DEVELOPMENT OF TWO AND THREE-DIMENSIONAL METHOD OF FRAGMENTS TO ANALYSE DRAINAGE BEHAVIOR IN HYDRAULIC FILL STOPES

Thesis submitted by

Kelda Shae RANKINE BEng(Hons)

in September 2007

for the degree of Doctor of Philosophy
in the School of Engineering
James Cook University

STATEMENT OF ACCESS

I, the undersigned, the author of this thesis, understand that James Cook University will make it available for use within the University Library and, by microfilm or other means, allow access to users in other approved libraries.

All users consulting this thesis will have to sign the following statement:

> **In consulting this thesis, I agree not to copy or closely paraphrase it in whole or in part without the written consent of the author; and to make proper public written acknowledgement for any assistance which I have obtained from it.**

Beyond this, I do not wish to place any restriction on access to this thesis.

_____   _____

Signature   Date

STATEMENT OF SOURCES

DECLARATION

I declare that this thesis is my own work and has not been submitted in any form for another degree or diploma at any university or other institution of tertiary education. Information derived from the published or unpublished work of others has been acknowledged in the text and a list of references is given.

_____   _____

Signature   Date

DECLARATION – ELECTRONIC COPY

I, the undersigned, the author of this work, declare that to the best of my knowledge, the electronic copy of this thesis submitted to the library at James Cook University is an accurate copy of the printed thesis submitted.

_____   _____

Signature   Date

Acknowledgements

The author wishes to thank,

My family – Dad, Mum, Tegan, Rudd, Shauna, Briony, Kirralee and Lachlan. Thankyou for being there through the good times and the bad, for sharing my laughter, tears, frustrations and achievements. I feel blessed to have the family that I have, and want to thank each and every one of them for always being there.

Another person who I am very thankful to who constantly provided their support, guidance, and encouragement is Assoc. Prof. Nagaratnam Sivakugan. Siva, you have taught me so much and have not only been an excellent teacher and mentor throughout my research, but you have also been a true friend for whom I will never forget and with whom I hope to share a friendship with for the rest of my life. You have helped me in so many ways, and for that I am forever grateful. Thankyou.

I would also like to thank Siva's wife Rohini, for her friendship and for sharing Siva and so much of his time with me.

Finally, I would like to thank the School of Engineering at James Cook University for allowing me to undertake this dissertation.

This work is dedicated to my wonderful family – Dad, Mum, Tegan, Rudd, Shauna, Briony, Kirralee and Lachlan

Abstract

The extraction and processing of most mineral ores, result in the generation of large volumes of finer residue or tailings. The safe disposal of such material is of prime environmental, safety and economical concern to the management of mining operations. In underground metaliferous mining operations, where backfilling of mining voids is necessary, one option is to fill these voids with a tailings-based engineered product. In cases where the fill is placed as a slurry and the fill contains free water, permeable barricades are generally constructed to contain the fill within the mining void whilst providing a suitable means for the drainage water to escape from the fill. Recent barricade failures, resulting from poor drainage, have led to an immediate need for an increased understanding of the pore pressure developments and flow rates throughout the filling operation. This thesis presents simple analytical solutions, based on the 'method of fragments,' for estimating discharge and maximum pore pressure for two and three-dimensional hydraulically filled stopes. Shape factors were developed to account for the inherent individuality associated with stope and drain geometry. The influence of scaling on discharge and pore pressure measurements is also investigated. The proposed solutions are verified against solutions derived from a finite difference program and physical modelling of a scaled mine stope and results showed excellent agreement. Using these analytical solutions developed for flow through three-dimensional hydraulic fill stopes, a user-friendly EXCEL model was developed to accurately and efficiently model the drainage behaviour in three-dimensional stopes. The model simulates the complete filling and draining of the stopes and was verified using the finite difference software FLAC^{3D}. The variation and sensitivity in drainage behaviour and pore water pressure measurements with, the variation in geometry, fill properties and filling-cycles of a three-dimensional hydraulic fill stope was also investigated.

List of Publications

Journals

Rankine, K.S. and Sivakugan N. (2007) "Application of Method of Fragments in Three-Dimensional Hydraulic Fill Stopes." *Journal of the Geotechnical Division ASCE, Under Review 3rd draft*

Sivakugan, N. and Rankine, K.S. (2006). "A simple solution for drainage through 2-dimensional hydraulic fill stope," Geotechnical and Geological Engineering, Springer, 24, 1229-1241.

Sivakugan, N., Rankine, K.J., and Rankine, K.S. (2006). "Study of drainage through hydraulic fill stopes using method of fragments," *Journal of Geotechnical and Geological Engineering*, Springer, 24, 79-89.

Sivakugan, N., Rankine, R.M., Rankine, K.J., and Rankine, K.S. (2006). "Geotechnical considerations in mine backfilling in Australia," *Journal of Cleaner Production*, Elsevier, 14(12-13), 1168-1175.

Refereed Conference Proceedings

Rankine K.S., Sivakugan N., Rankine K.J. (2007). *Drainage behaviour of three-dimensional hydraulic fill stopes: A sensitivity analysis*, 10th Australian and New Zealand Conference on Geomechanics – Common Ground, *Paper accepted*

Rankine, K.S. and Sivakugan, N. (2005). "A 2-D numerical study of the effects of anisotropy, ancillary drains and geometry on flow through hydraulic fill mine stopes," *Proceedings of the 16th ISSMGE*, Osaka, Vol.2, 955-958

Rankine, K.J., Sivakugan, N. and Rankine, K.S. (2004). Laboratory tests for mine fills and barricade bricks, *Proceedings of 9th ANZ Conference on Geomechanics*, Auckland, 1, pp. 218–224

Rankine, K.J., Rankine, K.S., and Sivakugan, N. (2003). "Three-dimensional drainage modelling of hydraulic fill mines," *Proc. 12th Asian Regional Conf. on Soil Mech. and Geotech. Engineering*, Eds. CF Leung, KK Phoon, YK Chow, CI Teh and KY Yong, 937-940.

Rankine, K.J., Rankine, K.S. and Sivakugan, N. (2003). "Quantitative Validation of Scaled Modelling of Hydraulic Mine Drainage Using Numerical Modelling," *Proc. of the International Congress on Modelling and Simulation, MODSIM 2003*,

Contents

List of Figures

List of Tables

List of Symbols

A = cross-sectional area

a = air content

B = stope width

C = Hazen's constant

C_{slurry} = percent solids of slurry

C_u = coefficient of uniformity

C_v = viscosity coefficient

C_0 = Terzaghi (1925) shape factor

C_2 = Kozeny-Carman (1938) shape factor

C_3 = Taylor (1948) shape factor

C_4 = Samarasinghe (1982) constant

C_5 = Amer and Awad (via Das, 2002) constant

c' = effective cohesional stress

D = drain height

D_r = relative density

D_s = effective particle dimeter

D_5 = the grain size for which 5% of the particles are finer

D_{10} = the grain size for which 10% of the particles are finer; effective grain size

D_{30} = the grain size for which 30% of the particles are finer

D_{50} = the grain size for which 50% of the particles are finer

$D_{60,}$ = the grain size for which 60% of the particles are finer

E_1, E_2 = material property constants, Carrier et al. (1983)

e = void ratio

e_{max} = maximum void ratio

e_{min} = minimum void ratio

F = drain width

Fr = Froude number

f = soil fabric

G = equivalent drain height

G_s = Specific gravity

g = acceleration due to gravity

H = height

H_w = height of water

h_i = head loss in i^{th} fragment

h_L = head loss

Δh = change in head between two points

i = hydraulic gradient

i_{entry} = entry hydraulic gradient

i_{exit} = exit hydraulic gradient

J = fill height increase per hour

K_0 = horizontal pressure coefficient (assumed to be 0.5)

k = permeability

$k_{0.85}$ = permeability at void ratio of 0.85

k_e = effective permeability

k_{equiv} = equivalent permeability for a layered system

k_h = permeability in the horizontal direction

k_v = permeability in the vertical direction

L = length

L_a = length of ancillary drain

m = soil compressibility

m_s = mass of solids

m_w = mass of water

N_d = number of equipotential drops

N_f = number of flow channels

n = porosity

n_{eff} = effective porosity

P_b = pressure exerted by the bulkhead on the fill

Q = discharge

q = discharge per unit length

Re = Reynold's number

R_s = solids filling rate

S = saturation

S_s = specific surface area of grains

S_v = grain surface per unit volume

s = shape factor

T = temperature

t = time

u = pore water pressure

u_{max} = maximum pore water pressure

v = discharge velocity

$V_{drained}$ = volume of water that has drained

V_f = volume of fill

V_{free} = total free water that is drainable

V_{in} = volume of water entering stope

V_{out} = volume of water draining from the stope

$V_{residual}$ = volume of residual water

V_s = volume of solids

$V_{to\text{-}drain}$ = volume of water that is yet to drain

V_v = volume of voids

V_w = volume of water

W = stope thickness

w = water content

w_{res} = residual water content

w_{sat} = saturated water content

w_{slurry} = water content of hydraulic fill slurry

X = drain length

α_{2D} = fraction of the head loss within fragment 2 for a two-dimensional stope that takes place in the horizontal segment of the largest stream line

α_{3D} = fraction of the head loss within fragment 2 for a three-dimensional stope that takes place in the horizontal segment of the largest stream line

Δh = change in head between two points

Φ = two-dimensional form factor for i^{th} fragment

Γ_i = three-dimensional form factor for i^{th} fragment

γ_t = total bulk unit weight of fill

γ_w = unit weight of water

η = dynamic viscosity

φ = effective frictional stress

κ = intrinsic permeability

μ = water viscosity

μ_T = water viscosity at T degrees Celsius

μ_{10} = water viscosity at 10 degrees Celsius

ρ_d = dry density

ρ_s = soil grain density

ρ_w = density of water

σ_h = horizontal/ barricade pressure

σ_h' = effective horizontal pressure

σ_v' = effective vertical pressure

τ_w = shear strength of rock-fill interface

ω = fluid surface tension

CHAPTER 1

INTRODUCTION

1.1. General

Minefill refers to any waste material that is placed into voids mined underground to dispose of mining waste (tailings) or used to perform some engineering function. In addition to this, minefill provides the following benefits:

- Effective means of tailings disposal,
- Increased local and regional rock stability,
- Improvement in ore recovery,
- Reduced environmental impacts of mining operations.

To accurately determine the support benefits that the minefill will provide, it is important that the geotechnical characteristics are properly understood. This will ensure that adequate provisions are made for the drainage, static and dynamic strength considerations. The static and dynamic strength stability requirements are typically imposed to ensure that the minefill has enough strength to prevent failure during the exposure of a minefill surface wall in the mining sequence and during blasting within the ore body. The dynamic and drainage requirements are linked inherently through the in-situ pore pressure in the fill mass. The major cause of failure in underground stopes is often attributed to the build-up of high pore water pressures behind the barricade, resulting in liquefaction due to blasting or piping (Bloss & Chen 1998; Grice 1998 a). Liquefaction occurs when the pore pressure increases dramatically, thus reducing the effective stress in the fill mass, to the point where the shear resistance of the soil is so low that the soil begins to "flow" like a liquid. If the fill mass liquefies, implications arise for the loading on the barricade walls which retain the fill in the stopes and prevent it from flowing into the mine. During liquefaction, all arching in the fill mass is lost and the loadings on the barricades will increase, which is significantly

greater than current design strengths for which barricade walls are designed. A flow of fill material would then follow, with potentially catastrophic consequences.

The open stoping mining method is a mining technique used as a means of obtaining ore from underground metalliferous mines. This method involves dividing the ore body into a series of prisms, approximately rectangular in geometry, called stopes. Blasting techniques are used to break down the ore within an individual stope to a size suitable for being removed via horizontal access at the bottom of the stope. Excavation initiates from the bottom of the stope and progresses upwards, so the ore falls to the base of the stope. Once the ore is extracted, it is processed, removing the valuable minerals from the rock and producing a waste material known as tailings. When used as minefill, these tailings are mixed with water and reticulated to an existing stope void. Where the walls of the fill mass are exposed by adjacent stoping, cement must be added to the minefill to provide sufficient strength to stabilize the fill over the exposed area.

To complete the extraction of an ore body, many stopes are required. These stopes are generally set out in a standard grid pattern, but specific details depend on the ore body geometry, the host rock and specific mine conditions. At any given stage of an underground mine operation, the excavation of several stopes will be under way at one time, and similarly several stopes will be in the backfilling stage. These individual stope operations are planned and sequenced to allow sufficient distance between excavations to avoid stability problems.

This research will focus on the drainage characteristics and associated properties of a particular type of minefill material known as *hydraulic fill* and issues related to using this fill material in underground mining operations. Hydraulic filling is one of the more popular backfilling methods used in Australia and worldwide and consists of deslimed tailings (i.e. finer fraction is removed via cycloning) and is placed underground hydraulically as a slurry. Hydraulic fills can be classified as sandy silts or silty sands with no clay fraction and are generally placed with a solids density of 65% − 75%.

Due to the high water content and permeability of hydraulic fill, free water exists in the placed fill and must be allowed to drain in order to minimize pore pressures

To contain the hydraulic fill, barricades are constructed at each of the entrances to the stopes. A schematic diagram of an idealized hydraulic fill stope is shown in Fig. 1.1. Barricade construction varies from mine to mine. In a number of cases, these barricades are made of special porous bricks that have permeabilities 2 – 3 orders of magnitude greater than those of the hydraulic fills (Rankine et al. 2004). These barricades contain the wet hydraulic fill, whilst draining the water into the drives thus reducing the build-up of pore water pressure behind the barricades. The remaining water either pools on the surface as decant water, or is retained in the interstices of the fill. Upon placement in the stope, the hydraulic fill rapidly develops sufficient shear strength to prevent transmission of geostatic (earth) pressure to the barricades. Therefore once dewatering is complete, pressures on the barricades are minimal. After dewatering and resulting consolidation in stopes underground, the fill becomes capable of accepting loads and the next stope is ready to be blasted.
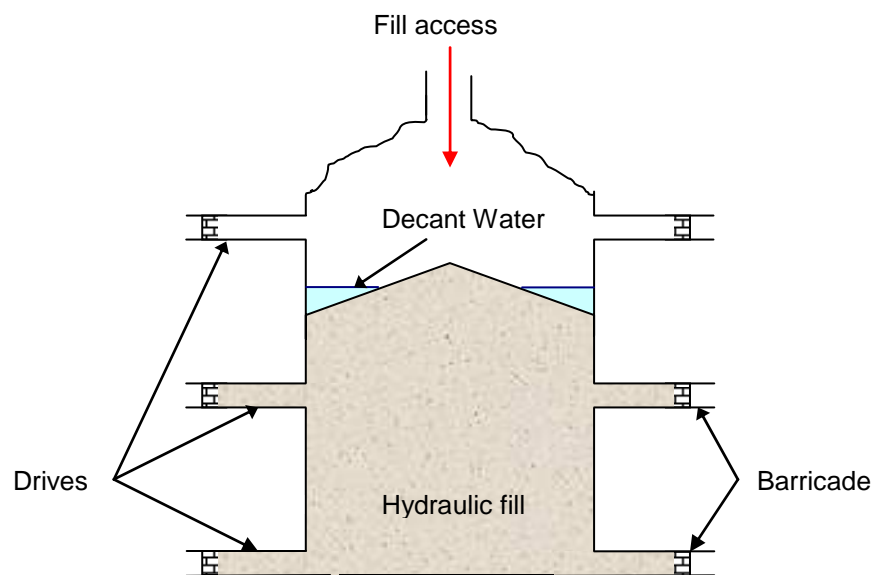
Fig. 1.1. Schematic diagram of idealized hydraulic fill stope

Recent barricade failures Grice, 1998 a; Torlach, 2000), resulting from poor drainage, have emphasized a need for an increased understanding of the pore pressure developments and flow rates throughout the filling operation. The primary objective of this thesis is the improvement in the filling and drainage operations through a greater understanding of the drainage behavior in hydraulic fill mines, as well as the means by which the drainage of these mines is analyzed.

1.2 Problem Statement

Hydraulic fill is generally placed in the form of a slurry with high water content for the ease of transportation and placement. The problem with high water content is that there is a substantial amount of water entering the stope. During the filling process and in the early stages of draining, several failures have occurred as a result of poor drainage of excess water from the stope causing substantial financial and human loss to the mines. As a result of these failures, there has been great importance placed on developments in drainage analysis of hydraulically placed minefill. Therefore, it is necessary to be able to predict the pore water pressure developments and flow rates throughout the filling process, so that barricade performance can be predicted and barricades can be engineered to prevent failure.

1.3 Objectives

The focus of this research is to study the fundamental aspects of the drainage behavior in hydraulic fill stopes. More specifically, this thesis aims to achieve the following objectives:

- To develop and verify simple analytical solutions, based on the 'method of fragments,' for estimating discharge and maximum pore pressure for two-dimensional hydraulically filled stopes.
- To extend method of fragments to three dimensional geometries and use this to develop and verify analytical solutions to predict the discharge rates and pore water pressures in three-dimensional hydraulic fill stopes.
- Develop a user-friendly *EXCEL* model to accurately and efficiently model the filling and draining of a three-dimensional minefill stope.

- Undertake a sensitivity analysis into the drainage behavior and pore water pressure measurements based on fill properties, geometries and filling schedules of a three-dimensional hydraulic fill stope.

1.4 Relevance of Research

The frequent historical occurrence of fill barricade failures around Australia and numerous underground mines worldwide has led to a need for an increased understanding of the factors which lead to failure of the fill in underground mining operations. Two major factors that have been identified are:

i) The flow of water through the hydraulic fill mass, and

ii) Poor drainage that leads to build-up of pore pressures, which results in piping, liquefaction and other forms of failures.

By understanding the processes that lead to failure, an increased level of confidence in design of hydraulic fills will be achieved. More efficient mining, safer minefilling practices and increased cost savings may also result from the introduction of new designs.

The drainage performance of hydraulic fill needs to be properly understood as it plays an important roll in the safety of underground hydraulic fill mining operations. Reliable knowledge of the drainage characteristics of underground hydraulic fill mines will improve mine safety and productivity through confidence in design and prediction.

1.5 Thesis Overview

Chapter 1 introduces the research problem, objectives and the relevance of the research. An overview of the major issues associated with the drainage of hydraulic fill mines and a brief description of the mining method have been presented. A broad overview of the thesis chapters is also discussed.

Chapter 2 presents a more detailed introduction into hydraulic fill. Initially an overview of minefill types and selections, the purpose of minefill and a brief historical overview of hydraulic filling practices within Australia are given. Research carried

out on the characterization of hydraulic fills and barricade bricks is also presented. As well as the current practices and recent developments with regard to underground hydraulic fill mining and drainage analysis and prediction, including physical modeling, in-situ monitoring and previous numerical modeling of the hydraulic fill stopes

Chapter 3 deals with the application of the method of fragments in two-dimensional stopes. Using method of fragments (Harr 1962, 1977) and the finite difference software *FLAC* (Fast Lagraingian Analysis of Continua, Itasca 2002), drainage and pore water pressure characteristics within a two-dimensional hydraulic fill stope were investigated in this chapter. Analytical solutions were proposed for determining the flow rate and the maximum pore water pressure within the stope. The proposed solutions were verified against solutions derived from the finite difference software package *FLAC* and were found to be in excellent agreement. The effects of ancillary drains and anisotropic permeability were also investigated.

Chapter 4 deals with the development of method of fragments in three-dimensions. This chapter provides simple analytical solutions and design charts for estimating the maximum pore water pressure and discharge within three-dimensional hydraulic fill stopes of varying geometries. Shape factors were developed to account for the inherent individuality associated with stope and drain geometry and the influence of scaling on discharge and pore pressure measurements were also investigated. Previously, method of fragments has only been applied in two-dimensions; this chapter extends the concepts into a three-dimensional analysis. The proposed solutions are verified against solutions derived from the finite difference software package $FLAC^{3D}$ and results are found to be satisfactory.

Using the analytical solutions developed for flow through three-dimensional hydraulic fill stopes in chapter 4, an *EXCEL* model was developed to accurately and efficiently model the drainage behaviour in three-dimensional stopes. This chapter discusses the development, application and verification of the *EXCEL* model which simulates the complete filling and draining of the stopes. Using this model, the sensitivity of

drainage behaviour and pore water pressure measurements with the fill properties, geometries and filling schedules of a three-dimensional hydraulic fill stope was investigated.

A summary of the findings from this research and recommendations for future research are presented in Chapter 6.

CHAPTER 2

LITERATURE REVIEW

2.6 General

Australians enjoy one of the highest living standards in the world and part of the reason for this is that we are a major trading nation. The minerals industry is one of the biggest contributors to Australia's export trade with estimated export earnings of $58.3 billion in 2004-2005 (**http://www.australianmineralsatlas.gov.au**).

The extraction and processing of most mineral ore, result in the generation of large volumes of finer residue or tailings. The safe disposal of such material is of prime environmental, safety and economical concern to the management of mining operations. For underground mines, the use of tailings in minefill not only reduces the environmental impact of surface disposal of tailings but also provides the base of an engineering material that can be used to improve both the ground conditions and economics of mining. Recent failures in Australia and worldwide have emphasized the need for proper understanding of underground filling practices, and in particular the use of hydraulic filling. Minefill refers to any waste material that is placed into voids mined underground for purposes of either disposal, or to perform some engineering function. This thesis is concerned with one particular minefill material, called *hydraulic fill*, which can be defined as deslimed mine tailings and a D_{10} value in excess of 10 μm. Hydraulic filling is one of the most popular minefilling methods used in Australia and worldwide.

The literature review is not only limited to this chapter which deals with the hydraulic filling of mine stopes; problems associated with hydraulic filling; and research carried out on the characterization of hydraulic fills and barricade bricks. A more extensive coverage on method of fragments, anisotropy, ancillary drainage, scale, numerical and physical modelling is given in latter chapters.

2.7 **Mining with Minefills**

There are two distinct types of mining methods: stable stope and caving, with a complete spectrum of methods available between these two extremes. The three stable stope methods which use minefill are the open stoping, room and pillar, and cut and fill mining methods. Caving is an unstable form of mining where ore is allowed to collapse under its own weight through prolific natural cracking and failures. In caving the ore will fail where undermined and will continue to fail while there is a void to fill and when there is sufficient cracking of the ore body. A comprehensive description of each of the mining methods is given by Brady and Brown (1985); Franklin and Dusseault (1991) and Reedman (1979). This research is based on the open stoping mining method in conjunction with hydraulic fill.

In an open stoping mining operation, the ore body is divided into separate stopes for mining. Fig. 2.1 illustrates a typical idealised plan view of an ore body, showing the typical stope extraction sequence in a nine-stope grid arrangement

Tertiary 6	Secondary 5	Tertiary 4
Secondary 3	**Primary 1**	Secondary 2
Tertiary 9	Secondary 8	Tertiary 7

Fig. 2.1. Plan view of an ore body showing typical stope extraction sequence in a nine-stope grid arrangement

In large scale, underground, mining operations, ore body extraction may result in stopes that are tens to hundreds of metres in depth. The stopes are created by carefully controlled sequences of blasts. On completion of extraction of the blasted ore the stopes are generally filled using the by-products of ore extraction and mineral processing, commonly known as tailings. Mine filling techniques, which generally use

these by-products, provide ground support to permit removal of adjacent, remaining ore, and are also effective means of disposal of waste materials. When hydraulic fill is used, barricades are constructed at each of the entrances to the stopes to contain the fill. These barricades can be made of special porous bricks that have permeabilities 2 − 3 orders of magnitudes greater than those of the hydraulic fills (Rankine et al. 2004). These barricades contain the wet hydraulic fill, whilst draining the water into the drives thus reducing the build-up of pore water pressure behind the barricades. The remaining water either pools on the surface as decant water, or is tied up in the interstices of the fill. After dewatering and resulting consolidation in stopes underground, the fill becomes capable of accepting loads and the next stope is ready to be blasted. It should be noted that for stoping sequences where adjacent stoping exposes the minefill, cemented hydraulic fill may be used and must cure to achieve the recommended design strength prior to adjacent stope extraction. A schematic diagram of an idealized hydraulic fill stope is shown in Fig. 2.2.
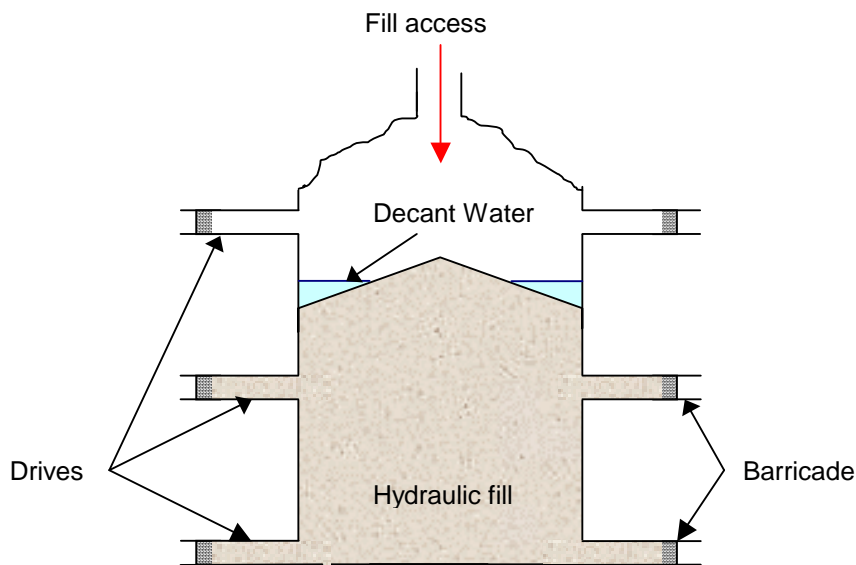
Fig. 2.2. Idealized hydraulic fill stope

2.8 **Purpose of Minefill**

Minefill refers to any waste material that is placed into underground voids, created by mining for the extraction of ore. Minefill is primarily used to maximise ore recovery

with the objective of optimising the economics of the mining operation. Minefill may be placed underground as a means of disposing it and to provide additional support for the remaining mine infrastructure (mine pillars etc). In addition to this, minefill provides the following benefits:

- Reduces the environmental impacts of the mining operations;
- Increases local and regional rock stability;
- Reduces risk of rockbursting;
- Provides an effective means of tailings disposal;
- Improves ore recovery;
- Reduces the need for large tailings dams; and
- Provides a working floor in minefill stoping methods.

To accurately determine the support benefits that the minefill will provide, it is important that the geotechnical characteristics of the fill are properly understood. This will enable adequate provisions to be made for the drainage, static and dynamic stability considerations. The static and dynamic strength stability requirements are typically imposed to ensure that the minefill has enough strength to prevent failure during the exposure of a wall in the mining sequence and during adjacent blasting within the ore body. The dynamic stability and drainage requirements are linked inherently through the in situ pore pressure in the fill mass. A brief overview of these requirements is given in section 2.4.

Nantel (1998) refers to the trend in Canada where future environmental legislations require the maximum quantity of mine waste to be returned to the underground workings. The obvious limit of this mining direction was reached when the Australian Federal Government recommended approving an alternative for the proposed Jabiluka Mine (JMA) whereby *all* mill wastes were required to be placed underground. Superficially, this may seem like a reasonable requirement based on a desire to preserve environmental integrity; however, such an approach may limit the financial viability of a significant number of mines (Grice, 1998 b). Grice showed that for one particular operation there was an excess mine volume of 46% which would have to be created to store all mill waste in the form of pastefill.

2.9 **Minefill Performance Requirements**

Minefill is an engineered product and in order to satisfy performance criteria as part of an economic mine plan, it must achieve defined static stability, dynamic stability and drainage requirements (where the mine fill is placed as a slurry and contains free water, as well as minimising environmental impact. Each of these requirements is discussed briefly below.

2.9.1 Static Requirements

Grice (2001) summarises the key static stability requirements as:

- Stand open in vertical faces when exposed by adjacent pillar mining;
- Support the weight of loading equipment when used as a mucking (trafficked) floor;
- Confine the rock mass surrounding the stope in order to maintain local and regional stability within mining areas;
- Permit mining underneath fill by production blasting for undercut ore extraction; and
- Permit mining through in development sized headings for the purposes of access or ventilation.

2.9.2 Dynamic Requirements

The key dynamic stability requirements are:

- Withstand the effects of close proximity blasting from production or development sized excavations; and
- Withstand the effects of regional seismic events

2.9.3 Drainage Requirements

Drainage is an important consideration in hydraulic backfilling where free drainage water is present. The main requirements include:

- Permit drainage of excess water from minefilled stope to reduce liquefaction potential

- Reduce potential excessive pore pressure being applied to stope access barricades that may fail as a result of high loading.

Excess water in stopes may come from three main sources including:
- Water used in transporting the fill material;
- Groundwater seepage from the stope walls; and
- Service water (e.g. machine water from drilling).

Generally the majority of the water to be drained through the fill mass comes from the water used to transport the fill to the site of deposition i.e. the water used to suspend the particles, as a hydraulic fill. Once placed, the solid particles tend to consolidate, leaving the water on top of the solidified material to percolate through the fill mass. Research undertaken by Thomas (1969) was instrumental in establishing and documenting the rule-of-thumb percolation rate for hydraulic fill as 100 mm/hr, which has been standard across the industry since around the 1950's (Nantel, 1998; Cowling, 1998; Keren and Kainian, 1983). With improved understanding into fill drainage and placement practices this standard has come under debate and the published permeability values of many hydraulic fills that are satisfactorily being used across Australia and worldwide fall well below this value (Brady and Brown, 2001; Herget and De Korompay, 1978; Pettibone and Kealy, 1971). It should also be noted that this value was often used as a good rate for cut and fill mining, which required relatively fast drainage to get back quickly on top of the fill with the mining equipment. In the 1980's and 1990's tailings became finer (due to finer grind) and this reduced percolation rates in the fill. For most open stoping methods, this was not as much of a problem because unlike cut and fill it was not necessary to be back on top of the fill within hours of placement. Also, cut and fill started reducing in popularity.

Minefill barricades are also typically designed to allow for the drainage of water from stopes. Sivakugan et al. (2006) conducted permeability testing on barricades which use porous bricks and hydraulic fills and found the ratio of the permeability of the brick to hydraulic fill to be in the range of 100 – 1500. Therefore it was assumed in this

dissertation that the fill-barricade interface is free draining and avoids any restriction to the flow of water from the stope and subsequent pore pressure buildup.

2.10   **Min efill Types and Selection**

There is a vast range of materials that can be used in minefill systems, including quarried rock, natural sands and gravels, total mill tailings, deslimed mill tailings, development mullock, open pit overburden, binders such as Portland cement, gypsum, lime, MINECEM and pozzolans (e.g. Flyash or slags) and chemical additives. Water is also required for the transport of hydraulic materials, hydration of binders and for dust control in "dry" systems. These materials provide a wide range of minefills that can be used in underground mines.

Dorricott and Grice (2002) discuss four major fill types used in Australia:
- *Hydraulic fill*: This may be produced directly from coarse sands and or mill tailings, or by desliming tailings with hydrocyclones to meet a nominal standard of <10% passing 10 μm and adequate drainage rates. Current industry practice suggests that provided the hydraulic fill meets this specification, drainage requirements will be met. Hydraulic fill slurries are usually placed at a solids densities ranging from 65% - 75%, to minimize the amount of excess transport water that must be drained and pumped to the surface.
- *Pastefill:* Consists of total mill tailings that are dried using filters and thickened to around 80% solids density. The size of tailings used in pastefill depends on what product is produced by the mill. Cement and water are added to the mix to achieve the required rheological and strength characteristics.
- *Rock fill:* Waste rock, quarry rock or aggregate are used as bulking materials. Depending on the engineering purpose of the fill, a hydraulic component (cement slurry or cemented tailings) can be combined with the bulking material to produce a cemented fill mass.

- *Blended fill:* Blended fills are created by adding rock or aggregate to sand, hydraulic or pastefill.

For mines that use minefill, the economics can be significantly influenced by minefill selection. The overall mine efficiency and viability is largely based on minefill selection and therefore minefill type is of paramount importance to the plan for the mining of an ore body.

For a more detailed description of fill types and production methods refer to McKinstry (1989) and Neindorf (1983). Table 2.1 illustrates the ten largest minefilling operations in Australia and the fill types used at each of these.

Table 2.1. Ten largest Australian mines using minefill (vide Dorricott and Grice, 2002)

Company	Mine	Fill Types*
BHP Billiton (WMC)	Olympic Dam	CAF, RF
MIM	Mt Isa Copper	CAF, CHF, HF
MIM	Enterprise	PF, CHF
Delta Gold	Kanowna Belle	CAF, PF
Normandy Yandal	Bronzewing	CAF, CHF, HF
MIM	George Fisher	CAF
BHP Billiton	Cannington	PF
Normandy NFM	Granites	CAF
Placer Pacific	Osborne	HF, RF
Normandy	Golden Grove	HF, RF

* CHF = cemented hydraulic fill, HF = hydraulic fill, PF = pastefill, PAF = paste aggregate fill, CAF = cemented aggregate fill, CRF = cemented rock fill, RF = rock fill

The type of fill used at a mine site is chiefly controlled by the on-site availability of the particular waste materials, financial costs involved with that minefill (e.g. are binders

required etc) performance characteristics and convenience of use. The selection of a minefill system involves a cost/benefit analysis of those systems that meet the basic technical and operational requirements. *EDUMine Online – Professional Development Underground Mine Backfill 1- Introduction* (2003) (www.civil.uwa.edu.au/teaching/MINE4162?f=130747) provides a design rationale for the minefill in six simple steps and is outlined below:

1. Specify the mining environment and mining system.

2. Identify the minefill purposes according to the mining system specified in step 1.

3. Define the target properties of minefill materials to serve the minefill purposes, based on the minefill purposes and mining condition.

4. Define the operating system so that minefill materials match target properties and the minefill operation itself. These include:

   ▪ Minefill material preparation;

   ▪ Minefill material transportation;

   ▪ Minefill material placement; and

   ▪ Minefill operation quality control and environment monitoring.

   To modify the design parameters, information monitoring at this stage will be fed back to earlier steps.

5. Do an economic evaluation of minefill system.

6. Document and implement minefill mining system.

This research deals with the placement, containment and drainage of hydraulic fill, which can be considered as the traditional tailings based mine filling practice (Thomas and Holtham, 1989). Therefore hydraulic fill and the drainage and containment of hydraulic fill within underground stopes will be discussed further.

2.11   Brief History of Minefill

The concept of using recycled extracted material for backfills in mines dates back hundreds of years. The original minefills in underground mines consisted mainly of waste rock and filling may have occurred naturally through caving of overlying strata or as part of a mining process to conveniently dispose of waste rock.

Over the past 150 years the Australian mining industry has developed into one of the world's leading mining nations. The gold rushes of the 1850's that put the Australian mining industry on the map have since expanded with the discovery of new minerals and resources. At present the Australian minerals industry is the third largest minerals sector by value of production of any country in the world (http://www.minerals.org.au/corporate). Fig. 2.3 depicts a brief timeline of Australian mines from the 1850's to that of present day. The export earnings from the past 25 years (1980 – 2004) have expanded from 7.2 billion to 52.2 billion dollars.
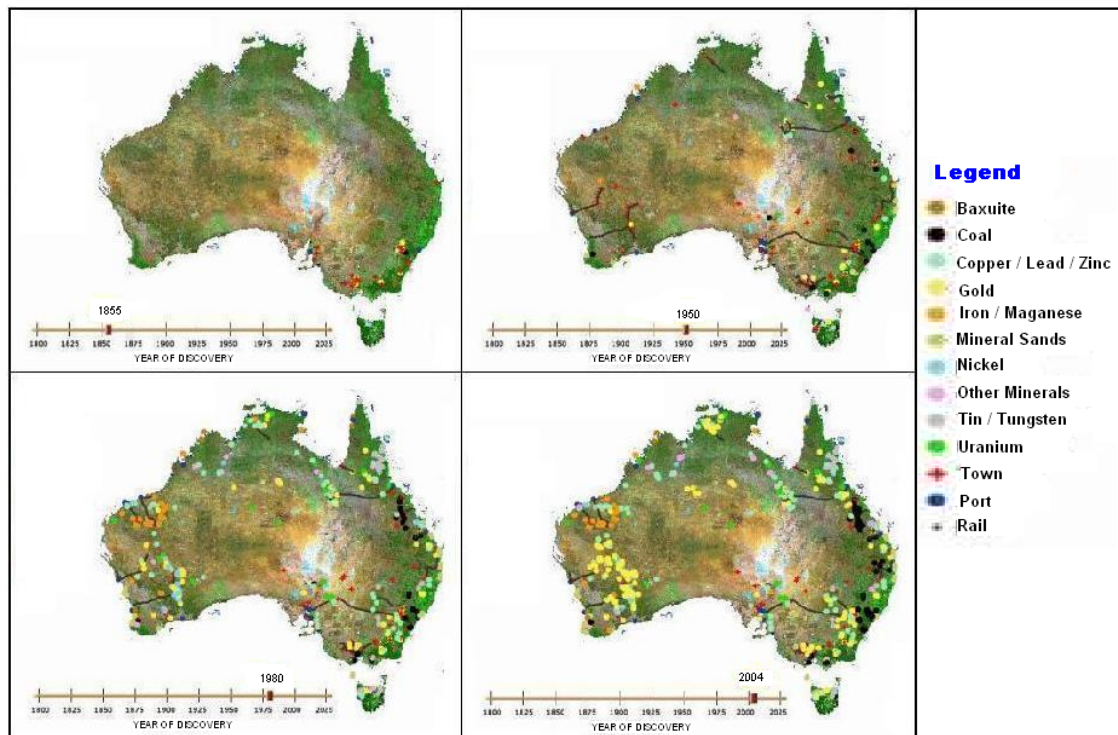
Fig. 2.3. Brief timeline of Australian mines from 1850 – 2004

One of the earliest recordings of the systematic use of fill is that of the use of mullock fill at Mount Lyell and North Lyell mines in Tasmania in 1915 (Murray, 1915). Barkley (1927) reveals that although the use of fill was only documented in 1915, the practice had been in progress since approximately the turn of the century.

The introduction of hydraulically transported fill in Australia was first reported by Black (1941) at the South Mine of Broken Hill South Limited, Broken Hill, New South Wales in 1939. By 1944, all underground transportation of fill within the South Mine was hydraulic.

Hydraulic fill has been used for a long time in the mining industry and remains the most commonly placed mine fill type (Potvin et al. 2005). The historical development of hydraulic fill practice in Australia runs roughly parallel with that in other countries. Hydraulic fill is now used extensively in underground mines throughout the world. Therefore, a move towards an improved understanding of hydraulic fill performance is needed.

The early days of fill in North America were not dissimilar to the Australian experience. Minefilling in Canadian mines has been practiced for close to 100 years and evidence suggests the application of minefill technology at an increasing rate during this decade (Nantel 1998, Udd and Annor 1993). The evolution of minefill technology is closely related to the establishment of new mining methods.

2.12 **Hydraulic Fill**

The most common source of material for hydraulic fill is the finely ground residues of mineral processing activities, however, they can be produced from a number of materials such as natural sand deposits and quarries. Hydraulic fills are simply silty sands or sandy silts with no clay fraction, which classify as ML or SM under the Unified Soil Classification System. The clay fraction is mostly removed through a process known as desliming, where the entire fill material is processed through hydrocyclones, and the fine fraction is sent to the tailings dam. The coarse fraction (referred to as hydraulic fill) is reticulated in the form of slurry through pipelines to the underground voids. Hydraulic fill is mostly commonly prepared using hydrocyclones, however several other less conventional methods are available. These can include: mechanical classifiers and thickeners, with sieve bend, filtration, and flocculation systems also worthy of consideration perhaps in conjunction with other more conventional processes (Thomas and Holtham, 1989). Differences in mineralogy,

particle shape and size distribution can affect transport, placement, drainage and performance properties.

Over the past decade, there has been a steady increase in the solids content of the hydraulic fill slurry placed in mines in an attempt to reduce the quantity of water that has to be drained and to increase the solids proportion. The problem with high solid content is that it becomes difficult to transport the slurry through the pipelines due to rheological considerations. Currently, solids contents of the hydraulic fill typically range between 65% - 75%. (Sivakugan et al. 2006). Even at 75% solid content, assuming specific gravity of 3.00 for the solid grains, 50% of the slurry volume is water. Therefore, there is a substantial amount of water that has to be drained from the hydraulic fill stope.

To contain the fill, barricades or bulkheads generally block horizontal drives. The horizontal access drives are large enough to let the machinery in during the mining operation and are blocked by the barricades during filling. The drives are often located at more than one level. The upper level drains let the decant water out and also would serve as an additional drain when the fill slurry reaches this level (Refer to Fig. 2.2).

2.13   **Hydraulic Fill Properties**

Hydraulic fill is a tailings-based material that is sourced from a wide variety of rock types and processing techniques. Many geotechnical properties of typical hydraulic fills may be characterized or described within a range. The following section aims to detail some of the properties of hydraulic fills, commonly found within the mining industry.

2.13.1 Grain Shape, Texture and Mineralogy

Fig. 2.4 illustrates the typical grain shape of a hydraulic fill sample tested at James Cook University. As shown in Fig. 2.4 and reported by Pettibone and Kealy (1971) and Nicholson and Wayment (1964), hydraulic fills contain very angular grains, which is a result of the crushing of waste rock from the milling process.
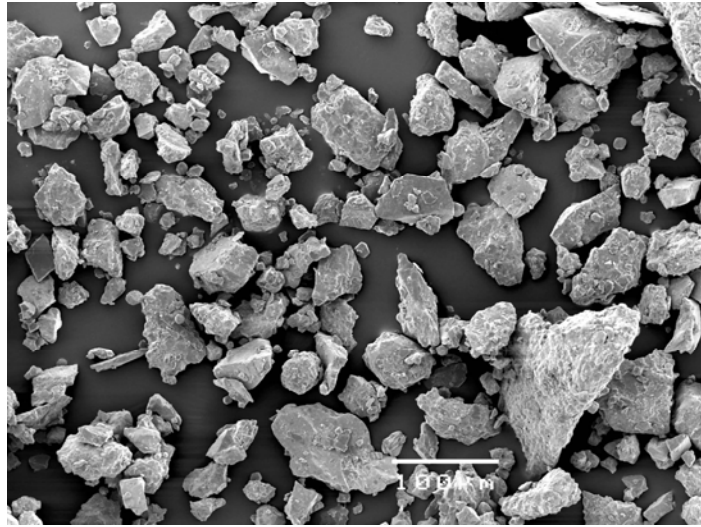
Fig. 2.4. Electron micrograph of hydraulic fill sample at James Cook University

Permeability of fill varies according to particle shape and texture of the soil. Generally, rough-surfaced particles produce a greater frictional resistance to fluid flow, thus reducing the permeability (Head, 1982). Irregular-shaped particles create longer, more tortuous flow paths for the fluid to flow through, thus reducing the permeability. Conversely, when particles are smooth and spherical, interlocking between particles is less and the flow paths are less tortuous, thus increasing permeability.

In fine-grained soils different types of minerals hold on to different thicknesses of adsorbed water and consequently the effective pore size varies. Thus, the mineral composition affects the permeability of clays, but has little effect on granular soils.

The mineral composition of the fill also indirectly affects the frictional resistance of the fill grains. Mineralogy controls important grain characteristics such as size, shape, surface attributes, angularity, and strength of particles Angular grains interlock more effectively than rounded ones, creating a larger friction angle and increasing the fill strength. Fill consisting of hard particles with rough surfaces that oppose grain movements off greater resistance to deformation and displacement.

2.13.2 Grain Size Distribution

Hydraulic fill is produced by passing the tailings from mineral processing in metalliferous mines through hydrocyclones to dewater and remove the fine fraction of the material. Research has suggested that the behavior of hydraulic fills depends critically on their grain size distribution (Clarke, 1988; Hinde, 1993). In general the smaller the grain, the smaller the voids between them and therefore the larger the resistance to flow of water. It is widely accepted within the mining industry that the effective grain size (D_{10} - *which is defined as the grain size for which 10% of the particles are finer than)*, most suitably defines the ability of a hydraulic fill to percolate water and settle from a slurry (Nicholson and Wayment, 1964; Thomas and Holtham, 1989). Current industry specification suggests that provided a hydraulic fill has less than 10% of the grain size distribution smaller than 10 μm, drainage requirements will be met (Grice and Fountain, 1991; Grice et al., 1993; Bloss and Chen, 1998, Dorricott and Grice, 2002). Herget and De Korompay (1978), quote 35 μm as the typical D_{10} value, whilst other researches including Kuganathan (2002) and Brady and Brown (2002) have quoted typical hydraulic fill D_{10} values in excess of 10 μm. The D_{10} range for fills tested by Rankine et al. (2006) fell between 12 μm and 43 μm. It should be noted that this criteria can vary, as long as the mining operation understands how their minefill drains and what it means for their mining process.

Wen at al. (2002) presents the results of a comparative study of particle size analyses by sieve-hydrometer and laser diffraction methods and suggests that laser diffraction methods should be adopted as the standard in geotechnical and geoenvironmental engineering. From the results, it was found that the sieve-hydrometer analysis underestimates the coarse silt and fine sand fractions which are the sizing that hydraulic fills fall within, and therefore this method may not be suitable or accurate. Due to the importance placed on the accuracy of the grain size distribution, all analysis is done through laser sizing in the mining industry.

More than 20 different hydraulic fills representing a wide range of mines in Australia were studied at James Cook University, and the grain size distribution for all these fall

within a narrow band as shown in Fig. 2.5. Along with them, the grain size distribution curve for a paste fill is shown. The addition of a very small percentage of cement has a limited effect on the grain size distribution. However, paste fills generally have a much larger fine fraction than hydraulic fills or cemented hydraulic fills as they contain the full plant tailings, but have negligible colloidal fraction finer than 2 μm.
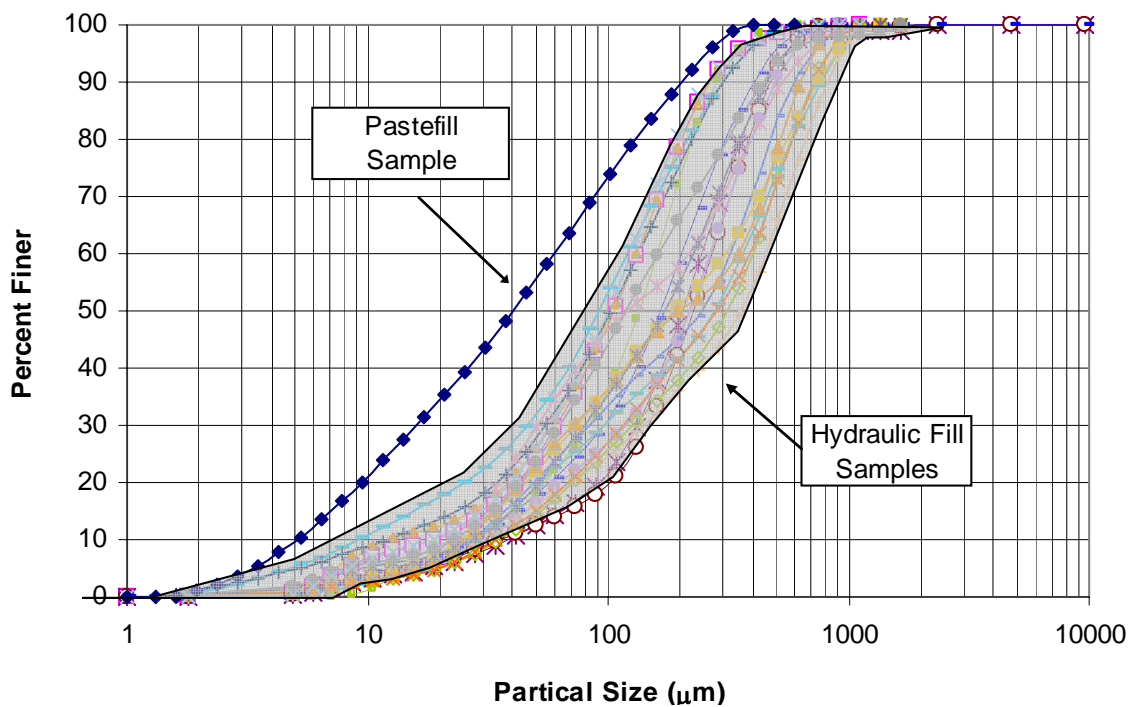
Fig. 2.5. Grain Size Distribution of Hydraulic Fills tested at James Cook University

Lamos (1993), Uys (1993) and Thomas (1978) suggest that the portion of particles finer then 10 μm in size (*ultrafines*) strongly influences the properties of minefills and in particular its permeability. Fig. 2.6 illustrates the decrease in minefill permeability with increased ultrafines content (Lamos, 1993).

The shear strength of a fill is also affected by the grain size distribution. As the friction angle increases so does the shear strength of a fill. Since well-graded fills have higher friction angles than poorly-graded fills, well graded fills tend to have a higher shear strength in the fill. Well graded fills also exhibit a large range of fine and coarse

particle sizes; this tends to decrease void space between grains, in turn increasing the frictional resistance of the fill particles.
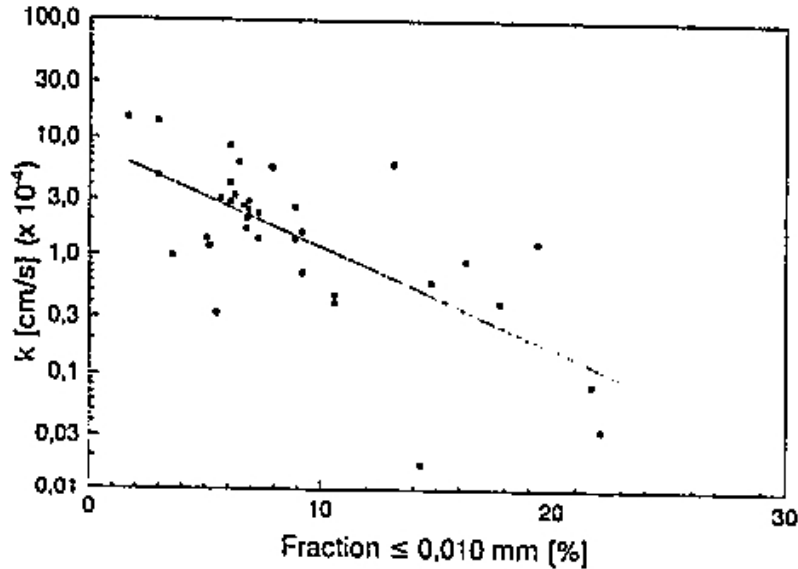
Fig. 2.6 Decrease in minefill permeability with increasing ultrafines content (Lamos, 1993)

2.13.3 Specific Gravity

Typically, the specific gravity of natural soil grains, falls within a narrow range of 2.6 – 2.9. However, due to the presence of heavy metals in the hydraulic fill tailings, the specific gravities vary significantly, ranging from approximately 2.8 – 4.4 for various Australian hydraulic fills tested at James Cook University (Sivakugan et al. 2005). These values agree well with the classified tailings tested by Pettibone and Kealy (1971) who recorded specific gravities ranging from 2.80 – 3.35. Table 2.2 presents a range of previously recorded specific gravities for a variety of minefills and in particular hydraulic fills.

Irrespective of specific gravity value, all hydraulic fills are generally placed into the stope at water contents of 30%-45%. At a certain solid content, the larger the specific gravity, the larger is the volume of water in the slurry, therefore the greater the volume of water that has to be drained from the stope.

Table 2.2. Specific gravity values for a range of hydraulic fills

Author	Material Type	Testing	Specific Gravity	No. of Samples
Rankine et al. (2006)	Hydraulic fill	Laboratory	2.80 - 4.40	24
Kuganathan (2001)	Hydraulic fill	Assumed	2.70 - 3.60	*NA*
Pettibone and Kealy (1971)	Hydraulic fill	Laboratory	2.80 - 3.35	9
Nicholson and Wayment (1964)	Hydraulic fill	Laboratory	2.82 - 2.96	4
Cowling et al. (1988)	Hydraulic fill	Assumed	2.90 - 3.00	*NA*
Qiu and Sego (2001)[1]	Mine tailings	Laboratory	1.94 - 3.17	4

[1]Tailings ranged from gold, copper, coal and consolidated tailings

2.13.4 Dry Density, Relative Density and Porosity

A common belief within the mining industry is that hydraulic fill settles to a dry density of approximately half the specific gravity of the material (Cowling, 1998). By simulating the hydraulic filling process in the mines, several laboratory sedimentation experiments were undertaken by Rankine et al. (2006). When these hydraulic fills, in the form of slurries at 65% - 75% solid content settled within the permeameter, they settled to porosity values in the narrow range of 36 – 49% and therefore it may be expected that the dry density is proportional to the specific gravity. Fig 2.7 illustrates the variation of dry density of the settled fill against the specific gravity, for hydraulic fills from several Australian and US mines as tested in the laboratory and in situ (Rankine et al. 2006).

In situ measurements both from overseas hydraulic fill mines (Pettibone and Kealy, 1971) and several Australian mines, agree well with the laboratory values tested at James Cook University (Rankine et al. 2004). From Fig. 2.7, Rankine et al. (2006) showed that the dry density of the hydraulic fill is directly proportional to the specific gravity and can be estimated by Eq. 2.1
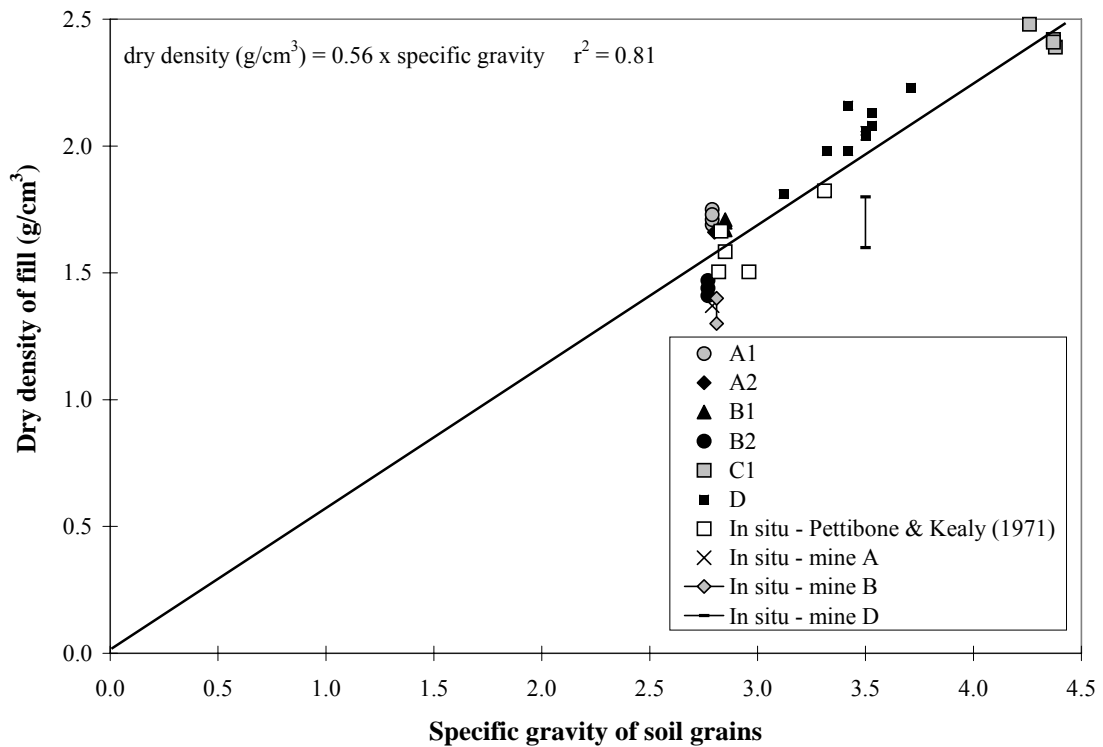
Fig. 2.7. Dry density versus specific gravity (Rankine et al. 2006)

Laboratory dry density (g/cm^3) = 0.56 x Specific gravity (g/cm^3)   (2.1)

The dry density (ρ_d) and void ratio (e) are related by:

$$\rho_d = \frac{G_s \cdot \rho_w}{1+e}$$ (2.2)

Brandon et al. (2001) conducted large and small scale testing on the fabrication of silty sand specimens and concluded that the density of the specimens along a vertical profile varied less than 6% from the average density. Sample sizes range from 3.1 by 7.6 cm in diameter to 1.5 by 1.5 m in diameter).

The porosity is given by:

$$n = \frac{e}{1+e} \qquad (2.3)$$

Grice (1998 b) assumes the porosity of a free-draining hydraulic fill to be approximately 50%, whilst published in situ values (Nicholson and Wayment, 1964; Pettibone and Kealy, 1971; Potvin et al., 2005) have been in the range of 30 % - 50%. A summary of several published porosity values for a number of hydraulic fills is recorded in Table 2.3.

Table 2.3. Published porosity values for hydraulic fills

Author	Material Type	Testing	Porosity (%)	No. of Samples
Potvin et al (2005)	Hydraulic fill	Assumed	29 - 50	NA
Nicholson and Wayment (1964)	Hydraulic fill	Laboratory	41 - 48	4
Grice (1998)	Hydraulic fill	Assumed	50	NA
Herget and De Korompay (1978)	Hydraulic fill	In situ	45 - 48	2
		Laboratory	37	1
Rankine et al. (2006)	Hydraulic fill	Laboratory	37 - 49	24

Relative density is a good measure of the density of the grain packing, and it depends on the maximum and minimum possible void ratios for the soil, still maintaining intergranular contact. The relative density can be defined as:

$$D_r = \frac{e_{max} - e_{current}}{e_{max} - e_{min}} \times 100\% \qquad (2.4)$$

The maximum void ratio is generally achieved by saturating the tailings and vibrating them to attain the densest possible packing whilst the minimum void ratio is generally determined by pouring the dry tailings from a fixed height so that the grains are placed at the loosest possible state. Using the two extreme void ratios and the current void ratio, the relative density of the fill is calculated from Eq. 2.4. Laboratory

sedimentation exercises at James Cook University laboratories (Rankine et al. 2004), showed that when the slurry settles under its self-weight, the relative density of the fill is in the range of 40%-70%. These values suggest that the hydraulic fills settle to a dense packing of grains. Extensive in situ testing at various hydraulic fill operations around the world indicate hydraulic fills are typically placed at a medium-dense state, with a relative density of approximately 55% (Nicholson and Wayment, 1964; Pettibone and Kealy, 1971; Corson et al., 1981). Refer to Table 2.4 for a list of various published relative densities of a number of hydraulic fills.

Table 2.4. Recorded relative density values of hydraulic fills

Author	Material Type	Testing	Relative Density (%)	No. of Samples
Pettibone and Kealy (1971)[1]	Hydraulic fill	Laboratory	44 - 66	4
Corson D.R. (1981)	Hydraulic fill	Assumed	55	NA
Nicholosn and Wayment (1964)[2]	Hydraulic fill	Laboratory	51 - 65	3
Rankine et al. (2006)	Hydraulic fill	Laboratory	50 - 80	9

[1]Mine H data omitted (Relative density = 11%), as was an anomaly in results

[2]Mine H data omitted (Relative density = 23%) as produced highly variable results

The relative density of the fill also affects the shearing resistance. As the void ratio decreases the amount of space between grains is reduced resulting in a denser fill. The increase in density of the fill implies an increase in interparticle contact area, and thus, in shearing resistance of the fill (Terzaghi et al., 1996). The closely packed grains of a dense fill give a greater resistance to shear forces, as grains must be forced up and around adjoining grains.

2.13.5 Friction Angle

Friction angle is an important parameter in the static and dynamic stability analysis of hydraulic fill mine stopes. Due to the limited access and safety issues, it is often difficult to carry out in situ tests within the stopes. Therefore laboratory tests such as direct shear testing on reconstituted samples are the preferred alternative.

Several hydraulic fills have been reported with friction angles between 30º and 47º Bloss (1992), and published triaxial test results on several hydraulic fill samples across the world also fall within this range (Pettibone and Kealy, 1971; Nicholson and Wayment, 1964). As the friction angle increases, so does the shear strength of the fill. It should be noted that the hydraulic fill sample with a friction angle of 47° recorded by Bloss (1992) was recorded for a high density sample.

Using reconstituted fills representing the in situ grain packing in the stope, a number of direct shear tests were conducted at James Cook University (Rankine et al. 2006). The tests reveal that the friction angles determined from direct shear tests are significantly higher than those determined for common granular soils. This can be attributed to the very angular grains that result from crushing the waste rock, which interlock more than the common granular soils. From limited experimental data, Rankine et al (2006) showed that a unique relationship exists between the friction angle of the hydraulic fill and the relative density.

2.13.6 Placement Property Test

The initial water content of hydraulic fill has significant influence on the in situ void ratio. A placement property test, proposed by Clarke (1988) is essentially a compaction test, where the compactive effort is applied through 5 minutes of vibration on a vibrating table. The main objective of the placement property test is to identify the optimum water content for the hydraulic fill that gives the minimum porosity and thus maximum dry density on placement in the stope. It is important to note that although this test provides us with the optimum water content, the rheological requirements required for ease of transportation through pipes generally results in water contents much higher than the optimum water content.

Fig. 2.8 illustrates porosity versus the water content for a sample tested at JCU (Rankine et al. 2006), where air contours are also shown. The shaded region, bounded by the horizontal maximum porosity (loosest state) and minimum porosity (densest state) lines at the top and bottom, and the saturation line on the right, is where the fill can exist with intergranular contact.   The intersection of the saturation line and the

minimum porosity line gives the theoretical optimum water content that can give the lowest porosity on placement. However, the fill materials are transported by pipes, and should have sufficient flow characteristics that require the hydraulic fill be transported and placed in the form of slurry, with water content higher than the optimum water content. The slurry follows the saturation line when settling under its self-weight and the density increasing with some vibratory loading. The placement property test is useful when assessing whether the fill will contract or dilate when subjected to vibratory loading such as blasting.
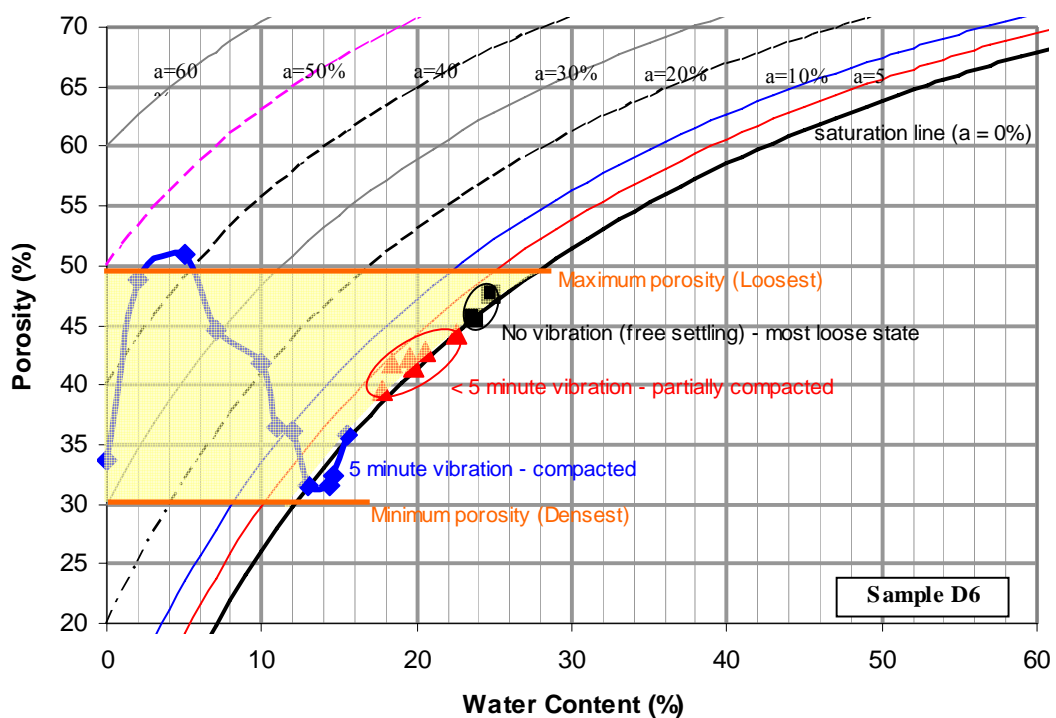
Fig. 2.8. Placement property curve of an Australian hydraulic fill (Rankine et al. 2006)

When the initial water content is very high, in the order of 40% - 50%, the suspension followed the saturation line and settled to a porosity value slightly less than the maximum porosity as shown by the two "■" symbols in Figure 2.8. The higher the water content of the suspension, the closer the porosity is to the maximum porosity. The points shown by the "▲" symbol were obtained from slurries mixed at water contents ranging from 20% to 50%, but were vibrated for less than 5 minutes. They

follow the saturation line in the shaded zone, and will move towards the optimum point with increased duration of vibration.

2.13.7 Degree of Saturation

Changes of the coefficient of permeability with less than 100% saturation are significant. Wallace (1975) showed that the higher the saturation the higher the percolation rate. Herget and De Korompay (1978) reported that a reduction in

saturation of approximately 10% could easily result in a percolation rate reduction of 50%. To develop a numerical relationship for this effect is not feasible, because of the fabric differences in various granular materials. Head (1982) also states that if the degree of saturation is less than about 85%, air is likely to be continuous, instead of being isolated bubbles. If this arises the permeability becomes also becomes function of saturation.

In this dissertation, it is assumed that the hydraulic fill beneath the water level is fully saturated. Fourie et al. (2001) observed from physical and laboratory tests that tailings could remain unsaturated below the phreatic surface.

2.13.8 Chemical Reactivity

Thomas (1969) states that in general, fill cannot be regarded as chemically inert, since it does react chemically with the solutions percolating through it and the gases they contain, as well as with atmospheric gases after dewatering. The rate of reactions is generally low though in certain circumstances it may become appreciable (Patton, 1957).

2.13.9 Permeability

Permeability is the measure of the ability of a fluid to percolate through a porous media. The permeability of hydraulic fill is the property of primary interest in hydraulic fill because it is commonly used as the sole criteria in establishing the suitability of a tailings product for placement as hydraulic fill (Corson et al., 1981;

Lamos, 1993; Thomas 1978).   The coefficient of permeability is a measure of the superficial velocity of water through the fill mass and is reported as meters per second at a unit gradient.   This is not the true velocity since the actual flow path is quite tortuous.

Approaches to both laboratory and field measurement of permeability through the hydraulic fill, are discussed by Herget and De Korompay (1978). Their results highlight that in many cases there is little consistency between permeability values observed in the laboratory and those existing in the field. Laboratory permeability values are referred to as 'absolute permeability' (k) and can be defined as the flow velocity for a fully saturated material at 20° Celsius under the influence of a hydraulic gradient of 1 unit of water head at 20° Celsius divided by the apparent flow path (Herget and De Korompay 1978). Refer Eq. 2.5 for absolute percolation rate definition.

$$k = \frac{QLC_v}{AH}$$ (2.5)

Here,

k = absolute percolation rate (cm/hr);

Q = flow rate (cm^3/hr);

L = length of sample (cm);

C_v = a dimensionless viscosity coefficient (the viscosity of water divided by the viscosity at 20º Celsius);

A = cross sectional area of sample (cm^2); and

H = height of water column (cm).

Effective permeability is the term used to describe permeability at a given saturation. In situ effective percolation rate studies were undertaken in the field, using three different permeameters as shown in Fig. 2.9.   Permeameters used include the tube permeameter, twin-rod permeameter and measuring electrode permeameter. Using the tube permeameter, the effective permeability was calculated from Eq. 2.6.

$$k_e = \frac{H}{t} \qquad\qquad\qquad\qquad\qquad\qquad\qquad\qquad\qquad (2.6)$$

Here,

k_e = effective permeability,

H = height between the electrodes, and

t = the time taken for the water level to fall between the two electrodes.
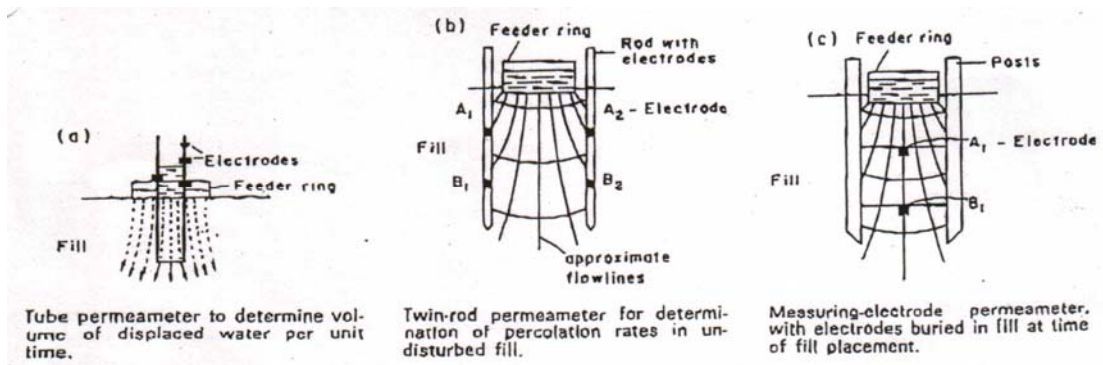
Fig. 2.9. Three field permeameters (Herget and De Korompay, 1978)

Both the twin-rod and measuring electrode methods illustrated above employed similar falling head analysis to calculate the effective permeability with more accurate measurements. The results obtained from the three different permeameters compared well, but these in situ permeability values varied considerably from the absolute permeability values calculated in the laboratory. When factors for the parameters that effect drainage were applied to the absolute values, they related well to the effective values (Herget and De Korompay, 1978).

A series of laboratory permeability tests were undertaken in 1981 as part of a research project by the United States Bureau of Mines, aimed at accurately defining the physical properties of hydraulic fill materials (Corson et al., 1981). The dependence of percolation rate on the void ratio of the material was identified, and as a consequence, a modified test that correlated the permeability of hydraulic fill to a range of densities was devised. This modified test is described in Wayment and Nicholson, (1964), and

the results may be used to estimate the flow of water through a fill material in a particular underground state. As discussed in section 2.8.5, most hydraulic fills commonly settle under self-weight in both laboratory tests and in situ conditions to relative densities and void ratios within a reasonably small band.

Martys et al. (2000) used image-processing techniques to capture the porous microstructure of a steady flow of water through soils. Images of soil microstructure were captured from soil specimens with the aid of an optical microscope and an image analysis system. Using image analysis of the soil samples, the average porosity and directional autocorrelation function of soil specimens were used to simulate the anisotropic three-dimensional microstructure of the soil specimens. The anisotropic permeability of the soils was then determined by the image processing techniques and numerical modelling of the pore structure. Several laboratory tests were carried out on a number of soil specimens to provide a comparison to the image processing techniques. For the test materials, the numerical values of permeability and the permeability anisotropy ratio compare well with experimental data.

The permeability of soil is generally determined in the laboratory by constant head permeability tests or falling head permeability tests. Constant head permeability tests are suitable for coarse-grained soils and falling head tests are suitable for fine-grained soils. Hydraulic fills, which contain a combination of sand-size and silt-size grains, may be studied using either of the two tests. Both tests are based on the application Darcy's law and assume laminar flow.

Darcy first investigated the flow properties of water through sand in 1856. Darcy developed the relationship relating the permeability, discharge velocity and hydraulic gradient of a soil, through a porous granular medium, under steady conditions and laminar flow as:

$$v = ki \qquad\qquad\qquad (2.7)$$

where:

v = discharge velocity (m/s),

k = coefficient of permeability (m/s)

i = hydraulic gradient (fall in hydraulic head per unit length)

Hansbo (1960) and Holtz and Broms (1972) found that there was a deviation from Darcy's Law for low permeability clays at a very low hydraulic gradient. This is in contrast to Mitchell's (1976) observations, who after reviewing a number of investigations regarding the applicability of Darcy's Law and stated that "with all else held equal, Darcy's Law is valid, even for fine grained soils at low hydraulic gradients". Mitchell (1976) cited the difficulties associated with obtaining accurate results with material of very low permeability, using laboratory test methods as the main source of deviation.

In a constant head test, water flows through the sample until discharge (Q) and the hydraulic head loss (h_L) has reached a steady state. The flow rate and head loss are then measured and the coefficient of permeability calculated using Eq. 2.8. A schematic diagram and an apparatus setup are shown in Fig. 2.10.
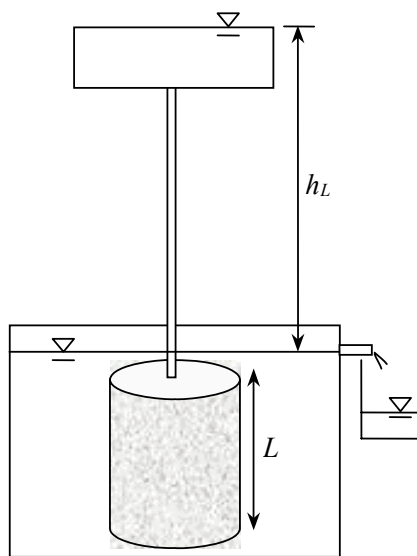
| (a) | (b) |

Fig. 2.10. Constant head permeability test (a) Schematic diagram, (b) Permeameter set-up in the laboratory

$$k = \frac{QL}{h_L A} \tag{2.8}$$

Here,

Q = the flow rate (cm^3/s),

L = sample length (cm),

A = sample cross-sectional area (cm^2),

h = the head loss (cm), and

k = coefficient of permeability (cm/s).

In a falling head permeability test, the water in the standpipe is allowed to fall during a period of time t, where the head drops from h_1 to h_2. A schematic diagram and experimental set-up is given in Fig. 2.11.

(a)   **(b)**
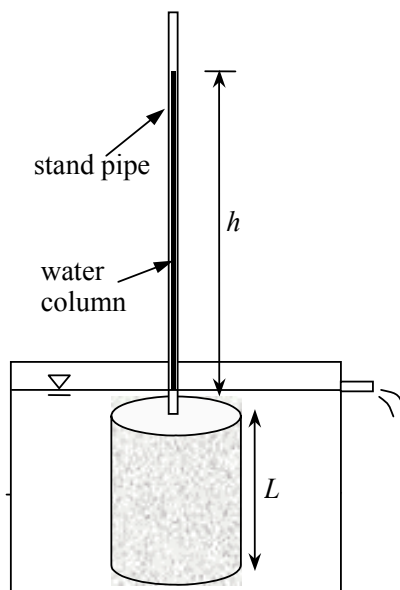
Fig 2.11. Falling head permeameter (a) Schematic diagram, (b) Actual permeameter set-up

Applying Darcy's law, it can be shown that the permeability is given by:

$$k = \frac{A_{s\tan dpipe}L}{A_{sample}t}\ln\frac{h_1}{h_2} \qquad\qquad (2.9)$$

where $A_{standpipe}$ and A_{sample} are the cross-sectional areas of the standpipe and the sample, respectively, and t is the time taken for height of water column h to drop from h_1 to h_2 in the standpipe. L is the length of the sample.

The constant head and falling head permeability tests carried out on hydraulic fill samples (Rankine et al., 2004) gave permeability values in the range of 7 - 35 mm/hour. In spite of having permeability values much less than the 100 mm/hr threshold suggested by Herget and De Korompay (1978) and Thomas (1979), all these hydraulic fills have performed satisfactorily in the mines, with no serious drainage problems reported. Anecdotal evidences and back calculations using the measured flow in the mine stopes suggest that permeability of the hydraulic fill in the mine is often larger than what is measured in the laboratory under controlled conditions. Table 2.5 details a list of permeability values recorded in literature for a range of hydraulic fills.

2.13.9.1   *Anisotropic Permeability*

Hydraulic fill materials, produced by crushing the waste rocks, have very angular grains as shown in the electron micrograph in Fig 2.4. When settling from the slurry they sometimes produce an anisotropic fill due to the finer fractions of the material settling with slower velocities than the coarser fractions. This stratification can lead to anisotropic behaviour in the permeability of the fill material. Fourie (1988) conducted Rowe cell testing to determine the variation in vertical and horizontal coefficients of permeability. The testing consisted of slurry mixtures set up at water contents of approximately 1.2 times the liquid limit. Fourie concluded that the ratio between horizontal and vertical coefficients of permeability were about unity for poorly graded coarse bauxite tailings, and increased to approximately ten for the well-graded fine-grained coal tailings.

Table 2.5. Published permeability values for a range of hydraulic fills

Author	Material Type	Testing	Permeability (mm/hr)	No. of Samples
Potvin et al. (2005)	Hydraulic fill	Assumed	1- 36	NA
Pettibone and Kealy (1971)[1]	Hydraulic fill	Assumed	22 - 76	NA
Herget and De Korompay (1978)[2]	Hydraulic fill	Field	89 - 93	2
		Laboraotry	37	1*
Nicholson and Wayment (1964)[3]	Hydraulic fill	Laboraotry	51 - 102	3
Grice (2001)	Hydraulic fill	Assumed	30 - 100	NA
Kuganathan (2001)	Hydraulic fill	Assumed	30 - 45	NA
Doricott and Grice (2002)	Hydraulic fill	Assumed	60 - 100	NA
Grice (1989)	Hydraulic fill	Field	14	1
Potvin et al. (2005)	Hydraulic fill	Assumed	1 - 36	NA
Rankine et al. (2006)	Hydraulic fill	Laboraotry	1 - 38	24
Brady and Brown (2002)	Hydraulic fill	Laboraotry	30 - 50	2

[1]Permeability values measured at void ratio of 0.8; Mine H data omitted

[2]Field permeability values recorded for porosity of 0.47 and adjusted for water temperature at 20 degrees Celsius and 100% saturation; Laboratory data recorded at porosity of 0.37, therefore adjusted to field porosity of 0.47

[3]Mine H data omitted as produced highly variable results

* Laboratory permeability value for porosity of 0.37. When sample was adjusted for porosity of 0.47 (as in the field case, permeability = 101mm/hr

Hatanaka (2001) conducted a series of permeability tests using a large-scale triaxial cell on high-quality undisturbed gravel samples recovered by the in situ freezing sampling method and also the reconstituted samples. Results suggest that:

- Although the data is limited, the permeability of gravel or sandy soils is not affected by the soil fabric. Therefore it can be concluded that the in situ

permeabilities could be estimated with a degree of confidence from the samples reconstituted in the laboratory.

- The coefficient of permeability in the horizontal direction is larger than that in the vertical direction. However the difference is below 70% and considered insignificant.

- The coefficient of permeability of gravely soils is almost the same as that of sandy soils, even though the 50% diameter of gravely soils is about ten to a hundred times that of sandy soils. This result implies that the large size particles of gravely soils are not significant in the permeability characteristics of gravely soils.

Using the image-processing techniques discussed by Martys et al. (2000) in section 2.8.10, the degree of anisotropy in the permeability was also determined for the varying sand types with values ranging from $1.10 - 1.30$. Most of the available measurements of the permeability anisotropy ratio are for cohesive soils and rocks that can be cut and tested in different directions (Chapius et al. 1989). Few reliable results are available for cohesionless soils. Chapius et al (1989) presented laboratory results on the effect of densification methods of a cohesionless soil. The permeability anisotropy ratio was lower than 1 ($\approx 0.87 - 1.00$) for dynamically compacted samples, whereas it was in the range of $1.33 - 1.83$ for static compaction. Mansur and Dietrich (1965) reported the ratio of horizontal to vertical permeability to vary in the range of $1.4 - 4.1$ with an average of 2 for granular soils.

Witt and Brauns (1983) also conducted some experimental testing using a permeameter with cube sample dimensions of 10 cm x 10 cm x 10 cm (similar to that used at James Cook University) which allows sedimentation of the particles parallel and perpendicular to the direction of flow. Results from his testing indicate an anisotropic ratio of approximately 2.3. However, the testing undertaken by Witt and Brauns used hydraulic oil as the fluid which has a much larger viscosity than that of water.

Anisotropic permeability has also been estimated by various other authors including Ouellet and Servant (1998) and Pettibone and Kealy (1971). Pettibone and Kealy (1971) estimated an anisotropic ratio 0.5 whilst Ouellet and Servant (1998) investigated k_h/k_v values of 10, 20 and 30 in their numerical model. Although these authors provide an insight into the degree of anisotropy associated with similar soil types, laboratory testing was undertaken on hydraulic fill samples at James Cook University to analyse the degree of anisotropy associated with the particular minefill investigated in this dissertation.

2.13.9.2 *The effect of cement on permeability measurements*

Previous experimental testing by Manoharen et al. (2002) and Pettibone and Kealy (1971) suggest that the permeability of cemented soil changes with time. This behaviour is expected, since the cement in the hydraulic fill material cures over time, the permeability value reduces. Cowling et al (1988) discusses the application of a finite difference seepage model to the prediction of pore water pressure and water levels during filling of underground mining excavations. Cowling's analysis utilises the model to investigate the effect of various backfill materials on drainage behaviour, in particular cemented hydraulic fill. However, the model uses a single permeability value to model the cemented hydraulic filled stope. As a result, Cowling noted a variation in the measured and computed heights of the fill and water levels within the stope. Although this dissertation concentrates primarily on the use of hydraulic fill in underground stopes, a preliminary investigation into the effect of cement on the permeability measurements was undertaken.

Using two different hydraulic fills (copper and zinc tailings), permeability tests were carried out to determine the effect of cement on permeability measurements. The binder MINECEM used in the testing produces a higher bond between the tailings than other binders such as Portland cement. For each of the samples tested, specific gravity, porosity and bulk density values were determined using the Australian standard testing procedures. The permeability testing for each of the samples (copper and zinc) consisted of:

- 3 x permeability tests with 5 % Minecem binder and;

- 1 x permeability test with no binder (control).

The cemented hydraulic fill samples were tested continuously for 28 days with hourly readings on the first day then readings at 3, 7, 14 and 28 days after the samples were prepared. The initial slurry was mixed at 33% water content, representing 75% solids by weight, which is similar to the consistency of the slurry placed in the mine. The cemented hydraulic fill sample was prepared in the permeameter and is shown in Fig. 2.12. Once testing was completed, the samples were removed using a mechanical extruder.

Fig. 2.12. Sample prepared in the permeameter – prior to testing

The variation in permeability of the cemented hydraulic fill (CHF) samples with time is shown in Fig 2.13 and Fig. 2.14 for the copper and zinc tailings respectively. A rapid decay of permeability, by an order of magnitude is evident in both fills, within 7 days. There is very little decay in permeability after 14 days, and it appears to reach an asymptotic value at the end of 14 days. Therefore constant head permeability tests was used for the initial permeability testing (i.e. hourly readings on the first day, 3 day, 7 day) and the falling head tests was adopted as a better alternative to the constant head permeability test from this point onwards (i.e. 14 day and 28 day permeability tests). Appendix A summarises the results for each of the samples tested including the initial and final water contents, void ratio, specific gravity dry and bulk densities. A summary of the permeability values recorded is also given in Appendix A.
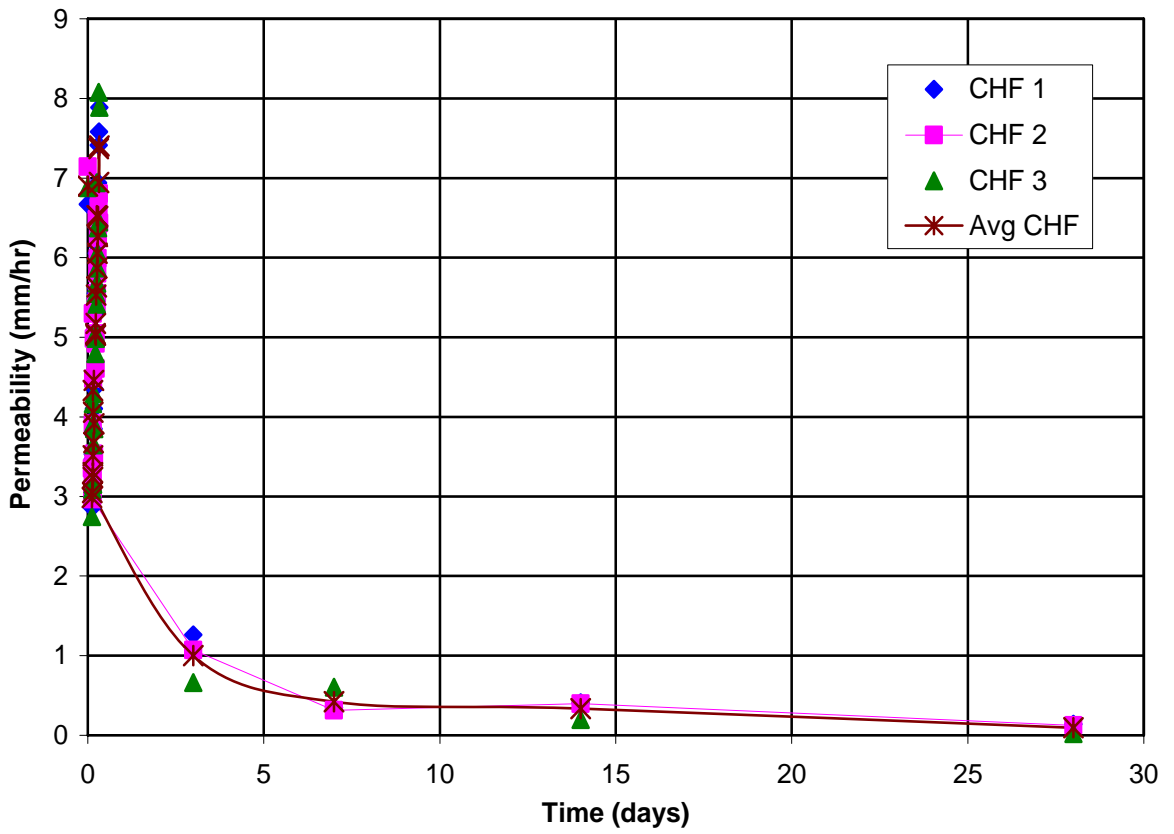
Fig. 2.13. Permeability Variation with Time for Copper CHF
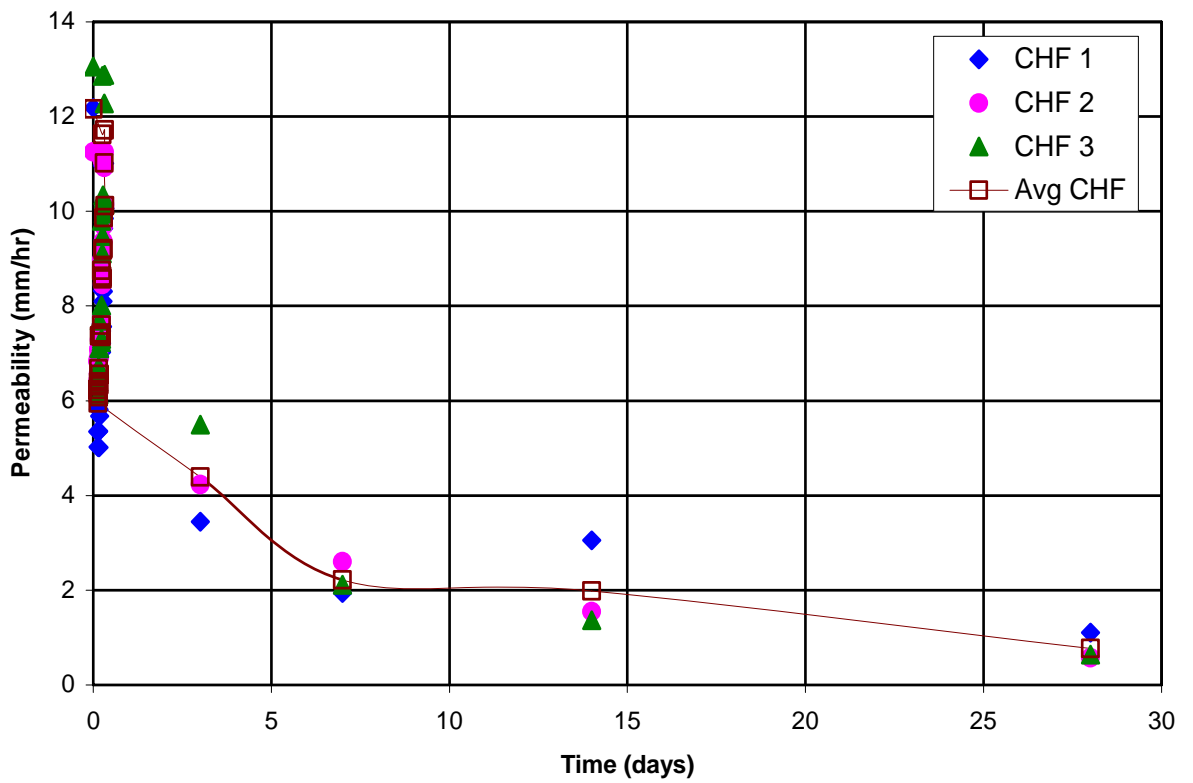
Fig. 2.14. Permeability Variation with Time for Zinc CHF

Empirical Relationships of Permeability

In 1880, Seelheim (vide Chapius 2004) wrote that permeability should be related to the squared value of some characteristic pore diameter. Since then, many equations have been proposed to predict the saturated hydraulic conductivity, k of porous materials. According to several publications (Scheidegger 1953, 1954, 1974; Bear 1972; Vukovic and Soro 1992; Mbonimpa et al. 2002; Aubertin et al. 2003; Chapius and Aubertin 2003), k can be predicted using empirical relationships, capillary models, statistical models and hydraulic radius theories.

The original Hazen equation developed in 1892 was defined as:

$$v(Darcy) = CD_{10}{}^2 (h / L)(0.70 + 0.03T) \qquad (2.10)$$

Therefore, Hazen's empirical relationship for the permeability can be calculated using:

$$k = CD_{10}{}^2 (0.7 + 0.03T) \qquad (2.11)$$

where v (Darcy) is the Darcy (1856) velocity expressed in m/d, h is the hydraulic head loss along the distance L (h and L have the same units), D is D_{10} in mm, T is the water temperature in degrees Celsius, and C is a constant close to 1000 in this system of units and k is the permeability in (m/d). Assuming T at 20 degrees Celsius and rearranging units, for the maximum void ratio, Eq. 2.11 becomes:

$$k = 1.50 D_{10}{}^2 \qquad (2.12)$$

where k represents the permeability in cm/s and D_{10} is the effective grain size in mm. Hazen formulated his empirical equation for permeability using clean filter sands in loose state. The effective grain size D_{10}, is an important value in regulating the flow through granular soils, including hydraulic fills (Budhu, 2000). There are a number of variations of Hazen's equation, however, it is generally written as:

$$k = CD_{10}{}^2 \qquad (2.13)$$

Several authors have suggested a Hazen's constant value of 1.0 (Lambe and Whitman, 1969; Freeze and Cherry 1979) However, several studies have been conducted and many geotechnical papers and textbooks cite a range of different values for Hazen's constant. Table 2.6 summarizes a range of values for Hazen's constant that have been published in geotechnical papers and textbooks.

Table 2.6. Hazen's constant values reported by various authors

Author / Textbook	Suggested Hazen's constant
Coduto (1999)	0.80 - 1.20
Das (1997)	1.00 - 1.50
Terzaghi et al. (1996)	0.50 - 2.00
Holtz and Kovacs (1981)	0.40 - 1.20
Lambe and Whitman (1979)	0.01 - 0.42
Cedegren (1967)	0.90 - 1.20
Terzaghi and Peck (1964)	1.00 - 1.50
Leonards (1962)	1.00 - 1.50
Taylor (1948)	0.41 - 1.46

Kozeny's (1927) formula and its modification by Carman (1938) use the relationship of permeability, particle size, porosity, angularity of particles, specific surface and viscosity of water. The equations are:

Kozeny (1927):
$$k = \frac{\rho_w g}{C_2 \eta_w S^2} \cdot \frac{n^3}{(1-n)^2}$$
(2.14)

Kozeny-Carman (1938):
$$k = \frac{\rho_w g}{C_2 \eta_w S^2} \cdot \frac{e^3}{1+e}$$
(2.15)

where:

k = coefficient of permeability (m/s);

ρ_w = density of water (1.00Mg/m^3);

g = acceleration due to gravity;

n = porosity;

η_W = dynamic viscosity of water at 20 degrees Celsius;

S_s = Specific surface area of grains (mm^2/mm^3);

C_2 = shape factor, varying depending on shape of particle, and ranges between 5 for spherical grains and 7 for angular grains.

Terzaghi (1925) also developed an empirical equation for estimating the permeability for sand.

$$k = C_0 \frac{\mu_{10}}{\mu_T} \left(\frac{n - 0.13}{\sqrt[3]{1 - n}} \right)^2 D_{10}{}^2 \tag{2.16}$$

where the constant C_0 equals 8 for smooth, rounded grains and 4.6 for grains of irregular shape (Terzaghi, 1925); and μ_{10} and μ_T are the water viscosities at 10 degrees Celsius and T degrees Celsius, respectively. For laboratory conditions, the data are usually given at T equals 20 degrees Celsius, for which the ratio of viscosities is 1.3.

Using Poiseuille's law, and considering flow through bundled capillary tubes, Taylor (1948) developed the following equation, which is in fact a simplification of Kozeny-Carman equation.

$$k = D_s{}^2 \frac{\gamma_w}{\mu} \frac{e^3}{1+e} C_3 \tag{2.17}$$

where:

k = coefficient of permeability;

D_s = effective particle diameter (m);

γ = unit weight of water (N/m^3);

μ = viscosity of water (m^2/Ns);

e = void ratio;

C_3 = shape factor (dimensionless).

For any clay, Taylor (1948) showed that by plotting e in arithmetic scale versus k in log scale, the trend could be approximated by a straight line. This was questioned by Samarasinghe et al. (1982). They showed that permeability of sands and clays could be related to void ratio by:

$$k = \frac{Ce^{C_4}}{(1+e)}$$

(2.18)

where the constant C_4 depends on the soil, with values of 3.2 for crushed glass, 4 for kaolinite, and 5.2 for Liskeard clay

The Naval Facilities Engineering Command (NAVFAC) design manual DM7 (NAVFAC, 1974) proposes a chart to estimate the saturated permeability of clean sand and gravel as a function of e and D_{10}. Analysing this chart, Chapius (2004) developed an equation given by Eq. 2.20 which relates the permeability, void ratio and D_{10} which is valid for parameters respecting the four conditions of NAVFAC (1974). These include:

- $0.3 < e < 0.7$,
- $0.10 < D_{10} < 2.0$ mm,
- $2 < C_u < 12$, and
- $D_{10}/D_5 < 1.4$.

where C_u is the coefficient of uniformity and is calculated by Eq. 2.19:

$$C_u = \frac{D_{60}}{D_{10}}$$

(2.19)

Where D_{10} is the effective grain size through which 10% of the particles are finer; D_5 is the grain size through which 5% of the particles are finer and D_{60} is the grain size through which 60% of the particles are finer.

Their equation is:

$$k = 10^{1.291e - 0.6435} |D_{10}|^{10^{0.294e + 0.5504}}$$ (2.20)

Carrier et al. (1983) showed that for slurried fine grained mineral wastes, including minefill and dredged materials, and remoulded clays, Eq. 2.21 provides a good approximation of the permeability value of these types of materials. E_1 and E_2 represent the material property constants and range from 10^{-13} to 10^{-9} m/s and $4 - 11$ respectively; e represents the void ratio of the soil and k is the permeability (m/s). Carrier et al. (1983) details more in depth explanations for the constants given by Carrier et al. equation of permeability (Eq. 2.21)

$$k = E_1 \frac{e^{E_2}}{1 + e}$$ (2.21)

Casagrande (vide Das 1997) suggested that for fine or medium clean sands the permeability relationship could be calculated using:

$$k = 1.4 k_{0.85} e^2$$ (2.22)

where $k_{0.85}$ is the coefficient of permeability of a void ratio of 0.85.

Several other relationships for the coefficient of permeability and void ratio are given in Eq. 2.23 – Eq. 2.25.

Lambe (1951): $\quad k \propto \dfrac{e^3}{1 + e}$ (2.23)

Karol (1960): $\quad k \propto e^2$ (2.24)

Das (1985): $\quad k \propto \dfrac{e^2}{1 + e}$ (2.25)

Qiu and Sego (2001) performed permeability tests at varying void ratios for four different types of tailings. Results agree well with those reported by Lambe and Whitman (1979) and are illustrated in Fig. 2.15.
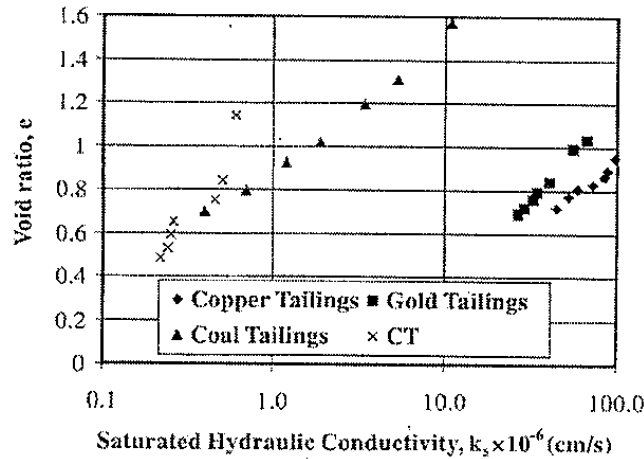
Fig. 2.15. Various laboratory measured soil permeabilities versus void ratios (Qiu and Sego, 2001)

As shown in Fig. 2.16 for all soils, *e* versus *log k* is a straight line (Lambe and Whitman, 1979). The permeability values documented by Lambe & Whitman (1979) are given for a wide range of different soils and were measured in the laboratory. All these developments suggest that *k* is proportional to e^n where *n* is a real number, and plotting *e* in arithmetic scale and *k* in log scale is approximated by a straight line.

Amer and Awad (vide Das 2002) suggest that the permeability of a coarse grained soil is related to the effective grain size, uniformity coefficient and void ratio and is given by Eq. 2.26.

$$k = C_5 D_{10}^{2.32} C_u^{0.6} \frac{e^3}{1+e}$$ (2.26)

where:

D_{10} = effective grain size (mm);

C_u = uniformity coefficient;

e = void ratio

C_4 = constant
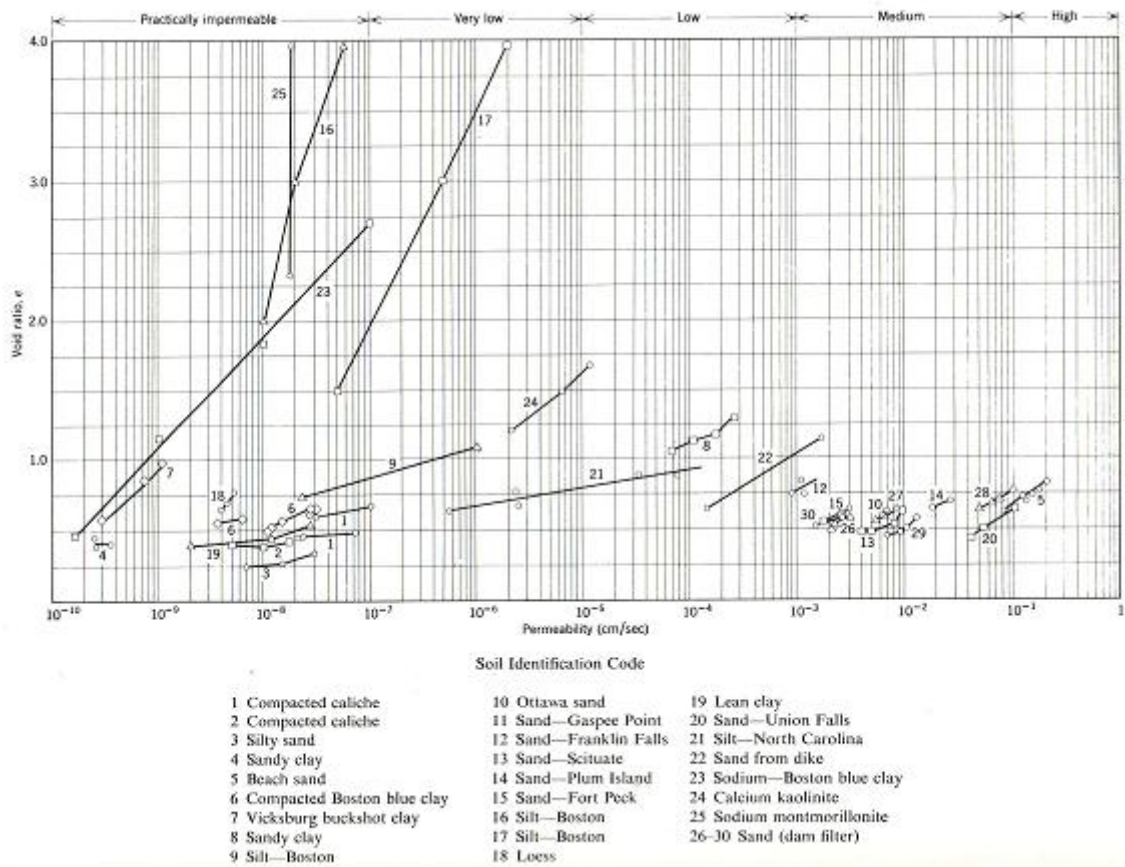
Fig. 2.16. Various laboratory measured soil permeabilities for various void ratios
(Lambe and Whitman, 1979)

In laboratory tests conducted by Cedegren (1989) it was shown that permeability values can vary by as much as one order of magnitude between the loosest and densest states of a soil.

2.14 Consolidation

According to Nicholson and Wayment (1964), "consolidation" is a term used to describe a volume change in saturated soil that is achieved under a constant load with the passage of time. This is different from "compression," which is used to describe a volume change due to an increase in load.

Carrier et al. (1983) states that if the solid particles are essentially sand to silt sized (e.g. hydraulic fill), the slurry material will sediment very rapidly to its final void ratio

and very little consolidation will occur as additional materials are deposited above. Thomas et al. (1979) noted that the consolidation of hydraulic fill is complete within a few seconds, whilst Clarke (1988) shows that consolidation of hydraulic fills results in a small initial volume reduction but no further changes occur with subsequent drainage.

Cohesionless materials, such as most hydraulic minefills, are not generally brought to maximum density by dynamic or static loading. Vibrators, however, very quickly bring this material to a high density provided the material is sufficiently free draining. This dissertation does not deal with the use of vibrators on hydraulic fill before placement. However the reader is directed towards Nicholson and Wayment (1964) for further information.

2.15   **Placement and Drainage**

Hydraulic fill placed into stopes, must be allowed to drain to remove transport water that exists as free draining water in the stope. The consequences of not meeting this requirement could lead to barricade failure, allowing a rush of fluidised fill into the mine workings with the possibility of tragic consequences.

In June 2000, a large brick barricade failed only three weeks after the start of the filling operation, killing three workers at the Normandy Bronzewing Mine in Western Australia. In the same year, two barricades failed at the Osborne Mine in Queensland. In both locations, hydraulic back filling was stopped for an extended period of time pending the outcomes of investigations. In the case of the Osborne Mine, fill activities were terminated for the remainder of 2000 and all of 2001 resulting in significant economic loss. Several other failures resulting in economic and human loss have been recorded within Australia and worldwide emphasizing the need for careful design and consideration of fill placement and drainage.

Potvin et al. (2005) discusses two important guiding principles and a number of conditions that should be met when designing the fill placement and drainage. The two guiding principles are:

- For a particular stope at any mine, there will be a rate of fill placement and resting time for drainage which should not be exceeded.
- If a mine employee has concerns about the safety of hydraulic filling operations that may result in an inrush situation developing, he/she should advise the supervisor to suspend fill placement. The supervisor should then warn and evacuate any personnel that may be exposed to an inrush of hydraulic fill.

The conditions detailed by Potvin et al. (2005) are as follows:
- Earth pressure and/or pore pressure loads applied to retaining barricades must be lower than the design strength of these structures,
- The excess transport water with which the hydraulic fill is delivered must be able to drain freely from the fill and the stope,
- The excess water should be minimised by:
    - Maximising slurry placement density, and
    - Reducing, diverting or eliminating flushing water delivered to the stope.
- The permeability of the fill and drainage system should be maximised by meeting or exceeding the permeability specification.

There are several approaches to the design of the filling schedule. In particular, the pour and rest times of the fill material. Drainage of excess transport water will commence immediately upon the start of placing fill and will continue while there is sufficient driving head to promote flow and the overall water content into the stope exceeds the residual moisture content (Cowling et al., 1988).

A number of authors have attempted to model fill placement and drainage process and most make some recommendation on pouring and resting regimes. Cowling et al. (1988) proposed a guideline for stopes at Mount Isa that are characterised by tall sublevel open stopes with multiple permeable masonry barricades located close to draw points. The filling schedules suggested by Cowling (see Table 2.7) were based on a fill rate of 300 t/hr at 72±2% solids content and a specific gravity of 2.90.

Table 2.7. Mount Isa fill and pouring resting regimes (Cowling et al., 1988)

Stope plan area m^2	Pouring time (hrs)	Resting time (hrs)
< 400	8	16
<1000	12	12
< 1600	16	8
> 1600	Unrestricted	N/A

Mitchell et al. (1975) describes a method of fill pouring based on monitoring the water balance in a filling stope. The criteria of the water balance method described by Mitchell et al. (1975) required that at any given time the total water content in a stope should not exceed 60% of the total water placed in the slurry. By measuring and subtracting the water drained out of the stope from the total water in the placed slurry, a continuous drainage state could be monitored. If the water in the stope exceeded the target figure, then filling must be suspended until that condition was satisfied. Likewise, if the water content was less than the target, then filling could either start or continue. The difficulties associated with the water balance method are accurately measuring the total quantity of water draining from the stope. Even for an isolated stope in good unfractured ground conditions, it is very difficult to capture all of the water. In most filling operations, there are filled stopes alongside or below that can be rewetted, or there are discrete water pathways in the rock that will result in missed measurements. However, drainage monitoring does provide an upper bound method that can highlight drainage problems. Since the unknown water losses cannot be measured, it is not possible to reliably set a lower target to compensate.

2.16   Barricades

Porous brick barricades can be used in underground mine operations to retain the hydraulic minefill that is used to fill the cavities created by mining. These barricades are designed to facilitate free drainage from the minefill. The rate and volume of water that drains is dependent on the initial density of the slurry and the residual water content of the minefill (Grice, 1998 a).

Barricade failures in underground mines are known to occur throughout the world. They are often catastrophic, generally resulting in substantial economic loss, and in some cases loss of life (Grice, 1998 a; Torlach, 2000). Barricade failure can lead to free flow of hydraulic fill slurry into the access tunnels, potentially trapping miners and machinery underground. Several mechanisms from piping to liquefaction have been suggested to explain barricade failures. Between 1980 and 1997, eleven barricade failures were recorded at Mount Isa Mines in both hydraulic and cemented hydraulic fill. Also, in 2000 a barricade failure in Normandy Bronzewing Mine in Western Australia resulted in a triple fatality, and another two permeable brick failures were reported later that same year, at Osborne Mine in Queensland.

As a result of several major bulkhead failures in the mid 1980's Mount Isa Mines instigated a research program aimed at developing an improved understanding of drainage behaviour. The research involved monitoring water flows and pressures in stopes, and testing the limiting strengths of barricade. The development of numerical models to predict seepage behaviour of the hydraulic fills was concurrently being undertaken, and the data gained from monitoring used to verify these models through back analysis (Isaacs and Carter, 1983; Cowling et al., 1988; Traves, 1988; Grice, 1989; Cowling et al., 1989). The research concluded that provided the barricades were free draining, insufficient pressure was built up behind the barricades to cause failure. The major cause of failure is often attributed to the build-up of high pore water pressures behind the barricade, resulting in liquefaction due to blasting or piping (Bloss and Chen, 1998; Grice, 1998).

The specialized barricade bricks often used for the containment of hydraulic fill in underground mines are generally constructed of a mortar composed of a gravel, sand, cement and water mixed in the approximate ratio of 40:40:5:1 respectively (Sivakugan et al. 2006). Fig 2.17 (a) shows a photograph of a barricade brick, and Fig. 2.17 (b) shows an underground containment wall constructed from the bricks. Traditionally, the walls were constructed in a vertical plane, but the recent industry trend has been to

increase wall strength by constructing them in a curved manner, with the convex side toward the hydraulic fill as shown in Fig 2.17 (b).

| (a) | (b) |
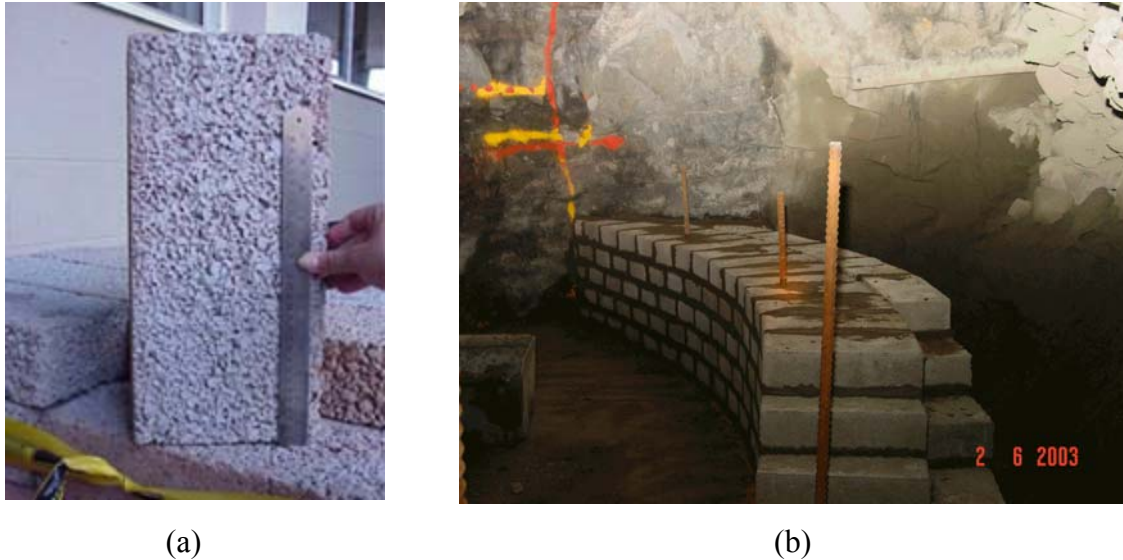
Fig. 2.17. (a) A brick used in the construction of barricades (b) A barricade wall under construction

According to Duffield et al. (2003), the design and construction objectives for brick barricades are:

- The barricade must have adequate strength to resist the pressure from the minefill (including initial hydrostatic pressure),
- The barricade must have adequate drainage/permeability (more than the minefill) to ensure minimal pore water pressure.

Rankine et al. (2004) conducted a series of laboratory tests on a number of typical Australian permeable bricks used for the construction of underground hydraulic fill barricades. The main objective of this testing was to study the drainage and strength characteristics of the barricade bricks, and their performance under pressures as high as 350 kPa. Typical barricade bricks were tested and showed porosities between the values of 18% and 24%, and a specific gravity range of 2.39 to 2.50 (Rankine et al. 2004).

Sivakugan et al. (2006) discusses permeability tests on barricade bricks that were carried out using a special pressure chamber, to study the one dimensional flow characteristics of barricades in the axial direction, under water pressures as high as 350 kPa. Three methods of determining the permeability of underground permeable barricade bricks were undertaken and the results were reproducible and correlated very well among all three methods.

From the results, it was shown that although there was substantial deviation in permeability between bricks, the average permeability of the barricade bricks has been quantified as two to three orders of magnitude larger than the values obtained for the hydraulic fill. The sizeable difference indicates that provided the barricades are built from the bricks in such a way that the construction or future migration of fines from the fill does not impede the drainage performance, for modelling purposes it may be assumed that the barricade does not contribute to the pore pressure development within the fill, and hence the drainage of the system is not related to the permeability of these bricks.

Rankine (2004) also conducted unconfined compressive strength tests on 9 longitudinally cored bricks, 95 lateral brick cores, 8 intact bricks and two specially cast cylinders. The bricks were sourced from three separate mines and were obtained by those mines from two different Australian manufacturers. The average unconfined compressive strength for the samples regardless of exposure condition was approximately 7.0 MPa, with a standard deviation of 2.8 MPa. Under in situ conditions, the bricks are saturated; therefore the effect of wetting the bricks was investigated by comparing dry and wet (7 days or 90 days wetted) samples (Rankine, 2004). Results indicated a distinct loss of strength in the order of approximately 25%, which is notable considering bricks are generally exposed to a saturated condition when placed underground, and manufacturer strength quotes are based on dry testing only.

Cowling et al. (1988) detail the specification of the bulkheads to be of approximately 10 MPa compressive strength and to remain porous. They use the general purpose

stress program BEFE (computer program for the static two and three-dimensional linear and nonlinear analysis of structures and solids using the Boundary Element (BEM) and/or the Finite Element (FEM) methods) to model the bulkhead stability. Based on the results of large-scale tests of bulkheads as reported by Grice (1989), elastic and strength properties were derived. From the analysis it was concluded that the standard bulkhead is more than adequate for all loading conditions likely to be experienced during filling operations, provided that they are constructed according to design.

Although it is known within the mining industry, that the porous bricks used in underground barricade construction are prone to variability in strength properties (Kuganathan, 2001), the manufacturers often guarantee a minimum value for uniaxial compressive strength for the bricks in the order of 10 MPa (Duffield et al. 2003). Kuganathan (2001) and Duffield et al. (2003) have reported uniaxial compressive strength values from 5 MPa to over 26 MPa.

Bridges (2003) discusses the use of field investigations for each type of barricade-fill combination. Experiments of controlled failures, like those conducted at Mt Isa mine in 1986 are required for each type of barricade, reasonably replicating the conditions in which barricades would be applied in the mine. Bridges (2003) suggests that a selection of stope barricades should be monitored for imposed fill pressures, displacements and flows of water during and after filling of stopes. Results from both types of investigations would be back analysed with numerical models to determine mechanisms of behaviour and design parameters that would be applied for future design and construction.

Duffield et al. (2003) utilized an analytical approach developed by Park and Gamble (2000), to model reinforced and un-reinforced concrete slab floors restrained on all four sides with the supports capable of resisting arch thrust, to compare predicted barricade strengths to those obtained experimentally by full-scale testing of an underground brick barricade at Mount Isa Mines in collaboration with CSIRO (Beer, 1986 vide Duffield et al., 2003; and Grice, 1989). The model predicted a failure

pressure of 427 kPa, which was well below the experimental failure pressure of 750 kPa for a 4 m x 4 m x 0.46 m thick barricade subjected to uniform loading (Duffield et al., 2003). This along with many other analytical methods of barricade performance contains too many simplifications, which extensively limits the reality of the predictions.

Potvin et al. (2005) analyses forces acting in the access drive including those exerted by fill earth pressure, seepage forces, shearing resistance along the drive rock wall and bulkhead pressure. These forces are illustrated in Fig. 2.18. The seepage force acting on the fill is given by $A.L.i.\gamma_w$ and is resisted by the lateral support given by the bulkhead and the contact shear resistance provided at the rock-fill interface along the access drive. If τ_w is the shear strength of the rock fill interface and P_b is the pressure exerted by the bulkhead on the fill then the force balance equation in the access drive is given by Eq. 2.27.
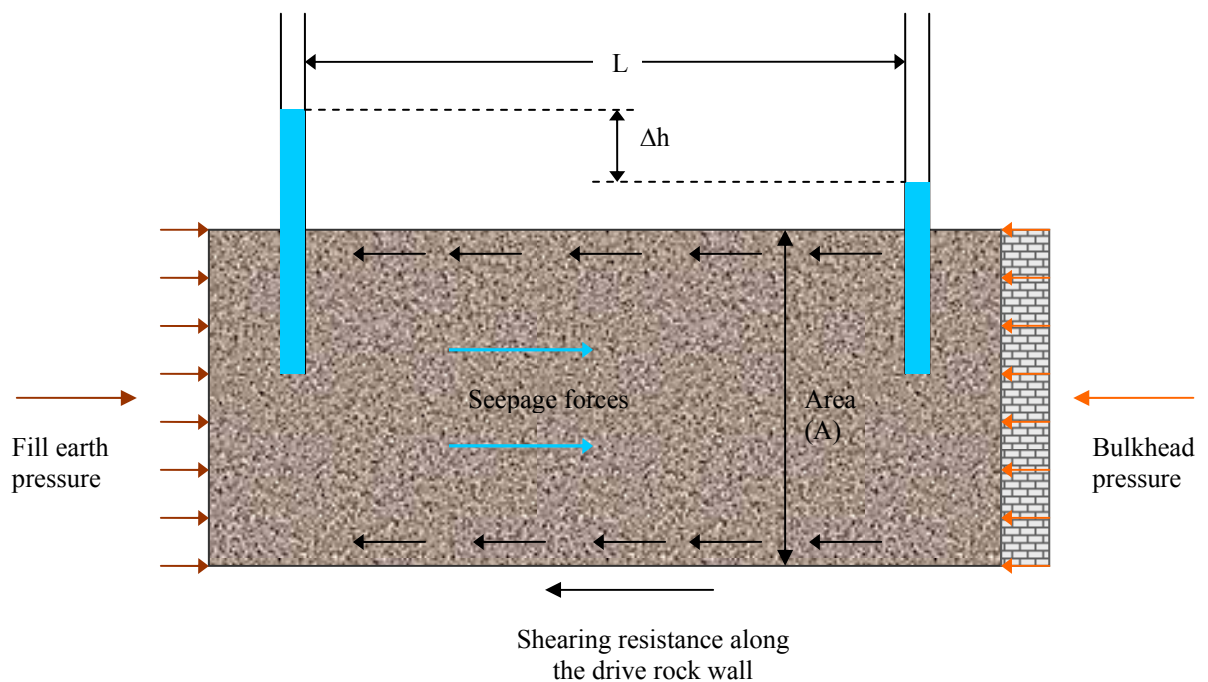
Fig. 2.18. Forces acting on the fill in an access drive (Potvin et al. 2005)

$$A.\sigma'_h + A.L.i.\gamma_w = P.L.\tau_w + A.P_b \qquad (2.27)$$

where:

A = area of access drive,

L = length of access drive at the bottom of a stope through which seepage occurs,

i = hydraulic gradient = $\Delta h/L$,

σ'_h = effective lateral earth pressure from the fill at the stope boundary,

τ_w = shear strength of rock-fill interface,

P_b = pressure exerted by the bulkhead on the fill,

γ_w = unit weight of water.

If the applied hydraulic pressure exceeds the strength of the barricade, then failure occurs. Bloss and Chen (1998) associate the failure behaviour depicted, with the piping mechanism described in geotechnical engineering by Terzaghi and Peck (1964). Piping is a condition where the pore pressures exceed the vertical effective stresses therefore causing buoyancy of the soil particles (this is commonly referred to as liquefaction or quick-condition) which propagates in the form of a pipe. Other descriptions and explanations of piping are clearly provided in Holtz and Kovacs (1981), Reddi (2004) and Harr (1962).

To improve the understanding of pipe formation and propagation, Bloss and Chen (1998) conducted a series of laboratory test simulations of the piping process. A constant head permeability apparatus was set-up with a standard uncemented minefill sample of 300 mm height. A two meter constant head of water was applied to the fill and a small hole was then created at the base of the column to provide a discharge location for water and eroded fill as shown in Fig 2.19.
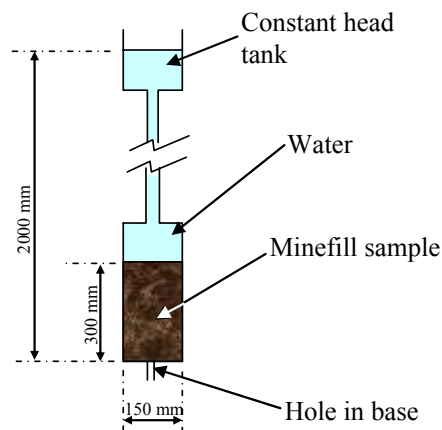
Fig 2.19. Test apparatus for observing the piping mechanism

The research described by Bloss and Chen (1998) illustrates three key issues:

- The significance of the piping mechanism in drainage-related bulkhead failures,
- The ease with which this piping can be initiated and propagate within the hydraulic fill, and
- The relatively poor understanding that exists in the area of piping in minefill.

The results confirm that to limit the occurrence of a pipe of this type developing in hydraulic fill stopes the slurry density should be maximised, thereby reducing the free water in the stope. The rate of fill and water heights in the stope should be monitored to reduce the amount of free water in the stope and regular inspections of bulkheads be undertaken to ensure minefill does not leak from them. Without a location for the minefill to discharge, the pipe will not generate.

The experimental investigation undertaken into the development of an erosion tube in hydraulic fill by Bloss and Chen (1998) described above, refers to a "piping" mode of failure and correctly describes the processes as follows:

> *"Piping will commence at a fill boundary where there is a hole sufficiently large to discharge the eroded fill (for example a hole in a bulkhead or adjacent country rock). The pipe will propagate into the fill given that the flow rate is sufficient to erode particles of fill and the result pipe structure. Piping by itself cannot pressurise a bulkhead; however if the pipe intersects a body of water such as water ponding on top of the fill surface, then the energy contained in the water will not be dissipated in the low permeability fill medium. In this case, pressure will be transmitted along the pipe to the surface where piping initiated."*

When leakage of fill is observed from a barricade, the failure would occur as detailed by Bloss and Chen (1998) with the development of the erosion tube initiating from the barricade. Several cases have been recorded whereby the erosion tube is the believed method of failure, but a leakage point on the barricade was not identified. Several reasons for this include.

- *Piping into a void behind a bulkhead*. When tight filling has not been achieved behind the barricade, a tube may propagate as a result of fill discharge into the void behind the barricade as shown in Fig 2.20 (Bloss and Chen, 1998). Minimising the distance between the stope edge and the bulkhead improves tight filling in the stope, therefore minimising the potential of piping. If an erosion channel were to initiate from a void, the overlying fill would continually erode into the gap, until it had been filled, in the form of 'slip'. Pressurization of the bulkhead can then occur without leakage of fill from the bulkhead.

Piping developing into unfilled access drive
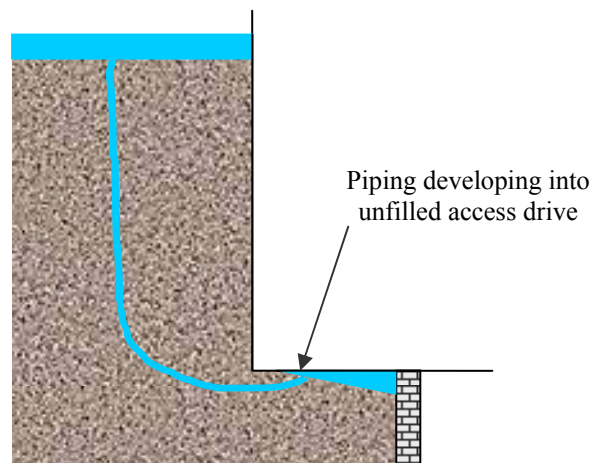
Fig. 2.20. Piping development in hydraulic fill due to unfilled access drive

- *Piping development in hydraulic fill due to fill escaping into fractures of the country or host rock* as shown in Fig. 2.21. The effect of arching can play a significant role in this case. The degree of arching within a stope depends on the geometry and location within the stope or drive (Rankine et al., 2004; Belem et al. 2004). Given the degree of arching that can occur in areas such as the stope drives, the vertical stresses in these areas can be very low. If an erosion tube develops from a region experiencing high degrees of arching, it is possible

that the pore pressures imposed by the erosion tube reaching the free surface would exceed the vertical stresses already reduced by arching. In this case liquefaction would occur and if this region of liquefaction propagates to the barricade, the full hydrostatic head of the free water would be applied to the barricade.
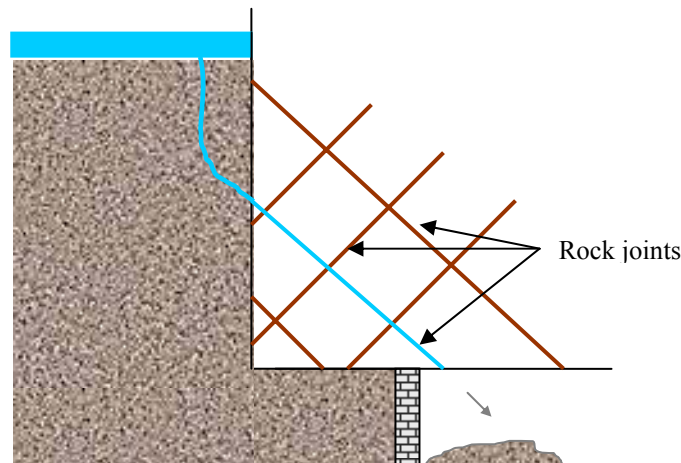
Fig. 2.21. Piping development due to fill escaping through rock joints

- *Development of a tube initiating from an unobserved leakage point* (Grice, 1998 a). Although possible, this is an unlikely scenario, as significant emphasis is placed on barricade safety and continual monitoring of barricades is generally undertaken in mining operations. Also, the quantity of fill that must escape for the tube to reach the surface is considerable; therefore it is unlikely that the barricade leak would go undetected.

Fig. 2.22 illustrates several examples of barricade failures.   Fig. 2.22 (a) illustrates an example of a pipe which has reached the upper surface (Grice, 1989). Whilst Fig 2.22 (b) illustrates a failed barricade whereby 100 m^3 of minefill ran into the drive and to an adjacent sump (Grice, 1998). The barricade shown in Fig. 2.22 (b) had a circular failure surface consistent with the application of a point load at the centre of the surface.   It was concluded by Grice, that a pipe had initiated at the site of the original leak and grew to meet the upper backfill surface. When it connected with the ponded water hydrostatic loads were applied, causing barricade failure. The ponded water and

the saturated backfill then rushed downwards through the pipe and into the access drive.
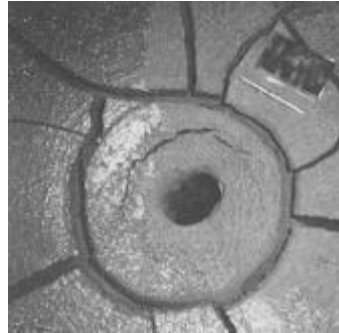
(a)
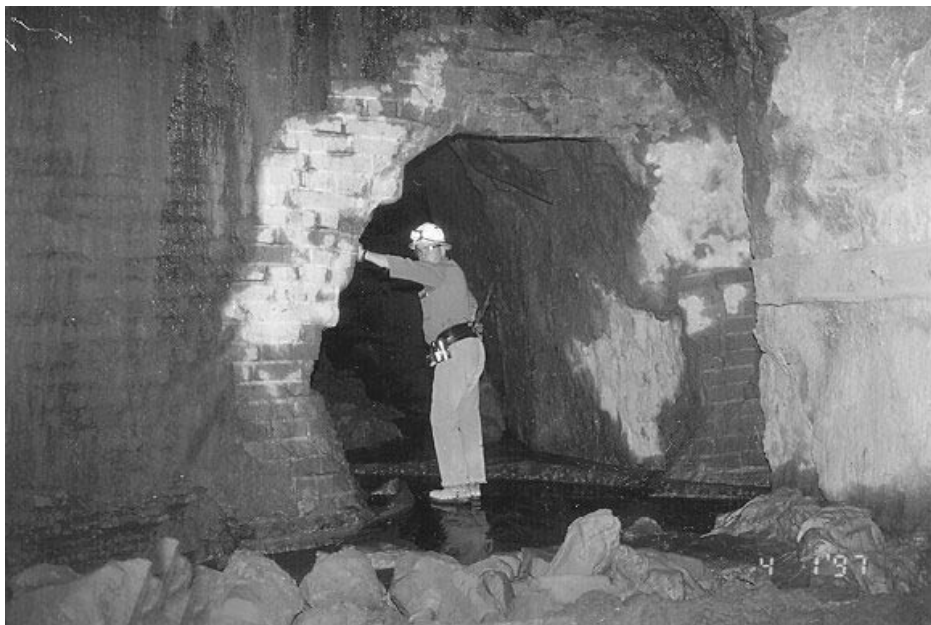
(b)

Fig. 2.22. (a) Erosion pipe seen during drainage trials (Grice, 1989) (b) Failed planar masonry barricade (Grice, 1998)

Kuganathan, (2001 a) used experimental and numerical modelling to identify the general failure mechanism of hydraulic fill barricades. Two case studies of barricade failure incidents in Australia were analysed to identify the key issues in barricade design and analysis. He suggests that there are four areas of concern when dealing with the drainage of a hydraulic fill system. They include:

- Preparation of fill mass within the stope,

- Fill in the access drive between the stope and the bulkhead,
- A properly designed drainage system, and
- Barricade design and installation.

Kuganathan suggests that for optimum safety in the hydraulic-filled stopes, careful attention is required to the design and details of the access drives. In particular the hydraulic gradient in the drive; size of the drive; offset distance between the stope and barricade; barricade construction; additional drainage behind the barricade; and the effective permeability of the hydraulic fill/brick system.

Kuganathan, (2001 b) designed an experiment to simulate the free draining bulkhead, which consisted of a 200 mm diameter galvanized steel pipe that was used to represent the drive in a real stope. The bottom end of pipe was closed and connected to a water supply through a 30 mm hole. Inside the cylinder a wire mesh and filter fabric were laid at the bottom and the cylinder was filled with hydraulic fill slurry until the fill solids level reached the top end of the cylinder. At the top end, a flat sheet plate with a 100 mm diameter hole was clamped to the cylinder. Care was taken to ensure there was no gap between the fill and steel plate. A 100 mm diameter perforated wooden disk was used at the top end of the cylinder to represent the model bulkhead. Geofabric filter cloth placed between fill and the model bulkhead prevented fill solids from leaking through the perforations, while allowing the water to drain freely. The model bulkhead was loaded to resist fill and water pressure during testing. First different water heads were applied at the bottom and the rate of water seepage was measured. Fill permeability was calculated from the seepage rates at various water levels. Water pressure was gradually increased until the model bulkhead failed. When the failure pressure was reached, the bulkhead was still draining freely. However, when the hydraulic gradient in the fill reached 30, a plug of fully mobilized fill pushed the bulkhead first and emerged through the failed bulkhead. Once the fill plug was pushed out, water was ejected from the failed bulkhead through erosion pipes, which developed after failure. The experiment was repeated with different sized model bulkheads and the failure mechanism was the same in all cases.

The experiment demonstrated that high seepage gradient in the fill caused it to fail, lose its strength and move like a heavy fluid to pressurize the bulkhead. The bulkheads fail under high pressure exerted by mobilized fill, and piping develops after the fill and bulkhead failure, due to the high pore water pressure that still exists in the fill. From these experiments, Kuganathan concluded that for from the analysis of his experiments, piping was not the cause of bulkhead failure; it is an after effect of bulkhead failure.

Martin (2001) performed test work to investigate the effects of introducing engineered drainage into a hydraulically minefilled stope. The tests were conducted in a laboratory environment using a custom built vessel to represent the stope. The tests incorporated the testing of drainage rates under two different conditions. The first test situation was to measure the drainage rate of the water in the stope through the simulated barricade, initially with no engineered drainage, and secondly, with engineered drainage.

The 450 mm (thickness) x 450 mm (depth) x 1100 mm (height) scaled stope was constructed of 3 mm sheet metal. Two drainage outlets were drilled into the base of the stope. Two fittings were also attached so that 5 mm copper tubing drainage pipes could be attached to the scaled stope. An access drive constructed of 75 mm square hollow tubing and measuring 45 mm in length, was welded to the sidewall of the tank. Holes were drilled along the length of the drive so that pressure readings could be taken. The internal drainage system was constructed out of 5 mm copper tubing. The copper tubing had 1 mm holes drilled along its entire length so that water would be able to percolate through the minefill and into the pipe. To prevent any fine particles from entering the pipe work, a geotextile fabric was placed over the pipe work. The vertical sections of the drainage pipe had 1 mm drainage holes drilled on both sides; whilst the horizontal sections had 1 mm drainage holes drilled on the upper surface. By simply removing the plugs that screwed into the bottom of the vessel drainage points, Martin was able to test the effect of engineered drainage on the stope.

The minefill mass in the stope vessel was placed under a constant head of water so that the pore water pressure in the access drive could be compared with and without

engineered drainage. Martin's results identified that engineered drainage reduced the flow of water through the barricade, and the pressure in the access drive behind the barricade. His results also concluded that lower moisture content developed in the stope with engineered drainage as opposed to the vessel with no engineered drainage. Although Martin produced various trends that will aid in the design and construction of drainage in minefills, there were a number of problems evident in his testing. These include:

- Scaling of the apparatus. Engineered drainage (5 mm copper tubing with 1mm holes drilled along its entire length) was not typical engineered drainage used in mines.

- The constant head of water applied to the minefill is not realistic in an actual operating drainage system.

2.17   **Physical Modelling of Hydraulic Fill Stopes**

The use of laboratory testing to study hydraulic fills is very attractive for the following reasons:

- Generally more economical then in situ testing,

- More controlled manner than at field scale,

- Possible to perform a larger number of tests and study the effects of several variables.

To the author's knowledge there has been no reported scale modelling data published on the drainage of hydraulic fill stopes. However, physical modelling of induced stresses within the fill mass using centrifuge testing and simulation of in-situ soil fabrics have been investigated and are briefly described below.

Previously, small, laboratory scale models of geotechnical structures, under gravity loads, lacked the proper similitude to generate the induced stresses within a fill mass. Using centrifuge testing, the modelling of such structures under an increased gravitational force has overcome this problem. Centrifuge testing has been frequently used as a modelling tool over the past 50 years. Studies on the static stability of cemented fills as well as the effects of blast loading on minefill using centrifuge

modelling have been reported in literature (Butterfield, 2000; Mitchell, 1998; Belem et al., 2004; Nnadi and Mitchell, 1991). More recently, laboratory modelling of hydraulic conductivity in centrifuges has been undertaken by Singh and Gupta (2000).

Brandon et al. (2001) used laboratory testing to investigate the fabrication of silty sand specimens for large and small-scale tests. The objective of their research was to simulate the in situ soil fabric and to allow for creation of a range of densities. Four alternate procedures were studied, including kneading, compaction, pluviation through air, pluviation through vacuum, and consolidation from a slurry. From his research, it was shown that slurry consolidation proved to be the best method to form silty sand specimens. The method approximates the natural formation process and leads to a specimen with a high degree of saturation. Densities can be varied over a wide range, and specimen structure is similar to that of silty sand in situ. Using this technique, Brandon conducts testing in the calibration chamber and concludes that the density of the specimens along a vertical profile varied by no more than 6% from the average density and their was little evidence of segregation of fines.

2.18   **In situ Monitoring**

In situ monitoring of hydraulic fill stopes provides several major advantages that are critical to underground operations. The measurements included pore water pressures, flow rates and fill/water heights. The advantages are:

1. Identifies abnormalities in the filling and draining process.
2. Provides data for the evaluation of numerical modelling techniques and empirical developments as prediction tools.

The disadvantages associated with the monitoring of hydraulic fill and barricade pressures and drainage include:
1. Very high expenses associated with the purchase of measuring and monitoring equipment.
2. The measuring equipment is typically non-retrievable.

Although the financial costs associated with monitoring hydraulic fill stopes are very high, the advantages well outweigh those disadvantages and many operations have successfully monitored the discharge rates and pore pressures during the filling and drainage of stopes (Grice, 1998 a; Ouellet and Servant, 1998; Brady and Brown, 2002). It is common practice these days to install monitoring equipment in stopes prior to filling.

One of the largest in situ monitoring programs in the world has been at Mt Isa Mines, with the results being successfully used to verify several numerical modelling drainage tools and gain invaluable knowledge and understanding into the drainage behaviour of stopes (Cowling et al. 1988). Some of the comprehensive measurements taken during the filling of stopes at Mount Isa Mines, have included pore water pressures, earth pressures, fill and water heights within the stope, water volumes discharged from the stope and barricade loading and deformation.

All instruments in the stope drainage trials were linked to a data acquisition system and results were recorded at 15 minute intervals throughout the 82 days of the project. Back analysis of the field measurements undertaken by Grice (1989), confirmed the application of a seepage model developed by Isaacs and Carter (1983).

Grice (1989) also conducted a series of tests to establish the performance of full sized concrete brick bulkheads. Three full sized bulkheads were built and tested underground and a modelling project with CSIRO Division of Geomechanics was initiated. The bulkheads were sealed then loaded and monitored until failure and the corresponding pressures and failure mechanisms recorded. The testing showed that pressure build-up was only possible if the bulkheads were sealed because of high permeability of the bulkheads. A sealed bulkhead is subjected to much higher pore water pressure loadings than one which is permitted to drain freely. A more detailed analysis of the in situ testing is provided by Grice (1989) and Cowling (1989).

Mitchell et al. (1975) present a case where the use of in situ monitoring was used to study the barricade pressures due to cemented hydraulic fill. Instrumentation was

placed in several heavily reinforced concrete barricades in a stope at Fox Mine in Northern Manitoba. The instrumentation included piezometers to measure the water pressures and pressure gradients, total pressure measurement devices which were incorporated in the barricade formwork, several 'mousetrap' drains and mid-level pressure gauges to detect if any water pressure was conveyed to the inner face of the barricade. The barricade stresses measured by Mitchell et al. (1975) were substantially less than values predicted based on using overburden weight (Eq. 2.28).

$$\sigma_h = K_0 H \gamma_t \tag{2.28}$$

Here,

σ_h = barricade pressure,

K_0 = horizontal pressure coefficient (assumed to be 0.5),

γ_t = total bulk unit weight of fill

H = the height of the minefill above the barricade.

Fig. 2.23 illustrates the results obtained from Mitchell et al. (1975) research and compares their results to predicted values based on Eq. 2.28.
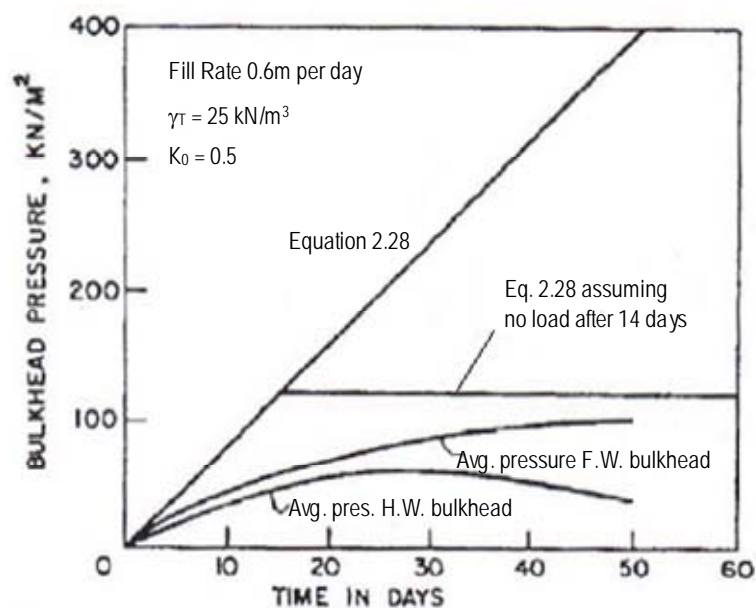
Fig. 2.23. Bulkhead pressure measurements (Mitchell et al. 1975)

The footwall bulkhead showed continually increasing pressures up to 50 days while the load of the hanging wall bulkhead decreased after approximately 30 days. From Fig. 2.23, Mitchell suggested that the gradual decrease in pressure transfer to the bulkheads was due to the strength gain in the cured minefill, and also due to the effects of arching (Barrett et al., 1978). The water balance study showed that the drainage characteristics of the hydraulic fill compared favourably to the predictions based on laboratory control specimens.

2.19 Numerical Modelling of Hydraulic Fill Stopes

With the development of higher powered and more affordable computers, numerical methods have been increasingly utilized in minefill design to identify areas of potential instability. Computer models play an important role with respect to understanding mechanisms of fill behavior and in designing economical strategies. Based on the results of this numerical modeling, a number of initiatives are proceeding with the objective of improving fill performance and economics.

Numerical simulation of hydraulic fill in mine stopes was initiated by a research contract between Mount Isa Mines (MIM) and L. Isaacs and J. Carter, which resulted in the development of a two-dimensional model, intended to provide a basic understanding of the concepts of the drainage of hydraulic fills in underground stopes (Isaacs and Carter, 1983). Through the use of this model, the developers were able to predict the drainage behavior of hydraulic fill throughout the filling and drainage of an underground stope. The model utilized limited parameter inputs, which were typical of very fine sand, and was restricted in its adaptability due to its fundamental geometric limitations. The barricades were assumed to be placed in flush with the stope, which is not very realistic. For safety reasons, barricades are always constructed at some distance from the stope. Work place health and safety requirements prohibit any access beyond the stope wall, into the unsupported empty stope. Therefore, barricades are always built at least a few meters away from the stope wall.

The model developed by Isaacs and Carter used an integrated finite difference solution method to determine the drainage configuration at each specified time step. The model

assumed the porous hydraulic fill material was homogeneous and isotropic and that Darcy's law for laminar flow was applicable. The top of the fill and the phreatic surface were assumed to be horizontal, and when the phreatic surface fell below the full height of the tailings, the upper boundary used for the seepage analysis was the phreatic surface. The position of the phreatic surface was calculated based on the quantity of water in the stope. When new hydraulic fill and water was added, the fill was added directly to the existing hydraulic fill and the water directly to the phreatic surface. Therefore, the addition of each pour had an immediate effect on the flow from the drains at the base of the stope. This introduced minor error in the times and quantities for predicted drain flows.

The results from the numerical model developed by Isaacs and Carter indicate that unless the pour rate was very low, the pore pressure developments within the stope were not significantly affected by the permeability of the hydraulic fill or the pour rate. They also concluded that the positioning of multiple drains had considerable impact on the pore pressure development within the system.

Although the research conducted by Isaacs and Carter has probably made the most significant contribution to date, to the understanding of the drainage behavior of hydraulic fill stopes, further evidence suggests that both pour rate and the hydraulic conductivity of the hydraulic fill do have a substantial effect on the pore pressure development within the system if the fill is not saturated. Considerable pore pressures may develop behind the wetting fronts in the hydraulic fill where the percolation rates have dropped significantly as a result of unsaturated flow (Wallace, 1975). The incorporation of saturated and unsaturated flow regimes would detect this effect. The other major shortfall of the two-dimensional model occurs in relating the output of the model to field measurements. The simplest method of in situ stope performance measurement is through outflow drainage rates from each of the barricades. The two-dimensional model developed by Isaacs and Carter only indicates the overall quantities for individual levels (Cowling et al., 1988). Individual drain discharge approximation may be made by dividing the total discharge for each level by the number of drains on that level.

Work was conducted which extended the program through field experiments and parameter studies including minefill type, pulp density, pour and rest time, stope dimensions, blocked barricades and flushing time, to provide field data from which to back analyze the model parameters and verify the value of Isaacs and Carter's program as a stope drainage prediction tool.

Isaacs and Carter (1983) provided valuable trends of drainage in stopes, the accuracy of the model's results was limited by the lack of laboratory and field measurements. Cowling et al. (1988) confirmed the application of the seepage model derived by Isaacs and Carter through the back analysis of field measurements. The work concluded that the coefficient of permeability values derived from this back analysis varied significantly from the laboratory values and that these values could only realistically be derived through the back analysis procedure. Cowling et al. (1988) determined that the influence the water content has on the effective porosity[1] is essential in the use of the model, and when accounted for provides close agreement with regard to pore pressure distribution as well as water balance within the system.

The two-dimensional model developed by Isaacs and Carter was further extended by Traves (1988). The model was advanced into a three-dimensional program, which incorporated several features allowing it to be more applicable to field conditions. The three-dimensional model was capable of simulating the filling and drainage of irregular stope geometries, with heterogeneous hydraulic fill, and provided predictions of pore pressures and flows at specific positions within the stope. Traves and Isaacs (1991) extended this model to three dimensions, but the model remains yet to be validated against field measurements.

Traves utilized a cells-based approach to model the geometry of the stope and the moisture flow through the fill. Flow simulation encompasses both the saturated and partially saturated regimes, allowing for the replication of the delays in time between

---

[1] Effective porosity accounts for the fraction of the voids that are active in conducting the water in the process of draining. It discounts the voids occupied by the residual water, which does not drain in engineering time.

the placement of a hydraulic fill pour, and the time in which the wetting front reached the phreatic surface. Traves' model was also able to permit spatial variability in hydraulic fill properties and provided output data, which was in an appropriate form for analysis and comparison to both the existing two-dimensional model and field data.

Ouellet and Servant (1998) analysed the findings from a series of two-dimensional finite element simulations for cemented hydraulic fill stopes. Ouellet and Servant hypothesised that the geometry of the drain system of a stope had a significant impact on the drainage of the stope and aimed their research on providing a better knowledge of the role the drain system has on the dewatering process of the stope. A cemented hydraulic fill stope was instrumented and daily records were taken during the entire filling process. These field observations and instrumentation data obtained confirmed findings previously reported by others. The 2-dimensional model developed by Ouellet and Servant was done in the commercially available finite element program SEEP/W, which was capable of modelling both saturated and unsaturated flow regimes. The results from the application of the model varied considerably from seepage simulation analysis reported from programs written by Traves and Isaacs and Carter, as well as others including Barrett and Cowling (1980) and Grice (1989 a). The simulation results could not be quantitatively verified against the field results as was done by the other researchers and a qualitative rationale whereby the movement of water in the vertical direction is less than the horizontal one due to layering effects was suggested by Ouellet and Servant to justify their findings.

Finally Rankine et al. (2003) developed two and three-dimensional drainage models in FLAC (*F*ast *L*agrangian *A*nalysis of *C*ontinua) and FLAC^{3D} to predict fill and water levels, discharge rates and pore pressures within two and three-dimensional hydraulic fill stopes as they are being filled and drained and verified it against the predictions from Isaacs and Carter (1983) model. These findings are discussed in further detail in chapters 3 and 4.

CHAPTER 3

APPLICATION OF METHOD OF FRAGMENTS TO TWO-DIMENSIONAL HYDRAULIC FILL STOPES

3.1   Overview

Using method of fragments (Harr 1962, 1977) and the finite difference software *FLAC* (Fast Lagraingian Analysis of Continua, Itasca 2002), the drainage and pore water pressure developments within a two-dimensional hydraulic fill stope were investigated in this chapter. Analytical solutions were proposed for determining the flow rate and the maximum pore water pressure within the stope. The proposed solutions were verified against solutions derived from the finite difference software package *FLAC* and were found to be in excellent agreement. Using these equations the effects of ancillary drains and anisotropic permeability were also investigated.

3.2   Introduction

In recent years, there has been an increasing trend to use numerical modelling as a prediction tool in studying the drainage of hydraulic fill stopes. Isaacs and Carter (1983) developed the first two-dimensional model which provided a basic understanding of the concepts of the drainage of hydraulic fills in underground stopes. Cowling et al. (1988) confirmed the validity of the seepage model developed by Isaacs and Carter through back analysis of the field measurements. Traves and Isaacs (1991) extended this into a three dimensional model however this is yet to be validated against field data. Rankine (2005) developed a two dimensional and more versatile three dimensional numerical model using *FLAC* and *FLAC^{3D}* respectively to study the pore water pressure developments and drainage with due considerations to the filling rate, slurry water content, tailing characteristics, etc. The model also allows for provision of multiple drains of different lengths and at different sub-levels. Although these models provide valuable information, they are often time-consuming and require specialist

knowledge of the numerical package used to model the stope. Using the parametric study carried out using *FLAC* and the method of fragments (Harr, 1962, 1977), this chapter presents an approximate solution for estimating the maximum pore water pressure and discharge within a two-dimensional hydraulic fill stope.

Method of fragments refers to an approximate analytical method of solution directly applicable to seepage problems where the flow rate, pore water pressures and the exit hydraulic gradients can be computed. The method was originally developed by Pavlovsky (1956) but was later bought to the attention of the western world by Harr (1962, 1977). The key assumption in this method is that the equipotential lines at some critical parts of the flow net can be approximated by straight vertical or horizontal lines that divide the flow region into fragments. (It should be noted that if the flow domain is tilted as a rigid body, these flow lines could be inclined.)

The flow region for the confined flow problem is divided into fragments by the vertical and/or horizontal equipotential lines. A dimensionless quantity, known as form factor (Φ_i) is then introduced for each fragment and is defined as:

$$\Phi_i = \frac{\text{No. of equipotential drops in i}^{\text{th}} \text{ fragment}}{\text{No. of flow channels}} = \frac{(N_d)_i}{N_f} \tag{3.1}$$

The flow rate can be given by:

$$q = kh_L \frac{N_f}{N_d} \tag{3.2}$$

Therefore, substituting Eq. 3.1 into Eq. 3.2, the flow rate can be calculated as follows:

$$\therefore q = \frac{kh_L}{\sum_{i=1}^{n} \Phi_i} \tag{3.3}$$

Since the flow rate is the same through all fragments,

$$q = \frac{kh_1}{\Phi_1} = \frac{kh_2}{\Phi_2} = ... = \frac{kh_i}{\Phi_i} = \frac{kh_L}{\sum \Phi} \tag{3.4}$$

where q, k, h_i and h_L are the flow rate per unit length, permeability, head loss in the ith fragment and total head loss across the flow domain respectively. The method of fragments, as described by Harr (1977), contained nine fragments (Type I, II … IX) given in Table 3.1. The first six fragments represent confined flow scenarios, whilst the remaining three consider unconfined flow cases.

Using method of fragments and numerical analysis, Griffiths (1984) condensed Harr's six confined flow fragments into two fragment types (Types A and B) and also introduced an additional fragment (Type C) as shown in Table 3.2. Griffiths presented a number of design charts for estimating the form factors (see Table 3.2) for varying geometries in which anisotropic soil properties can be accounted for directly. These form factors can then be used for estimating flow rates and exit gradients for various confined flow scenarios. The validity of the assumptions was assessed using finite elements and results indicate that the charts presented by Griffiths enable reliable estimates of flow rates and exit gradients to be made for a wide range of confined flow problems.

Sivakugan and Al-Aghbari (1993 a) carried out an optimization study on seepage beneath a concrete dam using the method of fragments. Initially, Sivakugan and Al-Aghbari also condensed Harr's six confined flow fragments to two main types (Types A and B) similar to Griffiths (1984). Then, using the charts and equations outlined in their paper, the effectiveness of using an upstream blanket and sheetpile on the quantity of flow rate, exit gradient and uplift was investigated. Sivakugan and Al-Aghbari (1993 b) compared the solutions from flow net and method of fragments, for seepage beneath concrete dams and sheet piles, and found excellent agreement between them. More recently, Mishra and Singh (2005) used the method of fragments to approximate the seepage through a levee with a toe drain resting on an impervious base. Their research was based on the unconfined flow fragment (Type VII) given by Harr (1977). Collectively these researchers have shown the method of fragments

Table 3.1. Summary of Harr's Fragments (Harr, 1977)
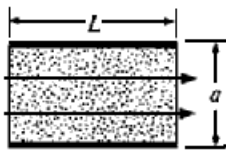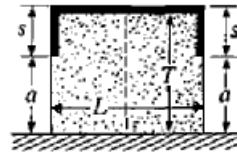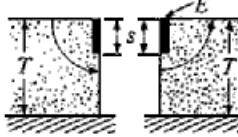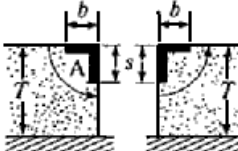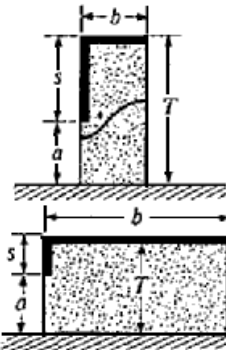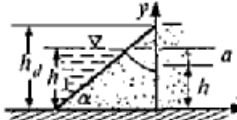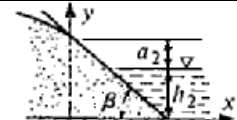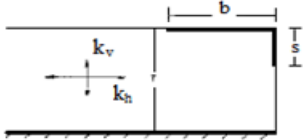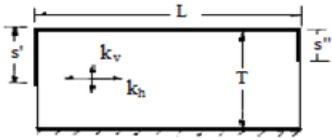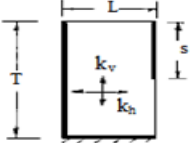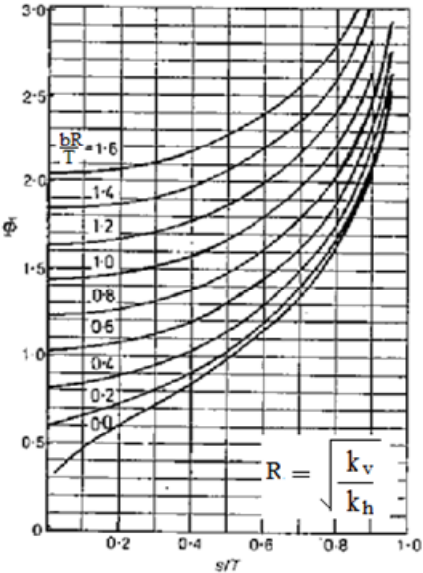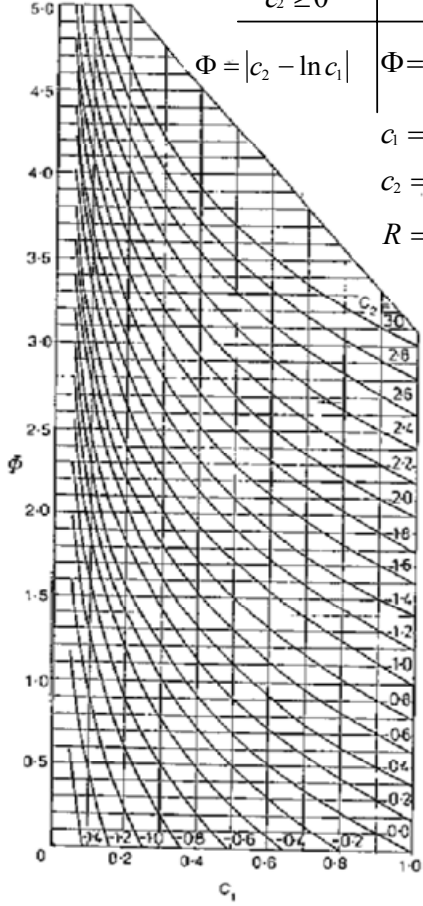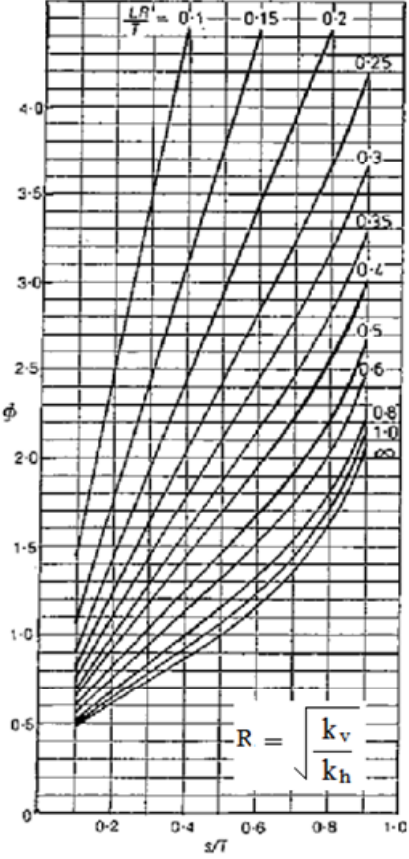
Fragment Type	Illustration	Form Factor, Φ	Fragment type	Illustration	Form Factor, Φ
I		$\Phi = \frac{L}{a}$	V		$L \le 2s$: $\Phi = 2\ln(1+\frac{L}{2a})$ $L \ge 2s$: $\Phi = 2\ln(1+\frac{s}{2a}) + \frac{L-2s}{T}$
II		$\Phi = \frac{1}{2}\left(\frac{kh}{Q}\right)$	VI		$L \ge s'+s''$: $\Phi = \ln\left[(1+\frac{s'}{a'})(1+\frac{s''}{a''})\right] + \frac{L-(s'+s'')}{T}$ $L \le s'+s''$: $\Phi = \ln\left[(1+\frac{b'}{a'})(1+\frac{b''}{a''})\right]$ $Where$: $b' = \frac{L+(s'-s'')}{2}$ $b'' = \frac{L-(s'-s'')}{2}$
III		$\Phi = \frac{1}{2}\left(\frac{kh}{Q}\right)$			
IV		$b \le s$: $\Phi = \ln(1+\frac{b}{a})$ $b \ge s$: $\Phi = \ln(1+\frac{s}{a}) + \frac{b-s}{T}$	VII		$\Phi = \frac{2L}{h_1+h_2}$ $Q = k\frac{h_1^2-h_2^2}{2L}$
			VIII		$Q = k\frac{h_1-h}{\cot\alpha}\ln\frac{h_d}{h_d-h}$
			IX		$Q = k\frac{a_2}{\cot\beta}\left(1+\ln\frac{a_2+h_2}{a_2}\right)$

Table 3.2. Summary of Griffith's form factors (Griffiths, 1984)

Fragment A	Fragment B	Fragment C

For Fragment B:

$c_2 \geq 0$	$c_2 < 0$
$\Phi = \left\vert c_2 - \ln c_1 \right\vert$	$\Phi = \ln\left[\dfrac{(2+c_2)^2}{4c_1}\right]$

$$c_1 = \left(1 - \tfrac{s'}{T}\right)\left(1 - \tfrac{s''}{T}\right)$$

$$c_2 = \frac{LR - (s'+s'')}{T}$$

$$R = \sqrt{\frac{k_v}{k_h}}$$

For Fragment A and Fragment C:

$$R = \sqrt{\frac{k_v}{k_h}}$$

is a simple and effective means of analyzing seepage for a wide variety of geotechnical problems.

3.3　Method of Fragments applied to a two-dimensional hydraulic filled stope

Initially, a simplified two-dimensional stope with no decant water, drain length (X), drain height (D), stope width (B), and height of water (H_w) was investigated and is shown in Fig. 3.1. Using *FLAC,* the flow net was developed for this stope and is shown in Fig. 3.2 (a). A few selected equipotential lines are shown in Fig. 3.2 (b). From this figure it is quite clear that, within the stope, above the height of B the equipotential lines are horizontal implying the flow is vertical. Similarly, beyond a distance of *0.5D* within the drain, the equipotential lines are vertical implying the flow is horizontal. Based on these observations, the flow domain was divided into three fragments given in Fig 3.2 (c) and the method of fragments was extended to quantify the flow rate and the maximum pore water pressure within a two-dimensional hydraulic fill stope. Form factors were then computed for each of the fragments given in Fig 3.2 (c). Fragments 1 and 3 within the stope, with one-dimensional flow, are of type I of Harr's fragments (see Table 3.1). Fragment 2 cannot be approximated by any of Harr's six confined flow fragments; therefore it was necessary to develop a new fragment and to compute its form factor. This was achieved through several numerical models developed in *FLAC*.
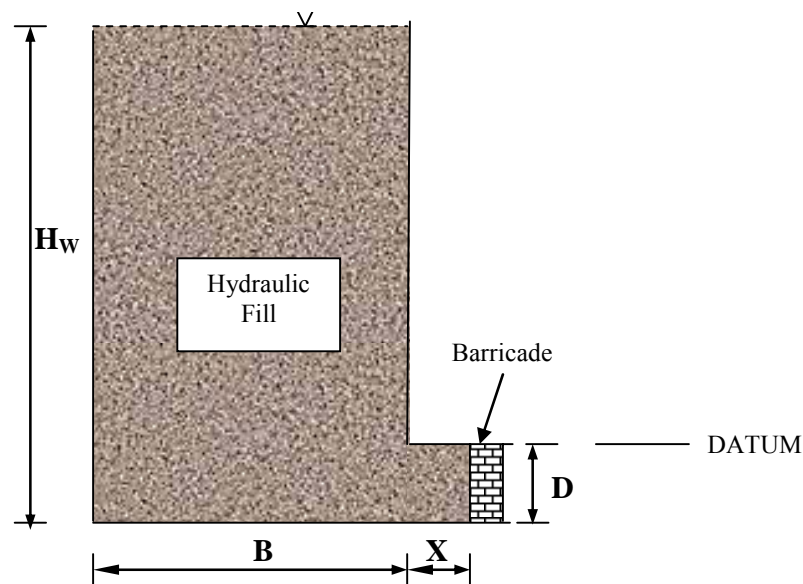
Fig. 3.1. Simplified schematic diagram of two-dimensional stope
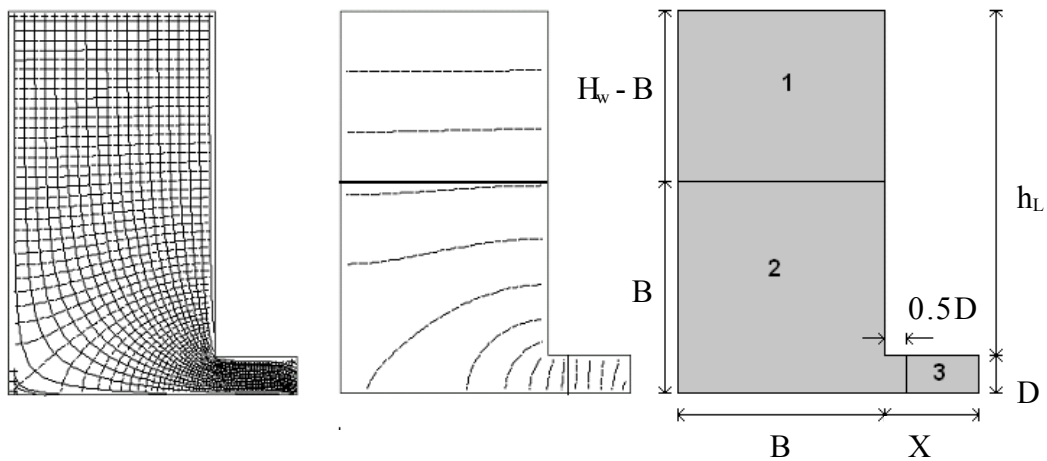
Fig. 3.2. Hydraulic fill stope with single drain (a) Flownet (b) Selected equipotential lines (c) Flow region and three fragments

3.3.1 Numerical Model

The finite difference package *FLAC* was used to model the two-dimensional stope illustrated in Fig. 3.1. The inbuilt programming language *FISH* was also used to write simple subroutines for functions that were not available in *FLAC*. The program written for this stope simulated a flow-only uncoupled analysis for a specified stope geometry and is given in Appendix B.

3.3.1.1   Numerical Package FLAC

FLAC is an acronym for **F**ast **L**agrangian **A**nalysis of **C**ontinua, and represents the name for a two-dimensional explicit finite difference program, which was originally developed by the Itasca Consulting Group to model soil and rock behaviour in geotechnical applications. The materials are represented by zones in a grid which may be moulded or adjusted to fit the geometry of the shape being modelled. The materials may yield and undergo plastic flow based on specified constitutive model behaviour, and in large-strain mode, the grid may deform and move with the material being modelled. The simulations detailed in this chapter, use *FLAC* Version 4.00, released in 2000.

FLAC contains a very powerful in-built programming language called *FISH,* which enables the user to implement special programming requirements by defining new

variables, functions and even constitutive models. For example, *FISH* permits user-prescribed property variations within the grid, custom-designed plotting and printing of user-defined variables, implementation of special grid generators, and specification of unusual boundary conditions, such as the changing boundary conditions required for the filling of a stope. Looping and conditional if-statements available in most programming languages (e.g., *FORTRAN, BASIC*) are also available through *FISH*.

The basic fluid-flow model capabilities in *FLAC* Version 4.00 are listed in the manual as follows (ITASCA, 2002):

1. *The fluid transport law corresponds to both isotropic and anisotropic permeability.*

2. *Different zones may have different fluid-flow properties.*

3. *Fluid pressure, flux, and impermeable boundary conditions may be prescribed.*

4. *Fluid sources (wells) may be inserted into the material as either point sources (interior discharge) or volume sources (interior well). These sources correspond to either a prescribed inflow or outflow of fluid and vary with time.*

5. *Both explicit and implicit fluid-flow solution algorithms are available.*

6. *Any of the mechanical models may be used with the fluid-flow models. In coupled problems, the compressibility of a saturated material is allowed.*

3.3.1.2   *Boundary Conditions and Assumptions*

To develop the two-dimensional numerical model in *FLAC*, several assumptions were made and are discussed below.

1. The simulation was a flow-only analysis for a completely saturated material. The calculations applied Darcy's law which is applicable to a homogeneous, isotropic fill material with laminar flow. The limited velocity by the flow of water through a fine grained soil such as hydraulic tailings justifies this assumption.

2. Since the deslimed hydraulic fills are granular, they consolidate quickly and the excess pore water pressure is assumed to dissipate immediately upon placement. Therefore, the numerical model was solved as a flow-only problem, where the soil mass acts as an incompressible skeleton.

3. Water enters at the top of the fill and exits through the drains. All other boundaries (see Fig. 3.1) are assumed to be impervious. In reality, there may be cracks on the surrounding walls, however, these are not considered in this analysis.

4. Sivakugan et al. (2006) studied two possible assumptions for the pore water pressure distribution along the fill-barricade interface (see Fig. 3.3).
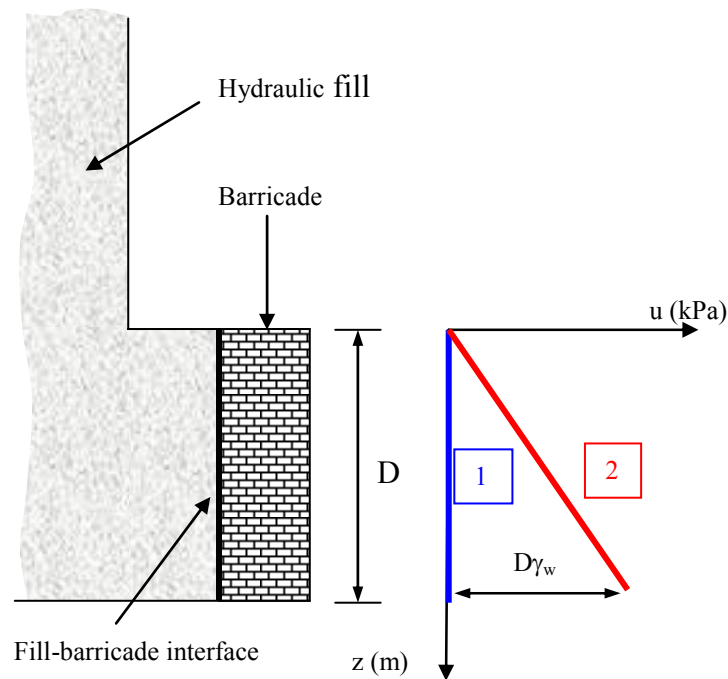
Fig. 3.3. Two possible pore water pressure distribution assumptions for fill-barricade interface

5. The most common assumption is that pore water pressure is zero along the fill-barricade interface (Isaacs and Carter, 1983; Traves and Isaacs, 1991; Rankine, 2005). Since the interconnected voids in the porous bricks are filled with water, it is more realistic to assume that the pore water pressure increases linearly with depth along the fill-barricade interface, with a value of zero at the

top and $D\gamma_w$ at the bottom, where D is the drain height and γ_w the unit weight of water. Nevertheless, Sivakugan et al. (2006) showed that the differences between the two assumptions was insignificant in the computed values of flow rate and maximum pore water pressure due to the height of the stope being much greater than that of the drain. Therefore the pore water pressure was assumed as zero along the fill barricade interface for all analysis made in this dissertation.

6. The fill and water levels were horizontal within the stope
7. The fill in the access drive was assumed to be tight filled.
8. Previous laboratory tests carried out at James Cook University on the porous barricade bricks have shown the permeability of the barricades that are used to contain the wet hydraulic fill, are 2 – 3 orders of magnitude larger than that of the fill (Rankine et al. 2004). Therefore, the barricade was assumed to be free draining.

3.3.1.3   *Grid Generation and Input Parameters*

The simulations were modelled with 1 m x 1 m grid spacing as this provided the right balance between accuracy and solution time. Fig. 3.4 and Table 3.3 illustrates various meshes investigated and the corresponding computational times taken to solve a sample stope with dimensions $H_w = 40$ m; $B = 40$ m; $D = 2$ m; $X = 2$ m.

(a)   (b)   (c)   (d)
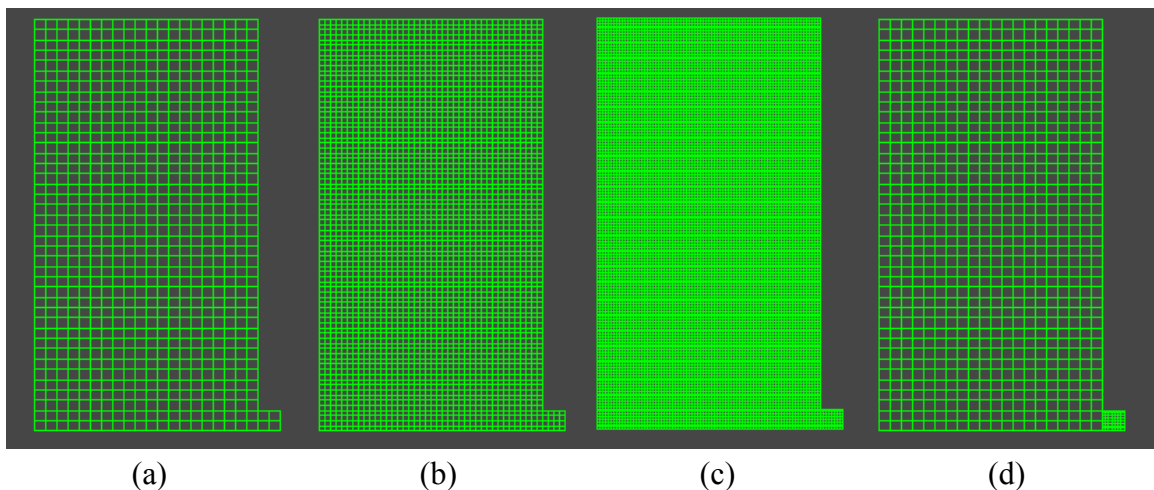
Fig. 3.4. Two dimensional meshes investigated (a) 1 m x 1 m mesh; (b) 0.5 m x 0.5 m mesh; (c) 0.25 m x 0.25 m mesh (d) combination of fine and coarse mesh (0.25 m x 0.25 m mesh in drain and 1 m x 1 m mesh in stope)

Table 3.3. Outputs by different mesh arrangements

Mesh Type	Mesh spacing	Actual running time	Output	
			u_{max} (kPa)	Flow rate (lit/min per m)
A	1m x 1m throughout	7 sec	248.6	1.847
B	0.5m x 0.5m throughout	4 min 25 sec	250.2	1.827
C	0.25m x 0.25m throughout	97 min 29 sec	250.8	1.818
D	1m x 1m in stope & 0.25m x 0.25m in drain	1 min 14 sec	248.9	1.840

It can be assumed that increasing the mesh fineness, increases the accuracy of the results. By comparing the overall difference in solution times between each of the meshes there is a difference of over 1.5 hours. However, the overall difference between the maximum pore water pressure and discharge is approximately 1% which is considered negligible. Therefore, for all remaining simulations a mesh of 1 m x 1 m was used.

The input parameters required in the model were determined from extensive laboratory testing carried out on hydraulic fills at James Cook University (Rankine et al., 2004).

3.3.2 Form Factors, Maximum Pore Pressure and Flow rate

Fig. 3.2 shows the two-dimensional stope broken down into three fragments. Since fragments 1 and 3 are of Type I of Harr's fragments (see Table 3.1), the form factors can be written as:

$$\Phi_1 = \frac{H_w - B}{B} \tag{3.5}$$

$$\Phi_3 = \frac{X - 0.5D}{D} \tag{3.6}$$

The form factor for fragment 2, Φ_2, cannot be approximated by any of Harr's six fragments and therefore it was necessary to develop a new fragment.

From Eq. 3.4, we know that

$$\sum \Phi = \frac{kh_L}{q}, \text{ and}$$

$$\Phi_2 = \frac{kh_2}{q}$$

where h_2 is the head loss within the 2nd fragment, and h_L $(= h_1 + h_2 + h_3)$ is the head loss across the entire stope, q is the flow rate and k is the permeability of the fill. Using the numerical model discussed in section 3.3.1. The form factor for fragment 2, Φ_2 was initially computed for case 1 where $H_w/B \geq 1$ and all three fragments were present in the stope. In this scenario, Φ_2 is a function of B/D. The relationship between Φ_2 and B/D was developed through several *FLAC* runs, is presented in Fig. 3.5. The graph illustrates B/D ratios ranging from 5 through 50. When B/D was less than 5, the chart can be extrapolated back to zero. However a stope with a geometrical ratio of B/D less than this is unrealistic and unlikely to occur.

To investigate the case when $H_w/B < 1$, which occurs at the start and end of the drainage process, several numerical models were run, where values of Φ_2 were computed for H_w/B ratios of 0.1, 0.2, … 1.0 and B/D ratios ranging from 5 through 50. The computed values of Φ_2 for all H_w/B ratios are shown graphically in Fig. 3.6. When extrapolating these results to three-dimensions (refer to chapter 4), these provided a more realistic range of geometries that may be observed in the mining industry.
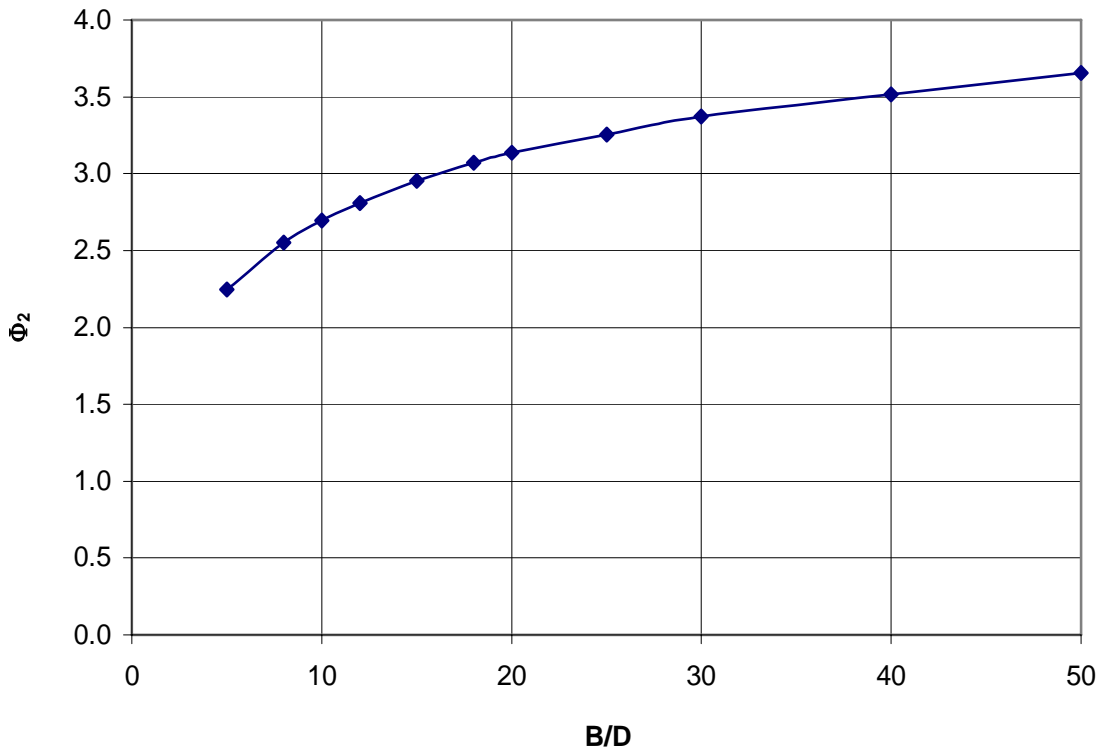
Fig. 3.5. Form factor for fragment 2 for case 1: $H_w/B \geq 1$
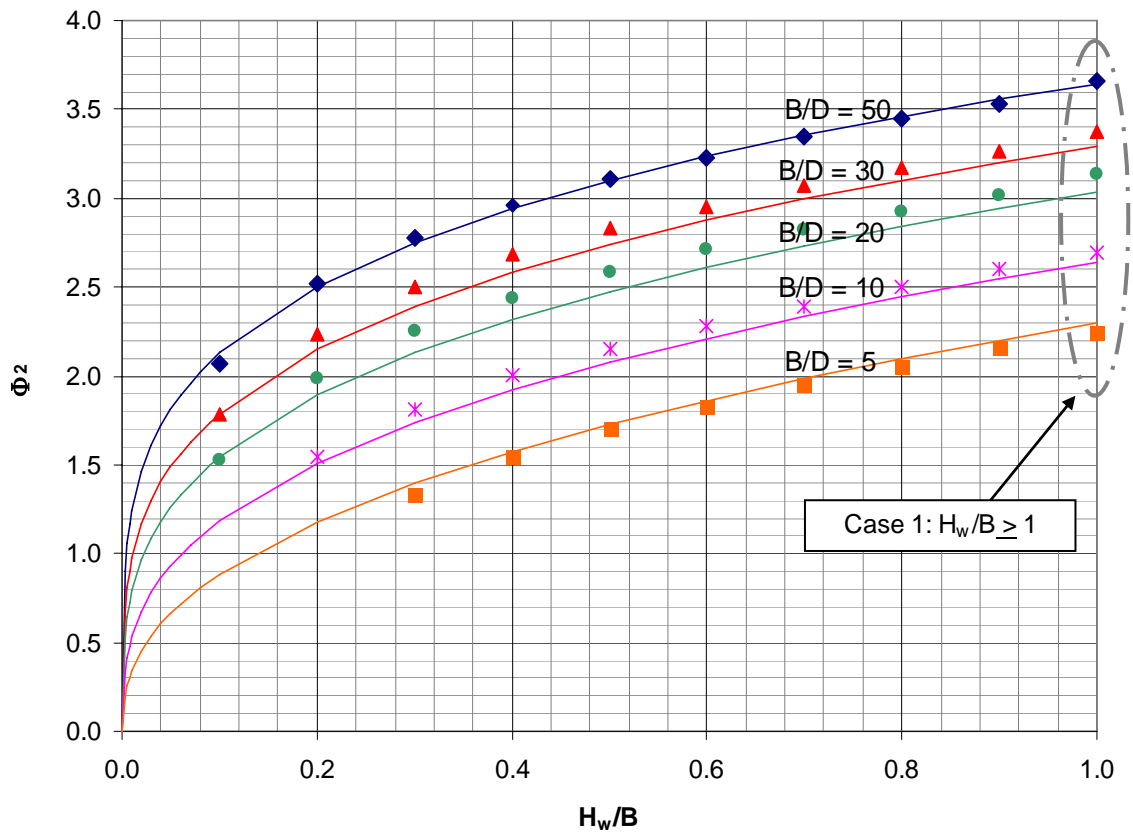
Fig. 3.6. Form factor for fragment 2 for all cases of H_w

Using these plots, equations of Φ_2 for all cases of H_w/B can be obtained. For $H_w \geq B$, when the height of water of fragment 2 is greater than or equal to B:

$$\Phi_2 = \frac{5}{3}\left(\frac{B}{D}\right)^{1/5} \tag{3.7}$$

For $H_w < B$, when the height of water is less than B, i.e. at the start and end of the drainage process:

$$\Phi_2 = \frac{5}{3}\left(\frac{B}{D}\right)^{1/5}\left(\frac{H_w}{B}\right)^{d} \tag{3.8}$$

where d is given by:

$$d = 0.62\left(\frac{D}{B}\right)^{1/4} \tag{3.9}$$

Values of Φ_2, computed using FLAC and the above equations are shown in Fig. 3.6 and an excellent fit can be seen. The curves plotted on Fig. 3.6 represent a graphical representation of Eq. 3.6 − Eq. 3.9 and actual FLAC results are given by the data points.

Intuitively and from the numerical model runs, it was evident that the maximum pore water pressure within the stope occurs at the bottom corner of the stope (point Q in Fig. 3.7). OPQRS and PQRS are the longest stream lines for case 1 *(Hw ≥ B)* and case 2 *(Hw ≤ B)* respectively. Here α_{2D} is the fraction of the head loss within fragment 2 that takes place in the horizontal segment of the largest stream line and ranges between 0 and 1. Denoting the head loss in fragment two as h_2, the head losses from Q to R and from P to Q can be defined as $\alpha_{2D}h_2$ and $(1 - \alpha_{2D})h_2$ respectively.

Assuming the top of drain as the datum, the total, elevation and pressure heads at the corner of the stope for case 1 (point Q in Fig. 3.7 a) are given by:

(a) Case 1: $H_w \geq B$ (b) Case 2: $H_w < B$
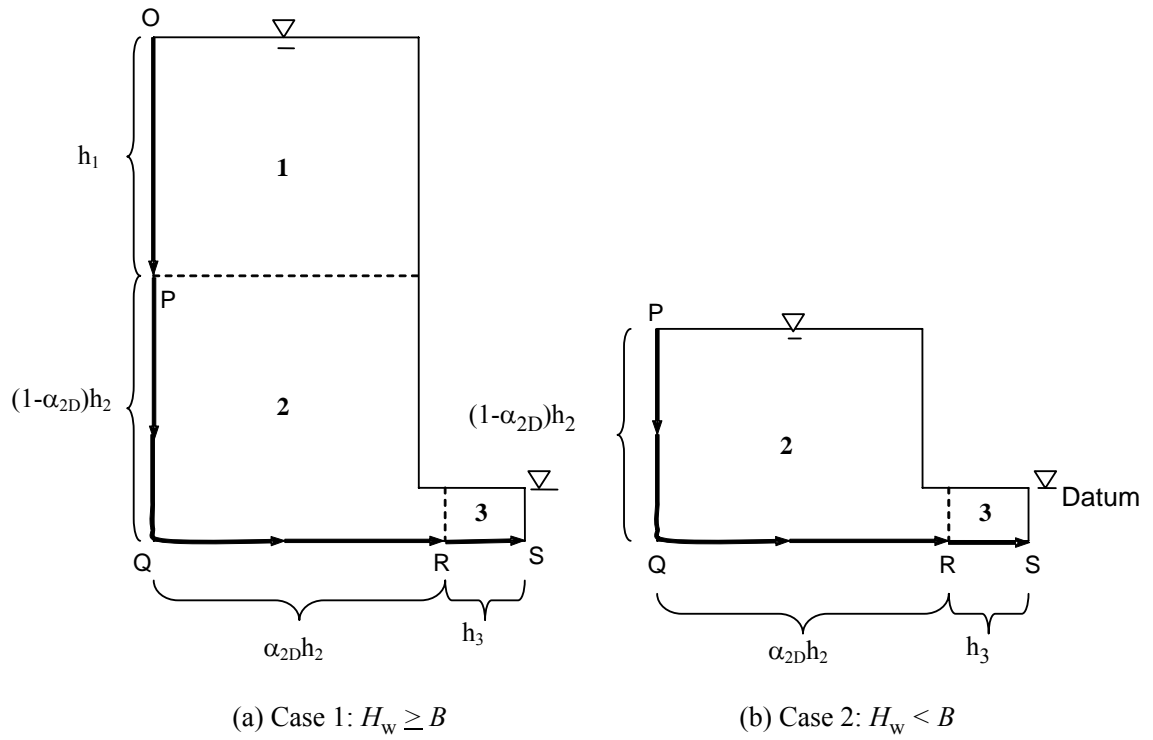
Fig. 3.7. Head losses within fragments

$$\text{Total head} = \alpha_{2D}h_2 + h_3 = \left(\frac{\alpha_{2D}\Phi_2 + \Phi_3}{\Phi_1 + \Phi_2 + \Phi_3} \right) h_L \tag{3.10}$$

$$\text{Elevation head} = \text{-D} \tag{3.11}$$

$$\therefore \text{Pressure head} = \left(\frac{\alpha_{2D}\Phi_2 + \Phi_3}{\Phi_1 + \Phi_2 + \Phi_3} \right) h_L + D \tag{3.12}$$

Therefore the maximum pore water pressure that occurs at the corner of the stope is given by:

$$u_{\max} = \left[\left(\frac{\alpha_{2D}\Phi_2 + \Phi_3}{\Phi_1 + \Phi_2 + \Phi_3} \right) h_L + D \right] \gamma_w \tag{3.13}$$

For case 2, when the height of water (H_w) is less than the stope width (B) as shown in Fig. 3.7 (b), fragment 1 does not exist and Φ_l equals zero.

Using *FLAC*, α_{2D} was computed for different values of *D/B* and H_w/*B* to represent typical stope geometries, these ranged from 0.02 to 0.20, and from 0.1 to 1.0 respectively. The variation of α_{2D} against these aspect ratios is shown in Fig. 3.8. As D/B is lowered, a larger head loss fraction occurs between Q and R, since more resistance has to be overcome in flowing from Q to R than from P to Q. Also, the greater the H_w/*B* ratio, the smaller the head loss fraction between Q and R.
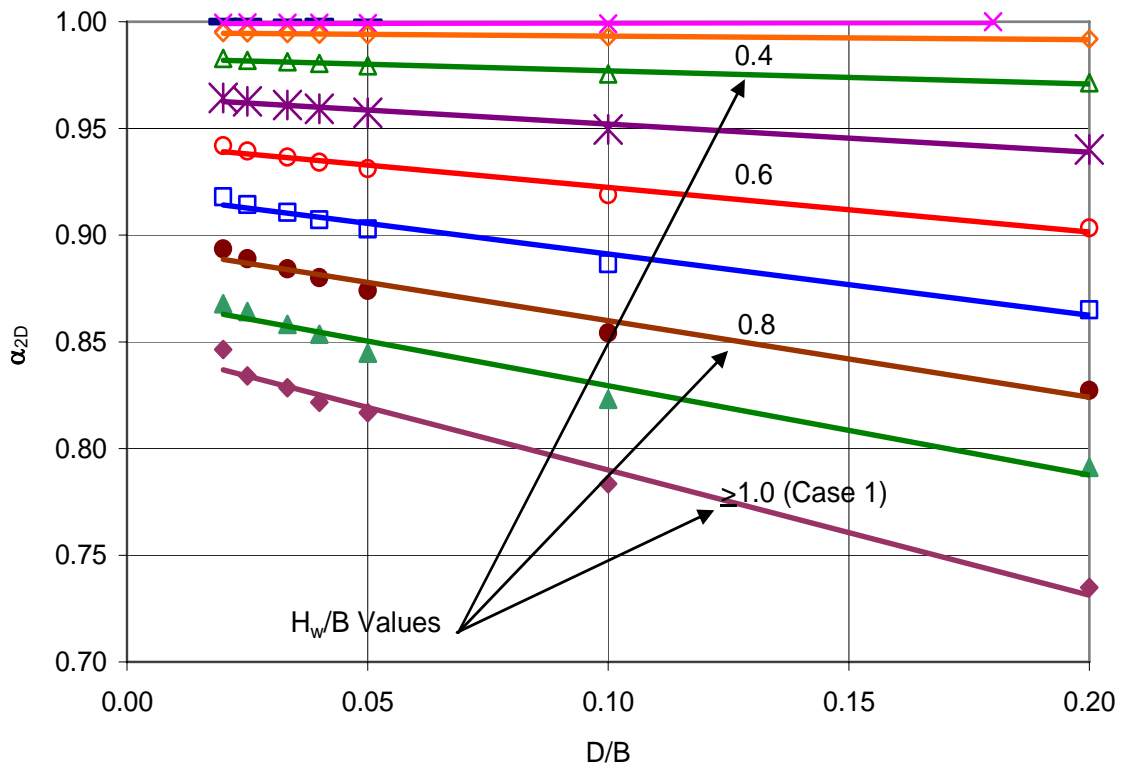
Fig. 3.8. Coefficient α_{2D} for fragment 2

It can be seen from Fig. 3.8 that the coefficient α_{2D} varies linearly with *D/B* for a specific H_w/*B*. Therefore can be expressed in the form:

$$\alpha = m(D/B) + c \tag{3.14}$$

where *m* and *c* are the slope and intercept on the α_{2D}-axis. Plotting the values of m and c separately against H_w/B shows that,

$$m = -0.7788 \frac{H_w}{B} + 0.2473 \tag{3.15}$$

$$c = -0.2193 \frac{H_w}{B} + 1.0689 \tag{3.16}$$

Here, the coefficients of determination (r^2) for Eq. 3.15 and Eq. 3.16 are 0.9741 and 0.9928 respectively, showing a very strong straight line fit between m and c against H_w/B. Substituting Eq. 3.15 and Eq. 3.16 in Eq. 3.14, α_{2D} can be written as:

$$\alpha_{2D} = -0.7788 \left(\frac{H_w}{B} \right) \left(\frac{D}{B} \right) + 0.2473 \left(\frac{D}{B} \right) - 0.2193 \left(\frac{H_w}{B} \right) + 1.0689 \tag{3.17}$$

For case 1 (Fig. 3.7 a), when $H_w/B \geq 1$, the value of H_w/B, when calculating Φ_2 and α_{2D} is equal to 1. Here, the flow domain above the height of B becomes fragment 1. Fig 3.8 also illustrates that when $H_w/B \leq 0.3$, the value of α_{2D} can be approximated as 1.

Fig. 3.5, Fig. 3.6 and Fig 3.8 present design charts to calculate Φ_2 and α_{2D} for typical stope geometries. Table 3.4 summarizes the equations used to calculate the maximum pore pressure, form factors and flow rate for a two-dimensional hydraulic fill stope with a single drain at the stope base and no decant water for all cases of H_w/B.

3.3.3 Fragment Comparison

It should be noted, that although none of Harr's six fragments could be used to estimate fragment 2 in the two-dimensional stope, Griffith's Type B and Type C fragments given in Table 3.2, can be used to approximate the form factors for the two-dimensional stope. Therefore, an overview of the various models was conducted to justify the need for the new fragments developed in Table 3.4.

Table 3.4. Summary of equations for two-dimensional analysis

Parameter	Equation	
Form Factor for fragment 1 Φ_1	$\Phi_1 = \dfrac{H_w - B}{B}$	
Form Factor for fragment 2 (Fig. 3.5 – Fig 3.6) Φ_2	$\dfrac{H_w}{B} \geq 1$	$\Phi_2 = c$
	$\dfrac{H_w}{B} < 1$	$\Phi_2 = c\left(\dfrac{H_w}{B}\right)^d$
	where:	$c = \dfrac{5}{3}\left(\dfrac{B}{D}\right)^{1/5}$ $d = 0.62\left(\dfrac{D}{B}\right)^{1/4}$
Form Factor for fragment 3 Φ_3	$\Phi_3 = \dfrac{X - 0.5D}{D}$	
Fraction of head lost in fragment 2 that takes place in the horizontal segment of the streamline (Fig. 3.8) α_{2D}	$\dfrac{H_w}{B} < 0.3$	$\alpha_{2D} \approx 1$
	$\dfrac{H_w}{B} \geq 0.3$	$\alpha_{2D} = \left(-0.78\left(\dfrac{H_w}{B}\right) + 0.25\right)\dfrac{D}{B} - 0.22\left(\dfrac{H_w}{B}\right) + 1.07$
Maximum pore pressure u_{max}	$u_{max} = \left[\left(\dfrac{\alpha_{2D}\Phi_2 + \Phi_3}{\Phi_1 + \Phi_2 + \Phi_3}\right)h_L + D\right]\gamma_w$	
Flow Rate q	$q = \dfrac{kh_L}{\sum\limits_{i=1}^{n}\Phi_i}$	

To provide a comparison between the models, several randomly selected stope geometries were analyzed and values of discharge were calculated using:

- The fragment types discussed in Table 3.4,

- Griffiths (1984) fragment types shown in Table 3.2, and
- Finite difference model

The results are illustrated in Fig. 3.9.
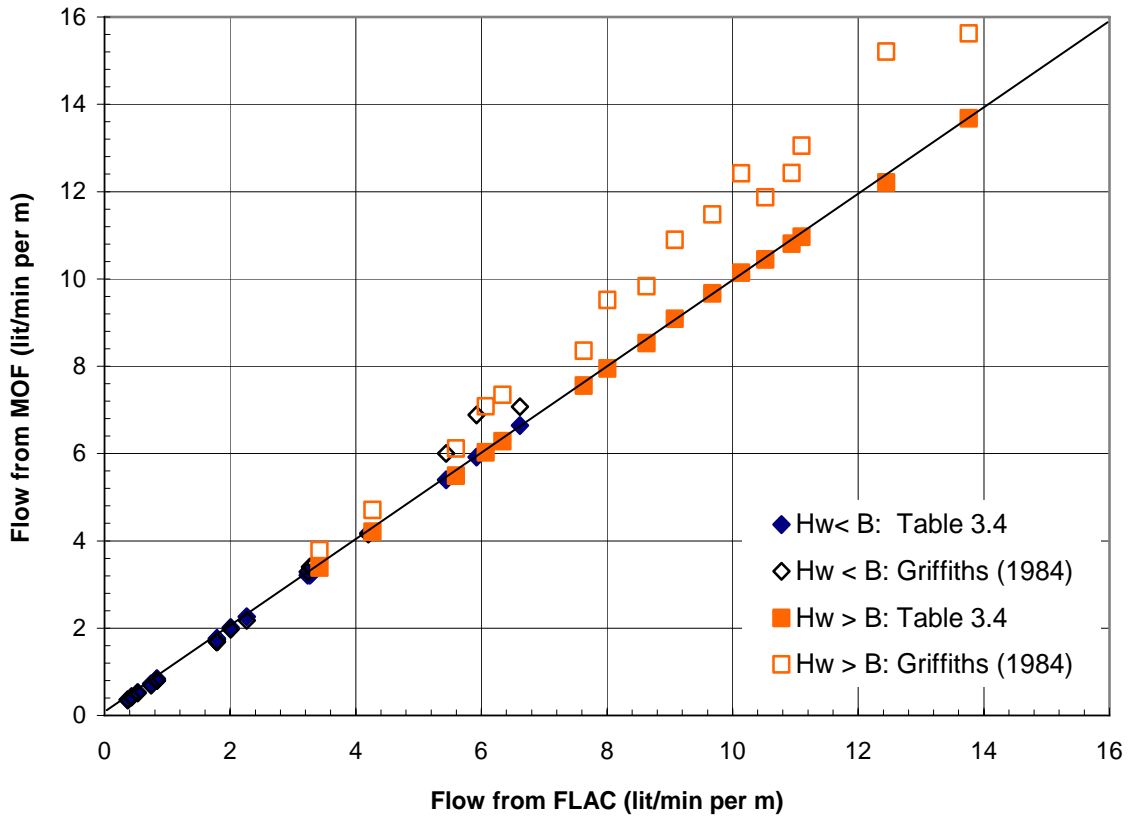
Fig. 3.9. Flow rate comparison using varying fragments including Griffiths (1984)
and Table 3.4 fragments against finite difference model *FLAC*

As shown in Fig. 3.9, the fragments developed and tabulated in Table 3.4, provide a much closer approximation than those suggested by Griffiths (1984). For the randomly selected samples, Table 3.4 fragments contained a maximum percent error of 2%, whilst Griffiths varied as much as 16%. This investigation illustrates that the application of Griffith's fragments to the two-dimensional stope contains significant percent error as opposed to those calculated using Table 3.4 fragments. Therefore when applying the method of fragments in two-dimensions, the fragments and analytical solutions given in Table 3.4 were used.

3.3.4 Decant Water in Two-dimensional Hydraulic Fill Stopes

Thus far it has been assumed that there is no decant water and the height of water (H_w) is equal to or less than the tailings height ($H_{tailings}$). If decant water is present in the hydraulic fill stope as (i.e. $H_w > H_{tailings}$) then $H_{tailings}$ should be substituted for H_w in the formulas outlined in Table 3.4. It is important to note that even when decant water is present, the head loss (h_L) remains the same (i.e. $h_L = H_{w\ (with/without\ decant\ water)} - D$).

3.3.5 Entry and Exit Hydraulic Gradients

One of the main objectives in the design of a hydraulic fill system is to remove the water from the stope as quickly as possible. This is often achieved by ensuring that the hydraulic fill has adequate permeability. Soil mechanics combined with simple mass balance can be used to define an upper bound value for the permeability of a specific fill to ensure there is no build up of decant water on the surface of the fill.

Since all other boundaries are assumed impervious and the only water entering the stope is via the slurry mixture, the volume of water entering the stope per hour (V_{in}) can be calculated by:

$$V_{in} = \frac{R_s w_{slurry}}{\rho_w}$$

(3.18)

where R_s is the solids filling rate (e.g. 250 t/hour), w_{slurry} is the water content of the hydraulic fill slurry and ρ_w is the density of water.

The volume of water draining from the stope every hour is:

$$V_{out} = k i_{entry} A$$

(3.19)

where k is the permeability, i_{entry} is the hydraulic gradient at the top of the water, and A is the plan area of the stope.

At a certain stage in backfilling, to ensure there is no more increase in water height, V_{out} must be greater than V_{in}. Therefore,

$$k \geq \frac{R_s w_{slurry}}{i_{entry} A \rho_{water}}$$
(3.20)

The above inequality is used to determine a threshold value for k, however, it often gives very high and unrealistic values for permeability, particularly stopes with small plan area. Here, i_{entry} varies with the height of water during the filling operation and subsequent draining.

A less conservative and more realistic approach is to allow the water to rise during the fill placement, but to remain below the fill level. This will ensure that there is no decant water at all times during filling. The derivation of the limiting value of permeability to ensure that water height remains below the fill height is given below.

$$\text{Volume of solids in every hour} = \frac{R_s}{G_s \rho_w}$$
(3.21)

Where G_s refer to the specific gravity of the fill and ρ_w refers to the water density.

$$\therefore \text{Increase in fill height per hour} = \frac{R_s}{G_s \rho_w} \frac{1}{(1-n)A}$$
(3.22)

Here n is the porosity of the settled hydraulic fill.

$$\text{Volume of water entering the stope per hour} = \frac{R_s w_{slurry}}{\rho_w}$$
(3.23)

$$\text{Volume of water leaving the stope per hour} = k\, i_{entry}\, A$$
(3.24)

$$\therefore \text{Net volume of water entering the stope per hour} = \frac{R_s w_{slurry}}{\rho_w} - k\,i_{entry}\,A \qquad (3.25)$$

$$\therefore \text{Increase in water height per hour} = \frac{\dfrac{R_s w_{slurry}}{\rho_w} - k\,i_{entry}\,A}{nA} \qquad (3.26)$$

To ensure there is no decant water above the fill, the increase in fill height has to be greater than the increase in water height every hour. Therefore,

$$\frac{R_s}{G_s \rho_w}\frac{1}{(1-n)A} \geq \frac{R_s}{\rho_w}\frac{w_{slurry}}{nA} - \frac{k i_{entry}}{n} \qquad (3.27)$$

Rearranging Eq. 3.27, the permeability (k) can be determined by:

$$k \geq \frac{R_s}{\rho_w}\frac{1}{A i_{entry}}\left[w_{slurry} - \frac{n}{(1-n)}\frac{1}{G_s}\right] \qquad (3.28)$$

In the absence of realistic values for i_{entry}, a gravitational gradient of unity is often assumed. Several runs in *FLAC* and *FLAC^{3D}*, for two and three dimensional stopes, show that the hydraulic gradients at the top of the water level can be significantly less than unity. Using the method of fragments, a simple expression is developed below for i_{entry} for a two-dimensional stope.

$$i_{exit} = \frac{h_3}{X - 0.5D} = \frac{\Phi_3}{\sum\limits_{i=1}^{i=3}\Phi_i}\frac{h_L}{X - 0.5D} \qquad (3.29)$$

From Eq. 3.18 and Eq. 3.29,

$$i_{exit} = \frac{1}{\sum\limits_{i=1}^{i=3}\Phi_i}\frac{(H_w - D)}{D} \qquad (3.30)$$

Therefore, i_{entry} can be written as:

$$i_{entry} = \frac{1}{\sum\limits_{i=1}^{i=3} \Phi_i} \frac{(H_w - D)}{B} \qquad (3.31)$$

It can be seen from Eq. 3.31 and in Fig. 3.10, that the hydraulic gradient at the top of the water level (i_{entry}) is a function of *X/D, D/B* and *H_w/B*.
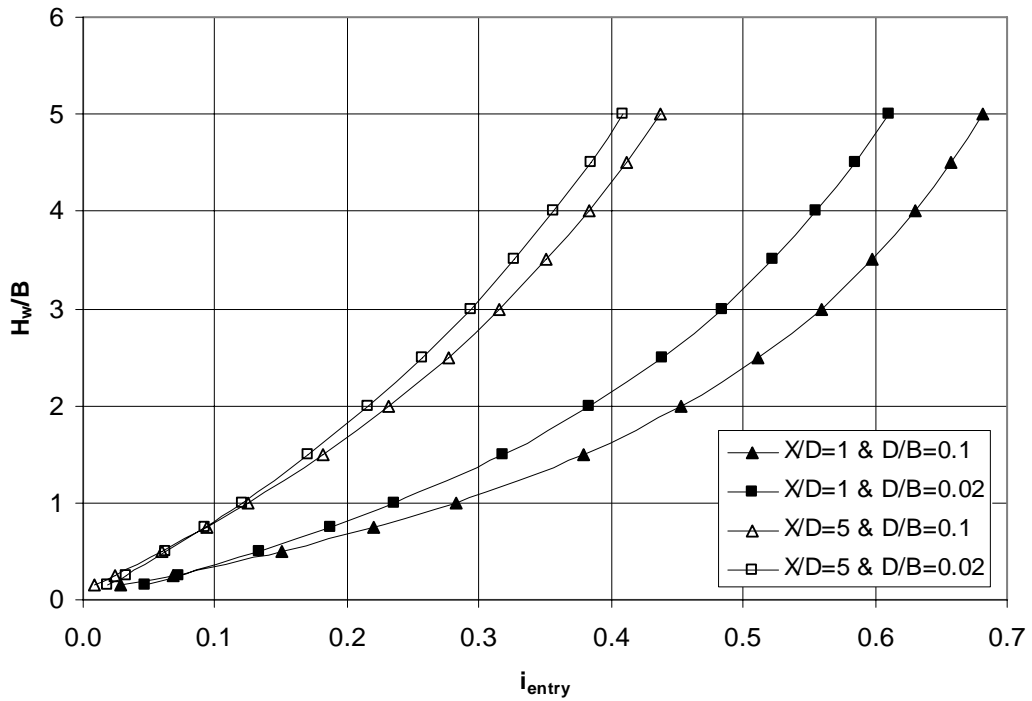
Fig. 3.10. Dependence of i_{entry} for several cases of X/D, D/B and H_w/B

For randomly selected values of *X, D, B* and *H_w* the hydraulic gradients at the top of the water level were computed using Eq. 3.31. In Fig. 3.11, *H_w/B* is plotted against i_{entry} without any considerations to the different values of *X/D* and *D/B*. From the figure, it is evident that as the water level rises, the hydraulic gradient increases. The hydraulic gradient at the top of the water level can be approximated as:

$$i_{entry} = 0.2\left(\frac{H_w}{B}\right)^{0.75} \qquad (3.32)$$
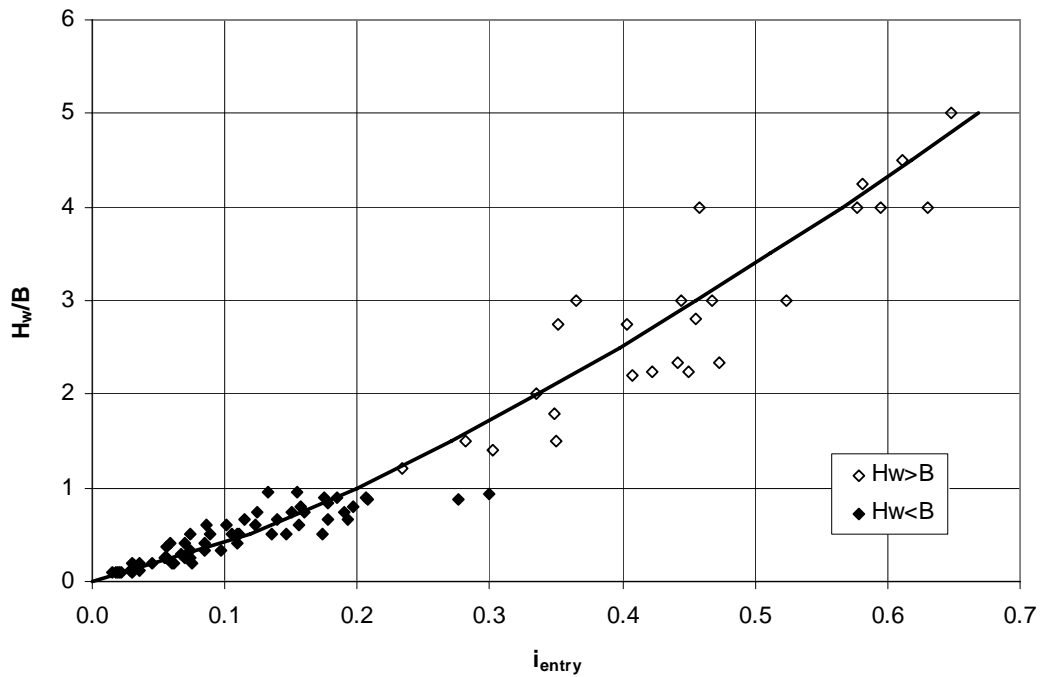
Fig. 3.11. H_w/B against i_{entry} for two-dimensional stopes

The curve in Fig. 3.11 illustrates the approximation of i_{entry} given in Eq. 3.32. The data points represent the theoretical values given by Eq. 3.31.

The use of Eq. 3.20, Eq. 3.28 and Eq. 3.32 is illustrated through a numerical example. For a 30 m wide stope with water height of 60 m, from Eq. 3.32, i_{entry} can be estimated as 0.34. For a filling rate of 5 t/hour per m and slurry water content of 33%, the permeability necessary to ensure no increase in water height can be estimated from Eq. 3.20 as 162 mm/hour. However, using a value of unity for i_{entry} would have grossly underestimated the required permeability as 55 mm/hr. From the permeability values computed using Eq. 3.20 (162 mm/hr); it appears that the permeability of the hydraulic fill has to be unrealistically large to ensure that there is no rise in water level. The more relaxed criterion of ensuring the fill rise is faster than the water (i.e. no decant water above the fill at any time) and assuming a porosity of 40% and specific gravity of 2.80 for the settled hydraulic fill, calculates that the permeability only as to be greater than 45 mm/hr (Eq 3.28.),

3.3.6 Scaling Effect on Method of Fragments

Method of fragments can also be used to explain the influence of scaling on pore water pressure measurements and flow rate from the stope. If a two-dimensional stope is scaled by a factor of x, as shown in Fig. 3.12, the entire geometry is scaled by a factor of x. Therefore, the total head loss across the stope, the head loss between each of the equipotential lines and the number of equipotential drops are also scaled by a factor of x. Hence the form factors (Φ_i) remain the same, even when the stope has been scaled. However, the permeability remains constant. Substituting the scaled geometries into Eq. 3.3 and Eq. 3.13, the flow rate and the pore water pressures scale by a factor of x for a two-dimensional stope.
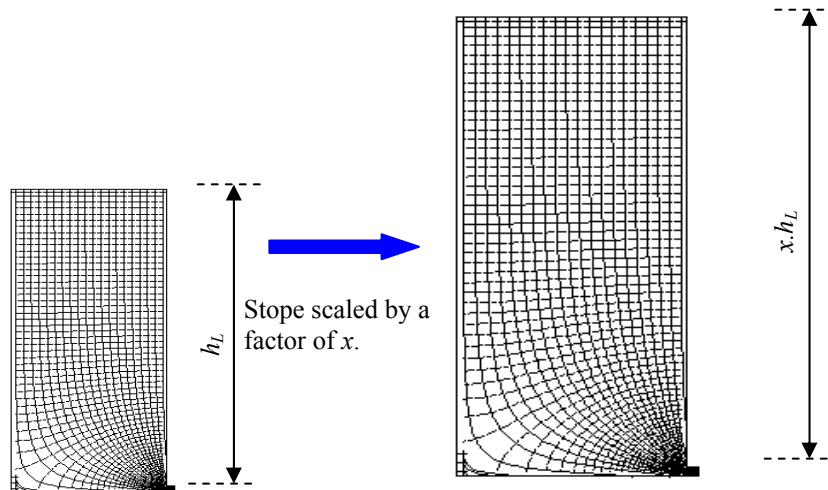
Fig. 3.12. Scaling of two dimensional stope and flow nets

3.3.7 Typical Stope Geometries

Typical stope geometries vary significantly in underground mining operations. The size of stope can depend on the ore body geometry, the geotechnical characteristics of the host rock and particular mine conditions. Stope widths and depths can vary between 20 m and 50 m and stope heights can be as high as 200 m. Drains are generally between 3 m and 6 m in width, which makes the drain typically between 9 m^2 - 36 m^2 in cross-sectional area. Drain lengths have a considerable influence on the pore pressure distribution as well as the discharge from the stope assuming that there is consistent permeability along the drain and that the drive is tight-filled. Increasing the drain length, often results in increased pore pressure and a reduction in drain discharge. Intuitively, as a barricade gets further from the stope, the flow path increases and the hydraulic gradient across the entire model decreases, resulting in

reduced flow velocity, and hence discharge. Pore pressure also increase with increasing drain length. It is for this reason drains are placed as close to the stope face as possible in practice, without compromising on safety.

The geometrical simplification required to model the three-dimensional problem as two-dimensional one does place limitations on the applicability of the results. To mimic a three-dimensional stope, an equivalent cross section of the drain, which falls within the typical range, is required. For example, for a two dimensional stope with a single drain at the base of the stope, and with a stope height (H_w) 50 m, stope width (B) 20 m, drain length (X) 5 m and drain height (D) 1 m, we could assume a stope depth of 20 m (assuming a square based stope) and multiply the two-dimensional flow rate (m^2/s) by 20 m (stope depth); to obtain an approximate three-dimensional discharge (m^3/s) for a 20 m x 20 m x 50 m (stope width × stope depth × stope height) stope with a 20 m^2 drain outlet (20 m depth × 1 m drain height) at a distance of 5 m from the stope face.

Although the two-dimensional analysis of hydraulic fill stopes provides valuable information regarding the drainage behaviour of hydraulic fill stopes, it does not allow for the investigation into the effects of various stope geometries. Since the stope has no depth, the user is unable to investigate the stope width to depth ratio. Also, for a two-dimensional geometry, the drain location, along the stope face cannot be analysed as well as drain shape etc. For this reason, this two-dimensional program has been extended into three-dimensions using $FLAC^{3D}$, to more realistically represent the geometry and is presented in chapter 4.

3.3.8   Validation of the Application of two-dimensional method of fragments

A systematic study was carried out to validate the application of the proposed model for estimating flow rate and the maximum pore water pressure in case 1 and case 2 described in the previous sections, for randomly selected values of X, D, B and H_w. The maximum pore water pressure within the stope and the flow rate were computed using FLAC and the equations given in Table 3.4 and are presented in Fig. 3.13 and Fig. 3.14 respectively, showing excellent agreement between the predictions from both methods.
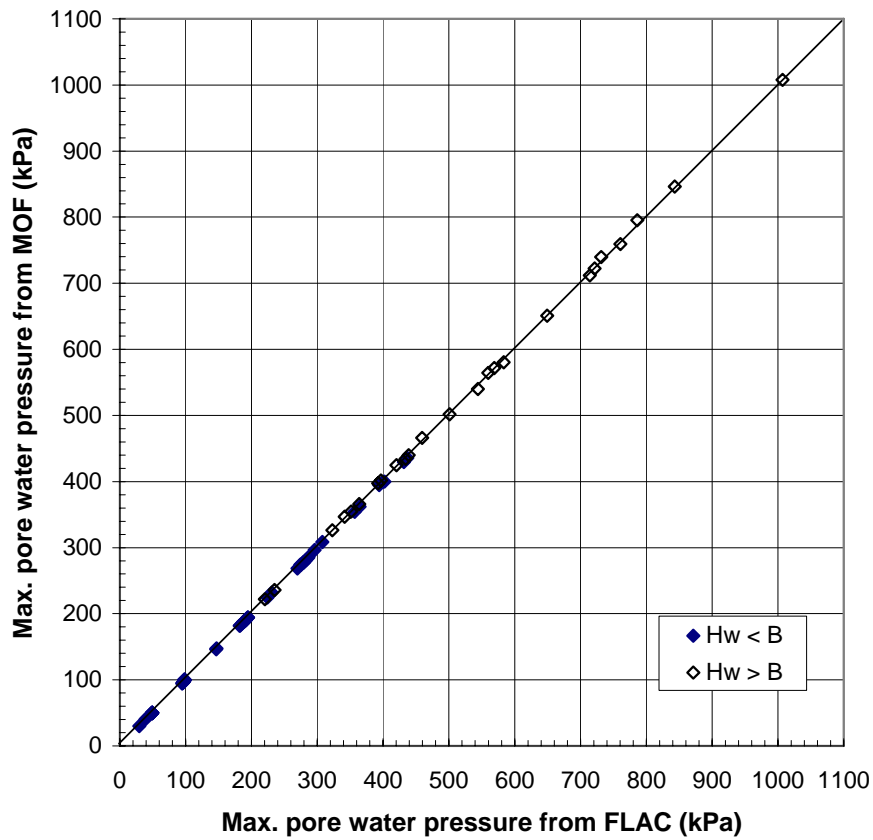
Fig. 3.13. Maximum pore water pressure comparison
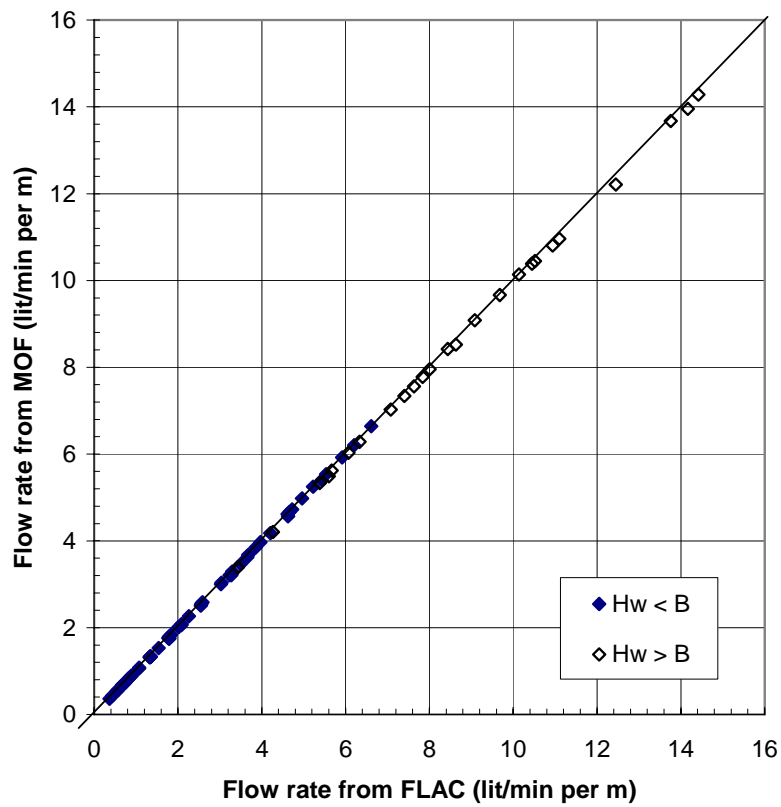
Fig. 3.14. Flow rate comparison

3.3.9 Further analysis of the pore water pressure in two-dimensional stopes

So far, the analysis of the two-dimensional hydraulic fill stope has only considered the most critical values for understanding the drainage and pore pressure development within a two-dimensional stope. These include the point of maximum pore pressure (point Q in Fig. 3.15) and discharge values for varying geometries. Using *FLAC* several other points were analysed and equations developed to determine the pore pressure development throughout the stope. Fig 3.15 illustrates the locations of several other points analysed.
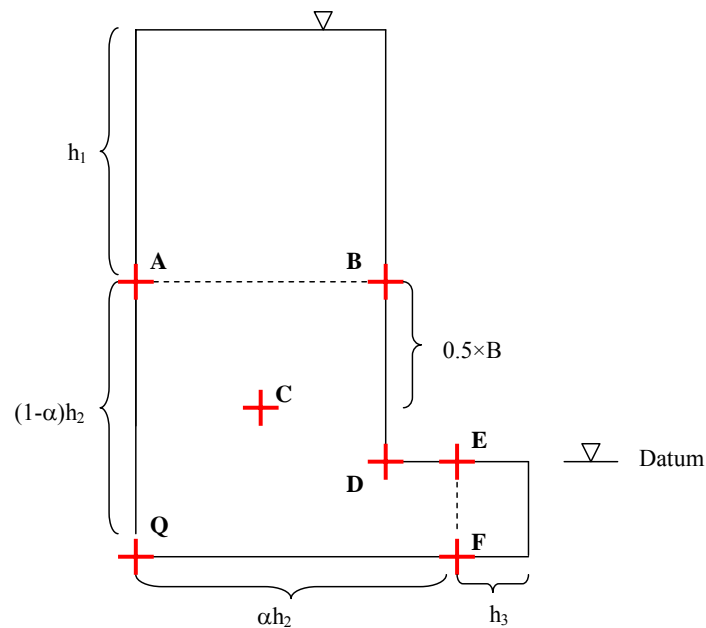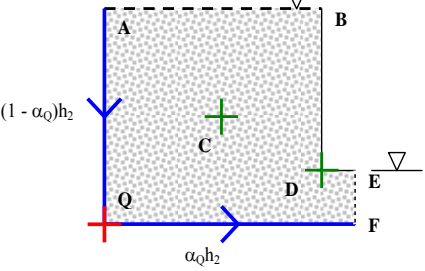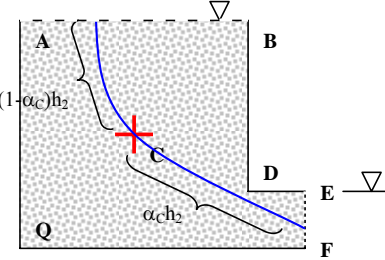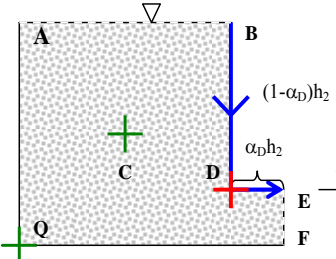
Fig. 3.15. Points for pore pressure analysis

Eq. 3.13 gives the maximum pore water pressure (point Q) for the two-dimensional stope shown in Fig 3.15. The pore water pressure at several other points shown in Fig. 3.15, are calculated using the equations given in Table 3.5. The coefficient α is the fraction of the head loss within fragment 2 and ranges between 0 and 1. This coefficient varies for each of the points being analysed and also varies with varying geometries, therefore design charts were developed for the points shown above and are given in Fig. 3.8, Fig 3.16 and Fig 3.17. To verify the proposed equations given in Table 3.5, several randomly selected geometries of the two-dimensional stope were modelled and compared with the equations given in Table 3.5. The validation plots for each of the points analysed are given in Appendix C and results show excellent agreement.

Table 3.5. Summary of pore water pressure equations and design charts for various points

Location	Pore water pressure (u_i)	α_i
Point A & B	$u_A = u_B = \left[\left(\dfrac{\Phi_2 + \Phi_3}{\Phi_1 + \Phi_2 + \Phi_3}\right)h_L + D\right]\gamma_w$	NA
Point Q – Maximum Pore Pressure 	$u_Q = u_{max} = \left[\left(\dfrac{\alpha_Q\Phi_2 + \Phi_3}{\Phi_1 + \Phi_2 + \Phi_3}\right)h_L + D\right]\gamma_w$	Refer to Fig. 3.8 or Eq. 3.14 – Eq. 3.16
Point C 	$u_C = \left[\left(\dfrac{\alpha_C\Phi_2 + \Phi_3}{\Phi_1 + \Phi_2 + \Phi_3}\right)h_L - (0.5B - D)\right]\gamma_w$	Refer to Fig. 3.16
Point D 	$u_D = \left[\left(\dfrac{\alpha_D\Phi_2 + \Phi_3}{\Phi_1 + \Phi_2 + \Phi_3}\right)h_L\right]\gamma_w$	Refer to Fig. 3.17
Point E	$u_E = \left[\left(\dfrac{\Phi_3}{\Phi_1 + \Phi_2 + \Phi_3}\right)h_L\right]\gamma_w$	NA
Point F	$u_F = \left[\left(\dfrac{\Phi_3}{\Phi_1 + \Phi_2 + \Phi_3}\right)h_L + D\right]\gamma_w$	NA
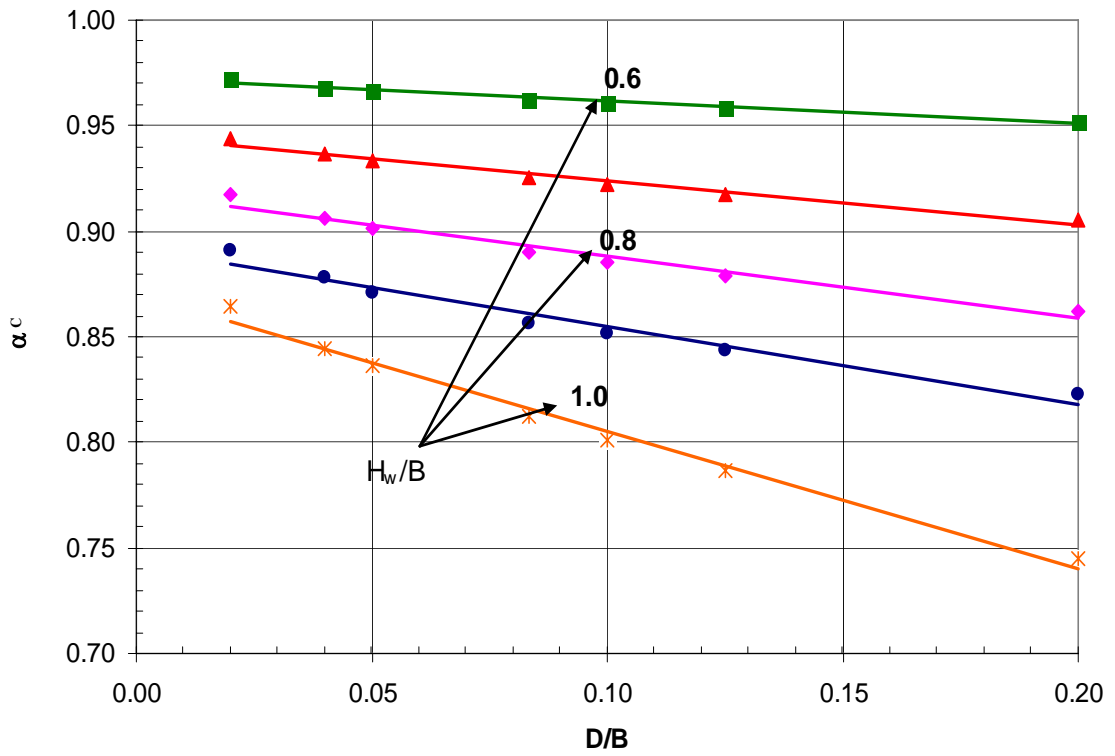
Fig. 3.16. Coefficient α_C for fragment 2 for point C
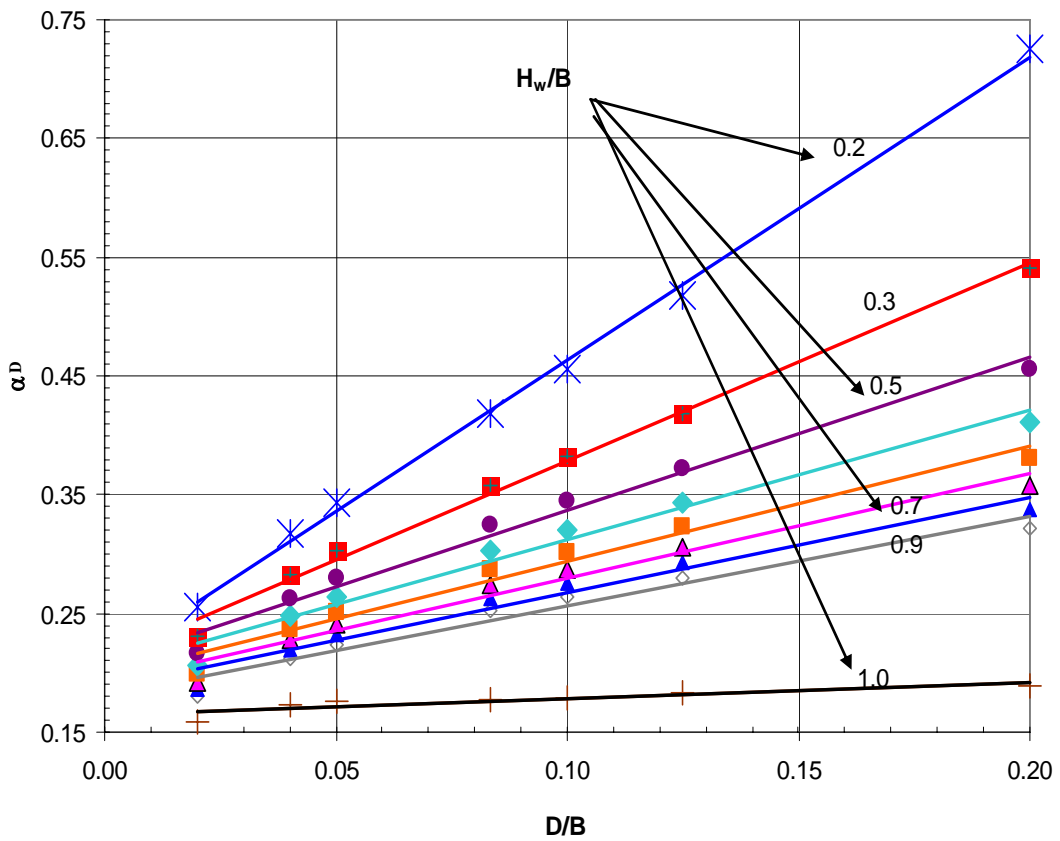
Fig. 3.17. Coefficient α_D for fragment 2 for point D

3.4   Anisotropy

Hydraulic fill materials, produced by crushing the waste rocks have very angular grains as shown in the electron micrograph in Fig 2.4. When settling from the slurry they sometimes produce an anisotropic fill due to the finer fractions of the material settling with slower velocities than the coarser fractions. This stratification can lead to anisotropic behaviour in the permeability of the fill material. Therefore, a preliminary investigation into the effect of the directional variation in permeability was undertaken using a combination of the finite difference program *FLAC* and method of fragments. A simple apparatus and method were developed for measuring the permeability variation within the hydraulic fill material. Using the apparatus, horizontal and vertical permeability values were measured for a variety of hydraulic fill samples. Although these results provide an indication into the degree of anisotropy, several problems were encountered in the testing; therefore results from previous laboratory testing and image processing techniques (Witt and Brauns, 1983; Martys et al., 2000; Mansur and Dietrich, 1965) along with those determined at James Cook University, were used.

3.4.1   Laboratory Testing

The permeability cell testing procedure is a modified version of the constant head permeability test outlined in AS 1289.6.7.1 (2001) and the test procedure developed by Witt and Brauns (1983). Using a 150 mm x 150 mm x 150 mm cubic permeability cell, simple laboratory test procedures were developed to measure the vertical and horizontal permeability for a reconstituted hydraulic fill sample as shown in Fig 3.18. Hydraulic fills were mixed at water contents that matched the placement water contents of the slurry at the respective mines.

The permeability cell was set up and saturated filter paper placed along all sides and base of the cell. Steel clamps and sealant were used to seal the cell as shown in Fig 3.18 (a). The slurry sample was then prepared to the specified solids content and placed evenly into the area of the mould in approximately 3 – 5 equal layers until the cell was completely full as shown in Fig 3.18 (b). The sample was left to stand untilthe build up of decant water was present on the surface. The decant water was

then removed and the filling continued until the entire cell was filled with the saturated fill. The final piece of filter paper was then saturated and lowered onto the top of the fill surface with careful attention to ensure no air voids were caught between the sample and the filter paper. The end caps were then attached to the apparatus and the end caps secured to the permeability cell using another clamp and sealant as shown in Fig. 3.18 (c). The void within the top end-cap was then completely filled with distilled water and the entire apparatus attached to the constant head assembly. A ring fastener was used to ensure the permeability cell setup and constant head apparatus were securely fastened. The overflow tank surrounding the permeability cell was filled with water to the level of the overflow pipe. The apparatus was then left to stand to ensure the flow had reached steady state. Standard constant head tests were then carried out on the sample, using the setup shown in Fig. 3.18 (d) and the permeability values were computed from the Eq. 3.33.

(a)

(b)

(c)

(d)
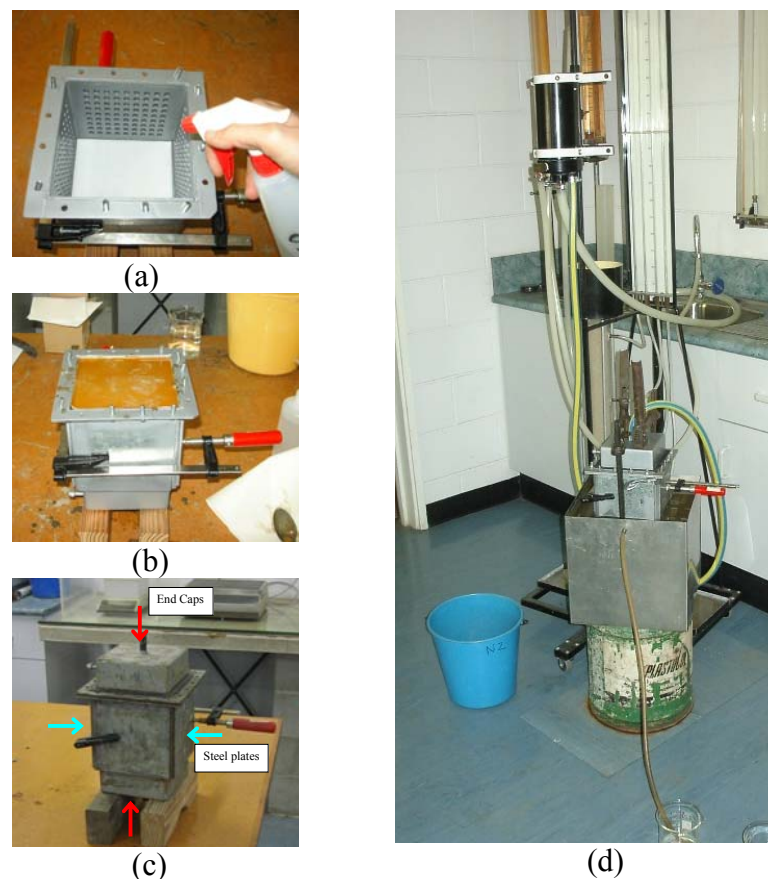
Fig. 3.18. (a) Permeability cell with filter paper (b) Placement of slurry in permeability cell (c) Secured permeability cell (d) Permeability cell connected to constant head apparatus

$$k = \frac{QL}{hA} \qquad\qquad (3.33)$$

where Q is the discharge per unit time, L is the length of the cell, h is the head, and A is the cross sectional area of the permeability cell.

Once the vertical permeability measurements were recorded, the cube was removed from the constant head apparatus setup and rotated 90 degrees to measure the horizontal permeability. The two end caps were exchanged with two-opposite steel plates surrounding the permeability cell and the apparatus set up as per the vertical permeability testing. It is important to note than whenever steel plates and end caps were secured using the clamps, sealant was applied to the connections and edges as an additional safety measure to ensure no leakage occurred during testing.

Previous laboratory testing that measured the degree of permeability (ratio of horizontal to vertical permeability) used two samples of soil. The first test would be carried out with flow in the direction of maximum permeability and the second with the flow at right angles to that in the first test. Difficulties with this approach could arise if the two samples were not exactly the same in terms of permeability characteristics. This testing procedure uses a single soil sample that is tested under the same conditions for both vertical and horizontal permeability measurements. However, during testing several problems were encountered with the permeability cell, these included:

- The movement of the cell when rotating it by 90 degrees may dislodge some particles and allow movement of soil grains within the sample, thus not accurately obtaining the 'true' horizontal discharge.
- During testing, several leaks were observed and were sealed using a silicone based sealant. However during the constant head permeability testing some of the apparatus was submerged in water, Refer to Fig 3.18 (d), therefore some leaks may have gone undetected which may have also influenced results.

- When measuring the horizontal permeability, it was necessary to switch the two end caps with two steel plates on opposite sides of the cell (see Fig 3.18 (c)). Once switched, the cell was resealed using the sealant and the remainder of the testing was undertaken. This part of the procedure is not practical and very labor intensive, therefore it is recommended that future testing on the degree of anisotropy is undertaken using an alternative testing procedure and apparatus.

- It would be more beneficial if vertical and horizontal permeability readings could be measured under confined pressures (as would be the case in the mines). This cell could only take measurements under the self weigh of the fill.

3.4.1.1   *Results*

Table 3.6 summarizes the results obtained from the anisotropic permeability testing using the permeability cell and also standard constant head permeability testing that was conducted from the same batch of hydraulic fill in 2004. Appendix D provides the full results. As was suspected, the degree of anisotropy in the three samples tested was very low. The results of vertical permeability from both test methods (standard constant head and the permeability cell) provided similar values for samples D3 and D4, however A1 was significantly higher than previously tested in 2004. In general, the overall degree of anisotropy for all three samples varied only slightly ranging from 1.28 – 1.34.

Table 3.6. Permeability anisotropy values for hydraulic fills

Sample	Specific Gravity	Permeability (mm/hr)			Degree of anisotropy
		$k_{V\,(2004)}$	$k_{V\,(2006)}$	$k_{H\,(2006)}$	k_H / k_V
D4	3.50	24.41	23.45	31.52	1.34
D3	3.53	37.84	51.47	71.72	1.39
A1	2.79	9.07	94.77	121.77	1.28

Using a combination of the finite difference program *FLAC,* EXCEL, method of fragments and the anisotropic values obtained from both previous and present testing,

the effect of anisotropic permeability was investigated. To take account of the anisotropic permeability, in-built functions in *FLAC* were applied to the model and the codes given in Appendix B. As mentioned previously, the maximum pore water pressure and flow rate are of interest mainly when the water height is quite significant, therefore only case 1 ($H_w > B$) was considered.   Based on previous literature and on the testing conducted at James Cook University, a permeability ratio of 1 – 3 was investigated in the numerical simulations.

3.4.2 Pore Water Pressure

When there is no directional variation in the permeability of hydraulic fill, the maximum pore water pressure is independent of the magnitude of permeability and the flow rate is proportional to permeability. However, if the hydraulic fill exhibits anisotropy with respect to permeability, the degree of anisotropy (i.e. k_h/k_v) can have significant influence on the maximum pore water pressure and flow rate. Fig. 3.19 and Fig. 3.20 illustrate the results for two cases that are modelled with typical aspect ratios encountered for a two-dimensional stope with varying degrees of anisotropy.   Case 1 considered a stope with a *D/B* ratio of 0.025 and an *X/D* ratio of 1, whilst case 2 considered a *D/B* ratio of 0.05 and *X/D* ratio 1.
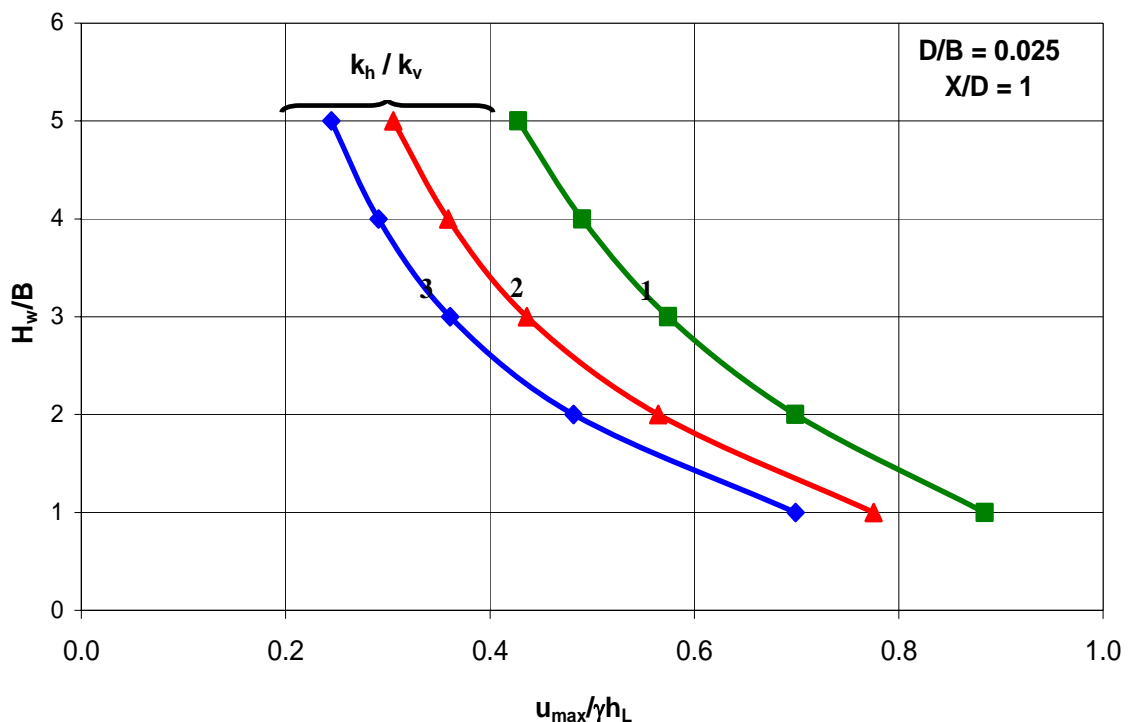
Fig. 3.19. Design chart for pore water pressure measurements for anisotropic fill material: D/B = 0.025; X/D = 1
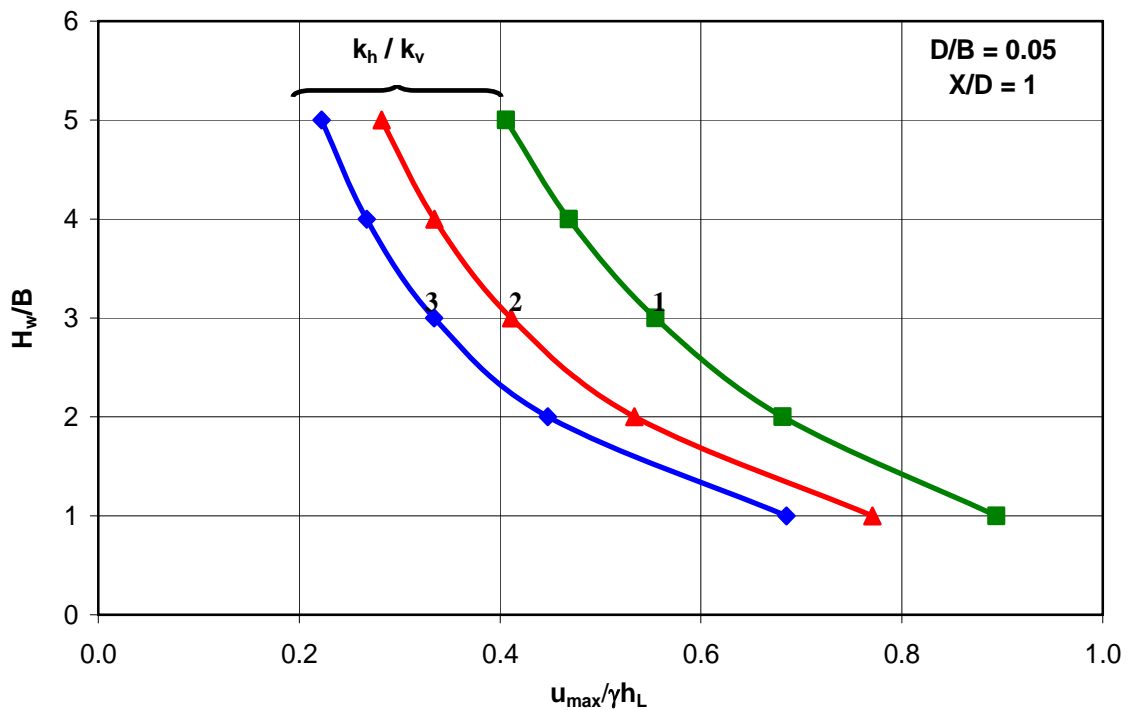
Fig. 3.20. Design chart for pore water pressure measurements for anisotropic fill material: D/B = 0.05; X/D = 1

These figures illustrate the effect of geometry and degree of anisotropy on the maximum pore pressure measurements. It is interesting to note that whilst the absolute magnitude of permeability has no influence on the pore water pressures within the stope, the presence of anisotropy in permeability reduces the pore water pressures quite significantly for a specific height of water.

3.4.3   Flow rate

The rate of drainage of water from the stope will be governed to some extent by the hydraulic properties of the fill material. With permeability being proportional to flow rate, it is obvious that materials of higher permeability will drain more quickly than those of lower permeability. However, the effect of anisotropic permeability on flow rate of hydraulic fill material has had little attention. Fig. 3.21 demonstrates the effect of varying anisotropic ratios on a stope with an *X/D* ratio of 1 and *D/B* ratio of 0.025.
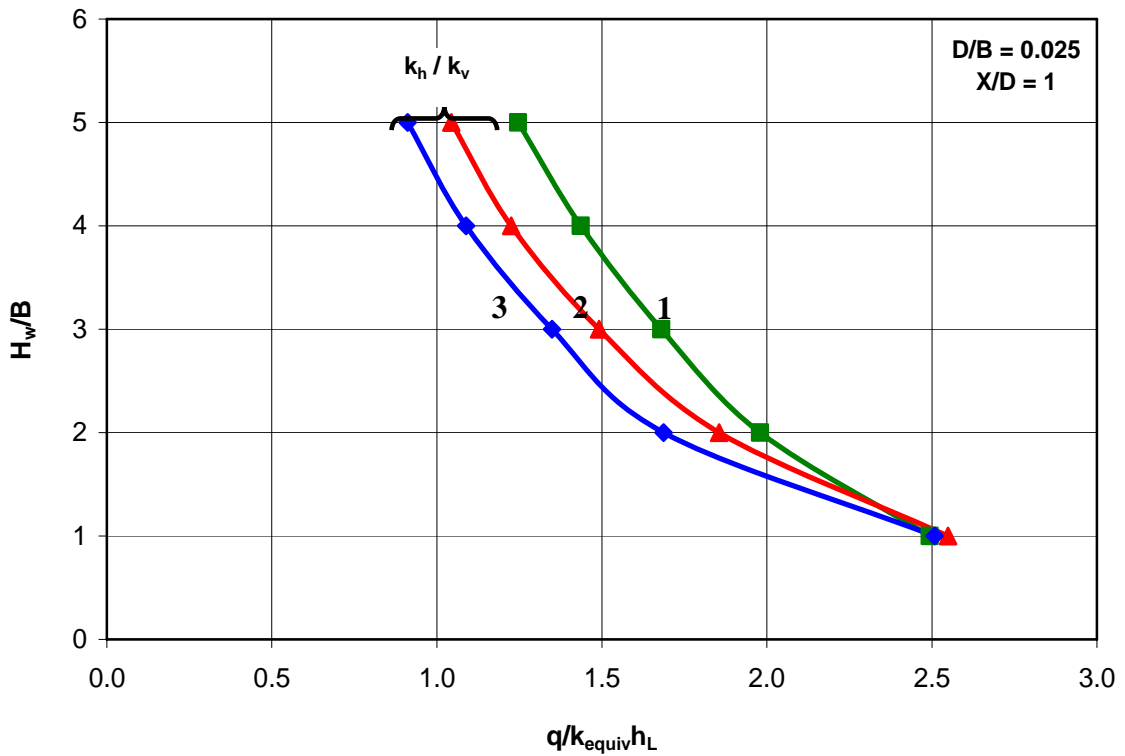
Fig. 3.21. Design chart: effect of anisotropic permeability on flow rate D/B=0.025; X/D=1

As shown in Fig. 3.21, as the anisotropic permeability and the H_w/B ratios increase within the stope, the flow rate decreases. When analysing Eq. 3.34 that calculates flow, the effect of the anisotropic permeability can be broken into two specific terms: $k_{equiv} = (k_h k_v)^{0.5}$ and N_f/N_d which equals the ratio of flow channels to equipotential drops. From Eq. 3.34, $\Sigma\Phi = kh_L / q$, which represents the *x*-axis in Fig. 3.21. Therefore, from the above figure, it can be deduced that for a specific geometry, as the anisotropic ratio increases, the equivalent permeability (k_{equiv}) increases and N_f/N_d decreases

$$Q = k_{equiv} h_L \frac{N_f}{N_d} = \sqrt{k_h k_v} \times h_L \frac{N_f}{N_d} \tag{3.34}$$

However, these terms are not proportional to each other, and care must be taken when analyzing the effect of anisotropic permeability on flow rate as the flow rate trends vary for differing geometries.

3.5   Ancillary Drainage in Two-Dimensional Hydraulic Fill Stopes

Upon discharge into a stope, hydraulic fill generally consists of a solids density of approximately 65% - 75% solids by weight and, because of its liquid nature, possess minimal shear strength. Before it can satisfactorily perform its function in the mining operation as an engineered backfill, it must go through a process of dewatering. Currently solids contents of 65 – 75% are used. Even at 75% solid content, assuming specific gravity of 3.00 for solid grains, 50% of the slurry volume is water. Although not all this water is required to drain i.e. some remains in the fill as residual moisture, there is still a substantial amount of water that has to be drained from the hydraulic fill stope. To expedite the drainage, there had been recent attempts to use prefabricated drains in vertical, horizontal and inclined positions within the stope, thus reducing the drainage paths (Kuganathan, 2001; Neindorf 1983).

Through the use of a two-dimensional model developed in *FLAC*, it can be shown that the prefabricated drains are effective in accelerating the drainage process and reducing the pore water pressures within the stope. Previously, prefabricated drains have been successfully used in consolidation of clays. However, this is the first numerical modeling study that looks at the effects of prefabricated drains on drainage through hydraulically filled mine stopes, where the material is granular and the prefabricated drains are used simply to shorten the drainage paths. Although, it would be premature to regard the two-dimensional model developed here as a proven design tool, it will provide a better understanding of the effect of using ancillary drainage in effectively draining a hydraulically filled stope.

The effects of ancillary drains on the pore water pressures and discharge were studied through a two dimensional numerical model developed in *FLAC*. Most of the runs were made on a 50 m wide stope containing hydraulic fill with a water level at 80 m height and with a 5 m long by 5 m high drain (Fig. 3.22). The ancillary drain is placed horizontally at the bottom of the drain. The first few trials were run with the above stope dimensions whilst varying the length of the ancillary drain. Later, a few more runs were made for stopes with different dimensions and drain lengths, to verify the findings.
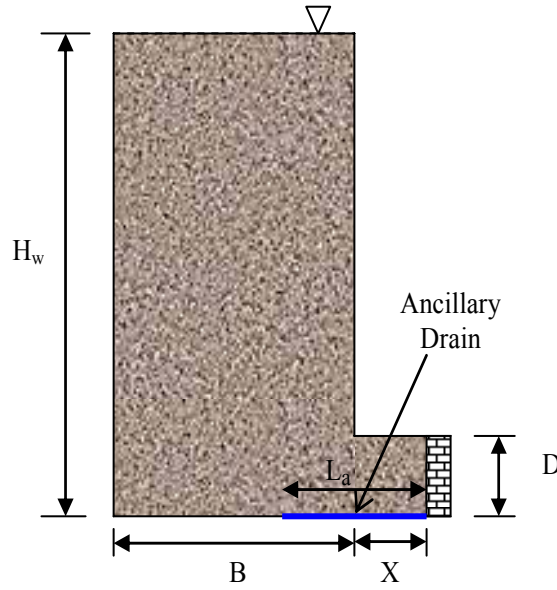
Fig. 3.22. Geometry of stope with ancillary drainage

3.5.1 Pore Water Pressure

As discussed in section 3.3.2, the maximum pore water pressure (u_{max}) within a two-dimensional hydraulic fill stope with no ancillary drain, occurs at the corner of the stope and can be calculated using Eq. 3.13, shown below.

$$u_{max} = \left[h_L \left(\frac{\alpha_{2D}\Phi_2 + \Phi_3}{\Phi_1 + \Phi_2 + \Phi_3} \right) + D \right] \gamma_w$$

Using *FLAC*, it was shown that for all values of ancillary drain lengths, the pore water pressures were still the maximum at the corner of the stope. For the 50 m wide stope described in (Fig. 3.22), the maximum pore water pressure, which occurs at the corner of the stope, decreases linearly with the drain length. This is shown in Fig. 3.23.

When the ancillary drain extends to the full width of the stope (i.e., $L_a = X+B$), the maximum pore water pressure is zero. This assumes the drain has infinite permeability i.e. no head loss along the drain. Therefore, for a given length of ancillary drain (L_a) the maximum pore water pressure can be simply interpolated, and can be expressed as:

$$u_{max} = \left(1 - \frac{L_a}{B+X} \right) \left[h_L \left(\frac{\alpha\Phi_2 + \Phi_3}{\Phi_1 + \Phi_2 + \Phi_3} \right) + D \right] \gamma_w \qquad (3.35)$$
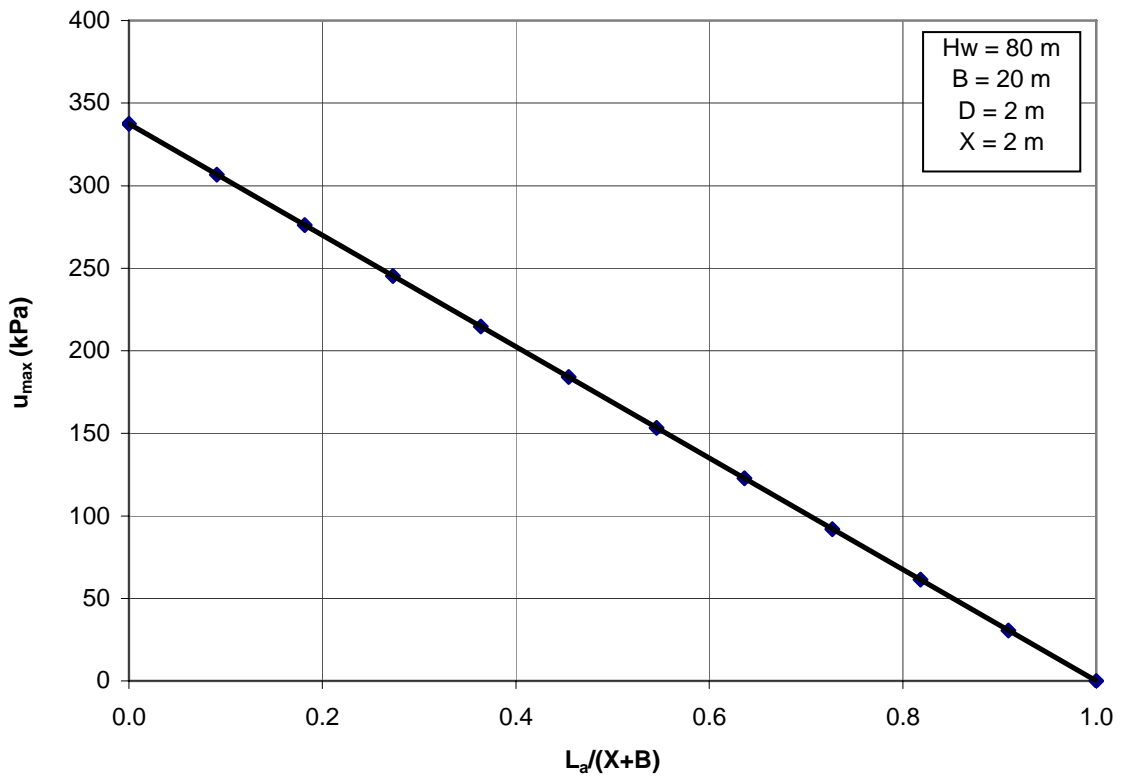
Fig. 3.23. Effects of ancillary drain on pore water pressure measurements

Fig. 3.24 illustrates the comparison between the maximum pore pressures calculated using Eq. 3.35 and those obtained from *FLAC* for varying geometries and ancillary drain lengths. As shown in the figure, Eq. 3.35 slightly overestimates the value of u_{max} when compared with those from *FLAC*. In other words, the equation provides an upper bound for the maximum pore pressure values. The actual values of u_{max} are almost certain to be less than those computed from Eq 3.35.

3.5.2 Flow rate

The values of flow rate (Q) were computed for a number of simulations with varying ancillary drain lengths in *FLAC*. These results are illustrated in Fig. 3.25. From this figure it is clear that as the ancillary drain length is increased, the flow rate also increases thus reducing pore pressure build-up behind the barricades. However, the cost and difficulty of installation is increased as the drain length increases, therefore it is important to reach a compromise between the two.
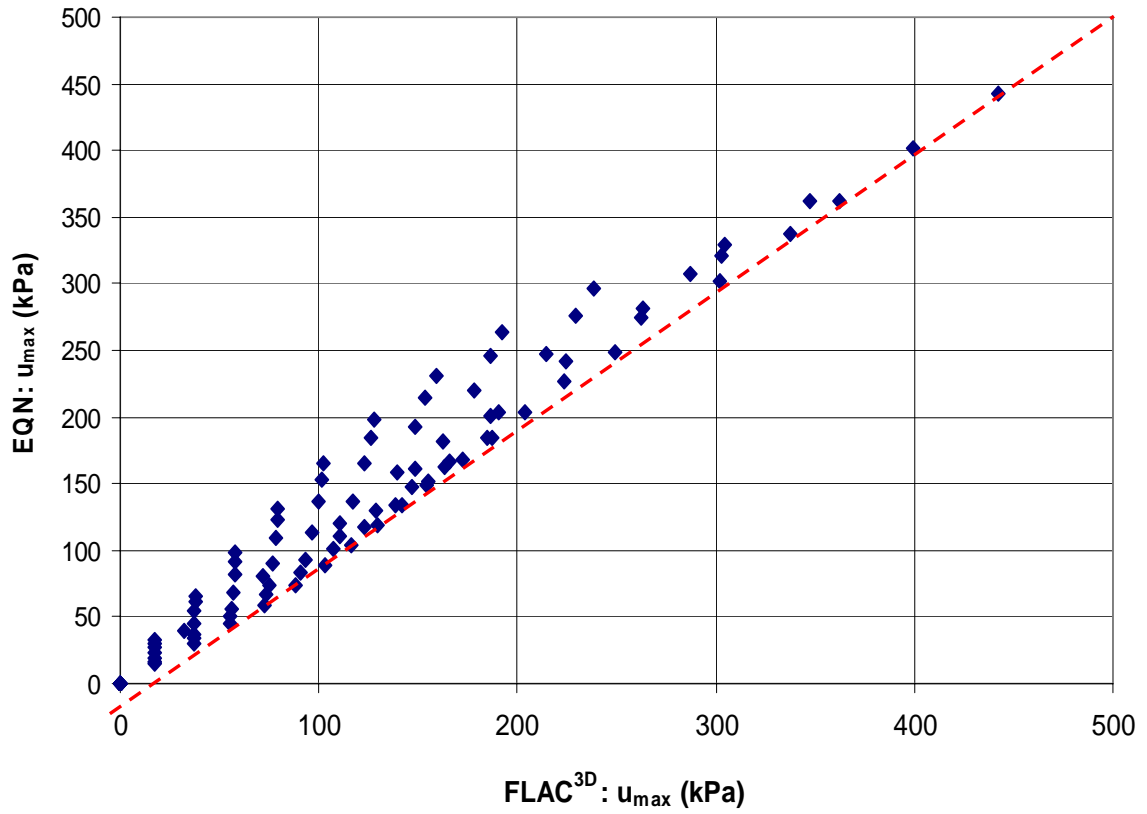
Fig. 3.24. Comparison between maximum pore water pressures obtained from *FLAC* and those calculated using Eq. 3.13
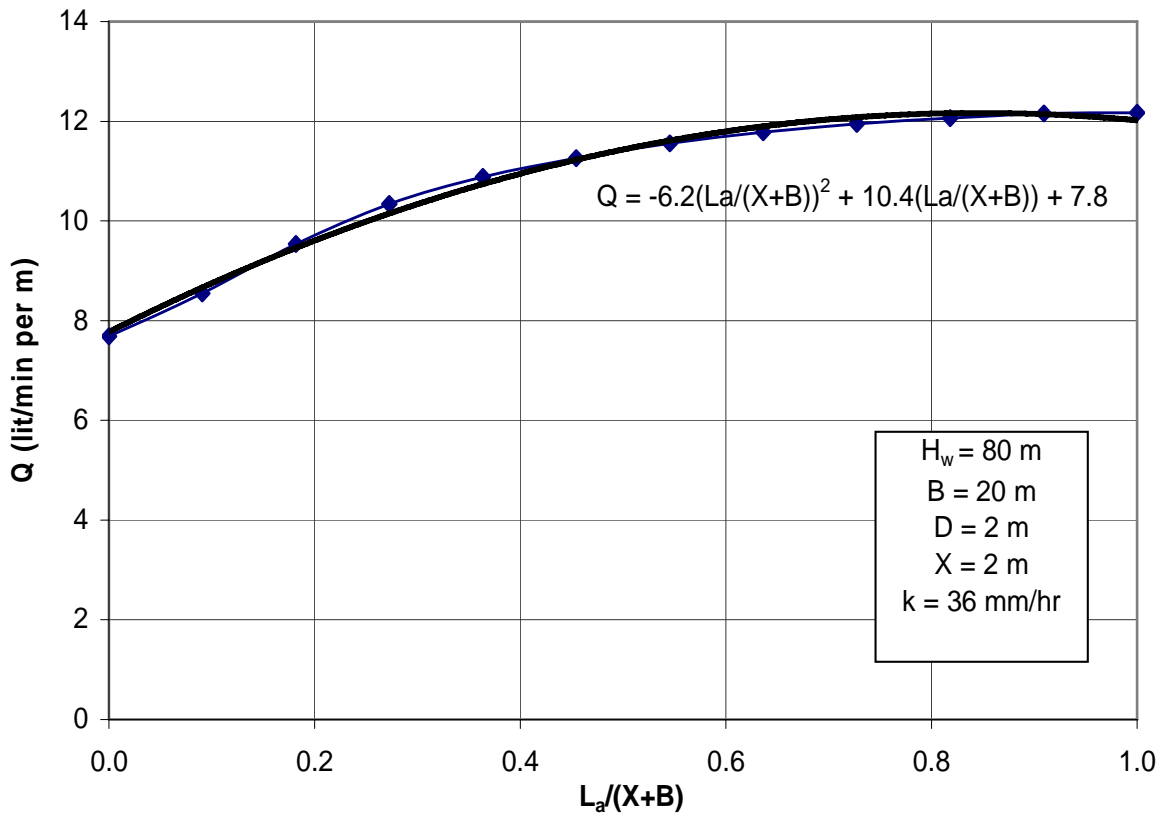
Fig. 3.25. Effect of ancillary drain on flow rate results

3.6 Summary and Conclusions

Using method of fragments (Harr 1962, 1977) and the finite difference software *FLAC*, the drainage and pore water pressure developments within a two-dimensional hydraulic fill stope were investigated in this chapter. It was shown that the flow region can be divided into three fragments, for which the form factors can be determined from the dimensions of the stope and the drain. The flow is vertical at heights above the stope width (*B*), and is horizontal within the drain a short distance (0.5*D*) from the stope face. At the bottom of the stope, up to a height of the stope width, flow is two-dimensional. Since the bottom of the stope (fragment 2) does not conform to any of the fragments suggested by Harr (1962), a new fragment was developed. The dimensionless form factor of the new fragments was expressed as a function of the dimensions of the stope and drain. Analytical solutions were proposed for determining the entry hydraulic gradient at the top of the stope, flow rate and the maximum pore water pressure that occurs at the bottom corner of the stope. The model was verified through several numerical examples of hydraulic fill stopes with randomly selected dimensions and was found to be in excellent agreement. Several other points within the two-dimensional stope were also analysed and equations developed to determine the pore pressure development throughout the stope. For all analysis in chapter 3, tight filling was assumed in the access drive.

The effect of anisotropic permeability in hydraulic fill material was investigated using *FLAC*, *EXCEL* and the method of fragments. From the results, it is evident that the anisotropic permeability has a significant effect on pore pressure development and discharge within the stope. As the anisotropy in permeability is increased there is a substantial reduction in pore pressure. A number of design charts were created to quantify the effect of varying anisotropic ratios and geometries on pore pressure and discharge within the stope.

Through the use of a two-dimensional model developed in *FLAC*, it was demonstrated that the use of ancillary drainage behind barricades is effective in accelerating the drainage process within a hydraulically filled stope - consequently, reducing the build-up of pore pressure behind the barricades, assuming tight filling of the drain. It was shown that the horizontal ancillary drain provided at the bottom of the drain reduces

the pore water pressure at all points within the fill, with the reduction being proportional to the length of the drain. A simple expression was developed to determine the maximum pore water pressure for the given stope and ancillary drain arrangement. The ancillary drain also increases the hydraulic gradient, thus the rate of flow, resulting in quicker drainage of the two-dimensional stope.

CHAPTER 4

APPLICATION OF METHOD OF FRAGMENTS TO THREE-DIMENSIONAL HYDRAULIC FILL STOPES

4.1 Overview

Underground stope arrangements are very much three-dimensional in geometry, and although the two-dimensional solutions discussed in Chapter 3 provide a valuable tool for drainage prediction, the inherent approximations required, substantially reduce the value of the model when dealing with complex three-dimensional stopes. This chapter provides simple analytical solutions and design charts for estimating the maximum pore water pressure and discharge within three-dimensional hydraulic fill stopes of varying geometries. Previously, complex numerical models were required to analyze these three-dimensional hydraulic filled stopes. Shape factors were developed to account for the inherent individuality associated with stope and drain geometry and the influence of scaling on discharge and pore pressure measurements were also investigated. The proposed solutions have been verified against solutions derived from the finite difference software package $FLAC^{3D}$ and physical modeling of a scaled stope and results are found to be satisfactory.

4.2 Introduction

As discussed in Chapter 3, several numerical models have been developed to simulate the drainage and pore water pressure developments within two and three-dimensional stopes. These included Isaacs and Carter (1983) two-dimensional model which provided a basic understanding of the concepts of the drainage of hydraulic fills in undergrounds stopes. Traves and Isaacs (1991) extended this model to three-dimensions; however the model remains yet to be validated against field measurements. More recently, Rankine (2005) developed several drainage models in $FLAC$ and $FLAC^{3D}$ with similar features and verified them against the predictions from

the Isaacs and Carter (1983) model. A major restriction with these models is that the simulations are often time consuming and in most cases, specialist knowledge of the corresponding software package is required. Therefore a quicker and less complicated solution was desirable.

Chapter 3 presents closed form solutions, based on the method of fragments and *FLAC* simulations that can be used to determine the discharge and maximum pore water pressures within a two-dimensional stope with a single drain at the stope base. However, many mine stope geometries are not two-dimensional, and a more adaptable three-dimensional solution was required. Using $FLAC^{3D}$ and the method of fragments, simple analytical solutions and design charts were formulated for estimating the maximum pore water pressure and discharge within three-dimensional hydraulic fill stopes of varying geometries. The three-dimensional solutions derived from $FLAC^{3D}$ were then compared with pseudo three-dimensional solutions derived in Chapter 3 using the Rankine (2005) model, Isaacs and Carter's verification problem and $FLAC^{3D}$ simulations.

4.3 Method of Fragments for Three-dimensional Hydraulic Filled Stopes

The three-dimensional flow net is approached in much the same manner as the two-dimensional net. However equipotential lines are viewed as equipotential surfaces, and the flow channels incorporate the third dimension. The total head loss (h_L) across the entire system is divided into a number of equipotential drops (N_d), which are defined by $N_d +1$ equipotential surfaces. The total head loss across the entire system is:

$$h_L = N_d \Delta h \tag{4.1}$$

As shown in the three dimensional stope depicted in Fig 4.1 (a), the equipotential surface within the stope, at the height of B above the bottom, is approximately horizontal as in the case with two-dimensional flow. Similarly, the equipotential surface within the drain, at a distance of $0.5D$ from the stope, is approximately vertical. Several $FLAC^{3D}$ runs, using various dimensions for the stope and the drain, were made

to justify these assumptions. Fig 4.1 (a) illustrates a few selected equipotential surfaces for a simplified three-dimensional stope. Only half the geometry is shown here.

Typical drain dimensions are generally, 3 m to 6 m wide and 3 m to 6 m high, and the barricades are located a short distance from the stope. As discussed by Rankine et al. (2003) the position of the barricade has considerable influence on pore water pressure and discharge measurements. As the position of the barricade progresses further from the stope face, the rate of discharge decreases. The closer the barricade the more efficient is the drainage. Intuitively, as the barricade gets further away from the stope, the flow path increases and the hydraulic gradient decreases. This results in a reduction in the velocity and flow discharge. For safety reasons, barricades cannot be constructed in flush with the stope face. Thus, for all modelling, the drain has been assumed to be located at a minimum distance of $0.5D$ away from the stope face. Also, the equipotential surface only becomes vertical, a short distance ($\approx 0.5D$) from the stope edge. These two equipotential surfaces divide the flow domain into three fragments similar to those in two-dimensions (see Fig. 4.1 b). In fragments 1 and 3, the flow is one-dimensional.

| (a) | (b) |
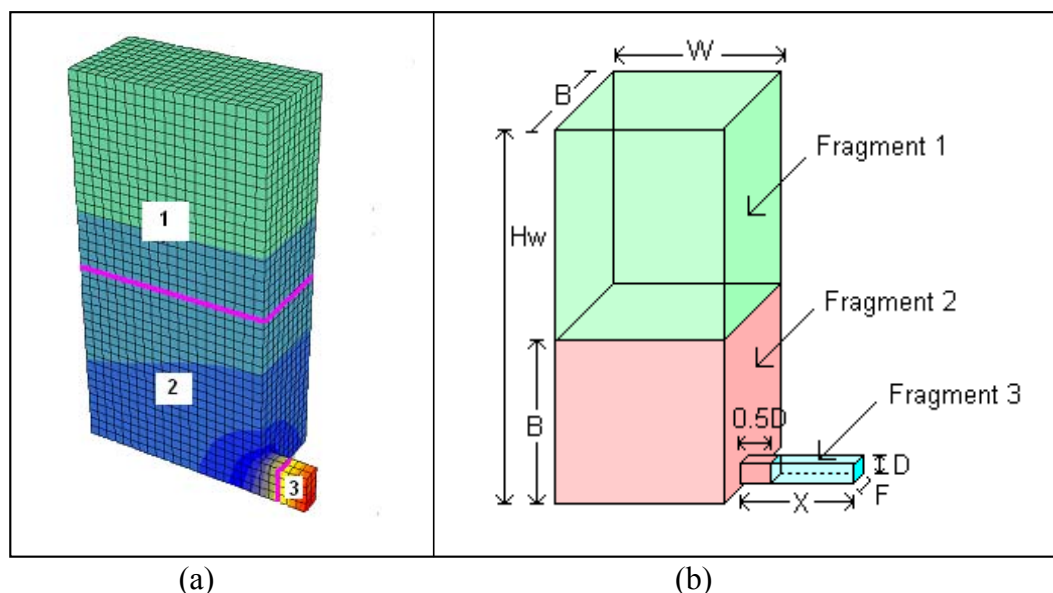
Fig. 4.1. Three-dimensional hydraulic fill stope (a) Selected equipotential surfaces
(b) Flow region, dimensions and three fragments of 3D stope

4.3.1 Numerical Model

The three-dimensional finite difference package $FLAC^{3D}$ was used to model the three-dimensional hydraulic fill stope illustrated in Fig. 4.1 b. The program written for the simulations undertaken in this dissertation was originally developed by Rankine (2005) for an uncoupled, flow-only analysis of a specified geometry. The inbuilt programming language *FISH* was also used to write simple subroutines for functions that were not available in $FLAC^{3D}$.

4.3.1.1 Numerical Package $FLAC^{3D}$

$FLAC^{3D}$ is an extension to the well established two-dimensional numerical modelling program *FLAC* developed by the Itasca Consulting Group (used in Chapter 3). Like *FLAC*, $FLAC^{3D}$ is an explicit finite difference program used in computational geomechanics. The numerical methods used in $FLAC^{3D}$ are essentially the same as *FLAC* but the simulations model the three-dimensional behaviour of structures built of soil, rock or other materials that undergo plastic flow when their yield criteria are reached. Both *FLAC* and $FLAC^{3D}$ allow the user to implement subroutines written in *FISH*.

Like *FLAC*, the variables involved in the description of fluid-flow through a porous media are the pore pressure (u), saturation (S), and the three components of the specific discharge vector (q_x, q_y, q_z). These variables are related through Darcy's law (the fluid transport law), the fluid mass-balance equation, the constitutive equation[2] and an equation of state for the unsaturated range which relates pore pressure to saturation. Assuming the volumetric strain rates are known, by substitution of the mass-balance equation into the constitutive relation, using Darcy's law, a differential equation in terms of pore pressure and saturation is formed. For a flow-only analysis such as the programs developed in this research, where grains are assumed incompressible, the volumetric strain rates are obviously not required. This differential equation may be solved for various geometries, properties, boundary and initial conditions.

---

[2] The constitutive equation specifies the fluid response to changes in pore pressure, saturation and volumetric strains

The discretization and finite difference methods follow the general scheme presented in the "Theory and Background" of the Itasca *FLAC*^{3D} manuals. Each brick-shaped element is further discretized into tetrahedra. The equations that describe pressures and saturation values are based on nodal or "gridpoints" calculations, and zone pressures and saturations are derived by simply averaging surrounding nodal values.

Attention is directed to two specifics of the numerical formulation:

1. All equations for both fluid analysis and boundary conditions in *FLAC* and *FLAC*^{3D} are expressed in terms of *pore water pressure* rather than *head*, which are more conventionally used in soil mechanics.

2. *Permeability*, described in *FLAC* and *FLAC*^{3D} refers to the mobility coefficient, the coefficient of the pore pressure term in Darcy's law. It is defined as the ratio of intrinsic permeability to fluid dynamic viscosity, (see– *FLAC* 4.0 Manual – User's Guide, 2.8 System of Units).

    In traditional soil mechanics, $v = ki = k\dfrac{dh}{dx}$, however, in *FLAC* computations $v = k\dfrac{du}{dx}$. Therefore, it can be shown that if *du* has the units of Pa, and *v* has the SI units m/s, the permeability (*k*) must have the units m^2/(Pa.s). The two permeabilities are related by:

$$k_{FLAC} = \frac{k_{\text{soil mechanics}}}{\gamma_w} \tag{4.2}$$

4.3.1.2 *Input Parameters, Boundary Conditions and Assumptions*

All material input parameters were identical to those used for the two-dimensional simulations performed in chapter 3, as were the boundary conditions and assumptions detailed in section 3.3.1.2. However, the three-dimensional problem investigated in this chapter does not need the geometrical simplification that was required in the two-dimensional solution as actual three dimensional geometries were modeled.

4.3.1.3 *Grid Generation*

The initial geometry investigated was a square based stope, with one drain located centrally along the base of one of the stope walls, as shown in Fig. 4.1 b. To ensure

the most accurate and efficient modelling, a sensitivity analysis of mesh spacing was undertaken. The meshes investigated are shown in Fig. 4.2 and include: (a) 2 m mesh spacing, (b) 1 m mesh spacing, (c) a combination of a fine and coarse mesh (0.5 m mesh spacing within drain with 1 m mesh spacing for the remainder of the stope) and (d) 0.5 m mesh spacing throughout the stope.

| (a) | (b) | (c) | (d) |
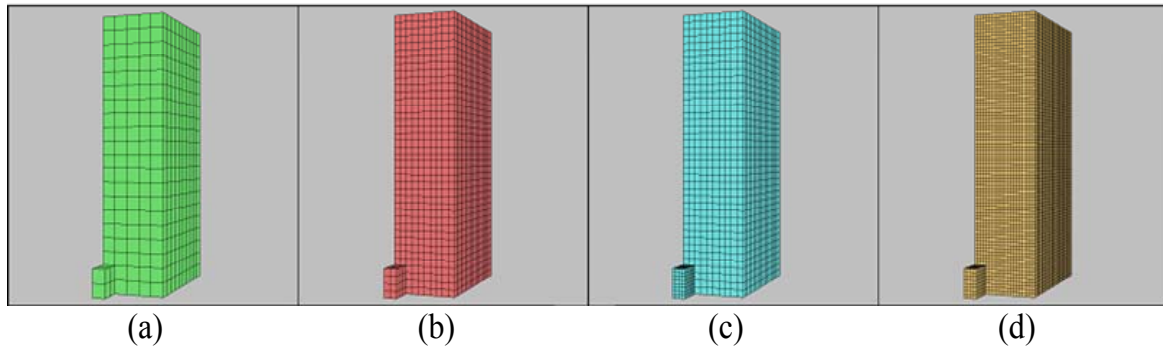
Fig. 4.2. Mesh sensitivity (a) 2 m mesh spacing, (b) 1 m mesh spacing (c)

Combination of fine and coarse mesh (d) 0.5 mesh spacing

Table 4.2 presents a summary of the output data from the various meshes investigated. The difference in maximum pore water pressure between these meshes was minimal with a variation of only 2%, whilst the difference in discharge varied as much as 10%. From Table 4.2, it is clear that as the mesh fineness increases, so too does the computational time. A 1 m x 1 m mesh shown Fig. 4.2 (b), was selected for use with the remaining simulations, as this provided an efficient balance between accuracy and solution time.

Table 4.1. Output for various three-dimensional meshes

Mesh Type	Mesh Size	No. of steps	Computational Time (min)	Output	
				u_{max} (kPa)	Flow rate (m^3/s)
a	2m x 2m mesh throughout	9096	0.8	327.3	0.464
b	1m x 1m mesh throughout	32988	22.3	329.3	0.450
c	Combination of 1m x 1m mesh in stope with 0.5m x 0.5m mesh in drain	132539	86.5	333.8	0.448
d	0.5m x 0.5m mesh throughout	114939	430.1	330.1	0.447

4.3.2 Developing Equations for Form Factors, Flow rate and Maximum Pore Water Pressure

In two-dimensional analysis, for the ith fragment, $\Phi_i = \dfrac{N_{d_i}}{N_f} = \dfrac{kh_i}{Q}$. This makes Φ_i a function of the fragment geometry, independent of flow net, and dimensionless. However, this will not be the case in three dimensions. Fig 4.1 (b) illustrates the three-dimensional stope broken down into the three fragments and the various dimensions used in analysis.

When defining the form factor (Γ) for a fragment in three-dimensions, it is necessary to ensure the following conditions:

a) The form factor is dimensionless,

b) $\Gamma_{stope} = \Gamma_1 + \Gamma_2 + \Gamma_3$,

c) Within the fragments, head losses (h_i) and the form factors (Γ_i) are in the same proportions. i.e., $h_1/\Gamma_1 = h_2/\Gamma_2 = h_3/\Gamma_3 = h_L/(\Gamma_1 + \Gamma_2 + \Gamma_3)$,

d) Form factor remains the same when the flow domain is scaled.

To satisfy the above conditions, Γ_i was defined as:

$$\Gamma_i = \frac{kh_L h_i}{Q} \quad \text{for i} = 1, 2, 3 \tag{4.3}$$

where h_i is the head loss within the ith fragment and h_L $(= h_1 + h_2 + h_3)$ is the head loss across the entire stope, Q is the flow rate and k is the permeability of the fill.

The flow rate (Q) is the same through all fragments, therefore, Eq. 4.3 can be written as:

$$Q = \frac{kh_L h_1}{\Gamma_1} = \frac{kh_L h_2}{\Gamma_2} = \frac{kh_L h_3}{\Gamma_3} = \frac{kh_L^2}{\Gamma_1 + \Gamma_2 + \Gamma_3} \tag{4.4}$$

Initially form factors were computed for the three fragments, on the basis that the stope and the drain have square cross sections and that the drain was located centrally at the base of the stope (see Fig. 4.1 b). Shape factors were later developed to account for non-square stope and drain cross-sections.

Case 1 illustrated in Fig. 4.1 (b) considers a square-based stope with a single drain placed in the centre at the base of one of the stope faces. The model also assumes no decant water is present.

From Darcy's law:

$$v = \frac{Q}{A} = ki = k\frac{\Delta h}{L} \tag{4.5}$$

where v is the velocity, i is the hydraulic gradient which is the ratio of the head loss (Δh) over a distance l, A is the area, k is the coefficient of permeability and Q is the rate of seepage. Therefore, through rearranging Eq. 4.5, the flow velocities within the fragments 1 and 3 are given by:

$$Q_1 = v_1 A_1 = \frac{kh_1}{H_w - B} \times B^2 \tag{4.6}$$

$$Q_3 = v_3 A_3 = \frac{kh_3}{(X - 0.5G)} \times G^2 \tag{4.7}$$

where G represents the equivalent drain height for a non-square drain outlet and is given by:

$$G = \sqrt{D \times F} \tag{4.8}$$

where D and F represent the height of the drain and width of the drain respectively as shown in Fig. 4.1 (b).

Rearranging Eq. 4.4 and substituting it into Eq. 4.6 and Eq. 4.7, the form factors for fragments and 1 and 3 can be written as:

$$\Gamma_1 = \frac{kh_L h_1}{Q} = \frac{kh_L h_1}{B^2 kh_1 /(H_w - B)} = \frac{(H_w - B)h_L}{B^2} \tag{4.9}$$

$$\Gamma_3 = \frac{kh_L h_3}{Q} = \frac{kh_L h_3}{G^2 kh_3 /(X - 0.5G)} = \frac{(X - 0.5G)h_L}{G^2} \tag{4.10}$$

The form factor for fragment 2 (Γ_2) cannot be derived in a straight forward manner since the flow is not one-dimensional within this fragment. Numerous simulations were undertaken for a wide range of stope dimensions using the three-dimensional model combined with Eq. 4.9 and Eq. 4.10. For each of these models, values of Γ_2, maximum pore water pressure and discharge were computed. The form factor, Γ_2, is a function of H_w/B and D/B and the results are presented graphically in Fig. 4.3.

The form factor for fragment 2, Γ_2 was initially calculated for the case where $H_w/B \geq 1$ and all three fragments were present in the stope (i.e. as was the case for the two-dimensional analysis). In this case, Γ_2, illustrates a linear relationship for the varying D/B ratios analysed and is given in Eq. 4.11. To investigate the case when $H_w/B < 1$, which occurs at the start and end of the drainage process, several numerical models were run, where values of Γ_2 were computed for H_w/B ratios ranging from 0.1 to 1.0 and D/B ratios ranging from 0.125 to 0.300. Fig. 4.3 presents a design chart for Γ_2 for all cases of H_w/B. The curves illustrated in Fig. 4.3 represent a graphical representation of Eq. 4.11 – Eq. 4.14, whilst the data points represent actual FLAC 3D results.

For $H_w \geq B$

$$\Gamma_2 = a\left(\frac{H_w}{B}\right) \tag{4.11}$$

For $H_w \leq B$

$$\Gamma_2 = a\left(\frac{H_w}{B}\right)^b \tag{4.12}$$

where the values of a and b are given by:

$$a = 0.82\left(\frac{D}{B}\right)^{-1.1} \tag{4.13}$$

$$b = 1.142e^{3.2\left(\frac{D}{B}\right)} \tag{4.14}$$
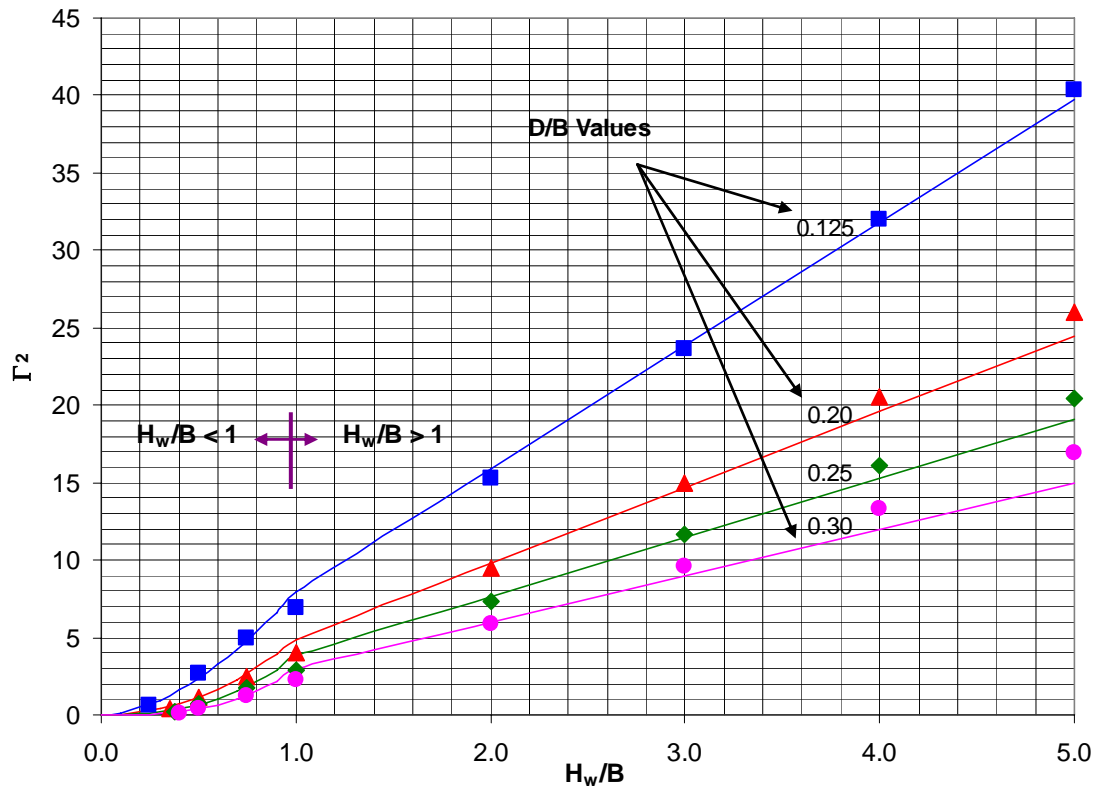
Fig. 4.3. Form Factor for fragment 2 (Γ_2) for a three-dimensional stope

Most of the time during the filling and drainage of a hydraulic fill stope, H_w is greater than B, and Γ_2 is proportional to the height of water H_w. When this is the case, the values computed using $FLAC^{3D}$ agree with Eq. 4.11 very well. When the height of

water is less than B, (i.e. at the beginning of filling and end of drainage) values of Γ_2 computed using Eq. 4.12 are only approximate (see Fig. 4.3). Nevertheless, when $H_w < B$, there is very little concern with the pore water pressure developments and liquefaction within the fill and the subsequent breach of the barricades. Therefore, the slight error in estimating Γ_2 using Eq. 4.12 for $H_w \leq B$ is considered acceptable.

The maximum pore water pressure within a hydraulic fill stope with a single drain at the bottom in the centre of the stope face, occurs at the two bottom corners furthest from the drain. The magnitude of this maximum pore water pressure is given by Eq. 4.15 and takes the same form as the maximum pore pressure for a two-dimensional stope.

$$u_{max} = \left[\left(\frac{\alpha_{3D}\Gamma_2 + \Gamma_3}{\Gamma_1 + \Gamma_2 + \Gamma_3} \right) h_L + G \right] \gamma_w \tag{4.15}$$

However, α_{3D} represents the fraction of head loss in fragment 2, (h_2) that is lost between the point of maximum pore water pressure and the barricade at the exit. $FLAC^{3D}$ was used to compute the values of α_{3D} for various values of H_w/B and D/B. These results are presented graphically in Fig. 4.4. When $H_w > B$, the coefficient α_{3D} is a function solely of B/D. When $H_w < B$, only two fragments are present and α_{3D} depends on H_w/B and D/B. In this situation (i.e. $H_w < B$), the pore water pressure is low and does not pose a serious threat.

The coefficient α_{3D} can be expressed mathematically as:

For $H_w/B \geq 1$

$$\alpha_{3D} = 1.0 - 0.56 \left(\frac{D}{B} \right) \tag{4.16}$$

For $H_w/B \leq 1$

$$\alpha_{3D} = \left(-0.8 \left(\frac{H_w}{B} \right) + 0.24 \right) \left(\frac{D}{B} \right) + 1 \tag{4.17}$$
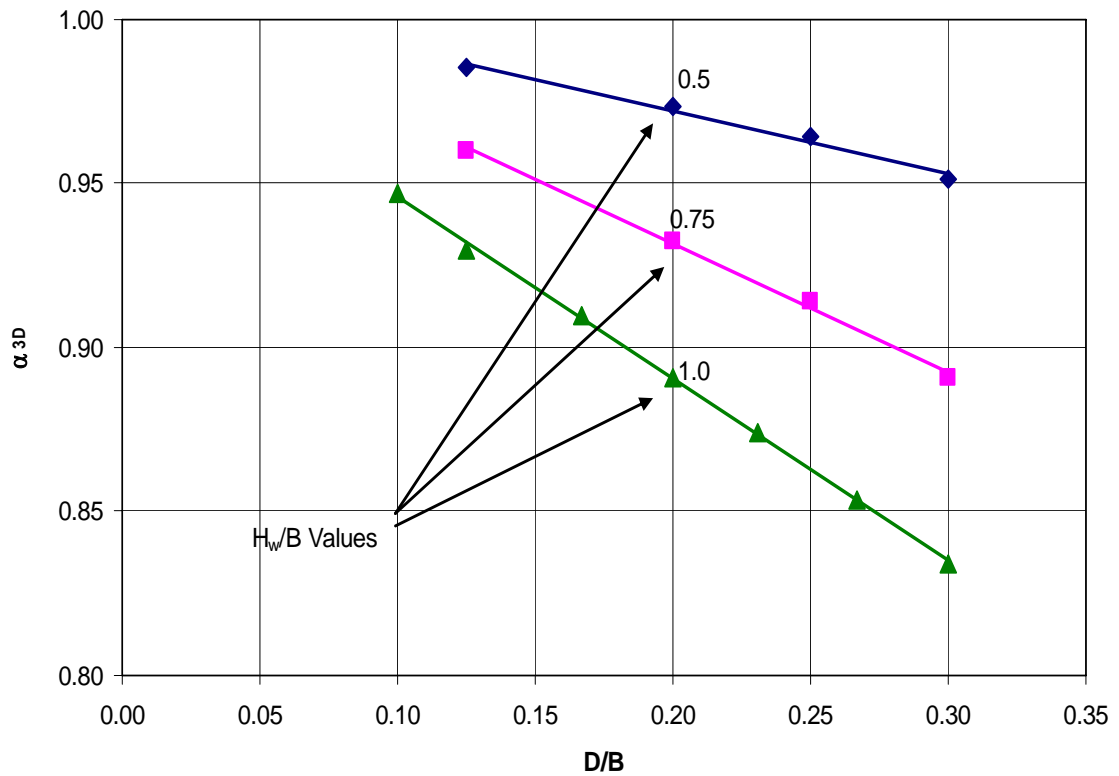
Fig. 4.4. Coefficient α_{3D} for fragment 2 in a three-dimensional stope

Realistically, it is unlikely that the stope dimensions have a square base and square drain; therefore it was necessary to explore varying stope dimensions. Several *FLAC^{3D}* runs were made with non-square drains and stopes, and the maximum pore water pressures and flow rates were compared with the results from stopes with square sections having the same cross sectional areas.

4.3.2.1 *Drain Shape*

To determine the effect of drain shape on discharge and pore pressure measurements, three types of drains with equivalent cross-sectional areas were investigated. They include:

  1) 4 m x 4 m drain (square cross-section as in case 1),

  2) 2 m x 8 m drain, and

  3) 8 m x 2 m drain.

Using these drain geometries, various ratios of H_w/B and D/B aspect ratios ranging from 1 – 3 and from 0.1 – 0.4 respectively, were investigated. In all simulations a drain length of 4 m was assumed. Fig. 4.5 and Fig. 4.6 illustrate dimensionless charts that

represent the effect of drain shape on pore water pressure and flow rates respectively. It is important to re-iterate that when calculating headloss an equivalent drain height (G) was used (See Eq. 4.8).
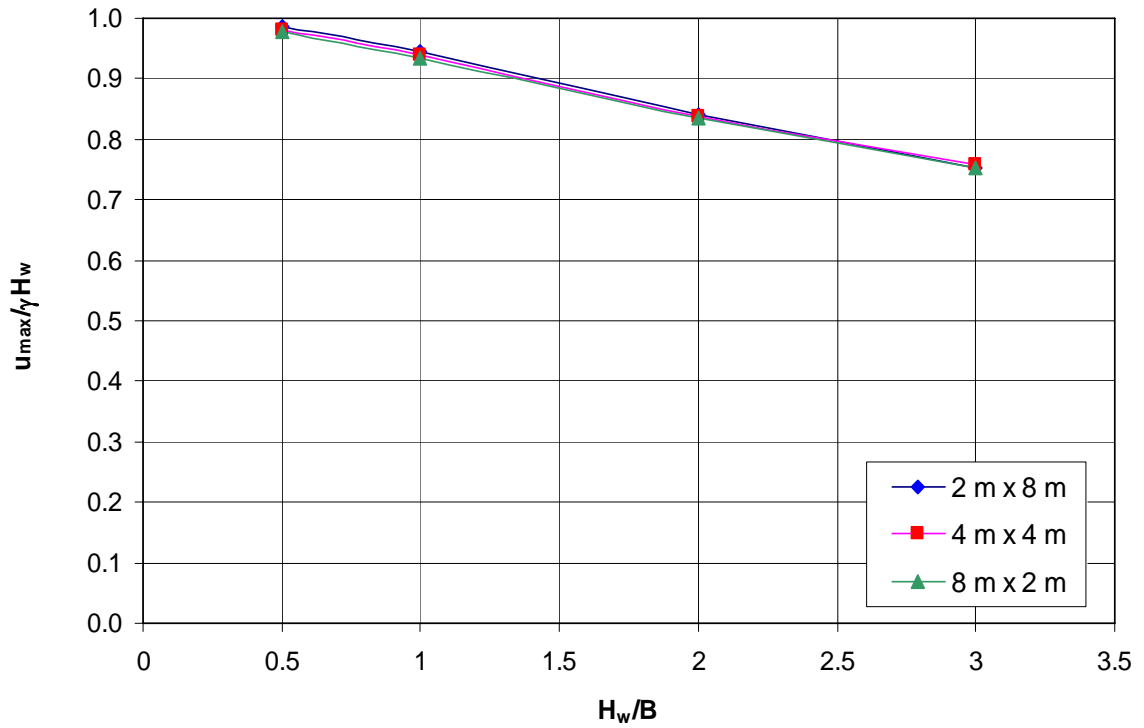
Fig. 4.5. Effect of drain shape on pore pressure measurements
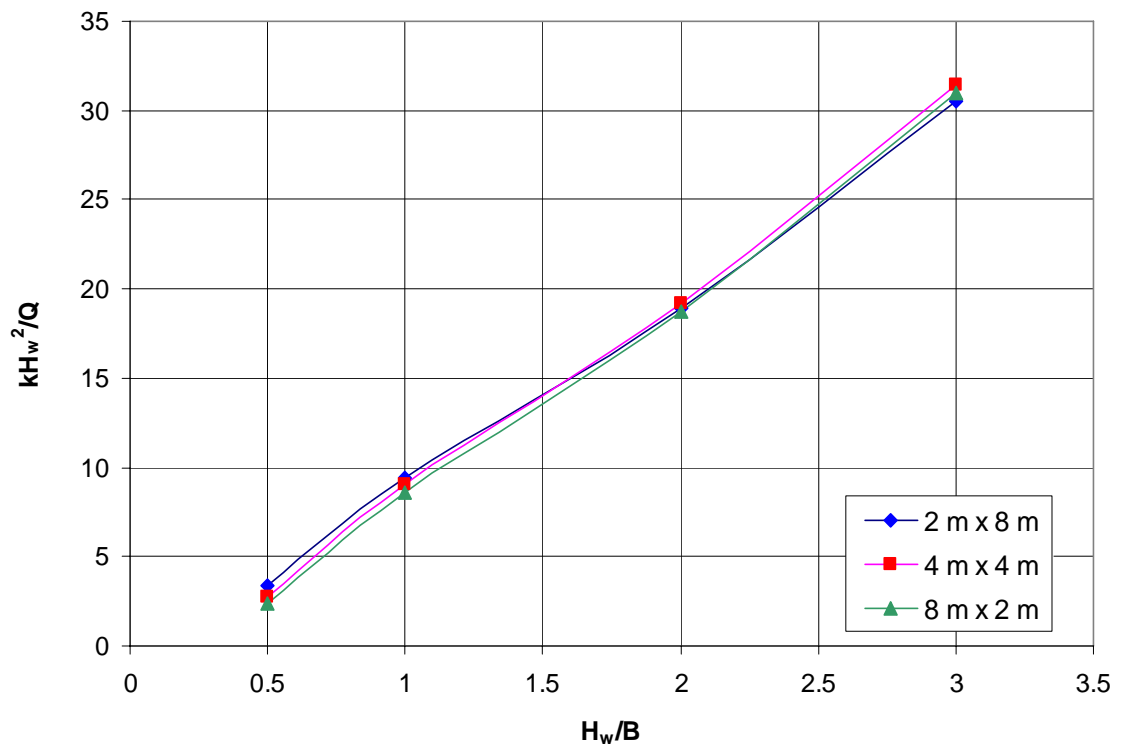
Fig. 4.6. Effect of drain shape on discharge measurements

From Fig 4.5, it is evident that for the geometries investigated, drain shape has negligible effect on pore pressure measurements within the three dimensional stope. Fig. 4.6 illustrates the effect of drain shape on discharge and shows that drain shape also has minimal influence on discharge when placed at the centre of the stope. However the drain shape has more effect on discharge when $H_w/B \leq 1$, then when H_w/B >1 at this drain location.

4.3.2.2 *Drain Location*

Sivakugan et al. (2005) showed using *FLAC* (2002) that even in the presence of sub level drains, most of the drainage occurs through the bottom drains; which is commonly observed in the mines too. Therefore, the drainage through hydraulic fills was studied by neglecting the flow through all upper drains. Only stopes with drains located at the base of the stope are considered within this dissertation.

To investigate the effect of drain location on pore water pressure and discharge measurements, two scenarios were considered and are illustrated in Fig 4.7. These include:

1) Centre square drain, Fig 4.7 (a)
2) Corner square drain, Fig 4.7 (b)

(a)   (b)
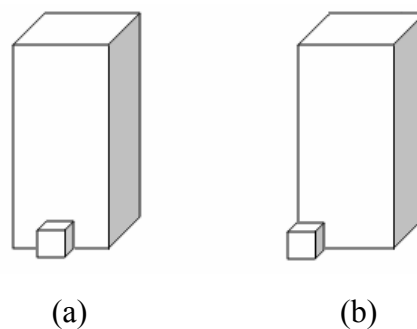
Fig 4.7. Drain Location Analysis (a) Centre Square drain (b) Corner square drain

Fig. 4.8 and Fig. 4.9 illustrate the effect of drain location on maximum pore water pressure and discharge measurements. From Fig. 4.8, it can be concluded drain location has negligible effect on the maximum pore pressure within a three-dimensional hydraulic fill stope when it is placed at the bottom of the stope face, as shown in Fig. 4.7. However, as shown in Fig. 4.9, drain location does have an influence on discharge measurements.
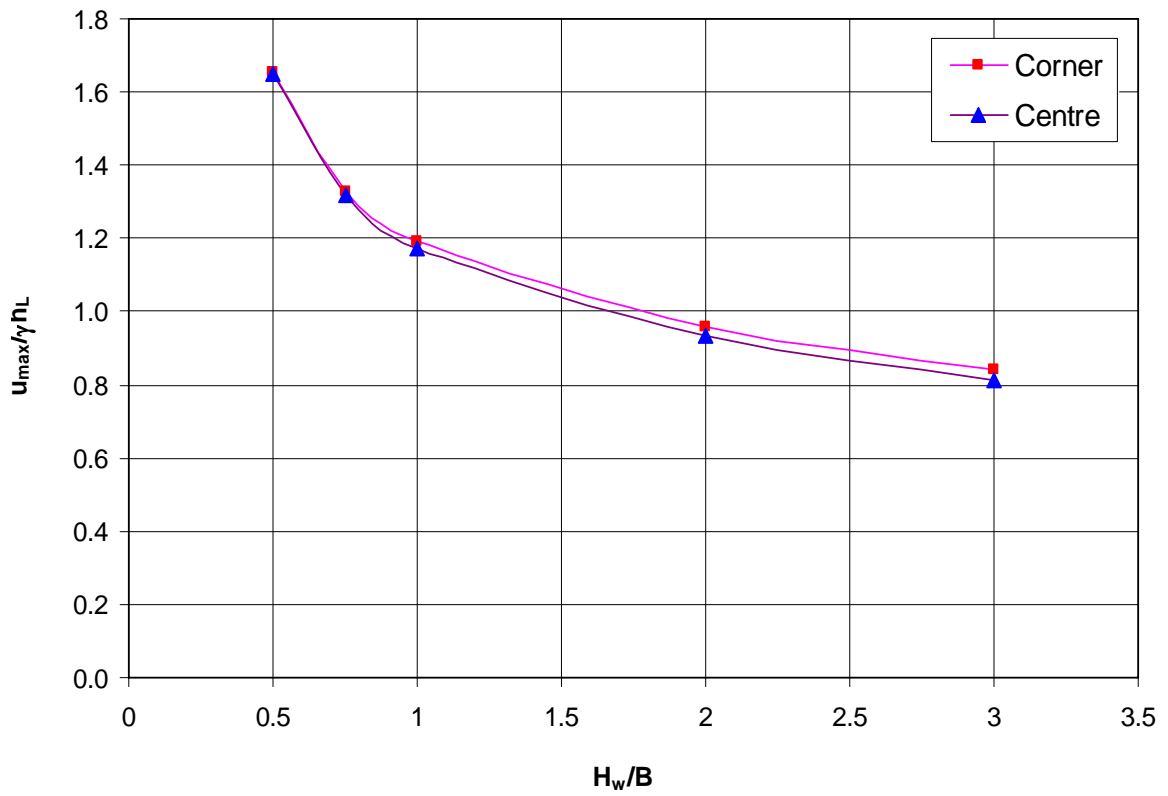
Fig 4.8. Effect of drain location on maximum pore pressure measurements
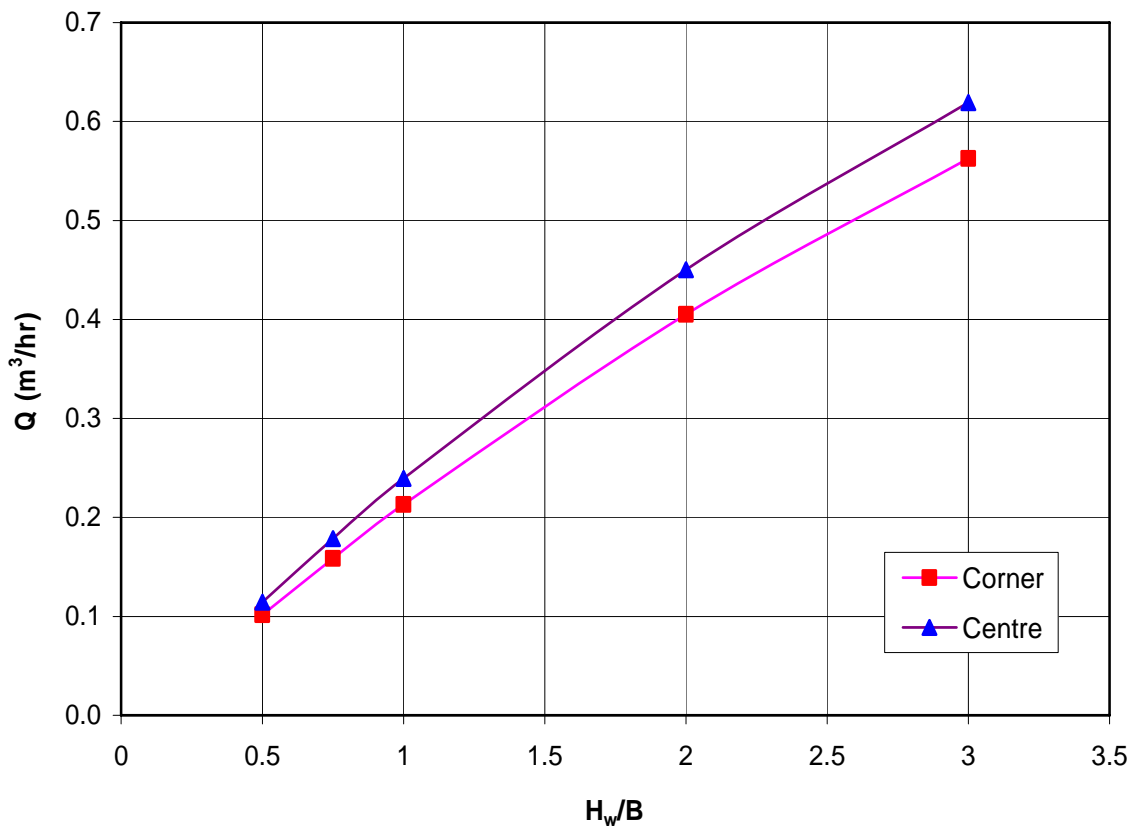
Fig. 4.9. Effect of drain location on discharge measurements

For the square drain modeled in Fig. 4.9, the centre drain consistently produced discharge approximately 10% greater than that of the corner drain. If we investigate the drain shapes discussed in section 4.3.2.1, we notice that the drain shape has an increased influence on discharge measurements when placed at the corner.

.

Table 4.2 summarizes the effect of varying drain locations and drain shapes on discharge measurements.

Table 4.2. The effect of drain location and drain shape on discharge measurements

Case	Geometry (m)						Corner		Centre		% Difference	
	H_w	B	W	X	D	F	u_{max} (kPa)	Q (m^3/hr)	u_{max} (kPa)	Q (m^3/hr)	u_{max}	Q
1	10	20	20	4			97.7	0.081	97.4	0.093	0.33	12.98
2	15	20	20	4			144.2	0.141	142.9	0.164	0.89	13.70
3	20	20	20	4	8	2	187.9	0.199	185.3	0.230	1.41	13.40
4	40	20	20	4			339.4	0.403	329.5	0.457	3.01	11.98
5	60	20	20	4			462.2	0.568	443.1	0.637	4.31	10.84
6	10	20	20	4			97.5	0.102	97.1	0.115	0.44	11.17
7	15	20	20	4			143.5	0.158	142.2	0.179	0.96	11.30
8	20	20	20	4	4	4	186.8	0.213	184.3	0.239	1.37	11.09
9	40	20	20	4			337.9	0.405	329.3	0.450	2.64	10.01
10	60	20	20	4			461.8	0.563	445.6	0.619	3.64	9.11
11	10	20	20	4			97.3	0.120	96.9	0.128	0.40	6.22
12	15	20	20	4			142.8	0.180	141.7	0.192	0.78	6.38
13	20	20	20	4	2	8	185.4	0.236	183.5	0.252	1.02	6.26
14	40	20	20	4			333.2	0.435	327.4	0.460	1.75	5.62
15	60	20	20	4			453.2	0.596	443.0	0.628	2.32	5.10

From Table 4.2, the following trends were present:

- As the H_w/B aspect ratio increases, the percent difference in discharge between the centre and corner drains is decreased.
- As the D/F ratio decreases, i.e. the drain is 'flattened' along the stope face; the difference in discharge between the centre and corner stopes is decreased.

- An increase in the percent difference of the maximum pore water pressure measurements is observed between the centre and corner drains with increasing H_w/B ratios

4.3.2.3 *Stope Shape*

To investigate the effect of stope shape on maximum pore water pressure and discharge measurements numerous $FLAC^{3D}$ models, for a wide range of stope dimensions were undertaken. The values of maximum pore pressure and discharge were recorded for each of these cases and shape factors were developed to take account of the varying W/B ratios. The shape factor coefficient given in Eq. 4.18, is applied to non-square stopes (i.e. where $W/B \neq 1$).

Therefore, to calculate the maximum pore water pressure and/or discharge for a non-square stope, the following steps are performed:
- Initially the problem assumes a square based stope with plan area of $B \times B$. The flow rate and pore water pressure are calculated using Eq. 4.4 and Eq. 4.15 respectively.
- The shape factor is then multiplied to these equations to approximate the discharge and pore water pressure for the non-square stope (refer to Eq. 4.19 and Eq. 4.20).

Simulations were undertaken for both corner and centre drain arrangements and based on cases where $W/B \geq 0.5$.

$$s = \left(\frac{W}{B}\right)^{0.11} \tag{4.18}$$

For non-square stopes the maximum pore pressure and discharge are calculated by Eq. 4.19 and Eq. 4.20.

$$u_{max} = \left(\left[h_L\left(\frac{\alpha_{3D}\Gamma_2 + \Gamma_3}{\Gamma_1 + \Gamma_2 + \Gamma_3}\right) + G\right]\gamma_w\right) \times s \tag{4.19}$$

$$Q = \left(\frac{kh_L^2}{\Gamma_1 + \Gamma_2 + \Gamma_3} \right) \times s \qquad (4.20)$$

These analytical solutions have been validated later in the chapter in section 4.5.

4.3.3 Scaling Effect on three-dimensional Method of Fragments

When a stope is scaled by a factor of x as shown in Fig. 4.10, all length dimensions of the stope are scaled by x (i.e. xB, xH_w, xW, xD, xF etc) and head losses are scaled by x (xh_L). Substituting these scaled values into Eq. 4.4 and Eq. 4.15, results in the flow rate being scaled by x^2 and the pore water pressure at any point in the flow domain being scaled by x. When the scaled geometries are substituted into the three-dimensional form factor equations, the form factors remain the same, as in the case of two-dimensional fragments. For example, when a prototype hydraulic fill stope is scaled down to a 1/50 laboratory model, the pore water pressures are scaled by 1/50 and the flow rate is scaled by 1/2500.
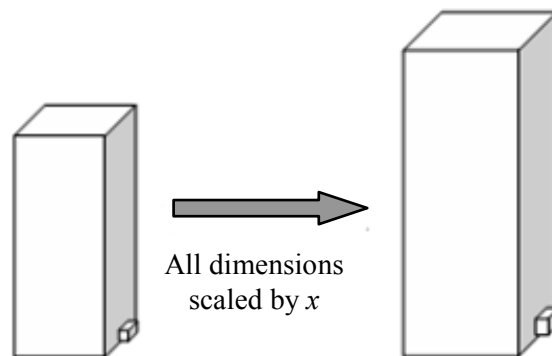
Fig. 4.10. Scaled three-dimensional stope

4.3.4 Summary of Equations

The expressions for computing the form factors, maximum pore water pressure and flow rate within a three-dimensional stope are summarized in Table 4.3.
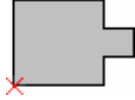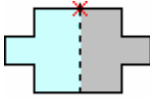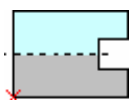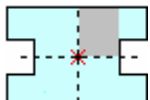
Table 4.3. Equations for three-dimensional hydraulic fill stopes

Parameter	Equation		
Form Factor for fragment 1 Γ_1		$\Gamma_1 = \dfrac{(H_w - B)h_L}{B^2}$	
Form Factor for fragment 2 (Fig. 4.3) Γ_2	$\dfrac{H_w}{B} \geq 1$	$\Gamma_2 = a\left(\dfrac{H_w}{B}\right)$	
	$\dfrac{H_w}{B} < 1$	$\Gamma_2 = a\left(\dfrac{H_w}{B}\right)^b$	
	where:	$a = 0.82\left(\dfrac{D}{B}\right)^{-1.1}$ $b = 1.142e^{3.2\left(\frac{D}{B}\right)}$	
Form Factor for fragment 3 Γ_3		$\Gamma_3 = \dfrac{(X - 0.5G)h_L}{G^2}$	
Fraction of head lost in fragment 2 (Fig. 4.4) α_{3D}	$\dfrac{H_w}{B} \geq 1$	$\alpha_{3D} = 1 - 0.56\left(\dfrac{D}{B}\right)$	
	$\dfrac{H_w}{B} < 1$	$\alpha_{3D} = \left(-0.8\left(\dfrac{H_w}{B}\right) + 0.24\right)\left(\dfrac{D}{B}\right) + 1$	
Maximum Pore Pressure u_{max} (kPa)		$u_{max} = \left[h_L\left(\dfrac{\alpha_{3D}\Gamma_2 + \Gamma_3}{\Gamma_1 + \Gamma_2 + \Gamma_3}\right) + G\right]\gamma_w$	
Discharge Q (m³/hr)		$Q = \dfrac{kh_L^{\,2}}{\Gamma_1 + \Gamma_2 + \Gamma_3}$	
Shape Factor S		$s = \left(\dfrac{W}{B}\right)^{0.11}$	

4.4 Possible Drain Arrangements

In hydraulic fill stopes, there can be more than one drain at any level and they can be placed at the centers or corners of the stope face. There are an infinite number of possible stope and drain geometry and size combinations, and therefore only a few typical arrangements and dimensions have been studied. Table 4.4 illustrates four common drain arrangements and their corresponding shape factors. The lines of symmetry used in the analysis, are shown as dashed lines and the point of maximum pore pressure is shown by the red cross on each of the cases shown in Table 4.4. These coefficients were obtained by considering the symmetry of the drain arrangements and the shape factor coefficient given in Eq. 4.18.

Table 4.4. Four common cases and corresponding equations for various Drain Arrangements**

Case	Plan View of Case	Shape Factor	Maximum Pore Pressure	Discharge
Case 1		1.00	$u_{max} = (u_{max})_{\text{case 1}}$	$Q = Q_{\text{case 1}}$
Case 2		0.93	$u_{max} = 0.93(u_{max})_{\text{case 1}}$	$Q = 1.85Q_{\text{case 1}}$
Case 3		1.08	$u_{max} = 1.08(u_{max})_{\text{case 1}}$	$Q = 2.16Q_{\text{case 1}}$
Case 4*		1.00	$u_{max} = (u_{max})_{\text{case 1}}$	$Q = 4Q_{\text{case 1}}$

* Use B/2 and W/2 for stope width and length as shown by shaded region, in computing flow rate and maximum pore water pressure.

** Cross section of stope and drain are assumed to be square

It should be noted, that because of the symmetry between some geometric configurations, these results may be used to provide discharge and pore pressure predictions for other stope arrangements.

4.5 Validation of MOF³ᴰ Analytical Solutions of Varying Stope Geometries

To verify the numerical integrity of the predictions of flow rate (Eq. 4.4) and maximum pore water pressure within the stope (Eq. 4.15), for square and non-square sections, a series of drainage problems were simulated for a number of stope geometries. Randomly selected values of H_w, B, W, X, D and F were used in this study to ensure that regardless of the stope and drain geometries, the above equations provide satisfactory solutions for the flow rate and maximum pore water pressure within a three-dimensional stope.

The maximum pore water pressure within the stope and the flow rate were computed using the equations and $FLAC^{3D}$, and the values are compared in Fig. 4.11 and Fig. 4.12 respectively. Since the situations when $H_w < B$ pose very little or no threat due to low values of flow rates and pore water pressures, most of the cases considered above were for $H_w > B$. From these two figures, it is evident that the proposed analytical solutions predicts the maximum pore water pressure and flow rate within 10% of what is given by $FLAC^{3D}$.
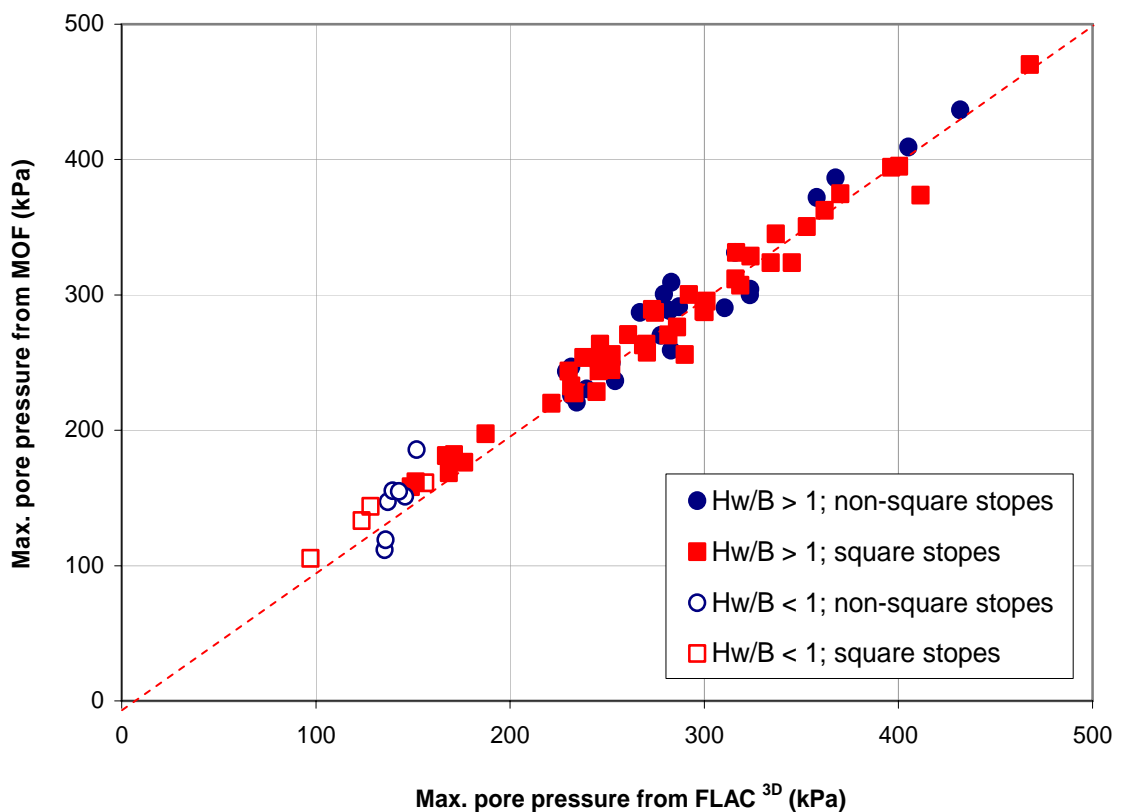
Fig. 4.11. Validation of pore pressure measurements for varying stope geometries
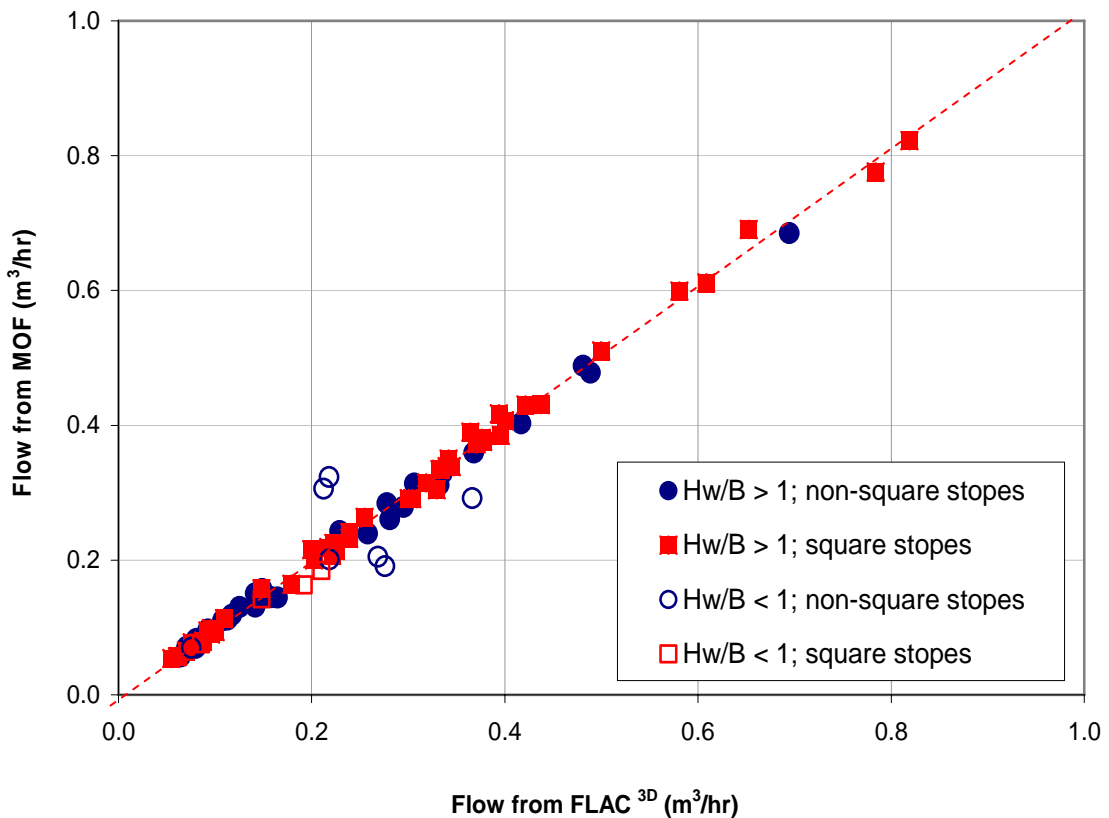
Fig. 4.12. Validation of discharge measurements for varying geometries

From Fig. 4.11 and Fig. 4.12, it is shown that when the height of water is greater than the stope width ($H_w/B > 1$), the equations given in Table 4.3 provide excellent agreement to those obtained from $FLAC^{3D}$ for both square and non-square stopes. When the height of water is less than the stope width ($H_w/B < 1$), the equations provide satisfactory agreement for square stopes. However, for non-square stopes with $H_w/B < 1$, the equations provide rough approximations.

4.6 Comparison of pseudo three-dimensional model with actual three-dimensional models

Chapter 3 discussed the use of a two-dimensional hydraulic filled stope. To mimic the three-dimensional problem in two-dimensions, an equivalent cross section of the drain, which falls within the typical range, was used. Three cases shown in Fig. 4.13 were investigated to determine the effect of simplifying the three-dimensional solution. It is important to note that when modelling this problem, an equivalent cross-section of the drain which falls within the typical range was used for all three models
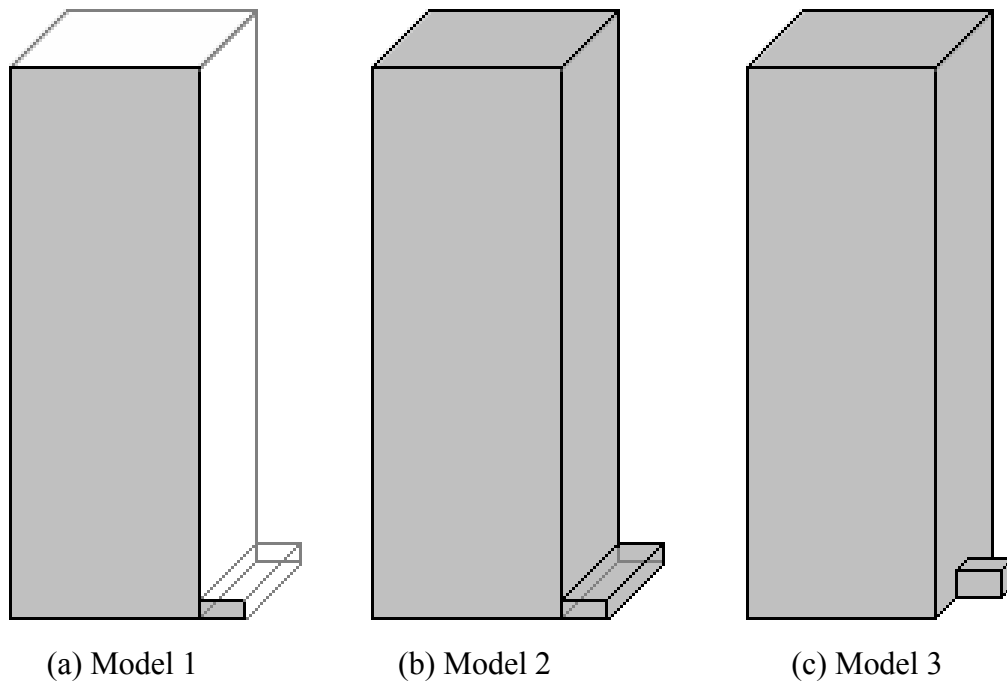
Fig. 4.13. Investigated two and three-dimensional models (a) Pseudo three-dimensional stope (b) Three-dimensional stope with long, flat drain (c) Three-dimensional stope with square drain of equivalent cross-section as Model 1 and 2

Model 1 illustrates a pseudo three-dimensional stope. Using *FLAC*, a simplified two-dimensional model is simulated. A stope depth equal to that of the stope width (*B*) was assumed and the two-dimensional discharge multiplied by the stope depth to obtain a pseudo three-dimensional discharge for the stope.

Model 2 was developed using *FLAC^{3D}* and contains the actual geometry of the pseudo three-dimensional model simulated in Fig 4.13 (a). That is, using *FLAC^{3D}* a three-dimensional stope with a drain of height and length equivalent to Model 1 and width equal to Model 3 was developed.

Model 3 consists of a three-dimensional stope with a single drain in the centre of one of the stope faces and contains an equivalent drain cross section to the models developed in Fig 4.13 (a) and (b).

Table 4.5 presents the results for the three models for a sample stope with $H_w = 40$ m, $B = 20$ m, $X = 4$ m and varying drain height depending on the model. (i.e. all drain cross-sections have equivalent cross-sectional area).

Table 4.5. Results of the investigated two and three-dimensional models

Model	Maximum Pore Pressure u_{max} (kPa)	Discharge (m^3/hr)
1	290.5	0.436
2	290.9	0.435
3	297.7	0.409

The results shown for the sample problem indicate that a pseudo three-dimensional problem simulated in two-dimensions provides a reasonably good approximation for three-dimensional stopes with equivalent cross-sections. However, there are numerous limitations for this pseudo three-dimensional solution including:

- Varying stope width to depth aspect ratios cannot be simulated,
- Varying drain locations,
- Varying drain arrangements,
- Varying drain geometries.

4.7 Physical Modelling of Flow through a Hydraulic Filled Stope

Physical modeling of flow through a hydraulic filled stope was undertaken using a scaled model and compared with the three-dimensional analytical solutions presented in Table 4.3 and also compared to numerical simulations undertaken in $FLAC^{3D}$.

The basis of all physical modelling is the idea that the model behaves in a manner similar to the prototype it is intended to emulate. Prototype usually refers to the real object whereas model refers to a scaled form of the prototype. A properly validated physical model can be used to predict the prototype under a specified set of conditions. This important concept allows us to perform model studies to obtain information that will aid in the design of the prototype and therefore avoid costly mistakes.

Prior to physical modeling, a dimensional analysis of the two systems was undertaken to ensure similitude between model and prototype.

4.7.1 Similitude and Dimensional Analysis

Similitude is a concept used in the testing of engineering models. A model is said to have similitude with the real application if the two share:

- Geometric similarity – The model is of the same shape as the application (usually scaled).

- Kinematic similarity – Fluid flow of both the model and prototype must undergo similar time rates of change motions (fluid streamlines are similar).

- Dynamic similarity – Ratios of all forces acting on corresponding fluid particles and boundary surfaces in the two systems are the same.

Using similitude, the flow through a scaled laboratory model of a three-dimensional hydraulic fill stope was investigated.

Geometric similarity is a similarity of shape. For a model and prototype to be geometrically similar they must have similarity of shape as well as similarity of solid boundaries that control the flow of a fluid. Simply, to satisfy this condition, the ratios of the respective lengths in the model and its prototype must be the same. The geometry of the scaled laboratory model consisted of a square based stope with one drain located centrally along the base of one of the stope walls with a scale ratio of 1/100. i.e. 1 cm in the laboratory model represented 100 cm in the prototype.

Kinematic similarity implies that, in addition to geometric similarity, the ratio of the *velocities* at all corresponding points in the flows are the same. That is, the velocities in the prototype (v_p) are equal to those in the model (v_m). Therefore, using Darcy's law:

$$v_m = v_p$$

$$\therefore k\left(\frac{\Delta h}{L}\right)_m = k\left(\frac{\Delta h}{L}\right)_p \tag{4.21}$$

Since the same soil is used for both model and prototype, the permeability (k) is the same. Also, assuming the model is scaled to $1{:}x$, the change in head (Δh) and length of flow path (L) are scaled to $1/x$, thus the hydraulic gradient remains the same at corresponding points in the model. Therefore, the seepage velocity remains the same, regardless of scaling.

For a model and prototype to be dynamically similar, they must have similarity of forces acting on the model through the flow. Obviously, to satisfy this condition there must also be geometric and kinematic similarities. There are many forces that affect fluid flow but in most cases, all of them may not exist or may be insignificant. So, a good understanding of the fluid phenomenon under study is necessary to determine the irrelevant forces. With such knowledge, the number of variables affecting a flow problem can be arranged into suitable dimensionless groups by dimensional analysis and insignificant parameters can be dropped out. By keeping the most important parameters the same for both model and prototype, we can simplify the analysis of the problem.

Butterfield (2000) described the general form of a typical soil-fluid flow problem in which flow occurs through a system of specific geometry, driven by a fluid head differential Δh, under a gravitational acceleration g. The absolute size of the system is fixed by a characteristic dimensional L as shown in Fig. 4.14.

For a general steady-state flow problem as described in Fig 4.14, Butterfield (2000) produces a list V of 16 variables required to define such a system:

$$V = \left\{\Delta h, L, D_s, \rho_s, \rho_w, \kappa, f, v, \mu, g, \sigma', u, m, \omega, \varphi', c'\right\} \tag{4.22}$$

where Δh equals the fluid head differential; L is the length of system; D is the characteristic particle dimension, which also characterizes a specific grading of
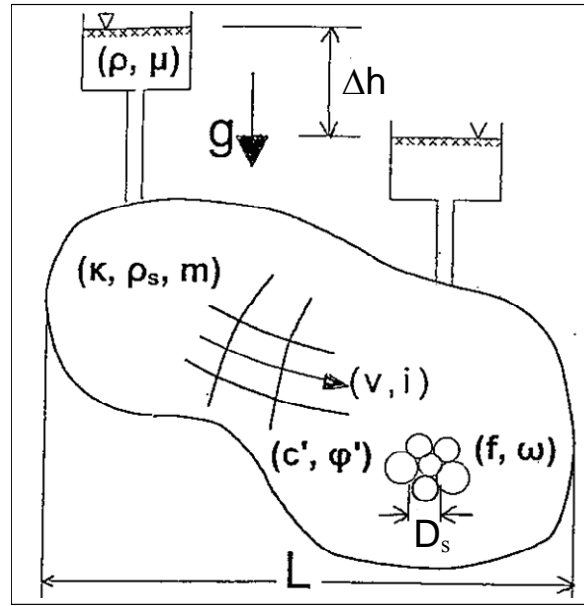
Fig. 4.14. General Form of the typical soil-fluid-flow problem (Butterfield, 2000)

particle sizes and shape; ρ_s is the soil grain density; ρ is the fluid density; κ is the intrinsic permeability; f is the soil fabric, signifying all aspects of its structure; v is the seepage velocity; μ is the kinematic fluid viscosity; g is the gravitational acceleration; σ' is the current effective stress regime, (in steady-state conditions this will not vary with time); u represents the pore water pressure; m equals soil compressibility; ω is fluid surface tension; φ is the effective stress frictional parameter; and c' is the effective stress cohesional parameter.

To simplify for dimensional analysis, Butterfield rearranged these 16 variables into 12 dimensionless groups. Using Buckingham pi theorem, Butterfield (2000) provided the following dimensionless groups (DG):

$$DG = \left\{ \frac{\Delta h}{L}, \frac{L}{D_s}, f, \frac{\rho_s}{\rho_w}, \frac{\sigma'}{\rho_s gH}, \frac{\sigma'}{\mu}, \sigma' m, \varphi', \frac{c}{\sigma'}\kappa, \frac{\rho vd}{\mu}, \frac{v^2}{gd}, \frac{\omega}{\sigma' d} \right\} \qquad (4.23)$$

For the model and prototype to be truly dynamically similar, all the dimensionless groups listed in Eq. 4.24 should be identical. However, as discussed previously, in

many cases not all forces acting on the model through the flow are significant and insignificant parameters can be dropped out. Butterfield (2000) provided an extensive dimensional analysis for each of the dimensionless groups above. This chapter is only concerned with the flow through a particular soil type (hydraulic fill); therefore, a new dimensional analysis was undertaken.

Douglas et al. (2001) investigated the study of flow through granular media and provides the following list of variables:

$$v = f\left(\rho, D_s, \mu, g, e, i\right) \tag{4.24}$$

where v is the seepage velocity based on the flow divided by the seepage area, D is the assumed particles size, ρ is the fluid density, μ is the kinematic fluid viscosity, e is the void ratio and i is the hydraulic head driving the flow.

The following assumptions were made when analyzing the two systems:
- The flow of water in soils is considered incompressible because density changes can be neglected at ordinary stress levels for most geotechnical engineering applications (Holtz and Kovacs, 1981).
- Hydraulic fill is generally classified as silty sand or sandy silt, with less than 10% passing 10 μm in sieve analysis. Therefore, it is assumed the hydraulic fill behaves as a granular soil.
- Since the deslimed hydraulic fills are granular, the consolidation is almost instantaneous and the excess pore water pressure is assumed to dissipate immediately upon placement (Potvin et al. 2006, Clarke 1988, Isaacs and Carter 1983).
- In the flow through porous or granular media it is usual to exclude the effect of capillary action and concentrate upon gravity-driven flow (Douglas et al. 2001).
- Since the same material (soil) is being used in both model and prototype, it is assumed they contain the same grain size distribution. Therefore, the characteristic particle diameter D_s is the same for both model and prototype.

- The dimensional analysis assumes a fabric scale ratio of 1 (Butterfield 2000). That is the soil fabric for both model and prototype is the same. This condition is unlikely to be met due to the inherent individuality in soils; however the effect of this on flow through hydraulic fill is considered insignificant.

- Preliminary testing of the effect of stress versus permeability for various hydraulic fills (C4, D6, C3, D3, A2) was tested at James Cook University and is shown in Fig. 4.15 (Singh, 2007). The results illustrate that although there is slight change in permeability with increased stress, the overall permeability remained relatively constant. Therefore a constant permeability was assumed for the entire stope.
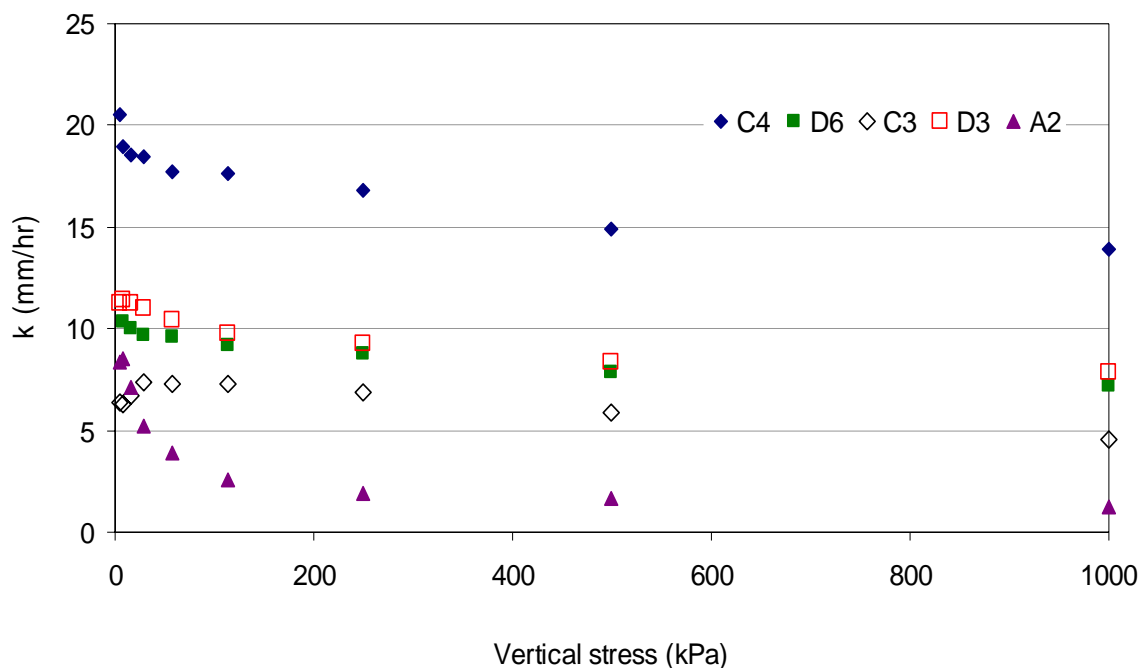
Fig. 4.15. Permeability versus vertical normal stress for various hydraulic fills tested at James Cook University (Singh, 2007)

- Surface tension forces are considered insignificant and ignored in the analysis.

- Since the same soil is being used in both systems, the permeability and soil particle density (ρ_s) for both model and prototype are considered equal.

- It is assumed that the water density remains the same for both systems. It should be noted that water density varies with temperature; therefore it is assumed both systems contain water at the same temperature.

- The way in which hydraulic fill is placed effects the size and nature of voids between particles thus affecting flow through a hydraulic filled stope. The greater the void ratio, the greater the permeability and thus the flow. However, research conducted by Carrier et al. (1983) states that if the solid particles are essentially sand to silt sized (e.g. hydraulic fill), the slurry material will sediment very rapidly to its final void ratio and very little consolidation will occur as additional materials are deposited above. Therefore, it is assumed that the void ratio will remain constant through the filling process even after additional materials are deposited above In situ and laboratory testing of hydraulic fill samples mimicking fill placement suggest void ratio values between 0.6 – 0.8 (Sivakugan et al. 2005).

Applying these assumptions, a list of parameters affecting flow through the hydraulic fill is given:

$$v = \{\rho_w, D, \eta, g, i, w, S\} \tag{4.25}$$

where v is the seepage velocity (m/s); D is the characteristic dimension, which is the effective diameter, D_{10}, of the soil grains; η is the dynamic viscosity (N.s/m^2); ρ_w is the density of water (kg/m^3); i is the hydraulic gradient, w is the moisture content; and S is the saturation of the hydraulic fill. It is important to note that the dimensional analysis and similitude carried out above, only applies to this case scenario i.e. flow through a hydraulic filled stope, where drainage is of primary concern. Using dimensional analysis and the Buckingham pi theorem, the following dimensionless groups were listed:

$$DG = \left\{ \frac{vD\rho_w}{\eta}, \frac{v^2}{gD}, S, w \right\} = \{Re, Fr, S, w\} \tag{4.26}$$

where Re is the dimensionless number known as Reynolds number and Fr is the dimensionless number referred to as Froude number. Therefore for specified moisture content for both models and assuming saturation, the dynamic similarity is:

$$\left(\frac{vD\rho_w}{\eta}\right)_{\text{prototype}} = \left(\frac{vD\rho_w}{\eta}\right)_{\text{model}} \qquad \text{and,} \qquad (4.27)$$

$$\left(\frac{v^2}{gD}\right)_{\text{prototype}} = \left(\frac{v^2}{gD}\right)_{\text{model}} \qquad (4.28)$$

As discussed in the assumptions the water used in both systems is assumed to be at constant temperature and thus ρ_w and η are equal for both systems. Gravity remains constant for both systems. Since the same fill is used in both, it can be assumed that the average diameter of the soil and permeability of the hydraulic fill is also equivalent. From kinematic similarity analysis, it is shown that the seepage velocity is also equivalent. Therefore, Reynolds and Froude numbers are equal in both systems and dynamic similarity is satisfied and similitude between the scaled laboratory model and prototype exists for the two systems when analyzing the flow through the hydraulic filled stopes.

4.7.2   Laboratory Setup

The laboratory model was designed and developed by the author and preliminary testing of the scaled stope was performed. Further testing was then carried out by the Hall (2006) and his more extensive results used in the analysis. The experimental apparatus shown in Fig 4.16 was constructed out of Perspex in the scale of 1:100. The model dimensions were 20 cm by 20 cm in plan area and 100 cm in height. A drive with dimensions of 4 cm by 4 cm was located at the bottom of the stope and is illustrated in Fig. 4.17. Several barricade attachments were constructed so as to enable laboratory testing of varying drain lengths (see Fig. 4.18). Note, the dimensions selected for the laboratory model were chosen, so as to represent a typical stope geometry in the mining industry (20 m by 20 m plan area at 100 m in height with a 4 m by 4 m drain).
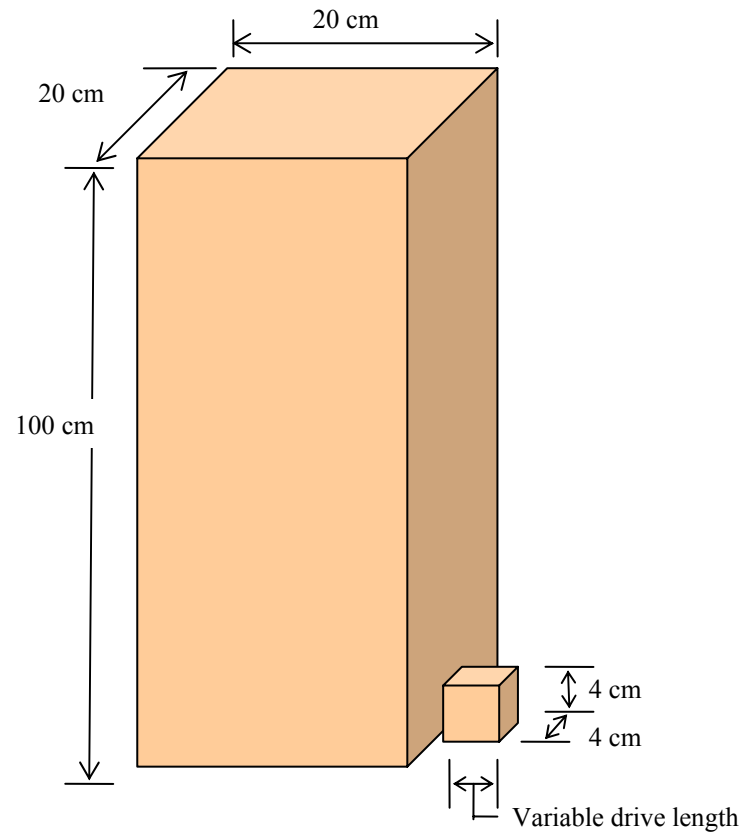
Fig. 4.16. Schematic diagram of Experimental Apparatus

20 cm

20 cm

100 cm

4 cm

4 cm

Variable drive length
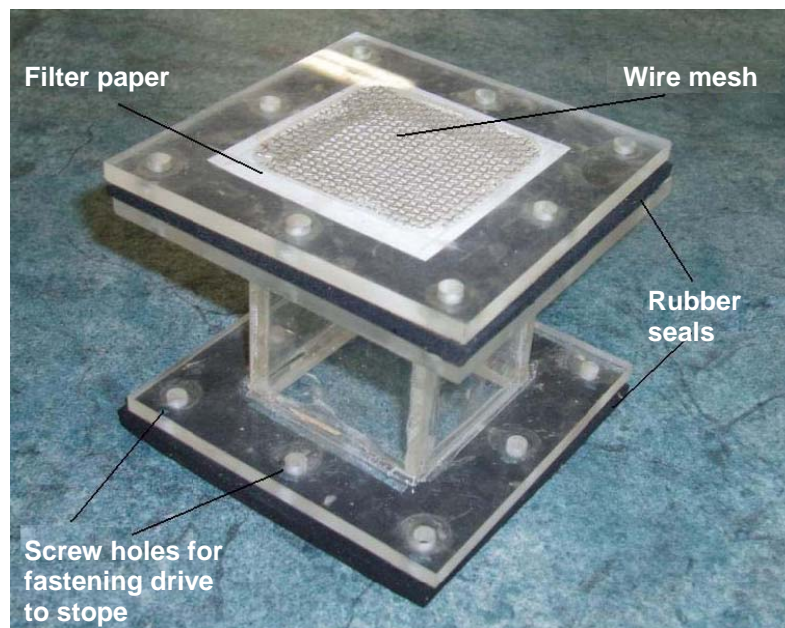
Fig. 4.17. Barricade (Hall, 2006)

Filter paper

Wire mesh

Rubber seals

Screw holes for fastening drive to stope
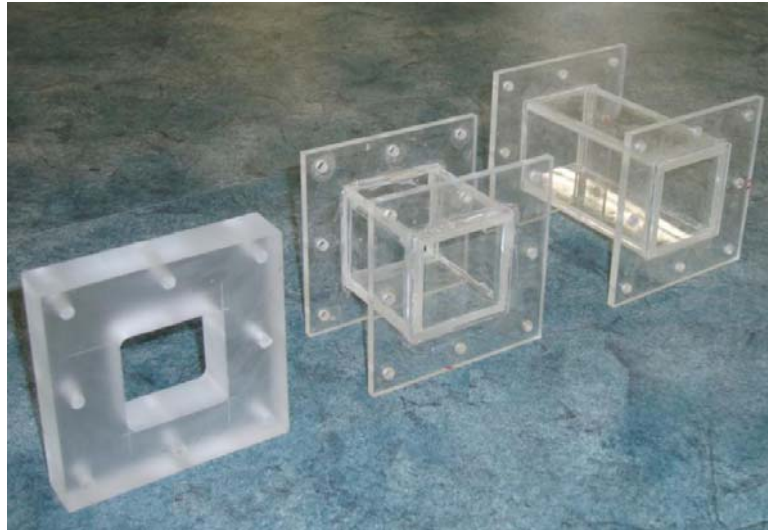
Fig. 4.18. Three different drain lengths of 5 cm, 20 cm and 14 cm (Hall, 2006)

Three different sand samples were used to fill the laboratory model to investigate the drainage in the three-dimensional stope. For each of the three samples investigated the following geometries were analyzed:

- Varying heights of material in the stope (*B, 3B, 5B* etc), and
- The location of barricade along the drive (5 cm, 10 cm, 14 cm).

The results obtained from the laboratory testing were compared with the three-dimensional closed form solutions given in Table 3.4 and numerical models developed in *FLAC³ᴰ*.

4.7.3 Sample material

Three samples labeled, S1 (dune sand), S2 (washed silica sand) and S3 (graded sand) were analyzed in the scaled laboratory model. Hall (2006) performed a number of standard procedures to determine the geotechnical parameters of the three types of sands. The tests and relevant Australian standards are:

- Grain Size Analysis (AS1289.3.6.1-1995),
- Particle Density Test (1289.3.5.1-1995),
- Maximum and minimum dry density tests (AS1289.5.5.1-1998),
- Moisture content test (AS1289.2.1.1-2005),

- Permeability Testing (Falling head AS1289.6.7.2-2001; Constant Head AS1289.6.7.1-2001).

Table 4.6 and Fig 4.19 provide a summary of the classification tests and grain size distribution for the three sand samples, showing the main parameters of interest. Hall then conducted several laboratory tests to determine the effect of relative density on permeability values and developed empirical relationships relating these parameters.

Table 4.6. Classification summary of sand samples

Sample	Description	D_{10} (mm)	C_c	C_u	G_s	e_{min}	e_{max}
S1	Dune sand	0.15	1.00	1.60	2.59	0.638	0.891
S2	Washed silica sand	0.18	1.24	3.06	2.62	0.575	0.819
S3	Graded sand	0.07	1.62	5.57	2.59	0.535	0.824
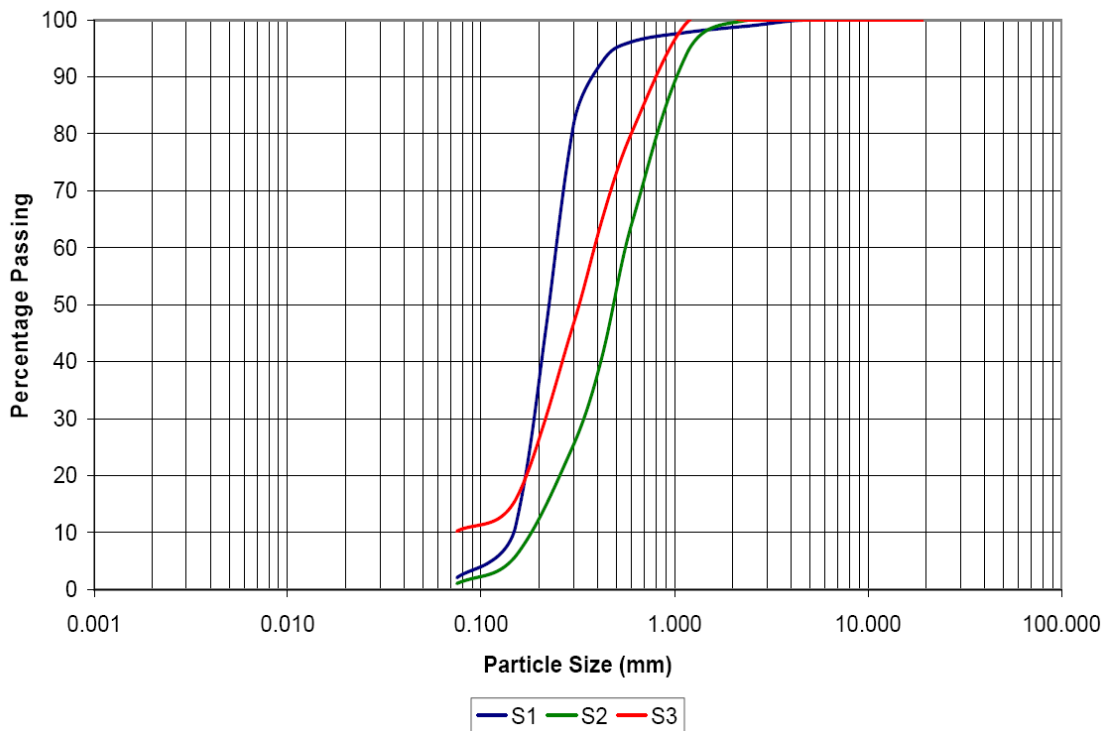
Fig. 4.19. Grain size distribution of sand samples (Hall, 2006)

Table 4.7 presents several empirical relationships developed by Hall (2006) for estimating the magnitude of permeability (cm/s) based on relative density for the three sands investigated.

Table 4.7. Hall (2006) empirical relationships

Sample	k - D_r Relationship
S1	$k = 0.032(D_r)^{-0.45}$
S2	$k = 0.047(D_r)^{-0.45}$
S3	$k = 0.042(D_r)^{-0.45}$

As expected, when the relative density of a soil increases, the permeability decreases. This is because as the relative density increases, the soil will become more compacted, thus will have a smaller amount of voids for water to flow through. Both constant head and falling head permeability tests were undertaken by Hall, however, the constant head permeability test data was used to develop the relationships relating the relative density and permeability of the various sand samples since this is the recommended permeability testing for granular materials. Table 4.8 presents the constant head permeability results for the various relative densities measured by Hall, 2006.

Table 4.8. Constant head permeability tests for various relative densities (Hall, 2006)

Sample	Dr (%)	k (cm/s) Measured	k (cm/s) Estimated (Table 4.7)	% Difference
S1-20	20.0	7.53E-03	8.31E-03	10.38
S1-40	40.2	6.58E-03	6.07E-03	7.74
S1-60	62.6	4.81E-03	4.97E-03	3.41
S1-80	84.4	4.65E-03	4.35E-03	6.49
S2-20	28.6	1.07E-02	1.04E-02	2.51
S2-40	40.3	8.73E-03	8.91E-03	2.02
S2-60	60.1	7.64E-03	7.44E-03	2.61
S2-80	80.2	6.40E-03	6.53E-03	2.10
S3-20	26.2	9.95E-03	9.66E-03	2.91
S3-40	45.7	7.38E-03	7.52E-03	1.91
S3-60	63.0	6.64E-03	6.51E-03	1.97
S3-80	76.4	5.38E-03	5.97E-03	10.94

As shown in Table 4.8, the variation of actual measured permeability values and those estimated using the formulas given in Table 4.7 vary by up to 11%.

4.7.4   Procedure

For the scaled laboratory testing, the following procedure was undertaken by Hall. Initially the vertical walls of the stope were marked at 20 cm intervals along the stope's height and the required drive length was attached to the stope using a screwdriver. The stope was placed on its support in the container of water so that the water surface was just at the top of the drain as shown in Fig. 4.20.

1. The stope was filled to a height of 20 cm with a known sample mass, so that the relative density could be calculated and therefore the permeability estimated using Hall's empirical relationships depending on the sand sample.
2. Water was then poured into the stope until there was a considerable amount of decant above the sand. The sample was allowed to saturate over time and it was paramount that no air was trapped in the drive of the stope.
3. When the sample was completely saturated, the water level was reduced so that it was just at the top of the sand. This was maintained during the experiment.
4. The mass of water escaping from the system was measured in five minute intervals, with the flow being recorded. To ensure steady-state was reached in the stope, several readings were recorded until a constant value was achieved.
5. The stope was then filled with more sand to a height of 60 cm and the procedure repeated.
6. Steps 3 – 5 were repeated with sand at a height of 100 cm.
7. The stope was then cleaned of the entire sand residue and the filter paper in the drain was replaced.
8. Steps 1 – 7 were then repeated using the remaining two samples.
9. The entire procedure was repeated again for each sample for the varying drain arrangements.

Fig. 4.20. Laboratory model stope setup

4.7.5 Numerical Modeling of Scaled Laboratory Stope

Using the *FLAC³ᴰ* numerical model developed by Rankine et al. (2003) as the base coding, simulations were developed for each of geometries investigated by Hall using the scaled laboratory model. To mimic the laboratory model, the required geotechnical parameters were determined in the laboratory (Hall, 2006) and were used as inputs in the numerical simulations. The output results from the program are summarized in Appendix E.

4.7.6 Interpretation of Results

Fig. 4.21 illustrates a comparison of the results obtained from the laboratory testing, numerical modeling and the closed form solutions derived and tabulated in Table 4.3. Refer to Appendix E for a table summary of these results.
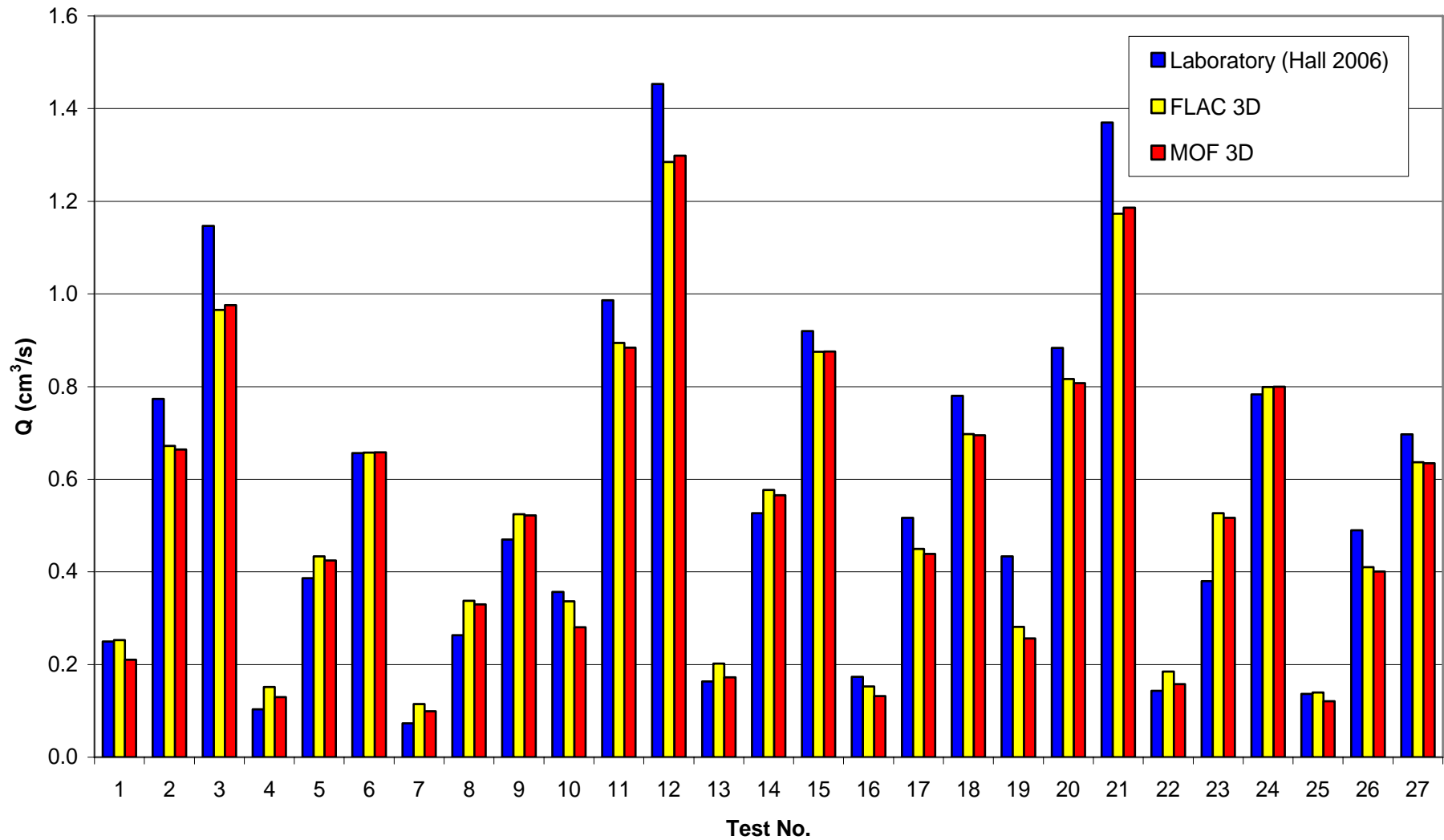
Fig. 4.21 Comparison between laboratory, numerical model and 3-D method of fragment solution

As shown in the figure, there is insignificant difference between the three methods of calculating flow. The slight discrepancies in Tests 3, 12 and 21 in Fig. 4.21, are most probably due to air bubbles in the drive or stope and/or leaks in the apparatus. However, these anomalies are only slight and in general, the results show excellent agreement between the various models and thus provide further verification of the closed-form solutions derived for the three-dimensional stope.

Fig. 4.21 illustrates several trends between the laboratory, numerical and analytical solutions these include:

- In general, the laboratory results tend to be more variable than the method of fragment solutions and the numerical results. This can be expected as the laboratory testing introduces human error, and relies on the experimenter obtaining a fully saturated test with no air voids.

- There are three significant anomalies in Fig. 4.21 shown in Test 3, Test 12 and Test 21. Possible sources of error for these tests include air voids in the apparatus, human error, and leakage in apparatus. In general, the results from the laboratory model tend to agree very well with the three-dimensional closed form solutions and the numerical simulations.

- For a given plan area, as the height of the saturated sand is increased in the model, the discharge is also increased. Instinctively, as the height of the saturated sand is increased, the hydraulic gradient increases, thus increasing flow in the laboratory stope.

- As the position of the barricade progresses further from the stope face, the rate of discharge decreases. It can be intuitively explained by saying that as the barricade gets further away from the stope, the flow path increases and the hydraulic gradient decreases. This results in the reduction in velocity and flow discharge. This has been observed in previous research conducted by Kuganathan (2001 a) and numerically by Rankine (2003).

As shown in Fig. 4.21, there are slight discrepancies between the results for each of the cases investigated. Since, the method of fragment equations can only provide approximate solutions, and the laboratory testing introduces human error, the

numerical modeling was assumed as the control when calculating percentage errors between the three models. Appendix E presents the percentage errors relative to the numerical modeling for all the results from the laboratory testing and the three-dimensional closed form solutions.

The overall average percent difference between the numerical model and the method of fragment solutions was 5.5% whilst the overall average percent error between the numerical model and the laboratory testing was 15.5%. A more detailed analysis of the variation in models is given in Table 4.9 and discussed below. The results have been broken down into two cases.

- Case 1: Investigates variation of H_w/B ratio. For each of the H_w/B cases investigated (H_w/B = 1, 3, 5), the X/D ratio was varied from 1.25 to 3.5. All three sand samples were considered when calculating the average percent difference.

- Case 2: Investigated the variation of X/D for all sand samples. For each of the X/D cases investigated (X/D = 1.25, 2.5, 3.5), the H_w/B ratio was varied from 1 to 5. All three sand samples were considered when calculating the average percent difference.

Table 4.9. Summarized comparison of percent difference in discharge results between the Numerical, Laboratory and MOF[3D] models for the varying stope geometries

Case study	Geometry		Average % difference for all sand samples	
	Hw/B	X/D	Laboratory - Numerical	MOF 3D - Numerical
Case 1	1	1.25 - 3.5	20.73	14.15
	3	1.25 - 3.5	15.27	1.81
	5	1.25 - 3.5	9.72	0.50
Case 2	1 - 5	1.25	15.97	5.42
	1 - 5	2.5	14.25	5.56
	1 - 5	3.5	15.51	5.48

From Table 4.9, the following trends were observed:

- In both comparisons (method of fragment solutions and the laboratory testing), the percentage error between the models increases as the H_w/B ratio decreases, particularly for the case when $H_w/B = 1$. As discussed in chapter 4, the closed form solutions gives greater error at H_w/B ratios less than or equal to 1. However, at these low H_w/B ratios, there is little concern with the pore pressure developments and liquefaction within the fill and the subsequent breach of the barricades. Therefore, these slight errors are deemed acceptable.

- Case 2 illustrates the variation of X/D on the discharge measurements. Both the laboratory-numerical model and the MOF[3D] – numerical cases illustrate little variation in percent difference for each of the X/D ratios investigated. The laboratory-numerical comparison contains an average of 14.25% - 15.97% error, whilst MOF[3D] – numerical model comparison vary from 5.42% – 5.56%.

- The method of fragment solutions produced less error in the discharge measurements than those obtained from the laboratory testing. This is a result of the same numerical package being used to model the laboratory stopes, as was used to develop the three-dimensional closed form solutions. Also, human error such as air voids in the laboratory apparatus may have contributed to the larger percent difference in the laboratory results. Another contributing factor which would have influenced the percent difference is the assumptions made during analysis.

4.8 Application of three-dimensional method of fragments

One of the primary purposes of developing equations for discharge and maximum pore water pressure for three-dimensional stopes was to provide quick and accurate solutions to the mining industry during the filling and drainage of the three-dimensional stope. Using *EXCEL* and the equations developed in this chapter, a user-friendly model was designed to simulate the drainage and filling of the stopes. The model, discussed in chapter 5, provides a user-friendly tool, for the mining industry

that can analyze the effects of varying stope geometries, input parameters and filling and draining cycles within a matter of seconds.

4.9 Summary and Conclusions

It was clear from various $FLAC^{3D}$ runs that the flow within the upper region of the stope, approximately above a height of B, is one-dimensional and vertical. Similarly, within the drain, at a distance greater than half the drain height, the flow is one dimensional and horizontal. This was also shown to be the case for two-dimensional stopes. On the basis of this observation, the flow domain was divided into three fragments, separated by equipotential surfaces, and form factors were developed for each fragment.

The three-dimensional model was first developed for a square stope with a single square drain in the middle at the bottom. It was shown through several $FLAC^{3D}$ runs that when the height of water is greater than the stope width ($H_w/B > 1$) the location of the drain on the base of the stope wall and the shape of the drain have little effect on the computed values of maximum pore water pressure and flow rate. However during the filling and drainage of the stope when the height of water is less than the stope width ($H_w/B < 1$) the location and shape of the drain have a noticeable influence on discharge and negligible effect on maximum pore water pressure.

A shape factor (Eq. 4.18) was proposed for non-square stopes, which is simply a multiplication factor on the flow rate and maximum pore water pressures computed assuming the stope is square with a stope plan area of $B \times B$. By considering the symmetry of drain arrangements, the proposed solutions can be applied to stopes with multiple drains at the bottom.

Initially the analytical solutions were validated against the predictions from $FLAC^{3D}$ and showed excellent agreement when the height of water was greater than the stope width for both square and non-square stopes. The analytical solutions developed for cases where the height of water was less than the stope width, displayed satisfactory agreement. However, for non-square stopes with $H_w/B < 1$, the equations provide

rough approximations and care should be taken when utilizing these equations for these cases.

Physical modelling was then conducted using a scaled laboratory stope and compared to the analytical solutions and $FLAC^{3D}$ simulations. The laboratory model was filled with three sand types for various geometries commonly observed in the mining industry. The results were compared with those obtained using the closed form solutions and numerical simulations. From these results, it was shown that:

- In general, the laboratory model provided satisfactory agreement between the closed form solutions and the numerical simulations developed in $FLAC^{3D}$.

- The discrepancies in the laboratory testing can be attributed to air voids within the testing apparatus and/or human error as well as the assumptions made in the three-dimensional method of fragment analysis.

- For a given plan area, as the height of saturated material is increased in the model, the discharge increases. Also, as observed by previous authors, as the position of the barricade progresses further from the stope face, the rate of discharge decreases.

- Taking into consideration the scaling of the stope, the laboratory model provides a useful means of calculating discharge measurements in actual stopes.

The laboratory model designed and tested provides further verification of the closed form analytical solutions. The method of modeling drainage through a scaled laboratory stope provides an adequate means of estimating the discharge, however, it was very time consuming and labour intensive and not recommended in practical mining applications. It is recommended that future modeling of drainage be undertaken using the three-dimensional method of fragments solutions, as these provide quick and reliable estimations of discharge.

CHAPTER 5

EXCEL MODEL

5.1 Overview

Using the analytical solutions developed for flow through three-dimensional hydraulic fill stopes, an EXCEL model was developed to accurately and efficiently model the drainage behaviour in three-dimensional stopes. The model simulates the complete filling and draining of the stopes and was verified using the three-dimensional finite difference program $FLAC^{3D}$ and the two-dimensional models Isaacs and Carter (1983) and Rankine (2005), and results showed excellent agreement. The model incorporates the complete filling and draining of the stopes and enables the user to input parameters such as filling schedule, slurry solids content, residual water content, geometry of stope, void ratio etc. This chapter investigates the variation and sensitivity in drainage behaviour and pore water pressure measurements with the fill properties and geometries of a three-dimensional hydraulic fill stope using the EXCEL model.

5.2 Verification Exercise

To verify the EXCEL spreadsheet a hypothetical problem was designed based on a simple in situ stope filling and draining regime. Results from the spreadsheet were compared and validated against results obtained from the identical simulation done in the existing two and three dimensional programs previously validated against in situ data. The verification exercise was designed to compare the water and tailings levels, the discharge during a specific filling schedule and the maximum pore water pressure development within the three-dimensional stope.

5.2.1 Problem Definition

A fictitious stope was designed based on typical input parameters, stope dimensions and fill properties, such that an identical data set could be used as input to provide a direct comparison between the two-dimensional Isaacs and Carter (1983) and Rankine

(2005) models; as well as the three-dimensional Rankine (2005) model that was developed in $FLAC^{3D}$.

5.2.2 Overview of Previous Drainage Models

Isaacs and Carter (1983) developed a computer program in FORTRAN for the analysis of drainage of a two-dimensional stope during hydraulic filling operations. Cowling et al. (1988) confirmed the validity of the seepage model developed by Isaacs and Carter through the back analysis of field measurements. Traves and Isaacs (1991) extended this model to three dimensions, but the model remains yet to be validated against field measurements. Rankine (2005) also developed a two-dimensional model to investigate the drainage of hydraulic fill stopes. The model developed in FLAC was used to compare the water and tailings levels and the discharge and pore pressure developments for a specific filling schedule of the two models. Later Rankine (2005) extended the model to three-dimensions using $FLAC^{3D}$. The numerical integrity of the program was verified using Isaacs and Carter (1983) two-dimensional model along with Rankine (2005) two and three-dimensional models. Pseudo three-dimensional models of the two-dimensional simulations (i.e. Rankine, 2005 and Isaacs and Carter, 1983) were utilized in the verification. These models consisted of a single drain located centrally along one wall as a two-dimensional problem; however, the drain is modeled as the full depth of the stope, with sufficient height to give an equivalent cross-sectional area as shown in Fig. 4.13 (b). These simulations were often time consuming and in most cases, specialist knowledge of the corresponding software package was required. Therefore a quicker and less complicated solution was desirable. Using the three-dimensional analytical solutions discussed in chapter 4, this chapter describes the use of an EXCEL spreadsheet that models the filling and draining of a three-dimensional stope.

5.2.3 Geometry and Boundary Conditions

As with previous models, the EXCEL model assumes that water enters at the top of the stope and exits through the drains and all other boundaries are assumed to be impervious. Also, the pore water pressure was assumed as zero along the fill barricade interface for all analyses.   For verification purposes, the EXCEL spreadsheet was

developed to model a square-based stope with a single square drain at the centre of one of the stope faces.

The geometry of the stope used in the verification exercise consisted of a 25 m wide 25 m thick stope at 150 m height. The stope contained one drain of cross-sectional dimensions 5 m x 5 m and was located centrally along the base of one of the stope walls (refer to Fig. 5.1). The two-dimensional program developed by Isaacs and Carter (1983) was not capable of modeling drain depth, therefore the depth was placed flush with the stope wall for all other models in the verification exercise to maintain consistency between the two and three-dimensional results.

The two-dimensional simplification to the drain geometry consisted of a 1m high drain flush with the stope wall (Fig 5.1 a) whilst the three-dimensional geometry consisted of a 5 m x 5 m drain flush with the stope as shown in Fig. 5.1 b. When comparing models, the two-dimensional stope was assumed to have a 25 m thickness, therefore providing an equivalent cross-sectional drain area of 25 m^2. This is referred to as the pseudo three-dimensional model and is given in Fig 5.2.
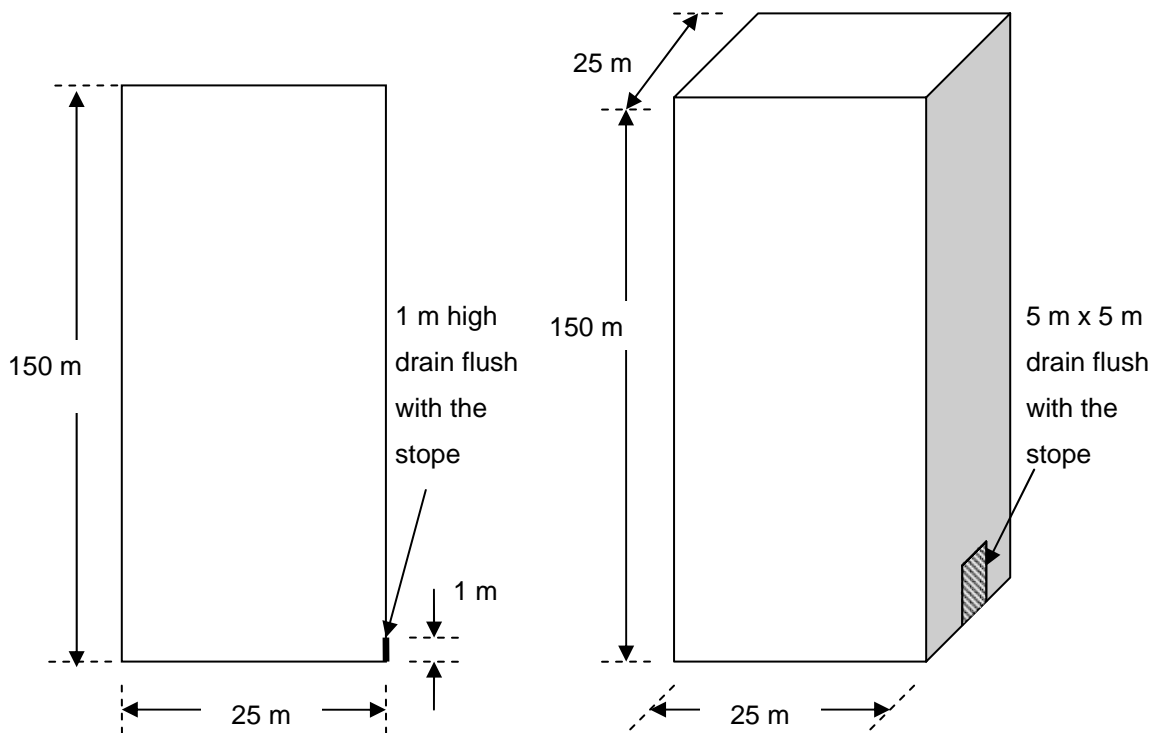
Fig. 5.1. Verification Geometry (a) Two-dimensional stope (b) Three-dimensional stope
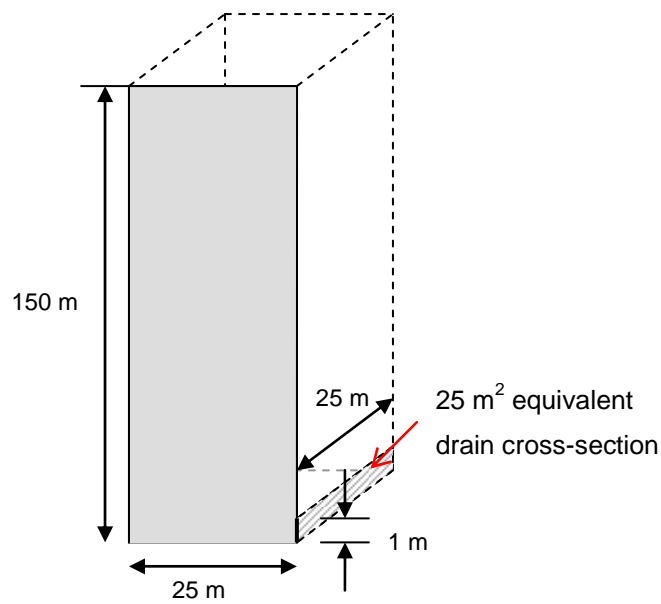
Fig. 5.2. Pseudo three-dimensional stope used for comparison of models

5.2.4 Input parameters

To ensure a direct comparison between each of the models, all material input parameters were identical for each of the four models used in the verification exercise and are given in Table 5.1. These models include:

- *FLAC* (Rankine, 2005),
- *FLAC^{3D}* (Rankine, 2005),
- Isaacs and Carter (1983), and
- EXCEL model.

Table 5.1. Input parameter for Verification Stope

Input	Value
Permeability, k	0.0054 m/hr
Specific gravity, G_s	2.9
Dry density of fill, ρ_d	1.4 t/m^3
Residual water content, w_{res}	25%
Percent solids of slurry placed	72%
Steady state time step	1 hour
Solids filling rate	250 t/hr
Filling cycle	12 hrs filling, 12 hrs resting

5.2.5 Simulation of filling schedule within stope

The filling schedule of the verification stope involved 12 hours of filling followed by 12 hours resting. The spreadsheet was cycled continuously until the fill height reached the height of the stope. To simulate this process in EXCEL, calculations were carried out at hourly intervals and the results were used to determine input conditions for the subsequent hour.

The fill height at each stage of solution was based on the quantity of dry tailings that had been placed into the stope at that given time. During filling, the fill slurry entered the stope and the fill height gradually increased by a height equal to the volume of dry hydraulic fill which would enter the stope for the input filling rate divided by the cross-sectional area of the stope. The volume of water in the stope was determined as the total volume of water that had entered the stope minus the total volume that had exited the stope, and provided the volume of voids within the fill matrix was larger than the volume of the water in the stope, the water level fell below the height of the fill. If the volume of water remaining in the stope was larger than the void volume, then there was decant water above the fill. With due consideration to these cases and the porosity of the fill, the water height was calculated for each hour. The quantity of discharge over this hour was recorded and added to the total water discharge from the stope for the calculation of water height for the next hour.   Once the tailings reached the height of the stope, the EXCEL model was solved as a continuously draining stope with calculations continued every hour.

It is important to note that no discharge calculations are performed until the hydraulic fill height passes the height of the drain i.e. in the very early stages of filling. Also, if decant water is present at the end of filling, it is assumed that the decant water drains from the top of the stope. i.e. the free water present as decant water is removed at the top of the stope.

5.2.6 Fill and water heights

Fig. 5.3 illustrates the water and fill heights during the first 500 hours of the filling schedule and the results compare very well for the verification exercise.   As shown in

Fig 5.3, the results illustrate a 'step-like' pattern which represents the pouring and resting of the hydraulic fill during the filling schedule. To amplify the difference between the programs, Fig. 5.3 was magnified over a 24 hour period and is shown in Fig. 5.4. Even when magnified, the comparison between all four models (*EXCEL, FLAC, FLAC^{3D}* and Isaacs and Carter) shows excellent agreement.
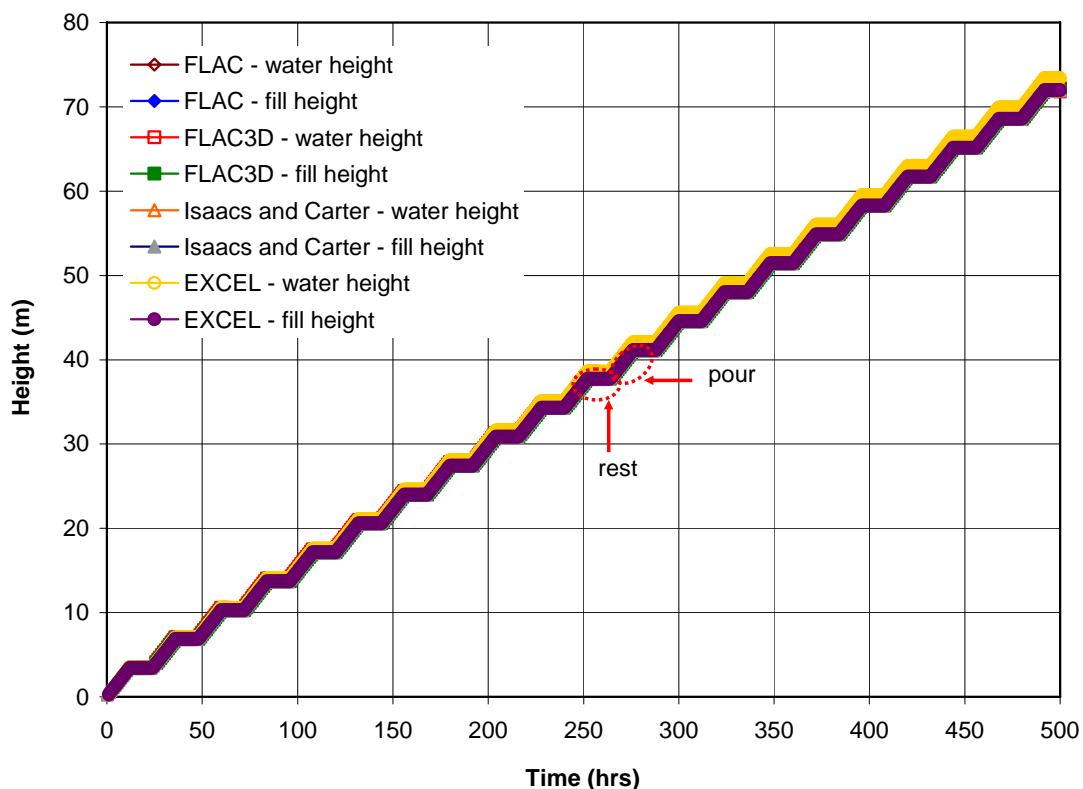
Fig. 5.3. Fill and water height comparison between Isaacs and Carter, *FLAC, FLAC^{3D}*, EXCEL for the verification problem

Fig. 5.5 illustrates the discharge comparisons for the first 500 hours of filling and resting of the verification stope. For the two-dimensional simulations (Isaacs and Carter and *FLAC*), the drain is modeled by extending it to the full length of the stope with sufficient height to give an equivalent cross-sectional area as the corresponding three-dimensional models as shown in Fig. 5.2. Thus, with the drain area located closer to the base and stretching the full depth of the stope, it is expected (and shown in Fig. 5.5) that the two-dimensional simulations would produce slightly higher discharge rates than the three-dimensional simulations.
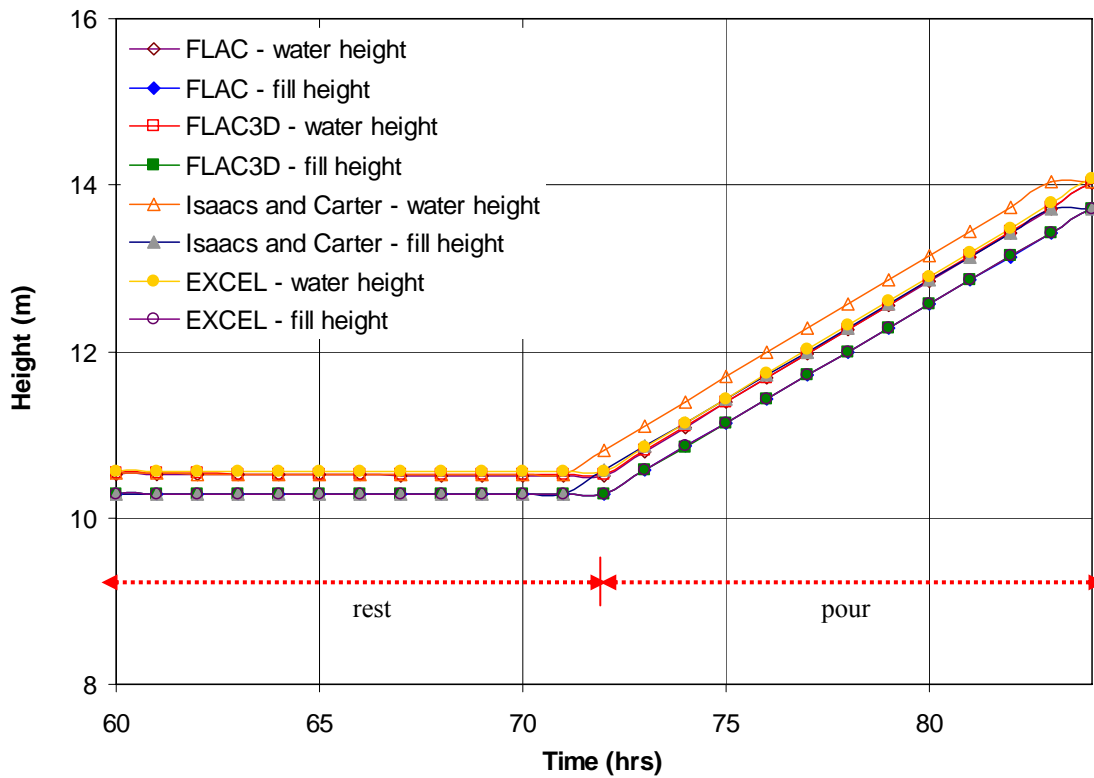
Fig. 5.4. Magnified fill and water heights for a 24 hour period
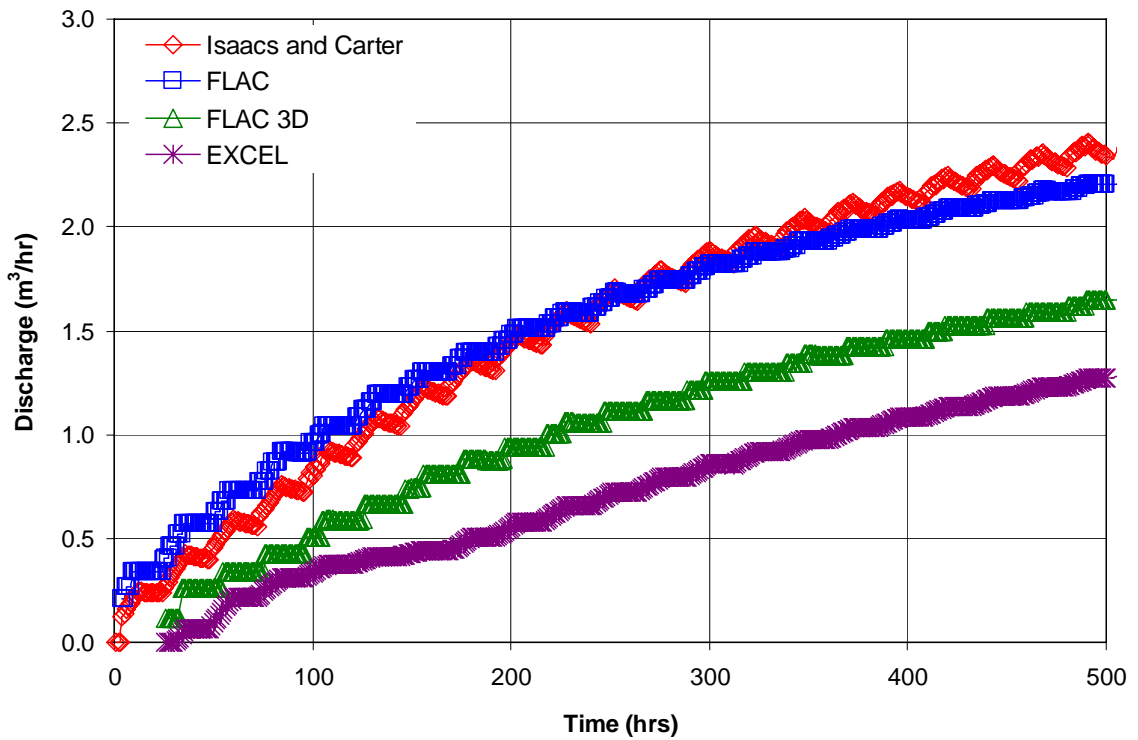
Fig. 5.5. Discharge rate comparison for between Isaacs and Carter, *FLAC, FLAC^{3D}* and EXCEL

To magnify the difference in discharge, Fig. 5.6 illustrates the initial 100 hours of the filling cycle.
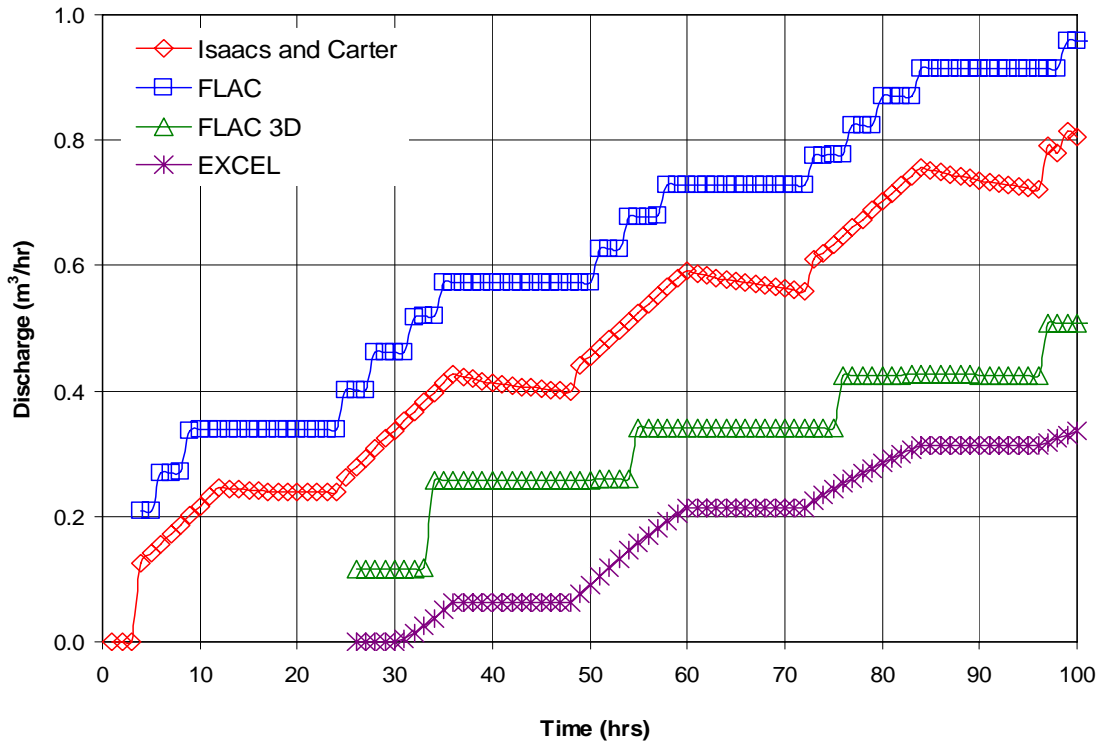
Fig. 5.6. Magnified discharge rate comparison for between Isaacs and Carter*, FLAC, FLAC^{3D}* and EXCEL

The discharge represents only a small proportion of the water in the stope; therefore the slight differences shown in Fig 5.5 and Fig 5.6 have little effect on the maximum pore water pressure measurements which are compared later in this chapter.

To investigate the effect of various filling schedules, numerous simulations of a three-dimensional stope with randomly selected values of geometry, filling schedules and geotechnical parameters were performed. Table 5.2 illustrates the inputs, for the range of stopes investigated, whilst Table 5.3 summarizes the results.

As shown from these tables, there is minimal difference in the maximum pore water pressure between the EXCEL and *FLAC^{3D}* simulations. The discharge values are also satisfactory, with a maximum variation of 8.2% between the two models.

Table 5.2. Input data for *FLAC³D* and EXCEL comparison

| Case | Dimensions (m) | | | | | | Filling Cycle | | | Input Parmaters | | | | |
	H_w	B	W	X	D	F	Solids Filling Rate t/m³	No. of hrs pouring	No. of hrs resting	k (m/hr)	G_s	ρ_d t/m³	w_{res}	% Solids of Slurry
1	40	16	16	4	6	6	240	8	16	5.40E-03	2.9	1.4	0.25	72
2	50	16	16	4	4	4	200	12	12	5.40E-03	3.5	1.7	0.25	75
3	40	20	20	4	4	4	240	12	12	5.40E-03	2.9	1.4	0.25	72
4	60	20	20	4	6	6	300	16	8	3.20E-03	4.3	1.7	0.25	70
5	40	16	16	4	6	6	240	12	12	5.40E-03	3.2	1.6	0.25	72

Table 5.3. Results for various simulations described in Table 5.2

| Case | *FLAC³D* | | EXCEL | | % Difference | |
	Q (m³/hr)	u_{max} (kPa)	Q (m³/hr)	u_{max} (kPa)	Q	u_{max}
1	0.596	251.7	0.631	250.2	5.9	0.6
2	0.470	347.3	0.488	345.1	3.9	0.6
3	0.440	330.2	0.449	334.3	2.0	1.2
4	0.536	374.1	0.580	361.3	8.2	3.4
5	0.596	251.7	0.616	246.6	3.4	2.0

5.3 Sequential Filling and Draining for Hydraulic Fill Stope Calculations

The fill and water heights for a particular filling schedule were calculated using simple phase relations, provided the material properties such as specific gravity, permeability, porosity of a settled fill and slurry water content are given. The input data of the EXCEL model can be broken down into three parts: dimensions, input parameters and filling schedule.

The input dimensions of the three-dimensional stope investigated within the EXCEL model are described below and are illustrated in Fig. 5.7.

- Height of stope, H_w, (m)
- Stope width, B, (m)
- Stope thickness, W, (m)
- Drain length, X, (m)
- Drain height, D, (m)
- Drain width, F, (m)
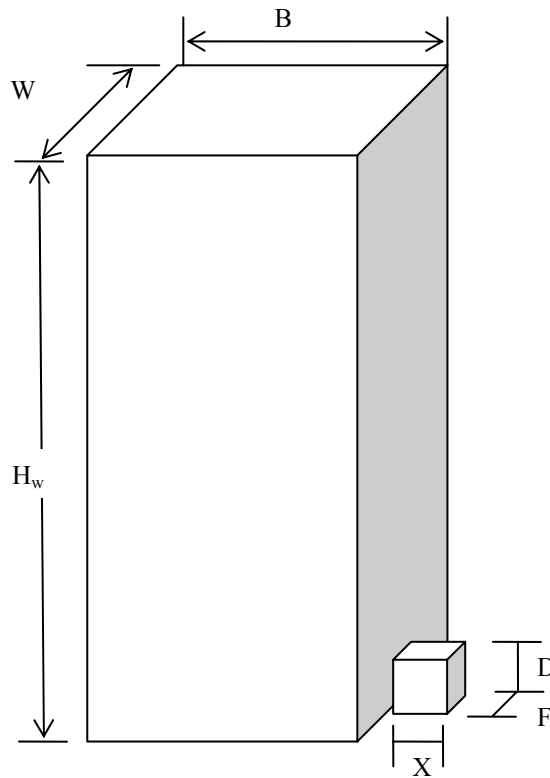
Fig. 5.7. Input dimensions of EXCEL model

From the geometry inputs, the EXCEL model calculates the stope base area (A), the equivalent drain height (G) and the head loss within the stope (h_L). These are given by:

Stope base area, $A = W \times B$

Equivalent drain height, $G = \sqrt{D \times F}$

Total head loss, $h_L = H_w - G$ (assuming datum at top of drain)

The geotechnical input parameters of the stope include:

- Permeability, k, (m/s)
- Specific gravity, G_s
- Dry density, ρ_d, (t/m^3)
- Residual moisture content, w_{res}
- % Solids of slurry, C_{slurry}

From the input parameters given above, the following properties were calculated:

Hydraulic fill void ratio, $e = \dfrac{n}{1-n}$ (5.1)

Hydraulic fill porosity, $n = 1 - \dfrac{\rho_d}{G_S}$ (5.2)

Saturation water content, $w_{sat} = \dfrac{e}{G_s}$ (5.3)

When the stope has fully drained, with all the free water removed, the water content is termed the residual water content (w_{res}). The residual water is not removed in engineering time and remains within the stope held within the voids. Previous recorded values range from 20% - 30%, therefore a residual moisture content of 25% was used for all models, unless otherwise specified.

The effective porosity (n_e) represents the voids that are effectively available to conduct water. The effective porosity can be written as:

$$n_e = n - \frac{G_s}{1+e} w_{res} \qquad (5.4)$$

The third section of input data is the filling cycle and includes the following inputs:

- Filling rate, R_s, (t/hr)
- Number of hours pouring, (hr)
- Number of hours resting, (hr)

Based on the input properties, geometry of the stope and the filling schedule the steady-state analysis of the filling and draining of the three-dimensional stope can be determined.

For a given stope arrangement,

Volume of fill, $V_f = AH_f$ $\qquad (5.5)$

Volume of solids, $V_s = AH_f(1-n)$ $\qquad (5.6)$

Mass of solids, $m_s = AH_f(1-n)G_s\rho_w$ $\qquad (5.7)$

Water content of slurry, $w = \dfrac{(1 - C_{slurry})}{C_{slurry}} \times 100\%$ $\qquad (5.8)$

Mass of water entering the stope, $m_w = m_s w$ $\qquad (5.9)$

Volume of water entering the stope, $V_w = AH_f(1-n)G_s\left(\dfrac{1 - C_{slurry}}{C_{slurry}}\right) = H_w An$ $\quad (5.10)$

To analyze the filling and draining of the stope, the EXCEL model performs calculations at hourly intervals, with each row in the spreadsheet assigned the values

for that specific hour. During the filling cycle, when the slurry is being poured into the stope, the fill height will increase by a constant height of J per hour. During the resting period fill height does not increase, but water height decreases due to the drainage from the stope drain. Assuming a constant filling rate i.e. the mass of solids poured per hour is R_s (t/hr)

The volume of solids poured per hour (V_s) is:

$$V_s(m^3 / hr) = \frac{R_s}{G_s \rho_w} = AH_f(1-n) \tag{5.11}$$

Rearranging Eq. 5.11, we can calculate the fill height increase per hour (J) in meters as:

$$J(m) = \frac{R_s}{G_s \rho_w A(1-n)} \tag{5.12}$$

To determine amount of water entering and leaving the stope, a water mass balance is analyzed. Refer to Fig. 5.8.
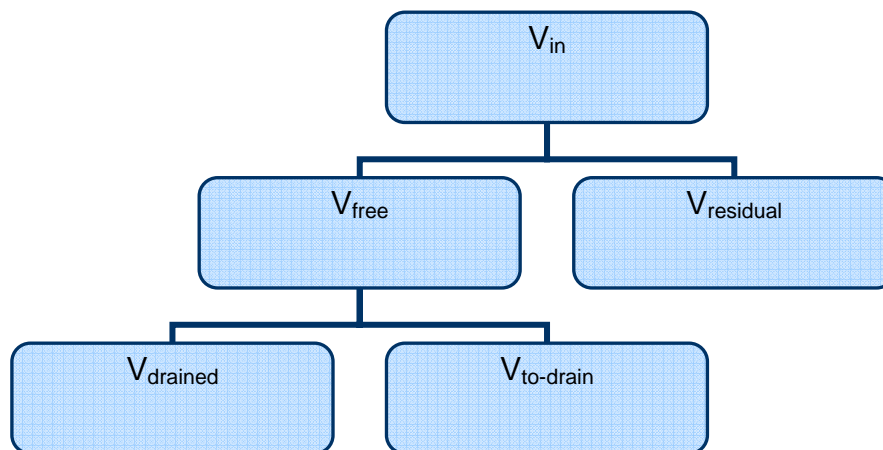
Fig. 5.8. Water mass balance

where:

V_{in} = total volume of water in the stope,

V_{free} = total free water that is drainable,

$V_{residual}$ = volume of residual water that remains within the stope and will not drain in engineering time,

$V_{drained}$ = volume of water that has drained so far,

$V_{to\text{-}drain}$ = volume of water that is yet to drain.

The volume of water entering the stope per hour can be calculated as:

$$V_{in}(m^3 / hr) = \frac{R_s}{\rho} w_{slurry} \tag{5.13}$$

The volume of water exiting the stope through drainage is calculated using the analytical solutions developed in Chapter 4 for a three-dimensional stope.

The volume of residual water is determined by:

$$V_{residual} = m_s w_{residual} \tag{5.14}$$

where m_s represents the total mass of solids in the stope at a specific time and $w_{residual}$ is the residual water content of the fill.

The volume of free water is calculated using:

$$V_{free} = V_{drained} + V_{to-drain} \tag{5.15}$$

At each time step, for example hourly intervals, calculations are undertaken with the new fill and water heights. Fill heights change during filling, however remain the same when in the resting part of the filling cycle. Water heights continually vary i.e. during filling and resting, until all free water has been completely removed.

After entering all the required inputs, the EXCEL model automatically gives the user the required time to fill the stope, the maximum pore water pressure and maximum discharge. Plots of water height, tailings height, maximum pore water pressure development and discharge during the filling cycle are also automatically given once the required inputs are entered.

5.4 Sensitivity Analysis

Using EXCEL the variation and sensitivity in drainage behaviour and pore water pressure measurements with the variation of the input properties can be determined. Initially the variation in geometry was undertaken, followed by variation in soil properties and finally the variation of filling schedule. This sensitivity analysis will provide a broader understanding of the varying effects of geometry, filling schedule and properties on discharge and pore water pressure developments within the stope.

5.4.1   Geometry

The geometry of the stope significantly affects the discharge and pore water pressure developments. The analytical solutions developed in Chapter 4 for calculating discharge and maximum pore water pressure are functions of the stope geometry and permeability. However, when considering the entire filling and draining of a three-dimensional stope other geotechnical properties including, specific gravity, residual water content, percent solids etc also effect these measurements. This is due to the properties affecting the amount of water and/or fill entering the stope. Using the analytical solutions described in chapter 4, design charts were developed to investigate the effect of varying geometries.

Typical geometric aspect ratios for a three dimensional stope were investigated and are illustrated in Fig 5.9 and Fig 5.10. These included H_w/B ratios ranging from 0 to 5; X/D ratios ranging from 0.5 to 2 and D/B ratios ranging from 0.2 to 0.3. The effect of stope dimensions on discharge and maximum pore water pressure were studied in this chapter and best presented by non-dimensionalizing the results such that the data may be presented in the form of design charts. From these charts, a user is able to

determine the discharge rate and maximum pore pressure values for stopes scaled from the ones used to develop the charts. The flow rate was represented by the dimensionless parameter $k(H_W)^2/Q$ which is equivalent to sum of the three-dimensional form factors $(\Sigma\Gamma)$, where k, H_w, Q and $\Sigma\Gamma$ are the permeability, height of water in the hydraulic fill stope, flow rate and sum of the three-dimensional form factors respectively. The maximum pore water pressure (u_{max}) for varying geometries was represented by the parameter $\dfrac{u_{max}}{\gamma_w H_W}$, where γ_w is the unit weight of water which equals 9.81 kN/m^3 and H_w represents the height of water for the specified geometry.

As shown in Fig. 5.9, the geometry of a specified stope has significant influence on the pore pressure distribution. The pore water pressure coefficient $\dfrac{u_{max}}{\gamma_w H_w}$ lies in the range of 0 – 1. For given stope and drain geometries and for a specific height of water, the maximum pore water pressure can be estimated using Fig. 5.9.
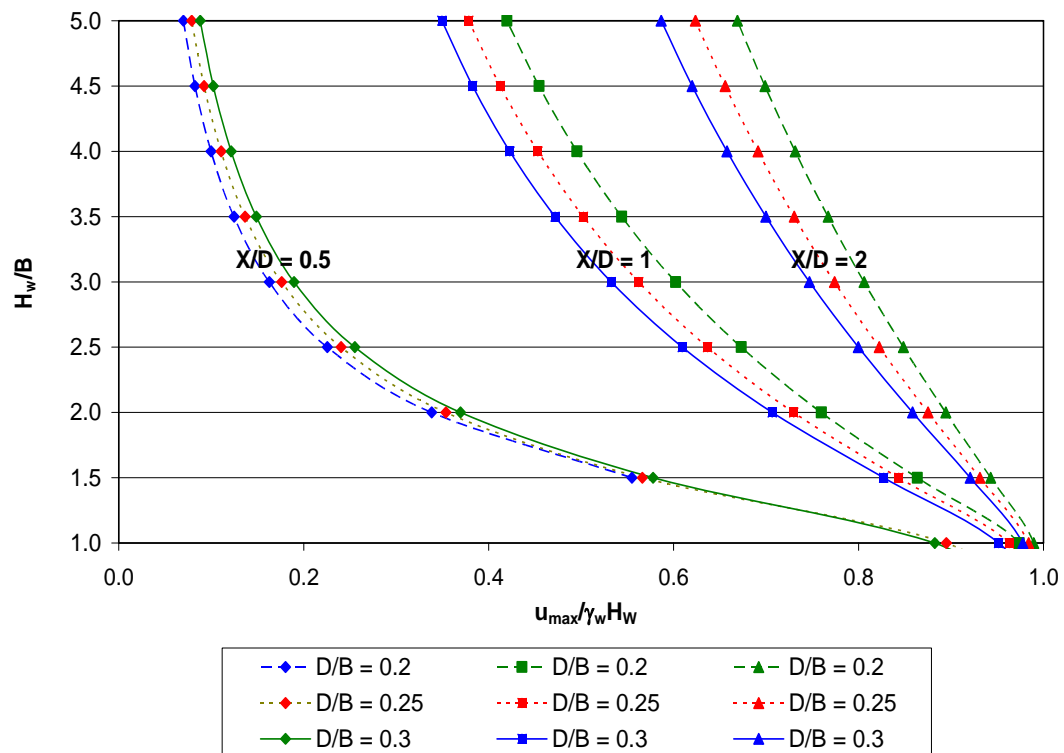
Fig. 5.9. Sensitivity analysis for varying geometries versus maximum pore water pressure

Fig. 5.9 also illustrates several other trends relating maximum pore pressure and geometry. For example, increasing drain length and/or decreasing drain height (i.e. increasing the *X/D* ratio) results in an increase in the maximum pore water pressure. Also when $X/D \geq 1$ the pore pressure increases with decreasing *D/B* ratios. However in the case of *X/D* = 0.5, there is a slight increase in pore pressure with increasing *D/B* ratios.

The variation of geometry with discharge is illustrated in Fig. 5.10.
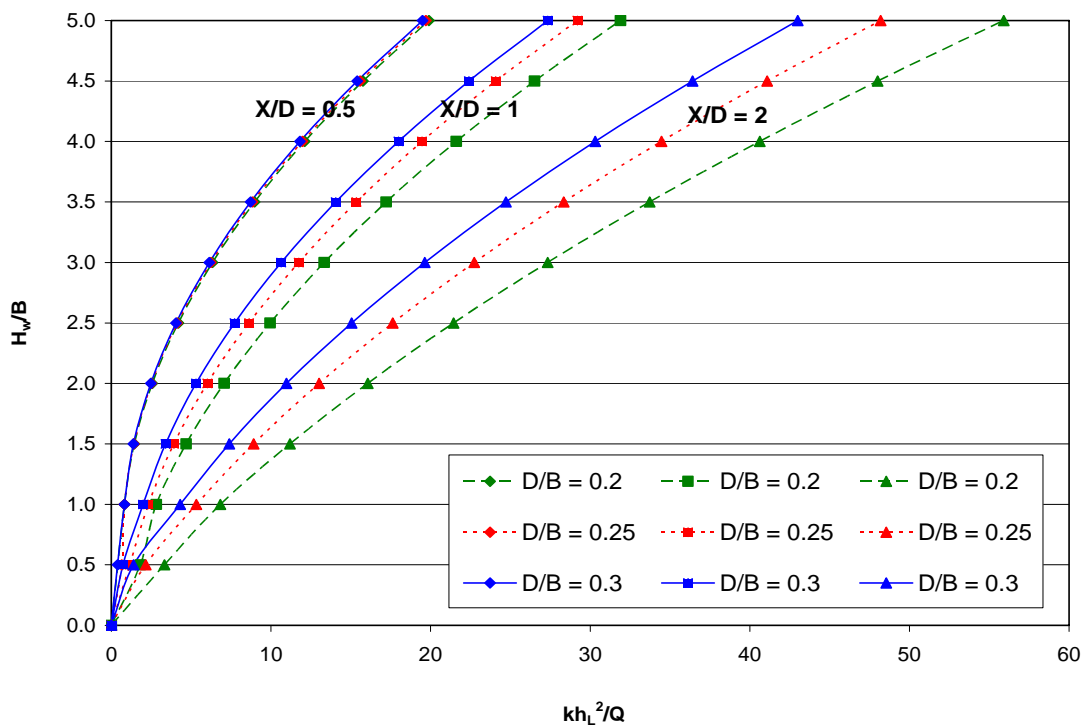
Fig. 5.10. Sensitivity analysis for varying geometries versus discharge

From this chart the following trends were observed.

- An increase in the *X/D* ratio results in an increase in the kh_L^2/Q ratio.
- Increasing the drain length results in a reduction in drain discharge. This can be intuitively explained because as the barricade gets further from the stope, the flow path increases and the hydraulic gradient across the entire model decreases, resulting in reduced flow velocity, hence discharge.
- As the drain gets larger for a specific geometry, the discharge increases, thus reducing the kh_L^2/Q ratio for a specified geometry.

- For increasing *D/B* ratios, there is a reduction in the kh_L^2/Q ratio.

- Another trend also present in Fig. 5.10 shows that for increased *X/D* ratios, there is a more prominent increase in variation of kh_L^2/Q for the increased *D/B* ratios. For instance when *X/D* is equal to 0.5, there is minimal variation for the three curves of *D/B* ratios. However, when *X/D* is increased to 2, there is a more distinct variation of kh_L^2/Q ratios for the varying *D/B* ratios.

5.4.2 Geotechnical Properties

Using the EXCEL model, a sensitivity analysis of the geotechnical properties was undertaken. These properties included permeability of the fill material, specific gravity, dry density, residual moisture content and percent solids of slurry. Previous laboratory testing carried out at James Cook University (Rankine et al. 2004) provided a range of values for the majority of the properties investigated. Residual moisture content has not been tested and previously published values are only estimates based on experience. For each of the parameters investigated, a sample stope with the dimensions shown in Fig. 5.11 was used. A filling schedule of 12 hours pour at 250 t/hr followed by 12 hours rest was assumed.
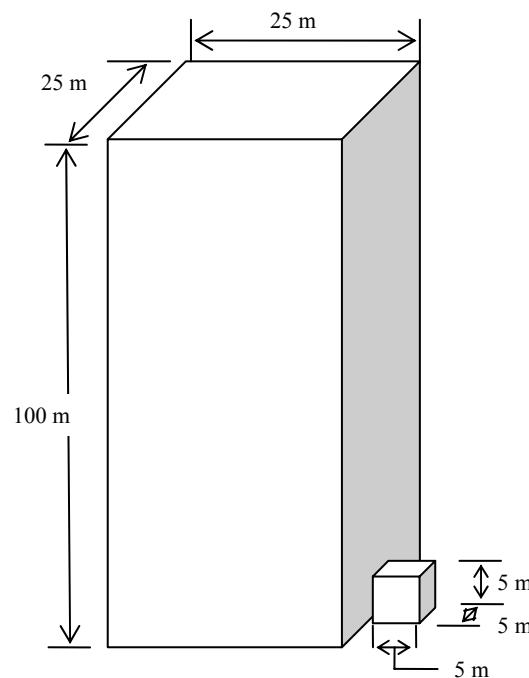
Fig 5.11. Dimensions of sample stope used in the geotechnical property sensitivity analysis

5.4.2.1 *Permeability*

The effect of permeability on the discharge and pore water pressure developments were investigated using previously published permeability values. Constant head and falling head permeability testing conducted at James Cook University on over 25 hydraulic fill samples, recorded a range between 2 mm/hr and 35 mm/hr which was used in the sensitivity analysis. For a given geometry, velocity is proportional to the permeability, thus, it can be expected that the rate of discharge also would be proportional to permeability. This is clearly evident in Fig 5.12 and Fig 5.13 below.

The effect of permeability values of 2 mm/hr, 10mm/hr, 20mm/hr, 30mm/hr and 36 mm/hr were investigated and results are summarised in Fig. 5.12 and Fig. 5.13.
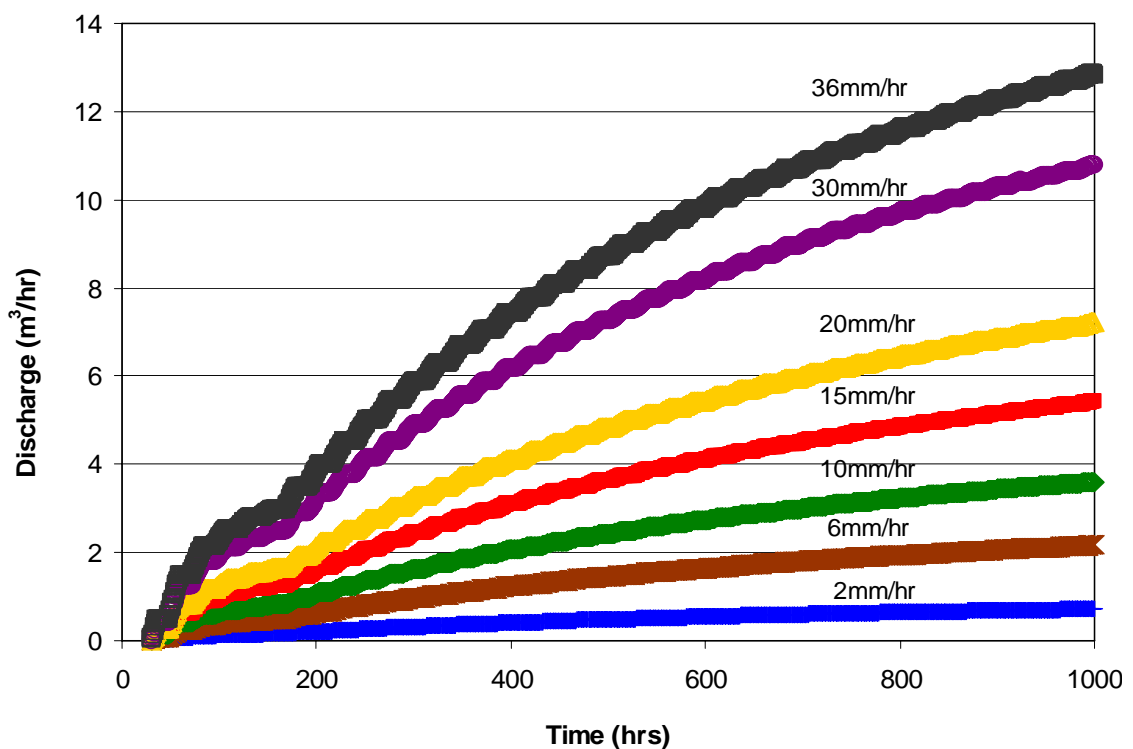
Fig. 5.12. Permeability versus discharge

The discharge with time plot (Fig 5.12) illustrates a marked difference in the water discharge rate from the stope for the typical range of fill permeability values. Velocity is proportional to the permeability (Darcy's law), thus, it can be expected that the rate of discharge also would be proportional to the permeability. This is clearly evident in

Fig. 5.12.   For all cases of permeability, the trend lines recorded for the discharge measurements, did not produce a smooth parabolic shape. Between approximately 168 – 184 hrs, each of the trend-lines showed a significant variation, and a step-like parabolic pattern was observed.   This can be attributed to the analytical equations developed in Chapter 4.   When the water height is less than the stope width, i.e. $\dfrac{H_w}{B} < 1$, the equipotential surfaces are not horizontal and new equations (Eq. 4.13 to Eq. 4.15) were required to calculate the form factor for fragment 2 for the three-dimensional stope.

However, the maximum pore pressure over time plot (Fig 5.13) shows little variation in permeability sensitivity. Since discharge water represents only a small proportion of the water placed into the stope, the relative influence the drainage rate has on the water height may be very small, as shown in Fig 5.13 by the minimal variation in pore pressure measurements between the ranges of permeability values.
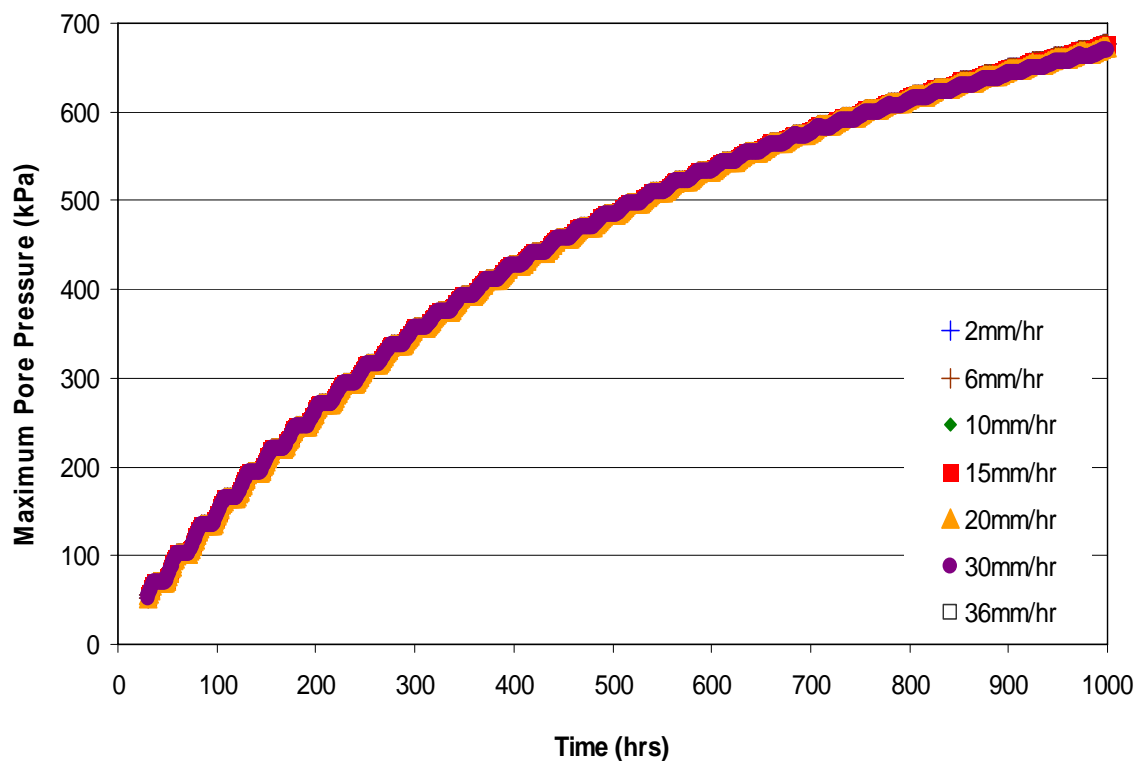
Fig. 5.13. Permeability versus maximum pore pressure

5.4.2.2 Specific gravity and dry density

Chapter 2 details the linear relationship developed between the dry density of the settled fill and the specific gravity of the hydraulic fill soil grains of previously tested hydraulic fills. This relationship is given in Fig 2.7 for hydraulic fills from several Australian and US mines. From the figure, it is shown that the dry density of the hydraulic fill is directly proportional to the specific gravity and can be approximated by:

Laboratory dry density (g/cm^3) = 0.56 x Specific gravity   (2.1)

Implying a void ratio of 0.786 and porosity of 44%. Therefore when analysing the sensitivity of the specific gravity within the drainage analysis, the dry density was approximated using Eq. 2.1 and a porosity of 44% was assumed for the settled hydraulic fill.

Hydraulic fill slurry is generally pumped at specific solid contents (e.g. 75% solids by weight). Therefore the quantity of water entering the stope is significantly influenced by specific gravity of the fill material. As the specific gravity increases, so does the quantity of water entering the stope for a specific slurry density. Fig 5.14 illustrates the fill and water heights versus time for various specific gravities for the specified stope at a specific solids content. From Fig 5.14 it can deduced that the water heights and the drainage times during any particular filling schedule will vary significantly with various specific gravities. In all three cases (G_s = 2.9 - 4.2) there was decant water present throughout the filling operations for the first 100 hours analyzed in Fig. 5.14. The rise in decant height relative to fill height with time increases with specific gravity. The maximum pore water pressure is dependent on the water height in the stope, therefore during filling; the maximum pore pressure will also be affected. From Fig 5.14, it is shown that the height of water is the greatest when the specific gravity is the lowest, therefore producing the greatest maximum pore pressure. However at higher specific gravities, the amount of decant water is greatest which can be of greater concern in the drainage of hydraulic fill stopes.
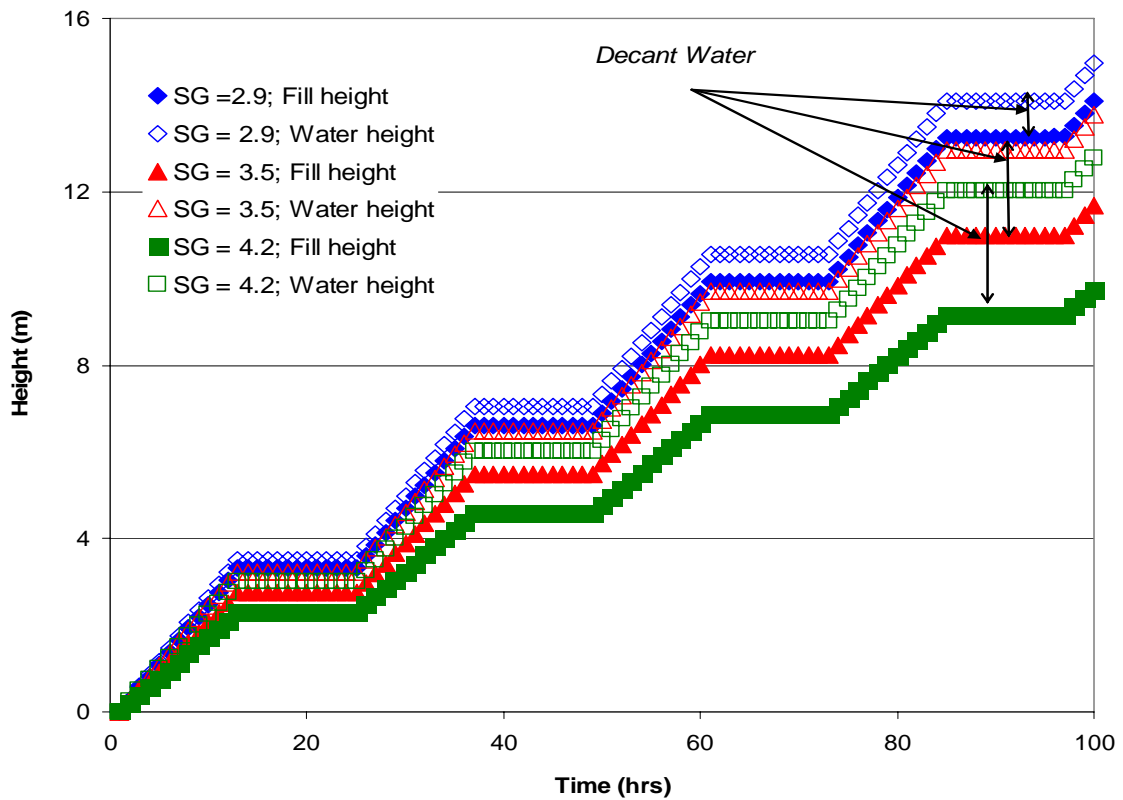
Fig. 5.14. Fill and water heights for varying specific gravity values at a constant solids content

It is important to note that there is significant difference between the rates at which the fill and water levels rise with the variation in specific gravity and therefore it is meaningful to also analyze the results when the stope is filled to a certain height (i.e. not at a certain time). For instance at an 8 m fill height, the decant water for the various specific gravities of 2.9, 3.5 and 4.2 are 8.2 m, 9.4 m and 10.3 m respectively, resulting in 0.2 m, 1.4 m and 2.3 m of decant water for the respective specific gravities (as shown in Fig. 5.14).

Fig 5.15 illustrates the maximum pore water pressure versus specific gravity for the first 500 hours of the filling cycle. As shown in the figure, for increasing specific gravity there is a decrease in the maximum pore water pressure within the fill. This can be expected since water height increases with decreasing specific gravity (see Fig. 5.14.). However, as noted previously, if the stope is analyzed at a certain height,

(rather than a certain time), the pore pressure would be greatest at higher specific gravities.
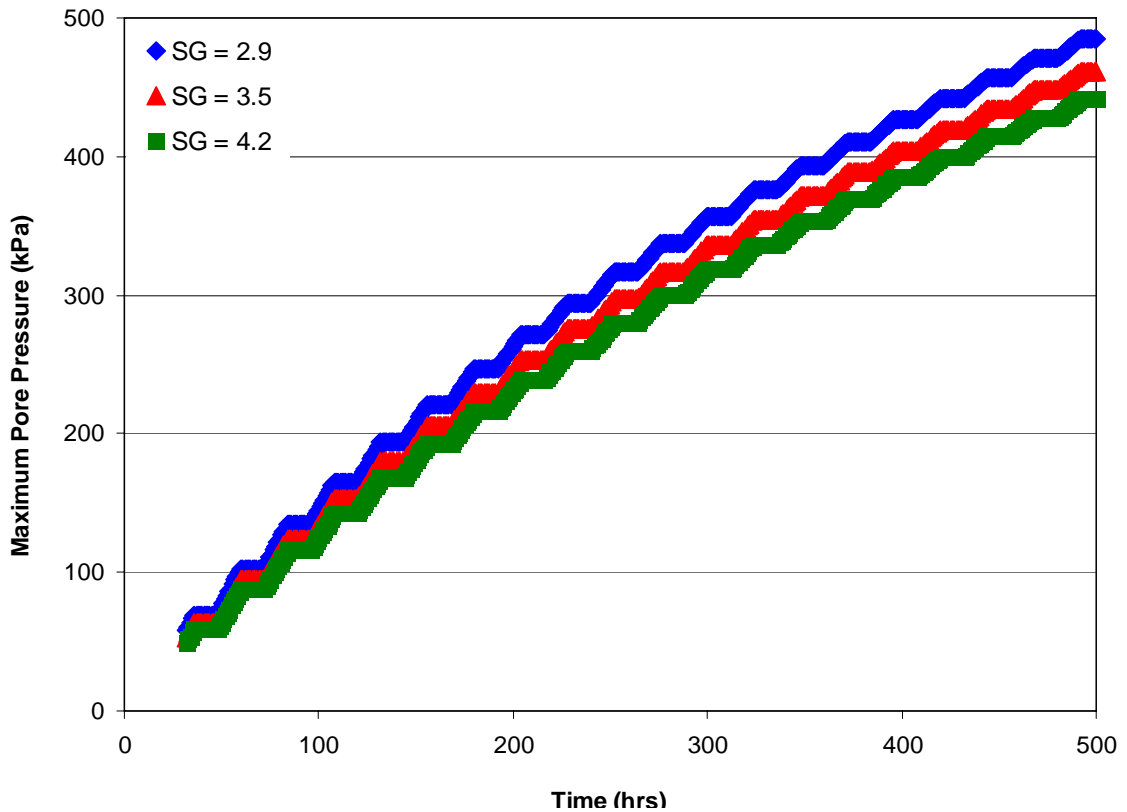
Fig. 5.15. Maximum pore pressure versus specific gravity

Fig. 5.16 illustrates discharge versus time for the various specific gravities investigated. Although the variation in discharge is minimal between the specific gravities, it is clear that the lower the specific gravity, the greater the discharge. From Fig. 5.14, we know that the lowest specific gravity produces the greatest fill and water heights. Therefore, applying these heights to the analytical equations developed in chapter 4 will result in increased discharge as shown in the figure.

5.4.2.3 Solids Content

For optimal economic advantage, stopes should be filled with a solids content that maximizes solid waste disposal, minimizes the quantity of water requiring removal, while still being sufficiently moist to meet rheological requirements. The tailings
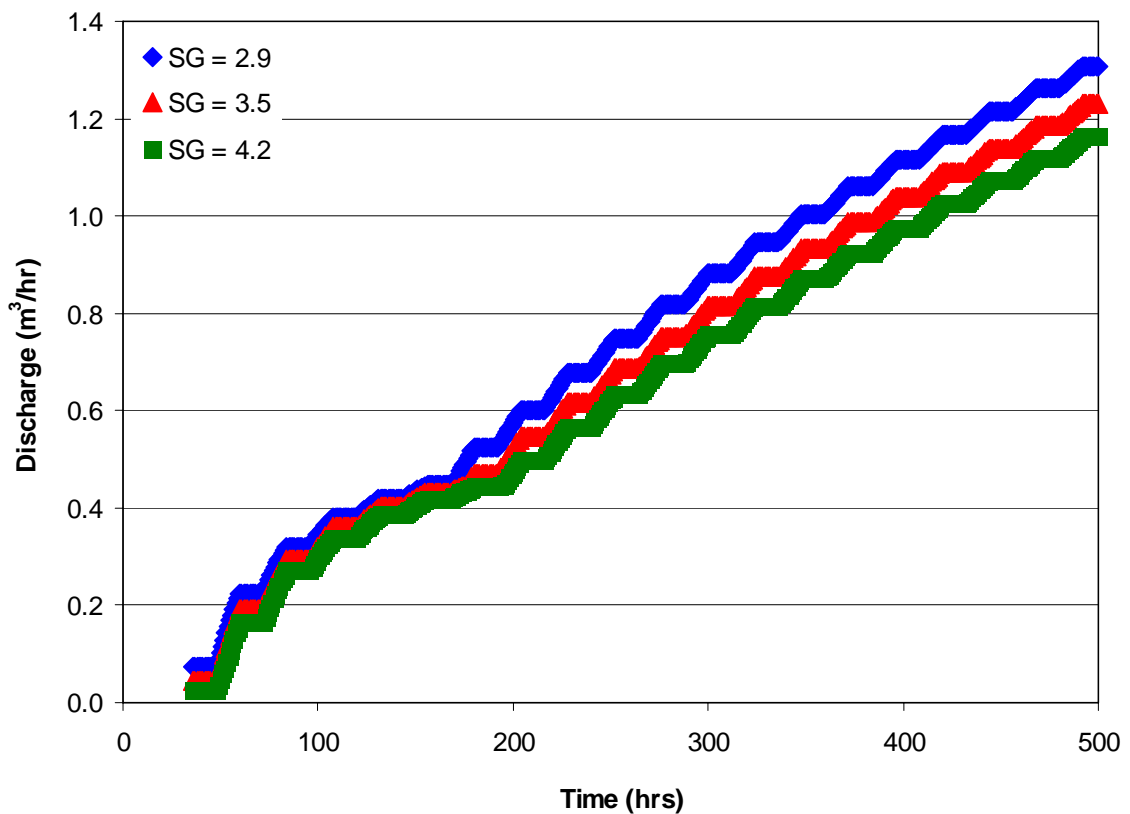
Fig. 5.16. Discharge versus specific gravity

slurry is dewatered to minimize the quantity of water that will be placed underground and must drain out of the fill during and after fill placement. However if the slurry is pumped at too high a solids content, the mine runs the risk of additional costs and schedule delays associated with blocked pipes. Each fill material has a specific optimum solids content for which the slurry best meets the balance between maximized solids disposal and minimized water added.

Tailings are supplied to the hydraulic fill plant at low density slurry. Hydrocyclones are commonly used to dewater the slurry to between 45% solid by volume and 50% solids by volume

Potvin et al. (2005) suggest a range of slurry densities that correspond to the common range of specific gravities encountered in hydraulic fill and these are illustrated in Fig. 5.17.
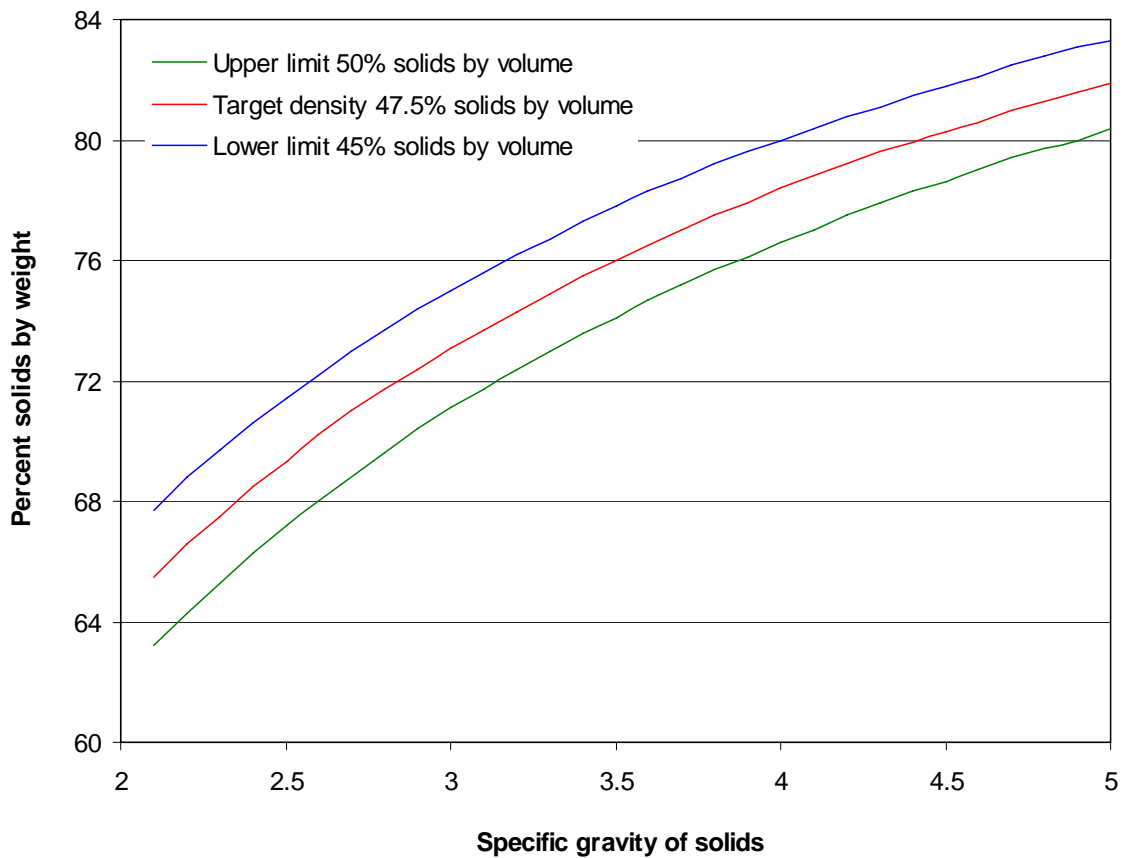
Fig 5.17. Hydraulic fill Slurry density ranges (Potvin et al. 2005)

Fig 5.18 illustrates the details of the fill and water heights for the first 500 hours of the filling schedule. As can be expected, as the percent solids content is increased, the volume of tailings is also increased. For each of the percent solids contents investigated, the mass of tailings entering the stope remained the same (250 t/hr) however; the amount of water was decreased with increased percent solids. This results in decreased water height in the stope with increased percent solids. To magnify the effect, Fig 5.19 illustrates the fill and water heights over a 24 hour period from 240 – 264 hours. As shown in the figure, at 70% and 72% solids content, the decant water is present in the stope contains, however, for the 74% solids content, there is minimal decant water and the tailings height and water height are roughly equal over the selected time period.
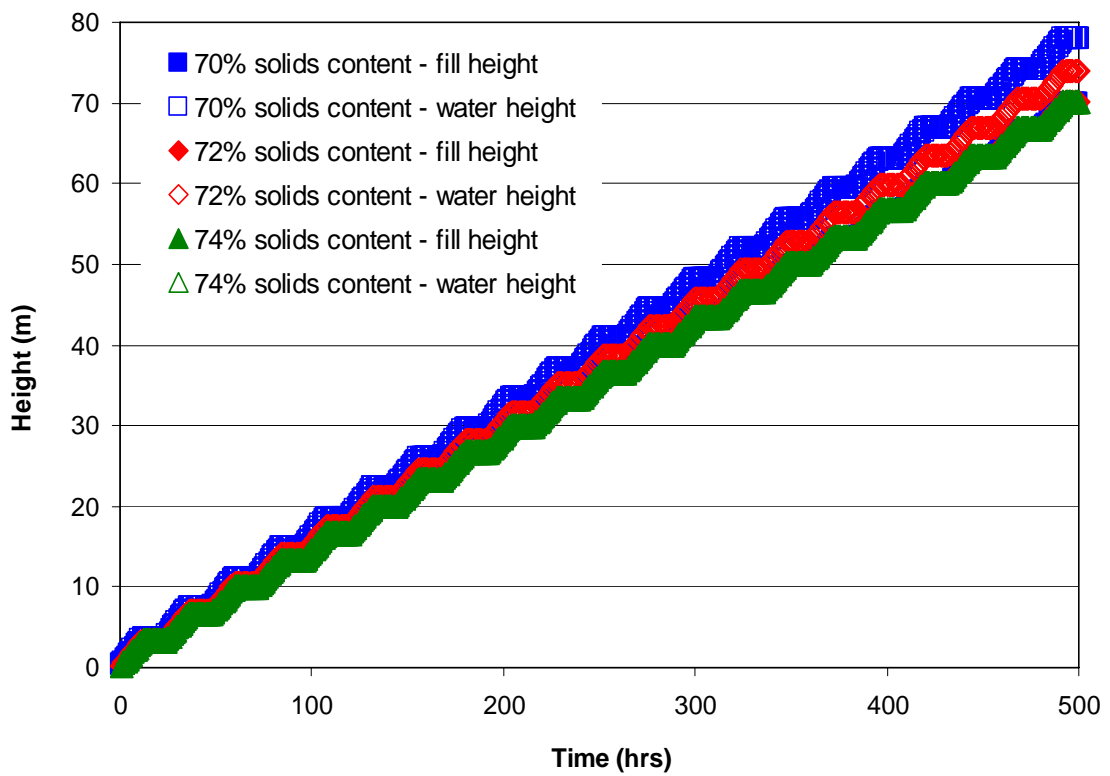
Fig. 5.18. Fill and water heights for varying solids content
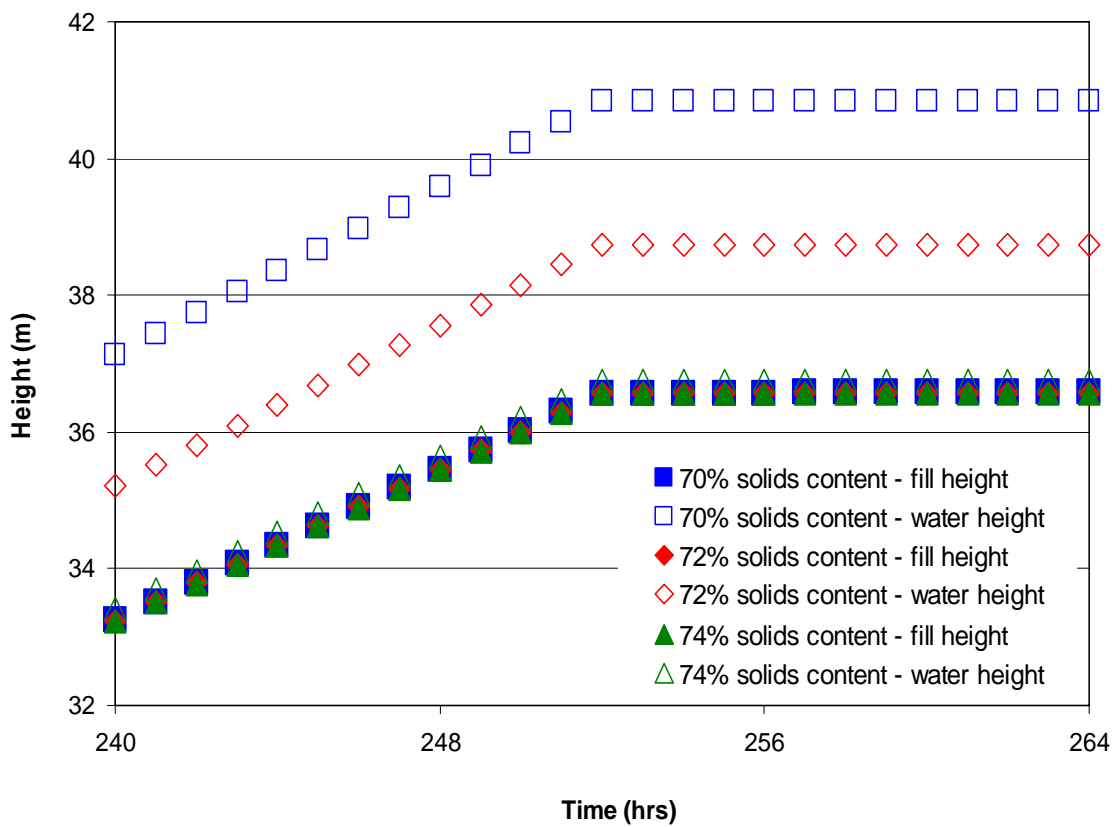
Fig. 5.19. Magnified fill and water heights for varying solids content

Fig. 5.20 and Fig. 5.21 illustrate the effect of solids content on discharge and pore water pressure within the three-dimensional stope.
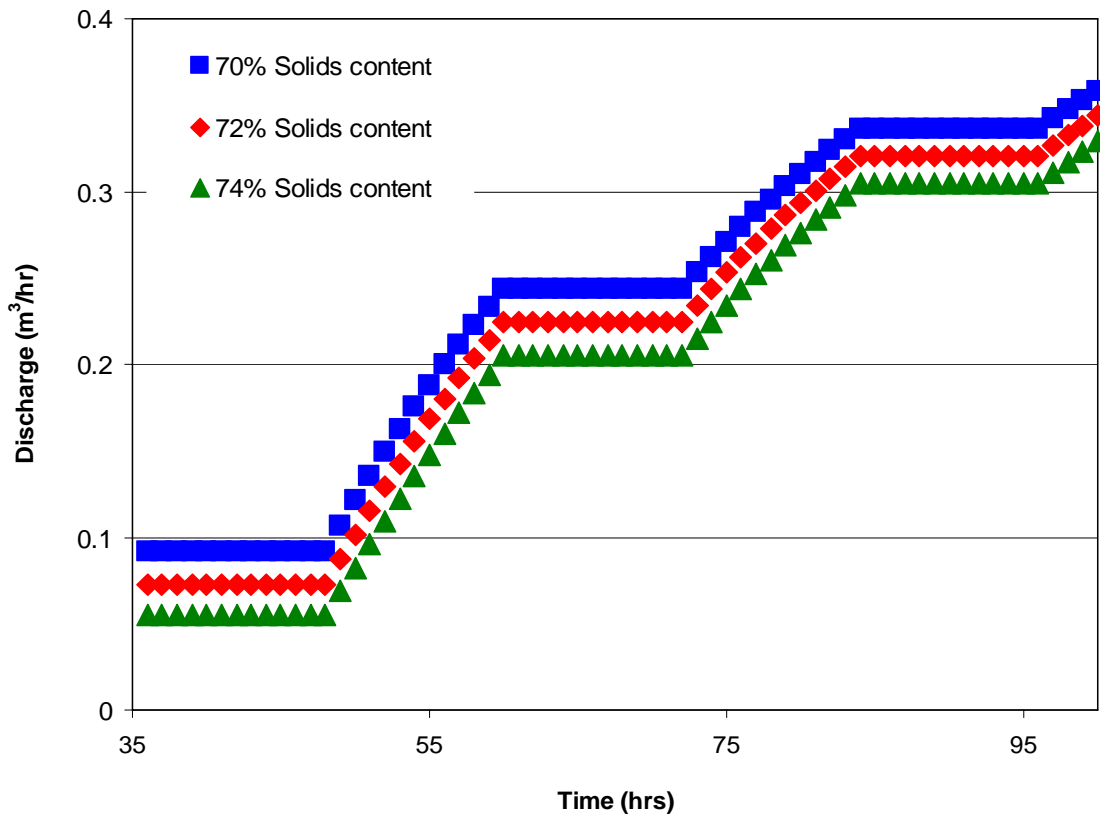
Fig. 5.20. Discharge versus solids content
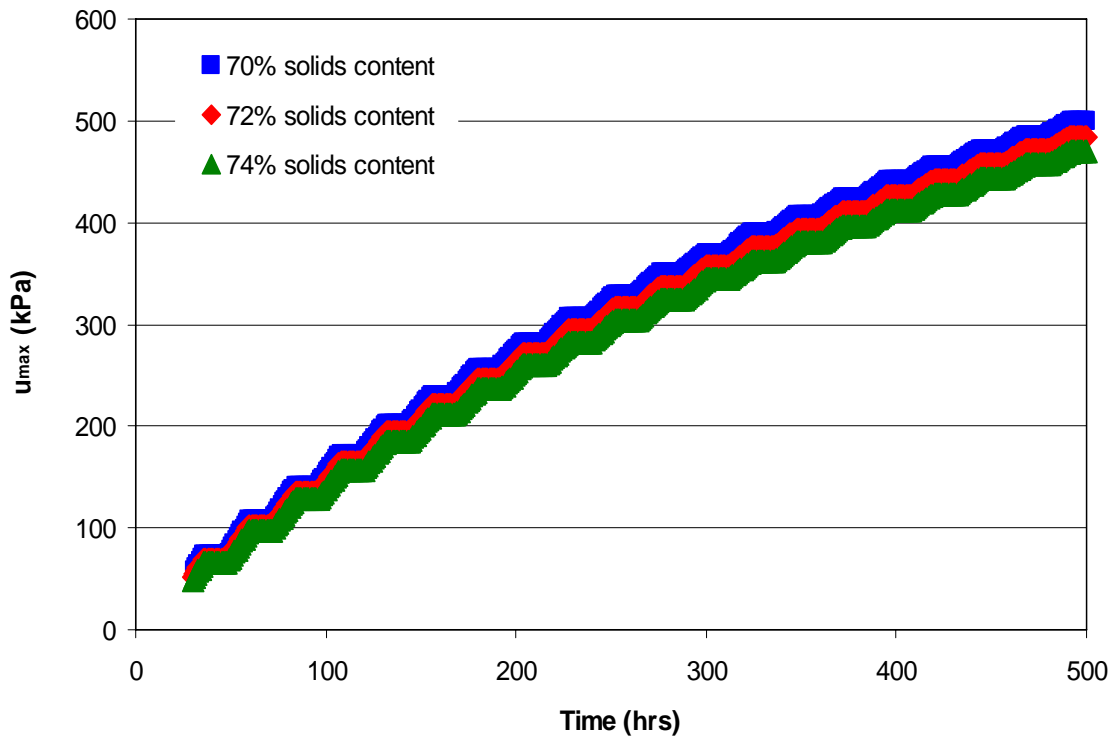
Fig. 5.21. Maximum pore water pressure versus solids content

Fig 5.20 illustrates the results for discharge versus time for the various percent solids investigated for the initial 35 – 100 hours of filling. (A smaller time interval was chosen for this figure, to magnify the effect of percent solids on discharge results). The discharge rates between the various percent solids does not vary significantly, however when magnified (as in Fig 5.20) it can be shown that with decreased percent solids there is a slight increase in discharge. Fig 5.21 illustrates the maximum pore pressure for the three solids contents investigated over the first 500 hours of the filling schedule. As illustrated, there is a slight increase in maximum pore water pressure with decreasing percent solids content, which would be a consequence of the increased water heights for the decreased solids content.

From these figures (Fig 5.18 – Fig 5.21), it can be concluded that the lower solids contents results in higher water levels, discharge rates and maximum pore pressures at a specific time, simply because more water has entered the stope. For the 72% solids content case, the results illustrated a slightly lower water level, lower discharge rate and marginally lower maximum pore water pressures. The pronounced step like pattern observed in all figures, is due to the fill and rest periods in the filling cycle.

5.4.2.4 *Residual water content*

Residual water content is the water content present within the stope, when the stope has fully drained. The residual water content is not removed in engineering time and remains within the stope held within the voids. When modeling the three-dimensional stope, the EXCEL simulation only models the flow of drainable water and not all the water that enters the stope.

Cowling et al. (1988) records the presence of residual moisture in a sample calculation. In his calculation, for every 200 t of hydraulic fill placed in a stope, 90 t of water is added, for a pulp density of 69% solids. During drainage only 40 t of water is discharged from the stope for every 90 t that are input. The difference, 50 t, is retained in the fill as residual moisture content, which is equivalent to 25 % residual moisture. Due to the generally large dimensions in hydraulic fill stopes, there is significant amount of immobile water that will not be drained in engineering times.

Using the EXCEL model, several simulations of a three-dimensional stope with dimensions given in Fig 5.11, where analyzed with varying residual moisture contents. As shown in the Fig. 5.22, the filling of the stope is not affected by the residual moisture content, however the drainage time required to completely remove all the free water from the stope is dependent upon this parameter. Once, the free water has been removed, the adjacent works may commence - thus providing a very valuable tool to assist with mine scheduling.
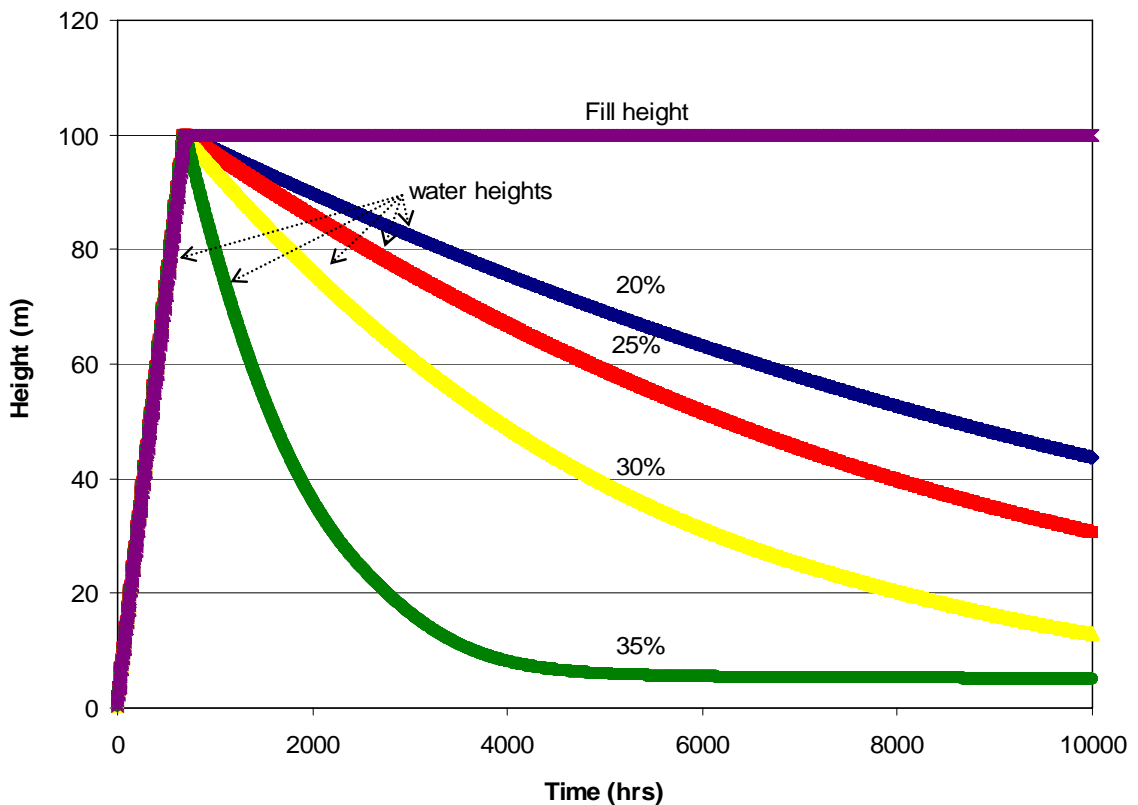
Fig. 5.22. Water and fill heights during filling and draining of three-dimensional stope with varying residual moisture contents

5.4.3 Filling Schedule

The EXCEL model was used to study the effect of varying filling schedules on the discharge and pore pressure measurements. When the slurry is placed into underground stopes, it is imperative that the stope be allowed to drain to remove the

transport water from the stope, reducing pore pressure build-up within the stope that could lead to barricade failure.   For a particular stope at any mine, there will be a rate of fill placement and resting time for drainage, which should not be exceeded.

Cowling et al. (1988) proposed a filling schedule for underground stopes at Mount Isa Mines. These guidelines were based on a filling rate of 300 t/hr at 72% $\pm$ 2% solids content with specific gravity of 2.9 and the stopes where characterized by tall sublevel open stopes.   Table 5.4 summarizes the suggested filling cycles.

Table 5.4 Suggested filling schedules (Cowling et al. 1988)

Stope plan area m^2	Pouring time (hrs)	Resting time (hrs)
< 400	8	16
<1000	12	12
< 1600	16	8
> 1600	Unrestricted	N/A

Fig 5.23 presents the fill and water heights for the various filling schedules suggested by Cowling et al. (1988) for the 100 m high stope given in Fig. 5.9 and with properties given in Table 5.2.

From the figure it is shown that provided the quantity of water discharged from the stope represents only a small percentage of the overall water placed into the stope, the filling schedule has little effect on discharge rates or pore pressures; it merely changes the time in which these values are experienced.

5.4.4. Filling Rate

As can be expected, the filling rate will influence the rate at which the fill and water levels raise, but have minimal effect on their heights relative to each other provided the discharge quantity represents only a small proportion of the total water placed in the stope. Also, the rate at which the stope is filled will have almost no influence on the
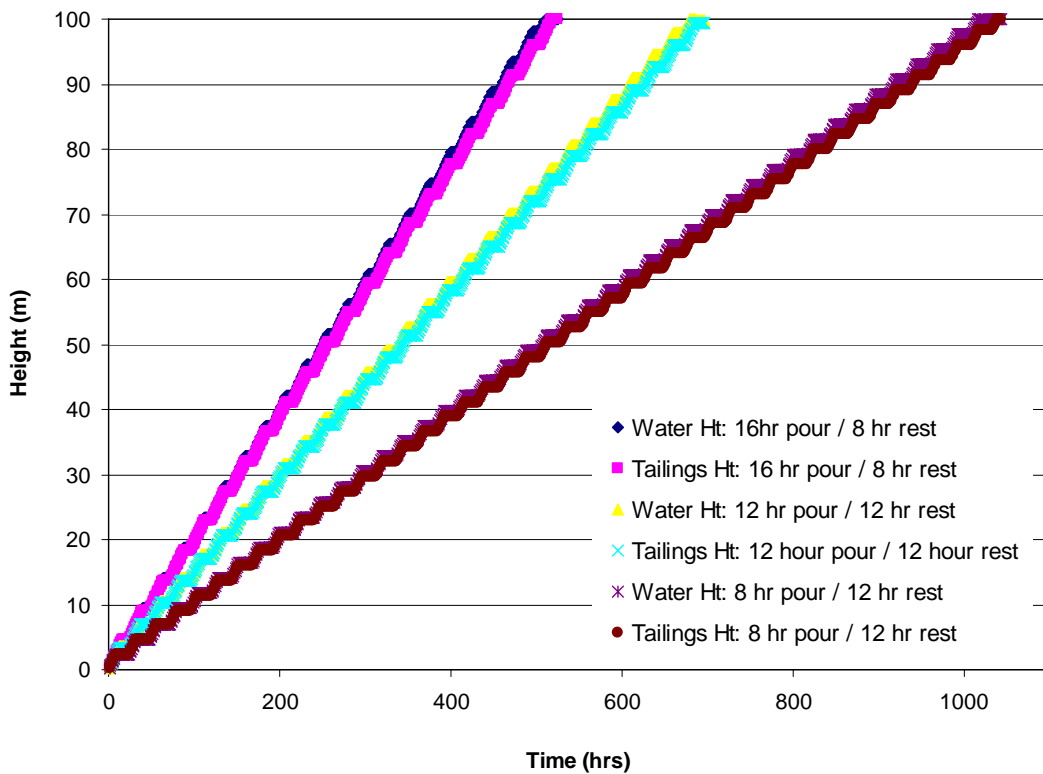
Fig. 5.23. Fill and water heights during filling for various filling schedules

values of discharge and pore water pressure at any given height, it will only influence the time in which these values are recorded (because the fill height increases more rapidly with increased filling rate).

5.5.   Two-dimensional versus Three-dimensional Stopes

The two-dimensional models and analytical solutions discussed in chapter 3 provide valuable information in the understanding of hydraulic fill drainage in underground stopes.   However, due to the geometrical simplification in the two-dimensional modeling, several shortfalls are present. These include:

- The distance between the drain exit and point of maximum pore water pressure is smaller for a two-dimensional analysis than for an identical sized stope in three-dimensions due to the geometrical simplification involved. Therefore, the maximum pore pressure measurements will be lower for two-dimensional analysis than it is for three-dimensional analysis, and hence the pore water pressure is lower.

- When comparing the two and three-dimensional solutions, the two-dimensional drain is modelled at the full depth of the stope with sufficient height to give an equivalent cross-sectional area of the corresponding three-dimensional models. Thus, with the drain area located more closely to the base and stretching the full depth of the stope, the two-dimensional simulations produce higher discharge rates than the three-dimensional simulations.

5.6. Summary and Conclusions

This chapter has developed, verified and implemented a three-dimensional model to simulate the complete filling and draining of a hydraulic filled stope. The EXCEL model is used to predict the fill and water levels, discharge rates and pore pressures within a three-dimensional hydraulic fill stope as they are being filled and drained. Using the model a sensitivity analysis on the drainage behavior and pore water pressure measurements with the fill properties, geometries and typical filling schedules of a three-dimensional hydraulic fill stope was undertaken.

To verify the EXCEL model, a hypothetical problem was designed and results from EXCEL were verified against results obtained from the identical simulation done in the existing two and three dimensional programs previously validated against in situ data. The verification exercise was designed to compare the water and tailings levels, the discharge during a specific filling schedule and the maximum pore water pressure development within the three-dimensional stope and results showed excellent agreement.

Using the EXCEL model a sensitivity analysis was undertaken for varying geometries, geotechnical properties and filling schedules. Several trends were observed and are briefly described below:

- As drain length increases and the drain cross-section area decreases, the maximum pore water pressure increases.
- As the barricade gets further from the stope, the flow path increases and the hydraulic gradient across the entire model decreases, resulting in reduced flow velocity, hence discharge.

- An increase in drain length results in a reduction in drain discharge and a slight decrease in the maximum pore pressure. Also, for increasing drain cross-sectional area discharge increases and pore water pressure decreases.

- Permeability has a significant influence on discharge. However, shows little variation in pore pressure measurements. For a given geometry, velocity is proportional to permeability, thus it is expected and illustrated in this chapter that the rate of discharge is also proportional to the permeability. Since the discharge water represents only a small proportion of the water placed into the stope, the relative influence the drainage has on the water height may be small, thus resulting in minimal variation in the pore pressure measurements.

- Also, the solids content and specific gravity of the slurry will have a significant influence on the relative fill and water heights with time, within the specified stope and minimal variation in discharge measurements. With all other parameters equal, the higher the specific gravity of the slurry, the greater the quantity of water entering the stope for a specific slurry density. Also, increasing the solids content decreases the excess water requiring removal within the stope. However, it is important that stopes be filled with a solids content that maximises the solids waste disposal, minimises the quantity of water requiring removal, while still being sufficiently moist to meet rheological requirements.

- The effect of residual moisture content was also investigated in the chapter. Results indicate that the filling of the stope is not affected by the residual moisture content, however the drainage time required to completely removing all the free water from the stope is dependent upon this parameter.

- Using EXCEL, several filling schedules and filling rates were analysed. Provided the quantity of water discharged from the stope represents only a small percentage of the overall water placed into the stope, the filling schedule and filling rate has little effect on the discharge rates or pore pressures, it merely changes the time in which these values are experienced. Careful attention should be directed towards these properties to prevent pore pressure build-up within the stope that could lead to barricade failure.

CHAPTER 6

SUMMARY AND CONCLUSIONS

This chapter presents a summary of the research carried out in this dissertation, conclusions and recommendations for future research.

6.1 Summary

The extraction and processing of most mineral ores, result in the generation of large volumes of finer residue or tailings. The safe disposal of such material is of prime environmental, safety and economical concern to the management of mining operations. Recent barricade failures, resulting from poor drainage, have led to need for an increased understanding of the pore pressure developments and flow rates throughout the filling operation. This dissertation is considers the drainage characteristics of hydraulic fill which is one of the most popular minefilling methods used in Australia and worldwide.

Hydraulic fills produced from tailings, are man-made and can therefore much more uniform in their characteristics than are most natural deposits. However, due to the wide range of geological conditions and mineralogical compositions from which the hydraulic fills may be sourced a wide range of specific gravity values for hydraulic fills has been observed across Australia. To ensure good drainage, backfilling operations typically ensure that the by-product (usually by hydrocyclones) has an effective grain size (D_{10}), no smaller than 10 μm. Commonly accepted industry rule-of-thumb standard suggests that the permeability of the hydraulic fill should be no less than 100 mm/hr but many Australian and worldwide mines that have operated satisfactorily for years quote hydraulic fill permeability values substantially less than this value. A review was presented on previous research conducted on the characterization of hydraulic fills and barricade bricks. An overview of the current

practices and developments reported in the literature with regard to the placement of hydraulic fill material in underground stopes was also undertaken. The review briefly discusses some of the details with regard to the design and construction of the barricades used to contain the hydraulic fill within the stope as it is being placed, the in situ monitoring techniques that have been used on site to study pore pressure developments and barricade loading, as well as some of the numerical and laboratory modeling techniques that have been used in the past to predict drainage behavior within hydraulic fill stopes.

In recent years, there has been an increasing trend to use numerical modeling as a prediction tool in studying the drainage of hydraulic fill stopes. Although these models provide valuable information, they are often time-consuming and require specialist knowledge of the numerical package used to model the stope. Using a parametric study carried out using the numerical packages *FLAC* and *FLAC^{3D}* and the method of fragments (Harr 1962, 1977), this dissertation presents analytical solutions for studying the drainage of hydraulic fills in two and three-dimensional stopes.

Initially a two-dimensional hydraulic fill stope was analyzed. It was shown that the flow region of the two-dimensional hydraulic fill stope can be divided into three fragments, for which the form factors can be determined from the dimensions of the stope and drain. The flow is vertical at heights above the stope width (*B*), and is horizontal within the drain a short distance (0.5*D*) from the stope face. At the bottom of the stope, up to a height of the stope width, flow is two-dimensional. Since the bottom of the stope (fragment 2) does not conform to any of the fragments suggested by Harr (1962), a new fragment was developed. The dimensionless form factor of the new fragments was expressed as a function of the dimensions of the stope and drain. Analytical solutions were proposed for determining the entry hydraulic gradient at the top of the stope, flow rate and maximum pore water pressure that occurs at the bottom corner of the stope. The model was verified through several numerical examples of hydraulic fill stopes with randomly selected dimensions and was found to be in excellent agreement.

Underground stope arrangements are very much three-dimensional in geometry and although the two-dimensional solutions provide a valuable tool for drainage prediction, the inherent approximations required, substantially reduce the value of the model when dealing with complex three-dimensional stopes. Using $FLAC^{3D}$ and method of fragments simple analytical solutions and design charts were developed to estimate the maximum pore water pressure and discharge within three-dimensional hydraulic fill stopes of varying geometries. Shape factors were developed to account for the inherent individuality associated with stope and drain geometry and the influence of scaling on discharge and pore water pressure measurements were also investigated. The proposed solutions were validated using the finite difference program $FLAC^{3D}$ and physical modeling of a scaled stope and results were found to be satisfactory.

Using the analytical solutions developed for flow through three-dimensional hydraulic fill stopes, an *EXCEL* model was developed to accurately and efficiently model the drainage behavior in three-dimensional stopes. The model simulates the complete filling and draining of the stopes and was verified using previously validated two and three-dimensional models and results showed excellent agreement. The model incorporates the complete filling and draining of the stopes and enables the user inputs such as filling schedule, varying stope geometries and geotechnical properties (e.g. specific gravity, slurry solids content, residual water content, void ratio etc). The variation and sensitivity of drainage behaviour and pore water pressure measurements with the fill properties, filling schedules and geometries was undertaken using the EXCEL model.

Catastrophic fill barricade failures in underground hydraulic fill mines in Australia and overseas have resulted in significant economic loss and loss of lives. The increased knowledge into the drainage behaviours of underground hydraulic fill stopes and the improved tools for analysis presented in this dissertation should produce an increased level of confidence in design of hydraulic fills, more efficient mining, increased cost savings and safer mine filling practices.

6.2 Conclusions

Initially this thesis applied the method of fragments to two-dimensional hydraulic fill stopes. The method, originally developed by Pavlovsky (1956) was used to divide the flow region into three fragments, for which the form factors were determined from the dimensions of the stope and the drain. Two simple expressions were developed for determining the discharge through the drain and the maximum pore water pressure within the stope. The proposed solutions were verified against solutions derived from the finite difference software package *FLAC* and results were found to be in excellent agreement. Later this method was applied to several other points within the two-dimensional stope and equations of maximum pore water pressure developed for each of the points considered. Using these analytical solutions, the use of ancillary drains and anisotropy was investigated. From the analysis the following conclusions were made:

- It was shown that ancillary drainage was effective in accelerating the drainage process within a two-dimensional hydraulically filled stope. Consequently, this accelerated drainage reduces the build-up of pore pressure behind the barricades.

- The horizontal ancillary drain provided at the bottom of the drain reduces the pore pressure at all points within the fill, with the reduction being proportional to the length of the drain

- Preliminary laboratory testing was undertaken to determine the degree of anisotropic permeability on several hydraulic fills. Using these results in combination with previously published values, varying degrees of anisotropic permeability was investigated using *FLAC* and method of fragments. From the results, it is evident that the anisotropic permeability has a significant effect on pore pressure development and discharge within the stope. As the anisotropy in permeability is increased there is a substantial reduction in pore pressure. Several design charts were created to quantify the effect of varying anisotropic ratios and geometries on pore pressure and discharge within the stope.

Using the method of fragment concepts and the three-dimensional finite difference software *FLAC^{3D}* simple analytical solutions and design charts were developed for estimating the maximum pore water pressure and discharge within a three-dimensional stope of varying geometry. The three-dimensional solutions were verified using the finite difference software package *FLAC^{3D}* and physical modeling of a scaled stope and results were deemed acceptable. It was clear from several *FLAC^{3D}* runs that the flow within the upper region of the stope, approximately above a height of the stope width (*B)*, is one-dimensional and vertical. Similarly within the drain, at a distance greater than half the drain height, the flow is one dimensional and horizontal. As was the case for the two-dimensional stope. On the basis of this observation, the flow domain was divided into three fragments, separated by equipotential surfaces and form factors were developed for each fragment. Initially the solutions were developed for a square based stope with a square drain outlet located centrally along the base of one of the stope faces. Using the three-dimensional analytical solutions, the following conclusions were drawn.

- Initially when the height of water is greater than the stope width the location of the drain on the base of the stope wall and the shape of the drain have little effect on the computed values of discharge and maximum pore pressure. However during the filling and drainage of the stope when the height of water is less than the stope width the location and shape of the drain have a noticeable influence on discharge and negligible effect on maximum pore water pressure.

- To take account of varying stope geometry, a shape factor was developed for non-square stopes, which is simply a multiplication factor on the flow rate and maximum pore water pressures computed assuming a square base stope and square drain outlet.

- By considering the symmetry of drain arrangements, values of discharge and maximum pressure can be computed for a wide variety of multiple-drain arrangements.

- For a given plan area, as the height of saturated material is increased in the model, the discharge increases. Also, as observed by previous

authors, as the position of the barricade progresses further from the stope face, the rate of discharge decreases.

The final part of this thesis consisted of developing an accurate and efficient three-dimensional model that can be used to simulate the complete filling and draining of a hydraulic filled stope. Previous models were often time consuming and in most cases, specialist knowledge of the corresponding software package is required. Therefore a quicker and less complicated solution was desirable. The well-known and user friendly package EXCEL was used to model the three-dimensional stope. The model is capable of predicting the fill and water levels, discharge rates and pore pressures within a three-dimensional hydraulic fill stope as they are being filled and drained. Using the model a sensitivity analysis on the drainage behavior and pore water pressure developments with fill properties, geometries and typical filling schedules of a three-dimensional hydraulic fill stope was undertaken.

To verify the EXCEL model, a hypothetical problem was designed and results from EXCEL were verified against results obtained from the identical simulation done in the existing two and three dimensional programs that have been previously validated against in situ data. The verification exercise was designed to compare the water and tailings levels, the discharge during a specific filling schedule and the maximum pore water pressure development within the three-dimensional stope and results showed excellent agreement.

Using the EXCEL model a sensitivity analysis was undertaken for varying geometries, geotechnical properties and filling schedules. Several trends were observed and are briefly described below:

- As drain length increases and the drain cross-section area decreases, the maximum pore water pressure increases.
- As the barricade gets further from the stope, the flow path increases and the hydraulic gradient across the entire model decreases, resulting in reduced flow velocity, hence discharge.

- An increase in drain length results in a reduction in drain discharge and a slight decrease in the maximum pore pressure. Also, for increasing drain cross-sectional area discharge increases and pore water pressure decreases.

- Permeability has a significant influence on discharge however shows little variation in pore pressure measurements. For a given geometry, velocity is proportional to permeability, thus it is expected and illustrated that the rate of discharge is also proportional to the permeability. Since the discharge water represents only a small proportion of the water placed into the stope, the relative influence the drainage has on the water height may be small, thus resulting in minimal variation in the pore pressure measurements.

- It was shown that the solids content and specific gravity of the slurry will have a significant influence on the relative fill and water heights with time, within the specified stope and minimal variation in discharge measurements. With all other parameters equal, the higher the specific gravity of the slurry, the greater the quantity of water entering the stope for a specific slurry density. Also, increasing the solids content decreases the excess water requiring removal within the stope. However, it is important that stopes be filled with a solids content that maximises the solids waste disposal, minimises the quantity of water requiring removal, while still being sufficiently moist to meet rheological requirements.

- The effect of residual moisture content was also investigated in the chapter. Results indicate that the filling of the stope is not affected by the residual moisture content, however the drainage time required to completely remove all the free water from the stope is dependent upon this parameter.

- Using the EXCEL model, several filling schedules and filling rates were analysed. Provided the quantity of water discharged from the stope represents only a small percentage of the overall water placed into the stope, the filling schedule and filling rate has little effect on the

discharge rates or pore water pressures, it merely changes the time in which these values are experienced. More attention should be directed towards these properties to prevent pore pressure build-up within the stope that could lead to barricade failure.

6.3 Recommendations for Future Research

Whilst there have been considerable advancements in understanding the drainage performance of hydraulic fill, there are still many areas that are deserving of further study. Recommendations for future research include:

- Only rectangular based and/or square based stopes were analyzed when developing the shape factor coefficient. It is recommended that shape factors be developed for more irregular shaped stopes.

- This thesis as assumed tight-filling in its analysis – it is recommended that several design charts be developed for stopes which have not been tight-filled.

- Extend the two-dimensional model described in chapter three to take into account multiple level access drives (i.e. more than one drain) and derive analytical solutions.

- The effects of cemented hydraulic fill be incorporated into the EXCEL model. i.e. the variation of permeability with respect to cement content and curing time would be investigated and applied to the EXCEL model. Although preliminary testing was conducted, further permeability testing on cemented hydraulic fills would be required to obtain a better understanding on the effect of varying cement contents on permeability; and the effect of curing on permeability.

- The effects of arching on the three-dimensional stope be investigated and implemented into the spreadsheet. Studies are currently being undertaken by a postgraduate student from James Cook University on the effect of arching on hydraulic fill material.

- Modeling of the bearing capacity of hydraulic fill i.e. the value of hydraulic fill as a working surface for underground personnel and machinery.

- Further investigation into the effect of consolidation on fill masses. Any attempt to incorporate coupling into the numerical model would require a thorough understanding of the consolidation characteristics of the hydraulic fills. Due to the rapid consolidation of the hydraulic fills observed in the standard oedometer tests at James Cook University, it is suggested that consolidation tests be carried out on much thicker samples (e.g. in a 150 mm diameter compaction mould) which would prolong the consolidation process, and enable determination of coefficient of consolidation c_v.

- The use of ancillary drainage in three-dimensional stopes. It was shown that ancillary drainage in two-dimensional stopes was effective in accelerating the drainage process within a hydraulically filled stopes, consequently, reducing the build-up of pore pressure behind the barricades. It is recommended that the use and placement of ancillary drainage in three-dimensions be investigated to enable the most effective and efficient drainage to be obtained. i.e. length and placement of ancillary drains

- Further investigation is suggested into the potential of migration of fines and the influence on the barricade drainage performance.

- It is recommended that the EXCEL model developed in this dissertation be modified to take into account inhomogeneity in the fill.

- Although the EXCEL model was verified against previously validated models, it is recommended that a direct comparison of in situ data be used in validation.

- The EXCEL model developed only considers the behaviour in hydraulic filled stopes. By understanding the behavior and requirements of other fill types, EXCEL models could be developed for each of the fill types and tied into the one spreadsheet.

It is anticipated that the EXCEL model developed in this dissertation will provide the building block for additional features (such as the static and dynamic requirements) in

understanding the behavior of three-dimensional hydraulic filled stopes with varying properties, geometries and filling schedules.

REFERENCES

Amer A.M., and Awad, A.A. (1974). "Permeability of cohesionless soils." *Journal Geotechnical Engineering Division ASCE*, 100(12), 1309-1216.

Aubertin, M., Li, L., Arnoldi, S., Simon, R., Belem, T., Bussiere, B. and Benzaazoua, M. (2003). "Interaction between backfill and rockmass in narrow stopes." *Soil & Rock America 2003*, Cambridge, Massachusetts, AA Balkema, Roterdam, 1157-1164.

Aubertin, M., Mbonimpa, M., Bussiere, B., and Chapius, R.P. (2003). "A model to predict the water retention curve from basic geotechnical properties." *Canadian Geotechnical Journal*, 40(6), 1104 – 1122.

Azizi F. (2000). *Applied Analysis in Geotechnics*, E & FN Spon, Taylor and Francis Group, New York, Chapter 13.

Barkley, E., (1927). "Stope filling at north Mount Lyell Mine." *The AusIMM Proceedings*, 66, 157-164.

Bear, J. (1972). *Dynamics of fluids in porous media*, Elsevier, New York, USA.

Black, A.B. (1941). "Pneumatic stowing of mill residues in underground stopes." Broken Hill South Limited, *Proc. Australian Institute Mining Metallurgy*, 123, 141-154.

Barnes, G.E. (2000). *Soil Mechanics – Principles and Practice*, 2nd Edition, MacMillan Press Ltd., London, 476.

Barrett, J.R. and Cowling, R. (1980). "Investigation of cemented fill stability in 1100 orebody, Mount Isa Mines, Ltd., Queensland, Australia." *Transactions, Institute of Mining and Metallurgy*, Section A, 89, A118-A128.

Barrett, J.R., Coulthard, M.A. and Dight, P.M. (1978). "Determination of fill stability." *Mining with Backfill, Proceedings of 12th Canadian Rock Mechanics Symposium*, CIM, 19, Sudbury, Ontario, Canada.

Belem, T., Harvey, A., Simon, R., and Aubertin, M. (2004). "Measurement and prediction of internal stresses in an underground opening during its filling with cemented fill," *Proceedings of the 5th International Symposium on Ground Support, Ground Support in Mining and Underground Construction*, Perth, Western

Australia, 619-130.

Bloss, M.L. (1992). *Prediction of cemented rock fill stability design procedures and modelling techniques*. PhD Thesis, Department of Mining and Metallurgical Engineering, University of Queensland, Brisbane, Australia.

Bloss, M.L. and Chen, J. (1998). "Drainage research at Mount Isa Mines Limited 1992 – 1997." *Proceedings of the 6th International Symposium on Mining with Backfill: Minefill '98*, Ed. M. Bloss, Brisbane, Australia, 111-116.

Brady, B.H.G. and Brown, E.T. (1985). *Rock mechanics for underground mining*, George Allen and Unwin, London.

Brady, A.C. and Brown, J.A. (2002). "Hydraulic fill at Osborne mine." *Proceedings of the 7th Underground Operators' Conference*, Townsville, Australia, 161-165.

Brandon T., Clough G., and Rahardjo P. (1991). "Fabrication of Silty Sand Specimens for Large-and Small-Scale Tests" *Geotechnical Testing Journal, ASTM*, 14, 46-55.

Bridges, M.C. (2003). "A New Era of Fill-Retaining Barricades," *Digging Deeper*, AMC Consultants, October, www.amcconsultants.com.au , 2-5.

Budhu, M. (2000). *Soil Mechanics and Foundations*, John Wiley and sons Inc., New York, USA, 557 pp.

Butterfield, R. (1999). Dimensional analysis for geotechnical Engineers, *Geotechnique*, 49(3), 357-366.

Butterfield, R. (2000). Scale-Modelling of Fluid Flow in Geotechnial Centrifuges, *Soils and Foundations*, Japanese Geotechnical Society, 40(6), 39-45.

Carman, P.C. (1938). "The determination of specific surface of powders." *J. Soc. Chem. Ind. Trans.*, 57, 225 pp.

Carman, P.C. (1956). *Flow of gases through porous media*, Butterworths scientific Publications, London, U.K.

Carrier III, D.W., Bromwell, L.G. and Somogyi, F. (1983). "Design capacity of slurried mineral waste ponds." *Journal of Geotechnical Engineering*, 109(5), 699-716

Cedegren, H. R. (1989). *Seepage, drainage and flownets,* Wiley, 3rd Edition, New York, USA.

Chapius, R.P. (2004). "Predicting the saturated hydraulic conductivity of sand and

gravel using effective diameter and void ratio." *Canadian Geotechnical Journal*, 41(5), 787-795.

Chapius, R.P. and Aubertin M. (2003). "On the use of the Kozeny Carman equation to predict the hydraulic conductivity of soils." *Canadian Geotechncial Journal*, 40(3), 616-628.

Chapius, R.P., Gill D.E. and Bass K. (1989). Laboratory permeability tests on sand: Influence of the compaction method on anisotropy." Canadian Geotechnical Journal, 26(4), 614 -622,

Clarke, I.H. (1988). "The properties of hydraulically placed backfill." *Proceedings of Backfill South African Mines*, Johannesburg, SAIMM, 15-33.

Coduto D.P. (1999). *Geotechnical engineering: Principles and practice*, Prentice-Hall, Upper Saddle River, N.J.

Corson, D.R., Dorman, R.K. and Sprute, R.H. (1981). "Improving the support characteristics of hydraulic fill." *Application of Rock Mechanics to Cut and Fill Mining, The Institute of Mining and Metallurgy*, Eds. O. Stephansson and M.J. Jones, 93-99.

Cowling, R. (1998). "Twenty-five Years of Mine Filling: Developments and Directions." *Proceedings of Minefill '98,* Brisbane, 3-10.

Cowling, R., Grice, A.G. and Isaacs, L.T. (1988), "Simulation of hydraulic filling of large underground mining excavations." *Proceedings of 6th International Conference on Numerical Methods in Geomechanics*, Innsbruck, Austria, 1869-1876.

Cowling R., Voboril A., Isaacs L.T., Meek J.L. and Beer G. (1989). "Computer models for Improved fill performance." *Proceedings of Innovations in Mining Backfill Technology*, Balkema, Rotterdam, 165 – 174.

Darcy, H. (1856). *Les fontaines publiques de la ville de Dijon*. Victor Dalmont, Paris, France.

Das, B.M. (2002). *Principles of Geotechnical Engineering*, 5th Edition, Brooks/Cole – Thomsom Learning, USA. 578 pp.

Das, B.M. (1985). *Advanced soil mechanics*, Hemisphere Publishing, Corporation, Singapore.

Das, B.M. (1997). *Advanced soil mechanics*, Taylor and Francis, Washington, D.C.

Douglas J.F., Gasiorek J.M. and Swaffield J.A. (2001). *Fluid Mechanics 4th Edition*,

Pearson, Essex, England.

Dorricott M.G., and Grice A.G. (2002). "Backfill – The environmentally Friendly Tailings Disposal System." *Proceedings Green Processing 02*, Australian Institute of mining and metallurgy, 265-270.

Duffield, C., Gad, E., and Bamford, W. (2003). "Investigation into the structural behaviour of mine brick barricades." *AusIMM Bulletin*, Institute of Engineers, March/ April, 45-50.

Franklin J.A. and Dusseault M.B. (1991). *Rock Engineering Applications 1st Edition*. McGraw Hill Professional, New York, USA.

Freeze, R.A. and Cherry, J.A. (1979). *Groundwater*, Prentice-Hall, Englewoods Cliffs, N.J.

Fourie, A.B., Hofmann, B.A., Mikula, R.J., Lord, E.R.F. and Robertson, P.K. (2001). "Partially saturated tailings sand below the Phreatic surface." *Geotechnique*, 51(7) 577 – 585.

Garett, W.S. and Campbell Pitt, L.T. (1961). "Design and Construction of Underground Bulkheads and Water Barriers." *7th CMMI Congress*, SAIMM, Johannesburg, 1285-1301

Grice, A.G. (1989). "Fill Research at Mount Isa Mines Limited." *Innovations in Mining Backfill Technology*, Balkema, Rotterdam, 15-22.

Grice, A.G. (1998 a). "Stability of hydraulic backfill barricades." *Proceedings of the 6th International Symposium on Mining with Backfill*, AusIMM, Brisbane, Australia.

Grice, A.G. (1998 b). "Underground mining with backfill." *Proceedings of the 2nd Annual Summit – Mine Tailings Disposal Systems*, Brisbane, Australia.

Grice, T. (2001). "Recent minefill developments in Australia." *Proceedings of the 7th International Symposium on Mining with Backfill: Minefill '01*, Seattle, USA, 351-357.

Grice, A.G., Wilwain, A, and Urquhart, K. (1993). "Backfilling operations at Mount Isa Mines 1998-1992." *Proceedings of the 5th International Symposium on Mining with Backfill: Minefill '93*, Johannesburg, South Africa, 369-373.

Grice, A.G. and Fountain, L.J. (1991). "The fill information system." *Second Australian Conference on Computer Applications in the Mineral Industry*, University of Wollongong, NSW, Australia.

Griffiths, D.V. (1984). "Rationalized charts for the method of fragments applied to confined seepage." *Geotechnique*., 34(2), 229 – 238.

Hall W.K. (2006). "Permeability Characteristics of Granular soils and hydraulic fill Drainage Modeling," B.E. Thesis, James Cook University.

Hansbo, S. (1960). "Consolidation of Clay with Special Reference to Influence of Vertical Sand Drains," *Proceedings No. 14, Sweedish Geotechnical Institute*. Sweeden.

Hatanaka, M., Uchida, A., Taya, Y., Takehara, N., Hagisawa, T., Sakou, N. and Ogawa, S. (2001). "Permeability characteristics of high-quality undisturbed gravely soils measured in laboratory tests." *Soils and Foundations*, 41(3), 45–55.

Harr, M.E. (1962). *Ground Water and Seepage*, McGraw Hill Book Company, New York.

Harr, M.E. (1977). *Mechanics of Particulate Media*, McGraw Hill Book Company, New York.

Hazen, A. (1892). "Some physical properties of sands and gravels, with special reference to their use in filtration." *24th Annual Rep., Massachusetts State Board of Health*, Pub. Doc. No. 34, 539 – 556.

Hazen, A. (1930). *Water supply. American Civil Engineers Handbook*, Wiley, New York, USA.

Head, K.H. (1980-1996). *Manual of Soil Laboratory Testing,* John Wiley and Sons; Vol. 1-3.

Herget, G. and De Korompay, V. (1988). "In situ drainage properties of hydraulic backfills," *Proceedings of Mining with Backfill, Research and Innovations*, CIM, 19, 117 – 123.

Hinde A.L. (1993). "Advances in Particle Sizing of Backfill." *Minefill 93*, SAIMM Johannesburg, 181 – 188.

Holtz, R.D. and Broms, B.B., (1972). "Long-Term Loading Tests at Ska-Edeby Sweeden." *Proceedings of the ASCE Speciality Conference on Performance of Earth and Earth-Supported Structures*, Purdue University, Vol 1, Part 1, 435 – 444.

Holtz, R.D., and Kovacs, W.D. (1981). *An introduction to geotechnical engineering*, Prentice-Hall, Englewood Cliffs, New Jersey, USA.

Hansbo, S. (1960). "Consolidation of Clay with Special Reference to Influence of

Vertical Sand Drains," *Proceedings* No. 14, Sweedish Geotechnical Institute.

Isaacs, L. T., Carter, J. P. (1983). "Theoretical study of pore water pressures developed in hydraulic fill in mine stopes," *Transactions of Institution of Mining and Metallurgy* (Section A: Mining Industry), 92, A93-A102.

Itasca, (2002). *FLAC version 4.0 Users Manuals*. Itasca Consulting Group, Thresher Square East, 708 South Third Street, Suite 310, Minneapolis, Minnesota, 55415 USA.

Itasca, (2002). *FLAC^{3D} version 2.1 Users Manuals*. Itasca Consulting Group, Thresher Square East, 708 South Third Street, Suite 310, Minneapolis, Minnesota, 55415 USA.

Keren, L. and Kainain, S. (1983). "Influence of tailings particles on physical and mechanical properties of fill." *Proceedings of the International Symposium on Mining with Backfill*, Eds. S Granholm, A.A. Balkema, Sweden, 21-29.

Karol, R.H., (1960). *Soils and Soil Engineering*. Prentice-Hall, Englewood Cliffs, New Jersey, USA.

Kozeny, J. (1927). "Ueber kapillare Leitung des Wassers im Boden." *Wien, Akad. Wiss.*, 136(2a), 271.

Kuganathan, K. (2001 a). "Design and Construction of Shotcrete Bulkheads with Engineered Drainage System for Mine Backfilling." *International Seminar on Surface Support Liners, Australian Centre for Geomechanics*, Section 8, 1-15.

Kuganathan K. (2001 b). "Mine backfilling, backfill drainage and bulkhead construction – A safety first approach." *Australia's mining monthly*, February, 58-64.

Kuganathan, K. (2002). "A method to design efficient mine backfill drainage systems to improve safety and stability of backfill bulkheads and fills." *Proceedings of the 7th Underground Operators' Conference*, Townsville, Australia, 181-188.

Kupper A., Morgenstern N, Sego D., (1992). "Laboratory tests to study hydraulic fill." *Canadian Geotechnical Journal*, 29, 405-417.

Lambe, T.W. (1951). *Soil Testing for Engineers*, John Wiley and Sons, New York, USA.

Lambe, T.W., and Whitman, R.V. (1969). *Soil Mechanics*, Wiley, New York, USA.

Lambe, T.W. and Whitman R.V. (1979). *Soil Mechanics, SI Version, Series in Soil*

Engineering, John Wiley and Sons, New York, USA.

Lamos, A.W. (1993). "An assessment of the effects of ultrafine aggregate components on the properties of mine backfills." *Proceedings of the 5th International Symposium on Mining with Backfill: Minefill '01*, Johannesburg, South Africa, 173-179.

Leonards, G.A. (1962). *Engineering properties of soils. Foundation engineering*, G.A. Leonards, ed., McGraw-Hill, New York, USA, 66 – 240.

Manoharan S., Pirahas B., Pirapakanara K. (2002). An experimental Study on the effect of Cement Stabilization on the Permeability and Compressive strength of a soil, *not published*.

Martin, D.M., (2001). *Effective drainage of Hydraulic Mine Backfill*, B Eng. Thesis, Western Australian School of Mines, Kalgoorlie, Australia.

Mansur, C.I. and Dietrich, R.S. (1965). "Pumping tests to determine permeability ratio." *Journal of Soil Mechanics and Foundations, ASCE*, 91(SM4), 151-183.

Martys, N., Masad, E., and Muhunthan, B. (2000). "Simulation of fluid flow and permeability in cohesionless soils." *Water Resources Research*, 36(4), 851 – 864.

McKinstry, J.D. (1989). "Backfilling operations at Mount Isa Mines Limited." *Proceedings of the fourth International Symposium on Mining with Backfill*, Montreal.

Mbonimpa, M., Aubertin, M., Chapius, R.P., Bussiere, B. (2002). "Practical pedaotransfer functions for estimating the saturated hydraulic conductivity." *Geotechnical and Geological Engineering*, 20, 235 – 259.

Mishra, G.C., and A.K. Singh. (2005). "Seepage through a Levee." *International Journal of Geomechanics.*, 5(1), 74-79.

Mitchell, J.K. (1976), *Fundamentals of Soil Behavior*, John Wiley and Sons, New York, 422.

Mitchell, R.J. (1998). "The Eleventh Annual R.M. Hardy Keynote Address, 1997: Centrifugation in Geoenvironmental Practice and Education." *Canadian Geotechnical Journal,* 35(4), 630-640.

Mitchell, R.J., Smith, J.D. and Libby, D.J. (1975). "Bulkhead Pressures Due to Cemented Hydraulic Mine Backfills." *Canadian Geotechnical Journal*, 12(3), 362-371.

Murray, R.M. (1915). "Mining methods at Mount Lyell." *The AusIME Proceedings,* 19, 125-139.

Murphy, G. (1950). *Similitude in Engineering*, Ronal Press Company, New York.

Nantel, J. (1998). "Recent Developments and Trends in Backfill Practices in Canada." *Proceedings of AusIMM '98 – The Mining Cycle*, Mt Isa, Australia, 11 – 14.

NAVFAC. (1974). "Soil mechanics, foundations and earth structures." *Naval Facilities Engineering Command (NAVFAC) design manual DM7.* U.S. Government Printing Office. Washington D.C.

Neindorf, L.B. (1983). "Fill Operating Practices at Mount Isa Mines." *Proceedings, Symposium 'Mining with Backfill*, Lulea, Sweeden, 179 – 187.

Nicholson, D.E. and Wayment, W.R. (1964). "Properties of hydraulic backfills and preliminary vibratory compaction tests." *United States Department of the Interior, Bureau of Mines, 6477.*

Nnadi, G.N. and Mitchell, R.J. (1991). "Use of centrifuge models to study simulated blast loadings on backfills." *Canadian Institute of Mining and Metallurgy, Rock Mechnaics Bulletin*, 84(951), 58-63.

Ouellet, J. and Servant, S. (1998). "Numerical simulation of the drainage in a mining stope filled with hydraulic backfill." *Proceedings of the 6th International Symposium on Mining with Backfill: Minefill '98*, Ed. M. Bloss, Brisbane, Australia, 105-110.

Park R.T. and Gamble, W.L. (2000). *Reinforced Concrete Slabs*. 2nd Edition, John Wiley and Sons, New York, USA.

Patton, F.E. (1957). Backfilling at Noranda. Mining in Canada, 6th Comm. Min. and Met. Congr: Toronto, Canada, 229 – 236.

Pavlovsky, N. N. (1956). Collected Works, Akad. Nauk USSR, Leningrad.

Peele, J. (1941). *Mining Engineers Handbook*, John Wiley & Sons, Inc. Canada.

Pettibone, H.C. and Kealy, C.D. (1971). "Engineering properties of mine tailings." *Journal of Soil Mechanics and Foundations Division*, ASCE, 97(SM9), 1207-1225.

Potvin Y., Thomas E., and Fourie A., (2005) *Handbook on Minefill*, Australian Centre for Geomechanics, Nedlands, Australia.

Qiu, Y. and Sego, D.C. (2001). "Laboratory properties of mine tailings." *Canadian Geotechnical Journal,* 38(1), 183-190.

Rankine, K. S. (2002). "Permeability and Drainage Characteristics of Hydraulic Fills in Underground Mines" B Eng. Undergraduate thesis, Department of Civil and Environmental Engineering, James Cook University, Townsville, Australia.

Rankine, K.J., Rankine, K.S., and Sivakugan, N. (2003). "Three-dimensional drainage modelling of hydraulic fill mines," *Proc. 12th Asian Regional Conf. on Soil Mech. and Geotech. Engineering*, Eds. CF Leung, KK Phoon, YK Chow, CI Teh and KY Yong, Singapore, 937-940.

Rankine, K.J., Sivakugan, N. and Rankine, K.S. (2004). Laboratory tests for mine fills and barricade bricks, *Proceedings of 9th ANZ Conference on Geomechanics*, Auckland, Vol. 1, 218–224.

Rankine, K.J. (2005). *An investigation into the drainage characteristics and behaviour of hydraulically placed mine backfill and permeable minefill barricades*. PhD Thesis, Department of Civil and Environmental Engineering, James Cook University, Townsville, Australia.

Rankine, K.J., Sivakugan, N. and Cowling, R. (2006). "Emplaced geotechnical characteristics of hydraulic fills in a number of Australian mines," *Geotechnical and Geological Engineering*, Springer, 24(1), 1-14.

Reddi, L.N. (2004). *Seepage in Soils – Principles and applications*, John Wiley and Sons, Inc., Hoboken, New Jersey, 383.

Reedman J.H. (1979). *Techniques in Mineral Exploration*. Applied Science Publishers, London, England.

Samarasinghe, A.M., Huang, Y.H. and Drnevich, V.P. (1982). "Permeability and consolidation of normally consolidated soils." *Journal of the Geotechnical Engineering Division,* ASCE, 108(GT1), 55-60.

Scheideeger, A.E. (1953). *Theoretical models of porous matter*. Producers Monthly, 10(17), 17-23.

Scheideeger, A.E. (1954). "Statistical hydrodynamics in porous media." *Journal of Applied Physics*, 25, 994-1001.

Scheidegger, A. E. (1974). *The physics of flow through porous media*, University of Toronto Press, Toronto, Canada.

Singh, S. (2007). *Personal Communication*

Singh, D.N. and Gupta, A.K. (2000). "Modelling hydraulic conductivity in a small

centrifuge." *Canadian Geotechnical Journal*, 37(5), 1150-1155.

Sivakugan, N. and Al-Aghbari, M.Y.S. (1993 a). "An Optimization Study on Seepage Beneath a Concrete Dam." *Proceedings of Structural Optimization '93, The World Congress on Optimal Design of Structural Systems*, Rio de Janeiro, 343-350.

Sivakugan, N., and Al-Aghbari, M.Y.S. (1993 b). "Method of fragments – quick solutions to seepage problems." *Environmental Management, Geo-Water & Engineering Aspects*, Balkema, 491-496.

Sivakugan, N., Rankine, K., and Rankine, R. (2006). "Permeability of hydraulic fills and barricade bricks." *Geotechnical and Geological Engineering*, Springer, 24(3), 661-673.

Sivakugan, N., Rankine, K.J. and Rankine, K.S. (2006). "Study of drainage through hydraulic fill stopes using method of fragments." *Journal of Geotechnical and Geological Engineering*, Springer, 24(1), 79-89.

Sivakugan, N., and Rankine, K.S. (2006). "A simple solution for drainage through a 2-dimensional hydraulic fill stope," *Journal of Geotechnical and Geological Engineering*, Springer, 24(5), 1229-1241.

Sivakugan, N., Rankine, R.M., Rankine, K.J., and Rankine, K.S. (2006). "Geotechnical considerations in mine backfilling in Australia," *Journal of Cleaner Production*, Elsevier, 14, 1168-1175.

Sivakugan, N., Rankine, K.J., and Rankine, R.M. (2005). Geotechnical Aspects of Hydraulic Filling of Underground Mine Stopes in Australia, *Chapter 18, Ground Improvements - Case Histories*, Eds. B. Indraratna & J. Chu, Elseveir, Netherlands, 515-540.

Taylor, D.W. (1948). *Fundamentals of soil mechanics*, Wiley, New York, USA.

Terzaghi, K., and Peck, R.B. (1964). *Soil mechanics in engineering practice*, Wiley, New York, USA.

Terzaghi, K., Peck, R.B., and Mesri, G. (1996). *Soil mechanics in engineering practice*, Wiley, New York, USA.

Terzaghi, C. (1925). Determination of the permeability of clay. *Engng News Rec.* 95, 832-836, 510.

Thomas, E.G. (1969). *Characteristics and Behaviour of Hydraulic Fill Material*,

PhD Thesis, Department of Mining and Metallurgical Engineering of the University of Queensland, Brisbane, Australia.

Thomas, E.G. (1978). "Fill permeability and its significance in mine fill practice." Mining with Backfill, 12th Canadian Rock Mechanics Symposium, Montreal, CIMM.

Thomas, E.G., (1979). "Fill permeability and its significance in mine fill practice." *Proc. Symp. Mining with Backfill*, Sunbury, Canada.

Thomas, E.G. and Holtham, P.N. (1989). "The basics of preparation of deslimed mill tailing hydraulic fill." Innovations in Mining Backfill Technology, Ed. Hassani et al., Rotterdam, Balkerna, 425-431.

Thomas, E.G., Nantel J.H. and Notley K.R. (1979). "Backfill technology in underground metalliferous mines." *International Academic Services*, Kinston, Ontario, Canada.

Torlach, J. (2000) Potential hazards associated with minefill, Safety Bulletin 55, *Department of Minerals and Energy of Western Australia.*

Traves, W.H. (1988). *A three dimensional model of the drainage of back-filled open stopes*, Masters Thesis, Department of Civil Engineering, University of Queensland, Brisbane, Australia.

Traves, W.H. and Isaacs, L.T. (1991). "Three-dimensional modelling of fill drainage in mine stopes." *Transactions of the Institution of Mining and Metallurgy, Section A (Mining Industry),* The Institution of Mining and Metallurgy, A66-A71.

Tritton, D.J. (1988). *Physical Fluid Dynamics 2nd Edition.*

Udd, J.E. and Annor, A. (1993). "Backfill Research in Canada." *Proceedings of the 5th International Symposium on Mining with Backfill: Minefill '93*, SAIMM, Johannesburg, South Africa, 361 – 368.

Uys, C.J. (1993). "The production of better backfill by the removal of ultrafine material." *Proceedings of the 5th International Symposium on Mining with Backfill: Minefill '93*, SAIMM, Johannesburg, South Africa, 159 – 167.

Vukovic, M., and Soro A. (1992). "Determination of hydraulic conductivity of porous media from grain size composition." *Water Resources Publications*, Littleton, Colorado, USA.

Wallace, K. (1975). "A procedure for numerical analysis of transient moisture in

saturated and unsaturated earth structures." Report, James Cook University, Townsville, Qld.

Wayment, W.R. and Nicholson D.E. (1964). "A proposed modified percolation-rate test for use in physical property testing of mine backfill" *Rep. Invest. U.S. Bureau Mines* 6562, 24 p.

Wen, B., Aydin, A. and Duzgoren-Aydin, N.S. (2002). "A comparative study of particle size analysis by sieve-hydrometer and laser diffraction methods." *Geotechnical Testing Journal*, ASTM, Dec, 25(4), 434-442.

Witt K.J., and Brauns J. (1983). "Permeability-anisotropy due to particle shape." Journal of Geotechnical Engineering, 109(9), 1181 -1187.

Hypertext References

www.civil.uwa.edu.au/teaching/MINE4162?f=130747

http://www.minerals.org.au/corporate

http://www.australianmineralsatlas.gov.au

Ore-age: a hybrid system for assisting and teaching mining method selection

APPENDIX A

Cemented hydraulic fill laboratory testing

A.1. Initial and Final Parameters for Copper Tailings

Parameters		Initial slurry			Final (At 28 days)			
		CHF 1	CHF 2	CHF 3	CHF1	CHF 2	CHF 3	HF
w	Water Content	0.33	0.33	0.33	0.196	0.19	0.194	0.171
G_s	Specific Gravity	3.69	3.69	3.69	3.69	3.69	3.69	3.69
e	Void Ratio	1.218	1.218	1.218	0.723	0.701	0.716	0.631
n	Porosity	0.55	0.55	0.55	0.42	0.41	0.42	0.39
ρ_d	Dry Density(t/m³)	1.85	1.85	1.85	2.14	2.17	2.15	2.26
ρ_m	Bulk Density(t/mᵌ)	2.45	2.45	2.45	2.56	2.58	2.57	2.65

A.2. Initial and Final parameters for Zinc Tailings

Parameters		Initial Slurry			Final (At 28 days)			
		CHF 1	CHF 2	CHF 3	CHF1	CHF 2	CHF 3	HF
w	Water Content	0.33	0.33	0.33	0.18	0.198	0.197	0.194
G_s	Specific Gravity	3.02	3.02	3.02	3.02	3.02	3.02	3.02
e	Void ratio	1.00	1.00	1.00	0.54	0.60	0.59	0.59
n	Porosity	0.50	0.50	0.50	0.35	0.37	0.37	0.37
ρ_d	Dry Density	1.51	1.51	1.51	1.96	1.89	1.89	1.90
ρ_m	Bulk Density	2.01	2.01	2.01	2.31	2.26	2.27	2.27

A.3. Grain Size Distribution Curves for Copper and Zinc Tailings tested in cemented hydraulic fill permeability testing
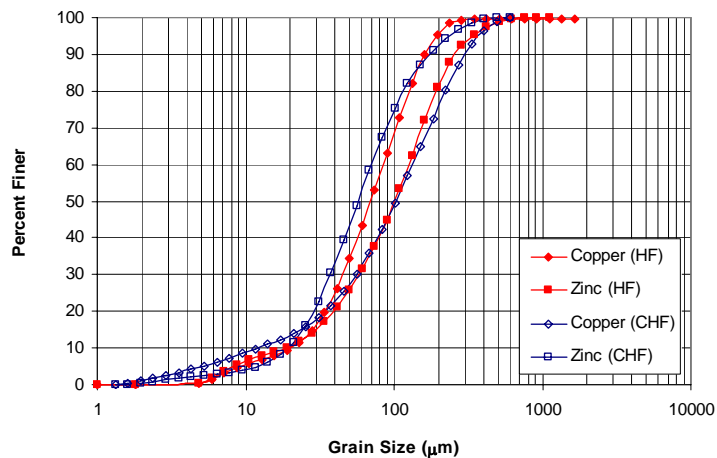
A.4. Summary of Copper Permeability Results

Time		Permeability (cm/s)						Permeability (mm/hour)					
		CHF1		CHF2		CHF3		CHF1		CHF2		CHF3	
days	hours	const.head	fall.head	const.head	fall.head	const.head	fall.head	const.head	fall.head	const.head	fall.head	const.head	fall.head
0.00	0	1.85E-04		1.98E-04		1.91E-04		6.67		7.14		6.88	
0.04	1	1.71E-04		1.80E-04		1.93E-04		6.15		6.48		6.94	
0.08	2	2.11E-04		1.89E-04		1.79E-04		7.58		6.80		6.45	
0.13	3	2.06E-04		1.84E-04		2.24E-04		7.41		6.62		8.08	
0.17	4	2.19E-04		1.79E-04		2.19E-04		7.89		6.44		7.89	
0.21	5	1.93E-04		1.74E-04		1.77E-04		6.94		6.25		6.37	
0.25	6	1.88E-04		1.66E-04		1.68E-04		6.75		5.99		6.06	
0.29	7	1.81E-04		1.61E-04		1.63E-04		6.50		5.80		5.87	
0.33	8	1.77E-04		1.54E-04		1.58E-04		6.37		5.55		5.68	
0.38	9	1.68E-04		1.51E-04		1.50E-04		6.06		5.43		5.41	
0.42	10	1.56E-04		1.51E-04		1.54E-04		5.62		5.43		5.55	
0.46	11	1.54E-04		1.37E-04		1.40E-04		5.55		4.92		5.05	
0.50	12	1.52E-04		1.28E-04		1.38E-04		5.49		4.61		4.98	
0.54	13	1.47E-04		1.40E-04		1.33E-04		5.30		5.05		4.80	
0.58	14	1.14E-04		1.38E-04		1.19E-04		4.10		4.98		4.29	
0.63	15	9.81E-05		1.47E-04		1.16E-04		3.53		5.30		4.16	
0.67	16	1.05E-04		1.24E-04		1.09E-04		3.79		4.48		3.91	
0.71	17	1.21E-04		9.81E-05		1.07E-04		4.35		3.53		3.85	
0.75	18	1.07E-04		9.81E-05		1.01E-04		3.85		3.53		3.65	
0.79	19	7.94E-05		9.31E-05		7.62E-05		2.86		3.35		2.74	
0.83	20	9.64E-05		9.11E-05		8.76E-05		3.47		3.28		3.15	
0.88	21	9.64E-05		1.09E-04		8.76E-05		3.47		3.91		3.15	
0.92	22	9.81E-05		8.41E-05		8.76E-05		3.53		3.03		3.15	
0.96	23	8.59E-05		8.24E-05		8.59E-05		3.09		2.97		3.09	
3.00	72	3.51E-05		2.98E-05		1.84E-05		1.26		1.07		0.66	
7.00	168	9.64E-06		8.76E-06		1.68E-05		0.35		0.32		0.60	
14.00	336		1.13E-05		1.10E-05		5.52E-06		0.41		0.40		0.20
28.00	672		3.92E-06		3.48E-06		6.08E-07		0.14		0.13		0.02

Permeability of (uncemented) hydraulic fill =   4.94E-04 cm/s   =   17.79   mm/hr   (approx)

215

A.5. Summary of Zinc Permeability Results

Time		Permeability (cm/s)						Permeability (mm/hour)					
		CHF1		CHF2		CHF3		CHF1		CHF2		CHF3	
days	hours	const.head	fall.head	const.head	fall.head	const.head	fall.head	const.head	fall.head	const.head	fall.head	const.head	fall.head
0.00	0	3.38E-04		3.13E-04		3.63E-04		12.18		11.25		13.05	
0.04	1	3.04E-04		3.07E-04		3.57E-04		10.96		11.06		12.86	
0.08	2	3.06E-04		3.13E-04		3.58E-04		11.01		11.25		12.88	
0.13	3	2.74E-04		3.04E-04		3.41E-04		9.85		10.93		12.28	
0.17	4	2.79E-04		2.82E-04		2.82E-04		10.06		10.15		10.14	
0.21	5	2.68E-04		2.69E-04		2.85E-04		9.64		9.69		10.27	
0.25	6	2.31E-04		2.60E-04		2.76E-04		8.31		9.37		9.95	
0.29	7	2.25E-04		2.53E-04		2.87E-04		8.10		9.11		10.34	
0.33	8	2.10E-04		2.40E-04		2.63E-04		7.57		8.65		9.48	
0.38	9	2.31E-04		2.35E-04		2.53E-04		8.32		8.46		9.11	
0.42	10	2.08E-04		2.49E-04		2.72E-04		7.48		8.98		9.80	
0.46	11	1.95E-04		2.15E-04		2.03E-04		7.03		7.74		7.30	
0.50	12	2.01E-04		2.10E-04		2.23E-04		7.22		7.55		8.01	
0.54	13	2.12E-04		2.06E-04		2.01E-04		7.62		7.42		7.24	
0.58	14	1.99E-04		2.02E-04		2.14E-04		7.15		7.29		7.69	
0.63	15	1.73E-04		1.97E-04		1.87E-04		6.22		7.09		6.72	
0.67	16	1.61E-04		1.95E-04		1.71E-04		5.81		7.03		6.14	
0.71	17	1.58E-04		1.92E-04		1.97E-04		5.67		6.90		7.11	
0.75	18	1.39E-04		1.92E-04		1.97E-04		5.02		6.90		7.11	
0.79	19	1.49E-04		1.90E-04		1.81E-04		5.35		6.83		6.53	
0.83	20	1.62E-04		1.92E-04		1.79E-04		5.82		6.90		6.46	
0.88	21	1.49E-04		1.83E-04		1.81E-04		5.35		6.57		6.53	
0.92	22	1.49E-04		1.81E-04		1.78E-04		5.36		6.51		6.40	
0.96	23	1.40E-04		1.79E-04		1.78E-04		5.02		6.44		6.40	
3.00	72	9.57E-05		1.17E-04		1.53E-04		3.45		4.23		5.49	
7.00	168	5.38E-05		7.22E-05		5.88E-05		1.94		2.60		2.12	
14.00	336		8.47E-05	4.29E-05		3.80E-05			3.05	1.54			1.37
28.00	672		3.07E-05		1.60E-05		1.78E-05		1.10		0.57		0.64

Permeability of (uncemented) hydraulic fill =	6.2582E-04	cm/s	=	22.53	mm/hr		(approx)

APPENDIX B

FLAC/FLAC^{3D} Codes

B.1.   Source listing *FISH* and *FLAC* code for program used to develop the two-dimensional form factor

```
;Program for validating Method of fragments in two-dimenisonal stopes

; Kelda Rankine
; James Cook University

config gw
grid 26,60                                      ; Change set up i-col j-row
model mohr

prop dens=1800 bulk=1e8 shear=0.3e8 coh=0 ten=0
prop perm=2e-10
set gravity=9.81
set flow = on mech = off
water dens=1000 bulk=2e9

gen 0,0 0,60 26,60 26,0

model null i=21,26 j=6,60                        ; Change for stope dimensions
apply pp=0  j=61 i=1,21                          ; Change set pp top of stope
fix sat j=61 i=1,21                              ; Change sat at top of stope
apply pp = 49.05e3 var 0 -49.05e3 i=53 j=1,6     ; Change set pp at drain exit
fix sat i=27 j=1,6                               ; Change sat at drain exit

set datum = 6                                    ; Change datum
plot hold model grid gn bou
his gpp i=1 j=1                                  ; Change max pp history
solve sratio = 1e-3

save kelflow.sav

plot hold fix bou                                ; Plots results
plot hold pp fill


; Calculating form factors for two-dimensional stopes

restore kelflow.sav

def formfac
  perm=2e-10
  sumflow=0
  loop j (1,6)                                   ; Change height of drain
```

```
sumflow = sumflow + gflow(27,j)              ;  Change  gridpoints  height  of
drain

end_loop
formfactor = perm*9810*55/sumflow            ;  Change  head  loss  for  specified
geometry
end

formfac

print formfactor

;***************

def formfaccheck
  perm=2e-10
  sumflow1=0
  loop i (1,21)                              ;  Change  gridpoints  widtth  of
stope
  sumflow1 = sumflow1 + gflow(i,61)          ; Change gridpoints stope height
end_loop
formfactorcheck = perm*9810*55/sumflow1      ; Change  head  loss  for  specified
geometry
end

formfaccheck

print formfactorcheck

;***************

def porepressures
ua=gpp(1,1)                                  ; Maximum pore pressure

end

porepressures

print ua
```

B.2. Source listing *FISH* and *FLAC* code for two-dimensional Anisotropic Permeability Analysis

```
; Anisotropic Permeability Investigation

; Kelda Rankine
; James Cook University

new

;SET UP MODEL

config gw
grid 42, 120                              ; Change stope geometry
model mohr

; SET UP PROPERTIES
prop den=1500 shear=3e8 bulk=5e8 coh=5e5 tens=1e10
prop k11=3e-9                             ;Change horizontal permeability
prop k22=1e-9                             ;Change vertical permeability

model null i=41,42 j=3,120
plot hold model grid bou
set gravity=9.81 flow=on mech=off         ; Flow only problem
water dens=1000 bulk=1e5

title
VERIFICATION OF SPREADSHEET

;SET UP PORE PRESSURE AND SATURATION ALONG BOUDNARIES
apply pp=0 j=121 i=1,41                      ;Change set pp at top of stope
apply pp=0 i=43 j=1,3            ;Change set pp at drain
fix sat j=121 i=1,41            ;Change fix sat at top of stope
fix sat i=43 j=1,3            ;Change fix sat at drain outlet
plot hold fix bou

set sratio 1e-3
step 140000

plot hold pp fill bou black


; TO COMPUTE FORM FACTOR AND FLOW

def flowout
```

```
        outflow=0
        loop j (1,3)                    ;Change height of drain
        outflow=outflow+gflow(43,j) ;Change gp at drain outlet

        end_loop
end

def flowin
        inflow=0
        loop i (1,81)                   ;Change gp at top of stope
        inflow = inflow + gflow(i, jgp)
        end_loop
end

flowout
flowin

hist gpp i=1 j=1

plot hist 1
print outflow inflow
print gpp i=1 j=1

save anisoF3.sav
```

B.3. Source listing *FISH* and *FLAC³ᴰ* code for program used to develop three-dimensional form factor

```
; Steady State Stope
;
; CASE 1 - Single drain, modelled in half symmetry
; Steady state simulations to develop design charts
;
; Kirralee Rankine modified by Kelda Rankine
; James Cook University
;
; *** Initial Input Parameters ***
; Specify Input Parameters
Define inputparameters
realfillperm=0.0054 ; m/hr
fillperm=(realfillperm/(60*60))/9810        ; FLAC3D units for permeability
fillspecgrav=2.9        ; Specific Gravity
filldrydens=0.5*fillspecgrav        ; Dry Density of Fill (t/m3)
fillmoistcont=0.25        ; moisture content
fillpor=1-(filldrydens/fillspecgrav)        ; fill porosity
fillvoidratio=fillpor/(1-fillpor)          ; fill void ratio
satmoistcont=fillvoidratio/fillspecgrav         ; saturated moisture content of fill
percentsolids=0.72        ; slurry percent solids
filleffpor=fillpor-(fillmoistcont*fillspecgrav/(1+fillvoidratio))        ; effective porosity
;
B=20   ; stope width (m)
hb=B/2          ; half stope width for half symmetry
x=4             ; drain length (m)
dw=2            ; square drain width (m)
hdw=dw/2
fullheight=100
;
; use 1 m grid spacing throughout
zonespace=1
xzones=x/zonespace
dwzones=dw/zonespace
hdwzones=hdw/zonespace
bzones=b/zonespace
hbzones=hb/zonespace
fullzones=fullheight/zonespace
;
; number of nodes
dwnodes=dwzones+1
hdwnodes=hdwzones+1
hbnodes=hbzones+1
```

```
bnodes=bzones+1
fullnodes=fullzones+1
;
; boundaries
xbound1=B+x+0.1
xbound2=B+x-0.1
xbound=B+x
stpoint=(B-dw)/2
endpoint=stpoint+dw
ppatbase=height*9.81*1000
;
end

inputparameters          ; run inputparamters
;
; FISH program to calculate discharge and store results in a table
; TABLE 1 => x=row number, y=water height
; TABLE 2 => x=row number, y=Discharge rate
; TABLE 3 => x=Hour number, y=Maximum Pore pressure
;
define calculatedischarge
        cumflow=0
        cumdischarge=0
        xcord=xbound ; x co-ordinate for drain node
        loop ynode (1,hdwnodes)
                ycord=((ynode-1)*zonespace)          ; y co-ordinate for drain node
                loop znode (1,dwnodes)
                        zcord=(znode-1)*zonespace   ; z co-ordinate for drain node
                        thenode=gp_near(xcord,ycord,zcord)
                        thenodeflow=gp_flow(thenode)
                        cumflow=cumflow+(-1*(thenodeflow))
                end_loop
        end_loop
hrdischarge=cumflow*3600*2          ; half symmetry
;
; Find Position and Value for Maximum Pore Pressure
 maxpp = 0
xcount=Bzones+1
ycount=hbzones+1
heightcount=heightzones+1
loop zpos(1,heightcount)
        zz=((zpos-1)*zonespace)
        loop xpos (1,xcount)
        xx=(xpos-1)*zonespace
                loop ypos (1,ycount)
                yy=(ypos-1)*zonespace
```

```
                        pppoint=gp_near(xx,yy,zz)
                        ppatpoint=gp_pp(pppoint)
                                if ppatpoint > maxpp then
                                maxpp = ppatpoint
                                end_if
                        end_loop
                end_loop
end_loop
;
        table(1,heightfac)=Height
        table(2,heightfac)=hrdischarge
        table(3,heightfac)=maxpp
;
end
;
; *** Model geometry ***
; Geomety
config fl
gen zone brick size Bzones,hBzones,fullzones p0 (0,0,0) p1 add (B,0,0) p2 add
(0,hB,0) p3 add (0,0,fullheight)
gen zone brick size xzones,hdwzones,dwzones p0 (B,0,0) p1 add (x,0,0) p2 add
(0,hdw,0) p3 add (0,0,dw)
;
;
define solveit
;

loop heightfac (1,20)
height=heightfac*B/2
Heightbound1=height+0.1
Heightbound2=height-0.1
ppatbase=1000*9.81*height
Heightzones=height/zonespace
Heightnodes=Heightzones+1
;
command
title
Case 1 - Single Drain with Half Symmetry
;
group fill range z -0.1 heightbound1
model mohr range group fill
model null range group fill not
prop dens=1500 shear=3e8 bulk=5e8 coh=5e5 fric=0 tens=0 range group fill
model fl_iso range group fill
prop perm fillperm por fillpor range group fill
set fl biot off
```

```
;
; --- Initial Conditions ---
ini fmod 1e3
ini sat 1 range group fill
ini pp ppatbase grad 0 0 -9.81e3 range group fill
apply pp=0 range x xbound1 xbound2 y 0 hdw z 0 dw
fix pp range x xbound1 xbound2 y 0 hdw z 0 dw
apply pp=0.001 range z heightbound2 heightbound1
fix pp range z heightbound1 heightbound2
;
; --- settings ---
set grav 0 0 -9.81
ini fdensity 1e3
ini ftens 0.0
set mech off
set fl on
;
set fluid ratio 1e-5
solve
calculatedischarge
print hrdischarge maxpp height
;
apply remove gp range x xbound2 xbound1 y 0 hdw z 0 dw
apply remove gp range z heightbound1 heightbound2
save stopeA.sav
end_command
end_loop
end
solveit
;
set logfile case stopeA
set log on
print table 1
print table 2
print table 3
set log
```

APPENDIX C

Validation plots for additional points on two-dimensional stope

C.1. Validation graphs for Point A and B on two dimensional stope
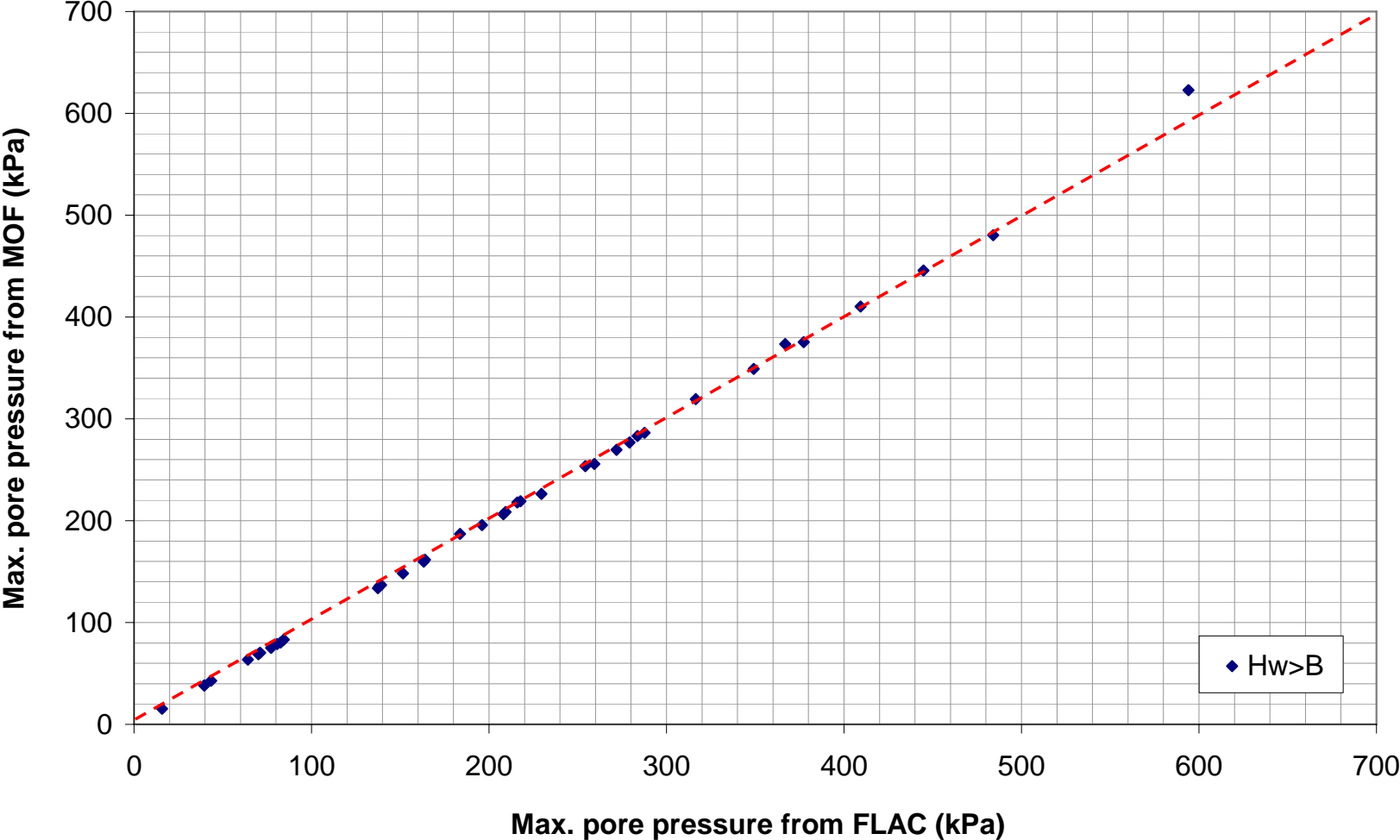
C.2. Validation graphs for Point C on two-dimensional hydraulic fill stope
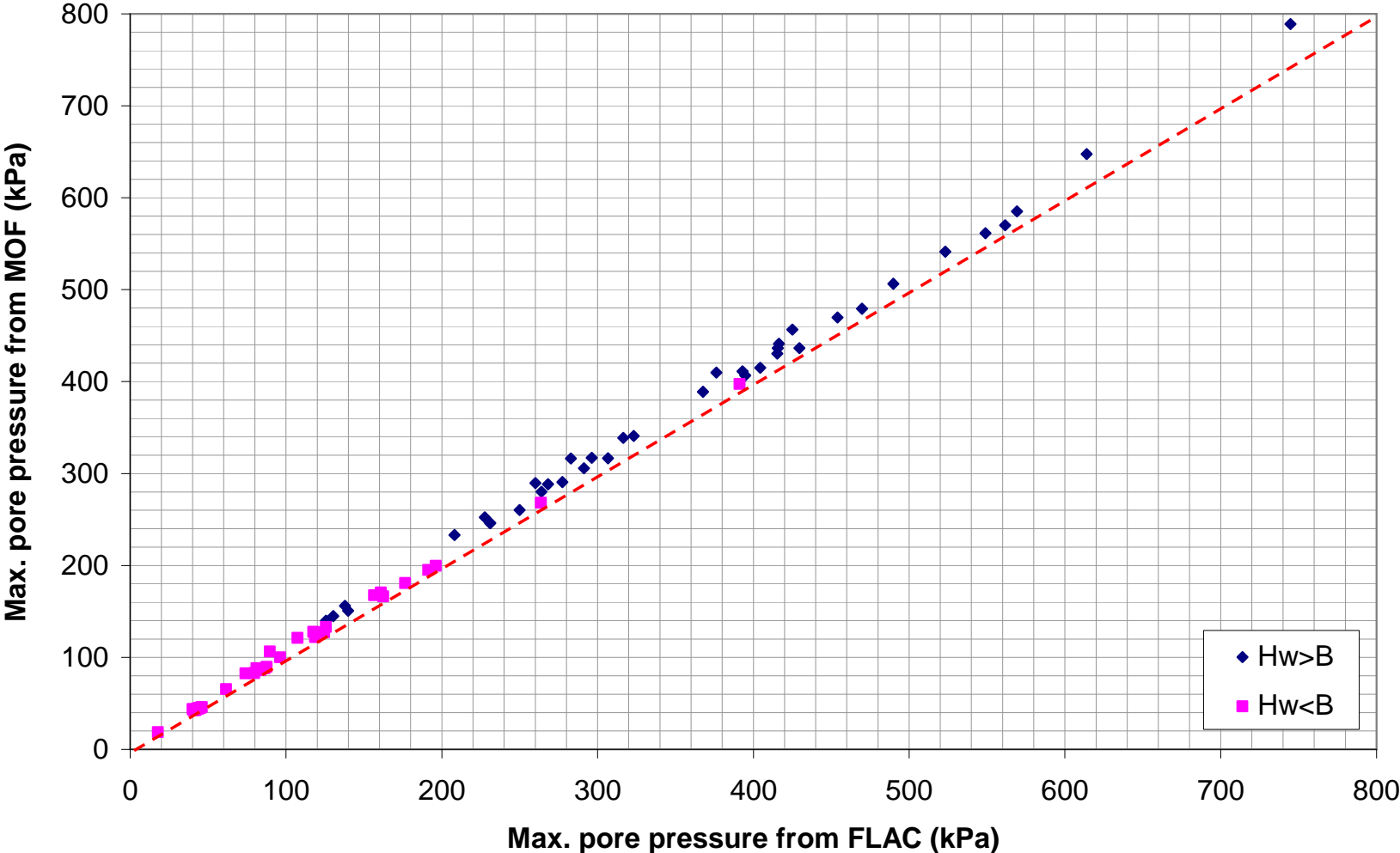
C.3. Validation graph for Point D on two-dimensional hydraulic fill stope
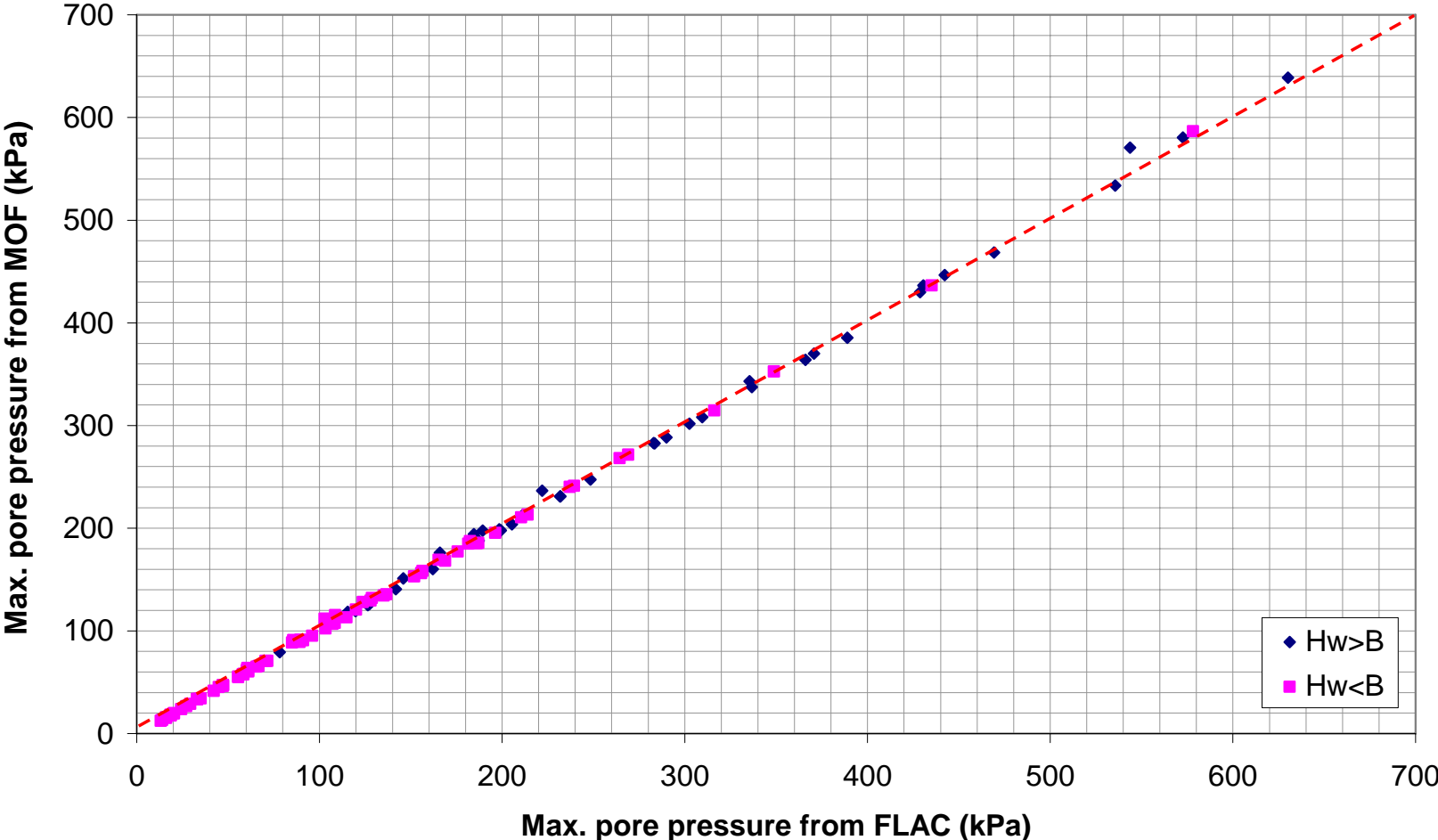
C.4. Validation graph for Point E and F on two-dimensional hydraulic fill stope
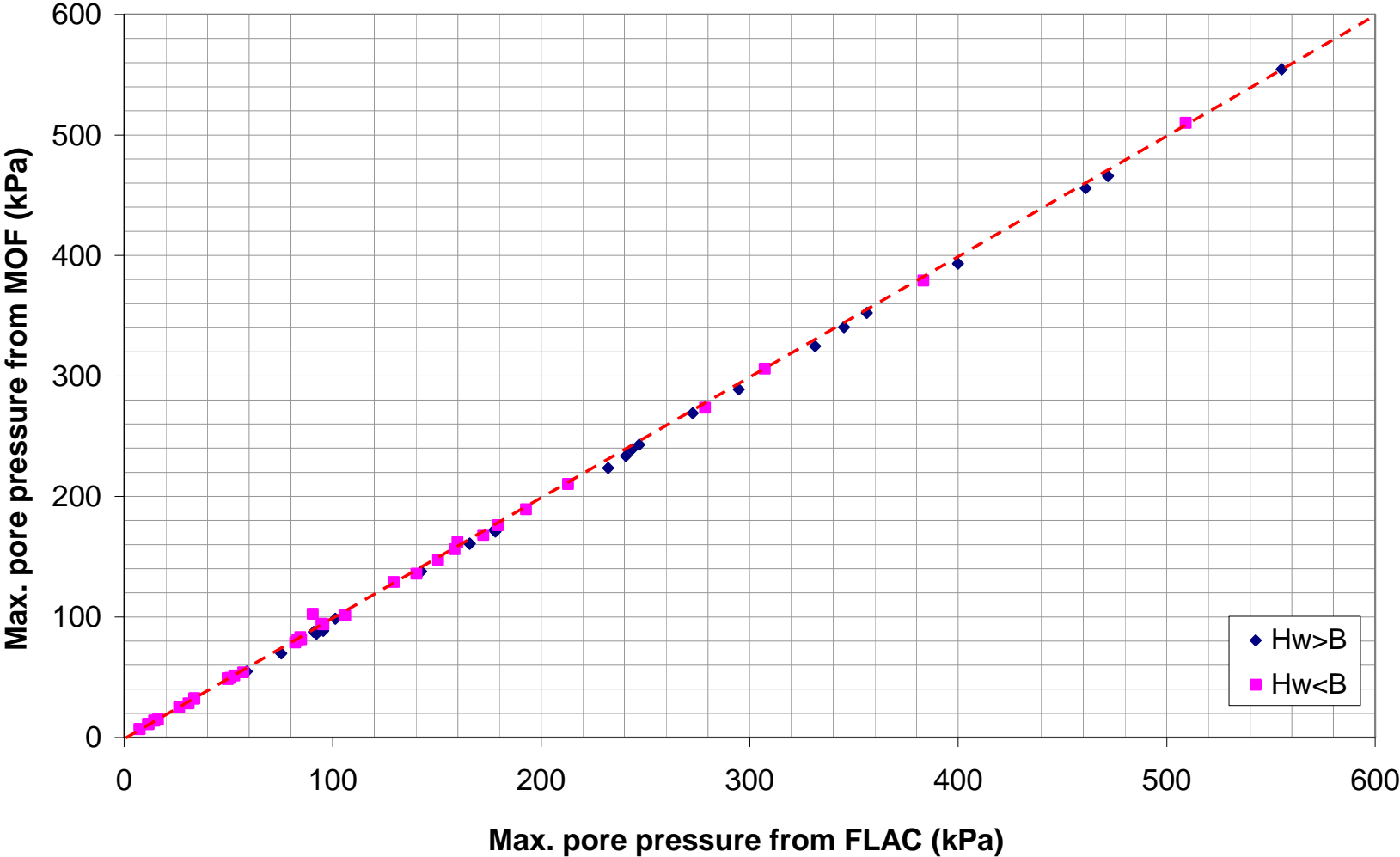
APPENDIX D

Anisotropic Permeability Cell Testing Results

D.1. Permeability Cell Testing on Sample D3

Trial	Flow Direction	Run #	Collection Time (mins)	Beaker mass (g)	Beaker + water (g)	Volume (cm³)	Head (cm)	k (cm/s)	k (mm/hr)	k_avg mm/hr	k_avg mm/hr	k_h/k_v
Head 1	Vertical	1	3.00	200	481	281	56	0.00183	66.01			
		2	3.00	228	498	270	56	0.00176	63.43			
		3	4.00	200	552	352	56	0.00172	62.02			
		4	3.00	228	528	300	56	0.00196	70.48	65.48		
Head 2		1	3.00	228	498	270	71	0.00139	50.03		56.14	
		2	3.00	200	499	299	71	0.00154	55.40			
		3	3.00	200	467	267	71	0.00137	49.47			
		4	3.00	228	509	281	71	0.00145	52.07	51.74		
Head 3		1	3.00	228	563	335	85	0.00144	51.85			1.28
		2	3.00	200	514	314	85	0.00135	48.60			
		3	3.00	228	577	349	85	0.00150	54.02			
		4	3.00	200	525	325	85	0.00140	50.30	51.19		
Head 1	Horizontal	1	3.00	200	495	295	55	0.00196	70.56			
		2	3.00	228	528	300	55	0.00199	71.76			
		3	3.00	228	552	324	55	0.00215	77.50			
		4	3.00	200	473	273	55	0.00181	65.30	71.28	71.78	
Head 2		1	3.00	228	590	362	65	0.00204	73.27			
		2	3.00	200	587	387	65	0.00218	78.33			
		3	4.20	228	734	506	65	0.00203	73.15			
		4	4.50	200	677	477	65	0.00179	64.36	72.28		

D.2. Permeability Cell Testing on Sample D4

Sample ID - *D4 ~ Permeability Cell (Anisotropic permeability)*   Date   17/01/2006

Sample Height	14.8	cm
Sample Length	15	
Sample width	15	cm
Sample Area	*225.00*	cm^2

Comments:

Trial	Flow Direction	Run #	Collection Time (mins)	Beaker mass (g)	Beaker + water (g)	Volume (cm^3)	Head (cm)	k (cm/s)	k (mm/hr)	k$_{avg}$ mm/hr	k$_{avg}$ mm/hr	k$_h$/k$_v$
Head 1	Vertical	1	5.00	228	388	160	58	0.00060	21.77			
		2	5.00	200	359	159	58	0.00060	21.64			
		3	5.00	228	396	168	58	0.00064	22.86	22.09		
Head 2		1	5.00	228	496	268	87.5	0.00067	24.18			
		2	5.00	228	511	283	87.5	0.00071	25.53			
		3	3.00	228	393	165	87.5	0.00069	24.81			
		4	3.00	200	368	168	87.5	0.00070	25.26	24.94	23.52	1.455
Head 1	Horizontal	1	3.00	228	371	143	55	0.00095	34.20			
		2	3.00	228	379	151	55	0.00100	36.12			
		3	3.00	228	370	142	55	0.00094	33.97	35.16		
Head 2		1	5.00	228	598	370	87.5	0.00093	33.38			
		2	5.00	200	568	368	87.5	0.00092	33.20			
		3	5.00	228	596	368	87.5	0.00092	33.20	33.26	34.21	

D.3. Permeability Cell Testing on Sample A1

Sample ID - *A1 ~ Permeability Cell (Anisotropic permeability)*   **Date**   **24/01/2006**

Sample Height	14.6	cm
Sample Length	15	
Sample width	15	cm
Sample Area	*225.00*	cm^2

Comments:

Trial	Flow Direction	Run #	Collection Time (mins)	Beaker mass (g)	Beaker + water (g)	Volume (cm^3)	Head (cm)	k (cm/s)	k (mm/hr)	k$_{avg}$ mm/hr	k$_{avg}$ mm/hr	k$_h$/k$_v$
Head 1	Vertical	1	3.00	200	555	355	50	0.00256	92.14			
		2	3.00	228	595	367	50	0.00265	95.26			
		3	3.00	200	568	368	50	0.00265	95.52	94.31		
Head 2		1	3.00	200	736	536	70	0.00276	99.37			
		2	3.00	228	761	533	70	0.00274	98.82			
		3	3.00	200	672	472	70	0.00243	87.51	95.23	94.77	1.28
Head 1	Horizontal	1	3.00	228	721	493	50	0.00355	127.96			
		2	3.00	200	689	489	50	0.00353	126.92			
		3	3.00	200	674	474	50	0.00342	123.03	125.97		
Head 2		1	2.50	200	747	547	70	0.00338	121.69			
		2	3.00	228	867	639	70	0.00329	118.47			
		3	3.00	228	835	607	70	0.00313	112.54	117.57	121.77	

APPENDIX E

Physical Modelling Results

E.1. Scaled Stope Analysis: Numerical / Laboratory / MOF³ᴰ results for scaled stope

Case	Hw	B	X	D	h_L	k (m/s)	D/B	X/D	Hw/B	$\Gamma_{1 \text{ (from eqn)}}$	$\Gamma_{3 \text{ (from eqn)}}$	$\Gamma_{2 \text{ (from eqn)}}$	$\Sigma\Gamma$ Eqn	α	$Q_{\text{full size Eqn}}$ (m³/hr)	$Q_{\text{scaled Eqn}}$ (m³/hr)	Experimental Q (m³/hr)	FLAC³ᴰ Q (m³/hr)
S11	20	20	5	4	16	6.58E-05	0.20	1.25	1.00	0.00	3.00	4.99	7.99	0.89	7.587	0.21	0.250	0.253
S12	60	20	5	4	56	6.58E-05	0.20	1.25	3.00	5.60	10.50	14.98	31.08	0.89	23.902	0.66	0.773	0.482
S13	100	20	5	4	96	6.58E-05	0.20	1.25	5.00	19.20	18.00	24.96	62.16	0.89	35.118	0.98	1.147	0.965
S14	20	20	10	4	16	6.58E-05	0.20	2.5	1.00	0.00	8.00	4.99	12.99	0.89	4.667	0.13	0.103	0.152
S15	60	20	10	4	56	6.58E-05	0.20	2.5	3.00	5.60	28.00	14.98	48.58	0.89	15.292	0.42	0.387	0.433
S16	100	20	10	4	96	6.58E-05	0.20	2.5	5.00	19.20	48.00	24.96	92.16	0.89	23.687	0.66	0.657	0.658
S17	20	20	14	4	16	6.58E-05	0.20	3.5	1.00	0.00	12.00	4.99	16.99	0.89	3.569	0.10	0.073	0.115
S18	60	20	14	4	56	6.58E-05	0.20	3.5	3.00	5.60	42.00	14.98	62.58	0.89	11.871	0.33	0.263	0.338
S19	100	20	14	4	96	6.58E-05	0.20	3.5	5.00	19.20	72.00	24.96	116.16	0.89	18.793	0.52	0.470	0.524
S21	20	20	5	4	16	8.76E-05	0.20	1.25	1.00	0.00	3.00	4.99	7.99	0.89	10.100	0.28	0.357	0.337
S22	60	20	5	4	56	8.76E-05	0.20	1.25	3.00	5.60	10.50	14.98	31.08	0.89	31.821	0.88	0.987	0.894
S23	100	20	5	4	96	8.76E-05	0.20	1.25	5.00	19.20	18.00	24.96	62.16	0.89	46.753	1.30	1.453	1.285
S24	20	20	10	4	16	8.76E-05	0.20	2.5	1.00	0.00	8.00	4.99	12.99	0.89	6.214	0.17	0.163	0.202
S25	60	20	10	4	56	8.76E-05	0.20	2.5	3.00	5.60	28.00	14.98	48.58	0.89	20.358	0.57	0.527	0.744
S26	100	20	10	4	96	8.76E-05	0.20	2.5	5.00	19.20	48.00	24.96	92.16	0.89	31.534	0.88	0.920	0.875
S27	20	20	14	4	16	8.76E-05	0.20	3.5	1.00	0.00	12.00	4.99	16.99	0.89	4.751	0.13	0.177	0.153
S28	60	20	14	4	56	8.76E-05	0.20	3.5	3.00	5.60	42.00	14.98	62.58	0.89	15.804	0.44	0.517	0.449
S29	100	20	14	4	96	8.76E-05	0.20	3.5	5.00	19.20	72.00	24.96	116.16	0.89	25.019	0.69	0.780	0.698
S31	20	20	5	4	16	0.00008	0.20	1.25	1.00	0.00	3.00	4.99	7.99	0.89	9.224	0.26	0.433	0.031
S32	60	20	5	4	56	0.00008	0.20	1.25	3.00	5.60	10.50	14.98	31.08	0.89	29.061	0.81	0.883	0.816
S33	100	20	5	4	96	0.00008	0.20	1.25	5.00	19.20	18.00	24.96	62.16	0.89	42.696	1.19	1.370	1.173
S34	20	20	10	4	16	0.00008	0.20	2.5	1.00	0.00	8.00	4.99	12.99	0.89	5.674	0.16	0.143	0.185
S35	60	20	10	4	56	0.00008	0.20	2.5	3.00	5.60	28.00	14.98	48.58	0.89	18.592	0.52	0.490	0.527
S36	100	20	10	4	96	0.00008	0.20	2.5	5.00	19.20	48.00	24.96	92.16	0.89	28.799	0.80	0.783	0.799
S37	20	20	14	4	16	0.00008	0.20	3.5	1.00	0.00	12.00	4.99	16.99	0.89	4.339	0.12	0.137	0.140
S38	60	20	14	4	56	0.00008	0.20	3.5	3.00	5.60	42.00	14.98	62.58	0.89	14.432	0.40	0.380	0.410
S39	100	20	14	4	96	0.00008	0.20	3.5	5.00	19.20	72.00	24.96	116.16	0.89	22.849	0.63	0.697	0.637